THE UNIVERSITY OF CALGARY

Molecular and Biophysical Analysis of the Delayed Rectifier K^+ Current in Bullfrog Atrium

by

Vicki L. Lowes

A DISSERTATION
SUBMITTED TO THE FACULTY OF GRADUATE STUDIES
IN PARTIAL FULFILLMENT OF THE REQUIREMENTS FOR THE
DEGREE OF DOCTOR OF PHILSOPHY

DEPARTMENT OF CARDIOVASCULAR/RESPIRATORY SCIENCES

CALGARY, ALBERTA
APRIL, 1998

Abstract

There is widespread interest in identifying the molecular structures underlying the slowly activating delayed rectifier K^+ current (I_{Ks}) in cardiac tissue. At the time this dissertation was started minK, a small 129 amino acid polypeptide, was proposed to encode I_{Ks}. There was a controversy, however, over whether minK formed a functional K^+ channel or acted as a regulator of protein(s) endogenous to *Xenopus* oocytes. The aim of this study was to provide a detailed quantitative comparison of the biophysical, pharmacological, and molecular properties of I_{Ks} with those of minK, to gain insight into whether minK could be responsible for I_{Ks}. The bullfrog atrium was used as a model of I_{Ks}, as the delayed rectifier K^+ current in this tissue (I_K) is composed of only a single slowly activating K^+ conductance.

I_K was recorded from isolated bullfrog atrial myocytes using standard whole cell patch clamp techniques. The characteristics of this current were compared to two-electrode voltage clamp recordings of rat uterine minK expressed in *Xenopus* oocytes. I_K and minK had very similar steady-state activation characteristics, current-voltage relationships, and selectivity for K^+; and both exhibited similar pharmacological sensitivity to the class III antiarrhythmic agents, azimilide and propenamide. These results suggest that minK forms at least part of the molecular structure underlying I_K.

Attempts to obtain evidence that minK is present in bullfrog atrium were unsuccessful, although two 3' splice variants of KvLQT1 were identified from bullfrog heart. KvLQT1 has recently been reported to coassemble with minK to encode I_{Ks}. At this time we have not been able to obtain functional expression of either splice variant.

During this study, we noted that efflux of K^+, due to activation of either minK or Kv1.2 expressed in *Xenopus* oocytes, caused significant depolarizing shifts in reversal potential, consistent with there being K^+ accumulation on the extracellular surface of the oocyte. A mathematical model was developed showing that a restricted diffusion layer on the surface of the oocyte, in combination with an unstirred fluid layer, can account for the K^+ accumulation.

Acknowledgements

I would first like to express my sincere thanks to my supervisor, Dr. Wayne Giles, whose support and guidance over the course of my studies has been greatly appreciated. He has been an excellent teacher and mentor, and his patience and concern will not be forgotten. I thank you Wayne for your genuine belief in me.

A sincere thank you also goes to Dr. Robert Clark (aka "The Fonz"), who was always there to answer my questions and whose patience was extraordinary. I don't believe there was ever a question he could not answer or a problem he could not fix, and he did so openly and uncritically.

An enormous thanks also goes to Robert Winkfein for his extensive work on cloning KvLQT1 from bullfrog heart, and also for guidance on the *in situ* hybridization experiments. Furthermore, I would like to thank Drs. Virginia Stroeher and Mark Heschl for preliminary work trying to identify minK in bullfrog heart, Mrs. Ewa Kinsberg for her help with the *in situ* hybridization experiments, Anders Nygren for doing the mathematical modelling of K^+ accumulation in *Xenopus* oocytes (and whose work is reported in Appendix 1 of this dissertation), Mrs. Leona Barclay for performing the electron and light microscopy of *Xenopus* oocytes, and Nishan Sharma for general technical assistance and moral support. Thank you also to Drs. Jaideep Bains, Jonathon Cordeiro, Mary Earle, Céline Fiset, Yakhin Shimoni, Hideo Tanaka, and Christopher Ward for invaluable criticism, advice and support.

I also wish to send a warm thankyou to all of my friends and family for their humour and understanding over the past several years. I hope this thesis teaches you that I do more in my life than just "suck cells". Finally, I want to acknowledge my son Connor, whose beautiful smile and laughter have put everything into perspective, and my husband Shawn, an incredibly wise and gentle man who was there for all of the ups and downs, and never once complained.

This work was supported by Studentships from the Heart and Stroke Foundation of Canada, the Medical Research Council of Canada, and the Alberta Heritage Foundation for Medical Research.

Dedication

To my parents, Peter and Carol Lowes, who instilled in me the love of learning and have always encouraged me to take on new challenges. I am forever grateful.

Table of Contents

List of Tables

List of Figures

CHAPTER 1: INTRODUCTION

Foreword

Potassium (K^+) channels play an important role in numerous cellular processes and have been found in virtually every type of excitable and nonexcitable cell examined. In cardiac tissue K^+ channels are responsible for action potential repolarization and maintenance of resting membrane potential. Dysfunctions of K^+ channels have been implicated in cardiac electrophysiological disorders associated with cardiac ischemia and some arrhythmias. A specific class of antiarrhythmic drugs, the Class III group, act mainly on K^+ channels. These agents lengthen the action potential and its refractory period and can interfere with ventricular tachycardia (Hondeghem, 1992). Examples of Class III antiarrhythmics include clofilium tosylate and azimilide, both of which have been found to block a component of K^+ current in mammalian cardiac tissue, the slowly activating delayed rectifier (I_{Ks}) (Arena and Kass, 1988; Busch et al., 1994a). This current is thought to be an important therapeutic target because, like other outward K^+ currents, blockade of this channel results in prolongation of action potential duration and the effective refractory period. Particularly advantageous, however, is the finding that agents which inhibit I_{Ks} do not exhibit reverse use-dependence, a phenomenon in which block becomes less effective at high heart rates, and which is characteristic of compounds which block the rapidly activating component of the delayed rectifier.

A small 129-130 amino acid protein which, when expressed in *Xenopus laevis* oocytes, elicits a current with many of the same biophysical and pharmacological characteristics of I_{Ks}, has been cloned from mammalian heart, kidney and uterus (for review see Kaczmarek and Blumenthal, 1997). This protein, named minK as a result of its 'minimal' size, is thought to underlie I_{Ks}, although to date no extensive quantitative comparison has been made between the cloned minK and I_{Ks} in native cardiac tissue. It is critical to have an in depth understanding of the molecular structure underlying I_{Ks} in order to improve the design and development of new antiarrhythmic agents, and also to better understand how this current contributes to normal cardiac function.

The aim of this study was to provide a quantitative comparison of the biophysical, pharmacological and molecular properties of I_{Ks} with minK. The model we chose to investigate the properties of I_{Ks} was bullfrog atrium, as the delayed rectifier K^+ channel in this tissue is composed of only a single slowly activating component. Thus, the following literature review will focus on three main areas; 1) A description of delayed rectifier K^+ currents in mammalian cardiac tissue; 2) A general background of the delayed rectifier K^+ current in bullfrog atria (in an effort to explain why bullfrog atrium is a good model to use); and 3) A review of the recent literature on the molecular structures thought to underlie I_{Ks}.

The Delayed Rectifier K^+ Conductance in Cardiac Tissue

The delayed rectifier K^+ current (I_K) activates during the plateau phase of the cardiac action potential and, in certain cardiac tissues (ie. bullfrog and guinea pig), is responsible for the initiation of repolarization. In other tissues (ie. mouse, rabbit, cat, dog, and human ventricle; see review by Rees and Curtis, 1996), rapid activation and then inactivation of the transient outward current starts early repolarization and contributes to the spike potential. This is then followed by opening of I_K, which repolarizes the membrane to a potential at which inward rectifier K^+ channels can open, which in turn mediates the final phase of repolarization. Three types of I_K have been described in single cardiac myocytes. These include the rapidly activating delayed rectifier (I_{Kr}) which has an inwardly rectifying current-voltage relationship, the slowly activating delayed rectifier (I_{Ks}) which has a linear or outwardly rectifying current-voltage curve, and the 'ultra' rapidly activating delayed rectifier (I_{Kur}) which also outwardly rectifies. These currents show variable tissue distribution, exhibit different sensitivities to pharmacological agents, and activate with different time- and voltage-dependence (For review see Sanguinetti and Jurkiewicz, 1994; Roden and George, 1996; Brown, 1997) . These unique characteristics can be used to advantage for study of each individual current component in isolation. This review will focus only on two of these components, I_{Ks} and I_{Kr}, but for a description of I_{Kur} see the recent review by Brown (1997).

Early Studies

Noble and Tsien (1969) were the first to provide a quantitative description of a time-dependent outward current in cardiac tissue. This current, identified in sheep Purkinje fibers, activated within the physiological range of membrane potentials, did not inactivate, and turned on very slowly relative to known Na^+ and Ca^{++} currents. The name 'delayed rectifier' was therefore given to this current as a result of its 'delayed' activation kinetics. Voltage-clamp experiments designed to characterize this outward current were interpreted in terms of two separate components, both of which were sensitive to changes in the concentration of extracellular K^+ but were not entirely K^+ selective. The first component, labelled i_{x1}, had a time course of activation of 500msec at -10mV and inwardly rectified at positive potentials. The second component (i_{x2}) activated with a time constant that was much slower (3.8 sec at -10mV) and its current-voltage relationship was relatively linear. This component was particularly non-selective, with a reversal potential between -50 and -20mV.

Two components of current similar to those described by Noble and Tsien (1969) have subsequently been described in multicellular preparations from other cardiac tissues. These include cat ventricular trabeculae (McDonald and Trautwein, 1978), frog sinus venosus (Brown et al., 1977), frog atrium (Ojeda and Rougier, 1974; Brown and Noble, 1969; Brown et al., 1976a; Brown et al., 1976b), rabbit atrioventricular nodal cells (Kokubun et al., 1982), and embryonic chick atrial cell aggregates (Shrier and Clay, 1986). Other reports, however, have identified only a single population of channels underlying the delayed rectifier. In rabbit sinoatrial node Noma and Irisawa (1976) described only a single component resembling i_{x1} of Noble and Tsien (1969), although this current was more selective for K^+. In addition, Bennett et al. (1985) reported that although the deactivation tail currents of the delayed rectifier in calf Purkinje fibers showed biexponential kinetics, both components shared the same reversal potential, suggesting that they may come from a single population of channels. The authors proposed that the delayed rectifier could be better described by a single population of channels having multiple-state kinetics including 2 closed and 1 open states, rather than

by two distinct channels activating together. It has also been suggested that the slow component of the delayed rectifier described by Noble and Tsien (1969), i_{x2}, may not represent a second population of channels, but might instead be an artifact of accumulation of K^+ in restricted spaces of the Purkinje fibers during the long voltage clamp steps needed to activate i_{x2} (Attwell et al., 1979). Alternatively, it could be that the variability between the different reports described above is simply due to species and/or tissue heterogeneity. This possibility will be discussed in more detail in the following sections.

Evidence for I_{Ks} and I_{Kr} from Single Cell Preparations

Since these early studies, many groups have investigated the properties of the delayed rectifier conductance in single-cell rather than multi-cellular preparations. These preparations are preferable for quantitative studies of biophysical properties as they minimize technical problems intrinsic to the latter system such as poor space clamp (Johnson and Lieberman, 1971), series resistance artifacts due to recording of large currents (see review by Johnson and Lieberman, 1971; Attwell and Cohen, 1977), and K^+ accumulation (Attwell and Cohen, 1977; Cohen and Kline, 1982; Kline and Morad, 1978; Noble, 1976; Attwell et al., 1979). In particular, one system where the different components of the delayed rectifier have been extensively studied is in isolated guinea-pig ventricular myocytes. Matsuura et al. (1987) identified a slowly activating delayed rectifier-type K^+ channel in this tissue that was half-maximally activated at -13mV and had a slope conductance of 12mV. This channel, although similar to i_{x2} described by Noble and Tsien (1969), was much more K^+ selective with a slope of 49mV/10 fold change in external K^+ concentration. Sanguinetti and Jurkiewicz (1990b) verified the presence of a slowly activating component of the delayed rectifier in guinea pig myocytes and labeled this current I_{Ks} (slowly activating I_K). In addition, they identified a novel (previously undetected) component of I_K that resembled i_{x1} from sheep Purkinje fibers (Noble and Tsien, 1969). E-4031, a class III antiarrhythmic that is a structural analogue of sotalol, was found to prolong action potential duration and also to inhibit the novel

component of outward K^+ current in these cells. An envelope of tails test confirmed the presence of two distinct currents, which could be separated based on their sensitivity to E-4031. The E-4031-sensitive component was inhibited with an IC_{50} of 397nM, activated rapidly (time constant of 15msec at +20mV), did not inactivate, and had an inwardly rectifying current-voltage relationship with negative slope at potentials more positive than 0mV. It was therefore referred to as I_{Kr} (rapidly activating I_K). Steady-state activation curves for I_{Kr} measured at the end of 550msec test pulses yielded a half-maximal activation of -21.5mV and slope factor of 7.5mV. Tests for K^+ selectivity revealed shifts in reversal potential of 54mV/10 fold change in external K^+ concentration, consistent with I_{Kr} being a K^+ selective current. In contrast, the E-4031-insensitive component of current (I_{Ks}) activated slowly with sigmoid onset kinetics, did not inactivate, and was less selective than I_{Kr} for K^+. This current had an outwardly rectifying current voltage relationship, a $V_{1/2}$ of +15.7 mV, and slope factor of 12.7mV, therefore closely matching the current described by Matsuura et al. (1987). Interestingly, at a potential of +10mV I_{Ks} was approximately ten fold larger than I_{Kr} in guinea-pig ventricle, suggesting it may be the major contributor to repolarization. The slow time course of this current, however, means that it will only be partially activated over the duration of the action potential. As a result, it is likely that both I_{Kr} and I_{Ks} are involved in repolarization (Sanguinetti and Jurkiewicz, 1990b). Mathematical modelling of the action potential in guinea pig ventricular myocytes has provided further insights into the role of both of these currents in action potential repolarization (Zeng et al., 1995).

Using a similar pharmacological and biophysical approach as that described above, two components of the delayed rectifier have also been identified in guinea pig atrial cells (Sanguinetti and Jurkiewicz, 1991). These currents share very similar properties to I_{Ks} and I_{Kr} identified in guinea pig ventricle. In atrial tissue, I_{Ks} has a half-point of activation of +24mV and slope factor of 15.7mV, whereas the corresponding values for I_{Kr} are -19.3mV and 5.2mV. One difference between the two tissues, however, is that I_{Ks} in atria is much more K^+ selective than in ventricular cells. Furthermore, in atrial cells the current density of I_{Kr} and I_{Ks} is 2-2.5 fold higher than in ventricle, perhaps

providing one reason why the action potential in guinea pig atrial myocytes is shorter than in ventricle (Sanguinetti and Jurkiewicz, 1991).

The different biophysical and pharmacological characteristics of I_{Ks} and I_{Kr} can be used to advantage for separating the components of the delayed rectifier in cardiac tissue. Thus, following the approach of Sanguinetti and Jurkiewicz (1990b) two components of current similar to I_{Kr} and I_{Ks} have been identified in human atrial appendages (Wang et al., 1994), and canine atrial and ventricular myocytes (Gintant, 1995; Liu and Antzelevitch, 1995; Liu et al., 1993; Gintant, 1996; Yue et al., 1996). In contrast, the delayed rectifier in bullfrog atria (Hume et al., 1986; Simmons et al., 1986), bullfrog sinus venosus (Giles and Shibata, 1985), and guinea pig sinoatrial node (Anumonwo et al., 1992) appears to consist of only a single current component resembling I_{Ks}, whereas the delayed rectifier in rabbit ventricular (Veldkamp et al., 1993; Howarth et al., 1996) and atrial (Muraki et al., 1995) myocytes, rabbit nodal cells (Howarth et al., 1996), fetal mouse ventricular myocytes (Wang and Duff, 1996a), and cat ventricular myocytes (Follmer and Colatsky, 1990; Furukawa et al., 1992) seems to be composed of a single population of channels resembling I_{Kr}. Others have identified a delayed rectifier too small to be accurately characterized in human atrial myocytes (Firek and Giles, 1995), and rabbit atrial and ventricular myocytes (Giles and Imaizumi, 1988), although Salata et al. (1996a) recently distinguished I_{Ks}- and I_{Kr}-like currents in a small proportion of rabbit ventricular myocytes.

It is apparent from the studies described above that there is substantial interest in investigating the properties of I_{Kr} and I_{Ks} in different cardiac tissues. Regional heterogeneity and differential distribution of these two components between tissues and species likely contributes to the observed variability in action potential shape and duration. This brief review has outlined only a few key studies and, in the interest of space, has omitted a large body of work. An extensive review of the properties of I_{Kr} is beyond the scope of this literature review, and the reader is referred to several recent reviews (Sanguinetti and Jurkiewicz, 1994; Kass, 1995; Sanguinetti and Keating, 1997) for a summary of the properties of this current. Rather, the following sections will centre

on the biophysical and pharmacological properties of I_{Ks} in cardiac tissue, since the properties of this current and the molecular structure underlying it are the focus of this dissertation.

Single Channel Properties of I_{Ks}

Several attempts have been made to obtain single channel recordings of I_K. Most studies have not distinguished between I_{Kr} and I_{Ks} and have described conductances ranging from 1.6 pS in 5.4mM external K^+ in rabbit nodal cells (Shibasaki, 1987), to 15 and 62pS in 4mM external K^+ in embryonic chick heart ventricle (Clapham and Logothetis, 1988). Single-channel recordings of I_{Ks} are complicated by the fact that I_{Ks} appears to have a very small single channel conductance (less than 1pS), despite being present in extremely high density in the sarcolemma (Walsh et al., 1991). Using cell-attached and inside-out patch-clamp recording Horie et al. (1990) identified two types of K^+ channels in guinea-pig atrial cells with unitary conductances of 10 and 3 pS. The larger conductance channel had biophysical characteristics resembling I_{Kr}, whereas the smaller conductance channel resembled I_{Ks}. This channel had a longer life time than the 10pS channel, a reversal potential of 0mV in symmetrical K^+, and plots of the ensemble tail currents revealed a slow time course of deactivation (1200 msec at -80mV; 419msec at -100mV). This 3pS channel was too small, however, to accurately resolve open and closed times and an in depth study of the single channel properties of I_{Ks} is still awaited.

I_{Ks} Physiology

A role for I_{Ks} in contributing to rate-dependent shortening of the action potential has been proposed by Jurkiewicz and Sanguinetti (1993). Rapid pacing of guinea pig ventricular myocytes increases the magnitude of I_{Ks}; as a result this current may fail to deactivate completely during rapid stimulation and contribute to the reverse use-dependent effects of I_{Kr} blockers on action potential duration (Jurkiewicz and Sanguinetti, 1993b). This 'accumulation' of I_{Ks} occurs as a result of its slow deactivation kinetics relative to I_{Kr} in guinea-pig heart (I_{Ks} vs I_{Kr} time course of deactivation: 212msec vs

~70msec at ~ -60mV in whole cell studies measured at 34-36°C (Matsuura et al., 1987; Sanguinetti and Jurkiewicz, 1990b); 1200msec vs 101msec at -80mV at 22-24°C in single channel studies (Horie et al., 1990)). Recent studies, however, have concluded that this role for I_{Ks} as a contributor to the reverse use-dependence of other class III antiarrhythmic agents may not be consistent between species. Gintant (1996) reported that the time constant for deactivation of I_{Ks} in canine ventricular myocytes, measured at -20 to -60mV, is actually much faster (150msec at -35mV) than for I_{Kr} (2-3sec at -35mV). In addition, at -85mV the time constant for I_{Ks} decreases to approximately 30msec suggesting that, contrary to guinea pig ventricular myocytes, it is unlikely that I_{Ks} in canine ventricle is involved in rate-dependent shortening of the action potential duration. Curiously, Heath and Terrar (1996b) have also reported faster deactivation kinetics for I_{Ks} relative to I_{Kr} in guinea pig ventricular myocytes. It is unclear why these results are so different to those of Sanguinetti and Jurkiewicz (1990b) in the same species, as the recording temperature and conditions were very similar in each study (Sanguinetti and Jurkiewicz, 1990b: 35°C, suction microelectrode technique, pipette resistance 4-8MΩ, pipette solution 1M K gluconate and 50mM KCl; Heath and Terrar, 1996b: 35-36°C, microelectrode technique, pipette resistance 18-25MΩ, pipette solution 0.5M K_2SO_4 and 10mM KCl). Rather, these differences could result from regional heterogeneity in the characteristics of I_{Ks} and I_{Kr} in guinea pig ventricle (see below) that is reflected in the different population of cells used in each study. Regardless, these studies do suggest that an involvement of I_{Ks} in contributing to reverse-rate dependence of class III antiarrhythmics may need to be specifically evaluated in each tissue.

Evidence for regional differences in the distribution of I_{Ks} and I_{Kr} within the same heart has been reported. Gintant (1995) reported that the density of I_K, measured by normalizing current amplitude to cell size, is greater in epicardial vs. midmyocardial myocytes in canine left ventricular free wall. This difference between epicardial vs. midmyocardial myocytes was enhanced with longer and more positive voltage-clamp steps. Furthermore, there was no change in either the time course or voltage dependence of activation or deactivation of I_K, or in I_{Kr} density, between these two groups of cells. In

combination, this data suggests that the increase in I_K is due entirely to a greater density of I_{Ks} in epicardial tissue. These results have been confirmed by a different group of researchers (Liu and Antzelevitch, 1995; Liu et al., 1993), and are in agreement with the fact that the action potential duration is shorter in canine epicardial vs. midmyocardial myocytes (Liu et al., 1993).

Regulation of I_{Ks}

There are marked changes in the levels of expression of I_{Ks} during different stages of development. In embryonic mouse hearts at mid-gestation (day 11-13) I_{Ks} can be detected by whole-cell patch clamp recordings in <2% of ventricular cells and not at all in atrial cells. By late-gestation (day 17-20), however, the amount of ventricular, but not atrial cells, expressing I_{Ks} increases to approximately 50%, with a current density of 1-2 pA/pF at +30mV. These changes are in contrast to I_{Kr}, whose expression levels do not change throughout prenatal development in mouse ventricle and atria (Davies et al., 1996a).

Wang et al. (1996b) have also investigated changes in the expression of the delayed rectifier in fetal, neonatal, and adult mouse ventricles and their results complement those of Davies et al. (1996a). At gestational day 18 the I_{Kr} blocker dofetilide completely inhibited the current tail of the delayed rectifier at the end of a five second voltage step to +10mV, suggesting that I_{Ks} is not present in this tissue. Indapamide, which has been reported to inhibit I_{Ks} but not I_{Kr} in guinea-pig ventricular myocytes (Turgeon et al., 1994), did not alter the duration of the action potential in fetal ventricle, supporting the voltage-clamp data. At neonatal day 1 and day 3 the level of expression of I_{Ks} increased to a current density of approximately 2 pA/pF and 5 pA/pF at +30mV, respectively, but then declined to undetectable levels in adult tissue. In contrast, levels of I_{Kr} were highest in fetal ventricular myocytes but then gradually decreased between this stage and neonatal day 1 and 3, and were not detectable in adult heart. Thus, it is clear that in mouse heart there are profound changes in the expression of both I_{Ks} and I_{Kr} during development, and it is probable that this variability in channel expression is responsible

for the shortening of action potential duration that occurs over the course of development (Wang et al., 1996b).

In addition to developmental regulation of I_{Ks}, there are also numerous studies describing modulation of this channel by intracellular messengers. External application of isoproterenol to activate β-adrenergic receptors increases the amplitude of I_{Ks} but not I_{Kr} in guinea pig ventricular myocytes (Sanguinetti et al., 1991). This effect on I_{Ks} is likely due to activation of the adenylate cyclase/cyclic AMP (cAMP) pathway, as application of either forskolin (to activate adenylate cyclase), the membrane-permeable cyclic AMP analogue 8-chlorphenylthio cAMP, or internal perfusion of the cells with cAMP or cAMP-dependent protein kinase, all increase the amplitude of I_K (Walsh et al., 1989; Heath and Terrar, 1996a; Walsh and Kass, 1991). This β-adrenergic modulation of I_K is sensitive to temperature and is most effective at temperatures of 30-37°C (Walsh et al., 1989). Also, activation of β-adrenoceptors with isoproterenol shifts the activation curve for I_K in the negative direction, but does not effect the slope of the curve (Walsh and Kass, 1991).

Stimulation of α-adrenoceptors with phenylephrine or methoxamine augments I_K in guinea pig ventricular myocytes (Walsh and Kass, 1991). Similar effects were also observed after activation of protein kinase C with the phorbol ester phorbol 12,13-dibutyrate (PDB), suggesting that this α-adrenergic effect might be mediated via the inositol triphosphate/diacylglycerol/PKC pathway (Walsh and Kass, 1988; Walsh and Kass, 1991). PKC regulates I_K in a different manner to PKA (see above), however, as application of PDB does not markedly shift the voltage-dependence of the activation curve but increases its slope. It is unclear whether these changes are due to effects on I_{Ks} or I_{Kr}, as this study did not differentiate between the two components of the delayed rectifier. However, the fact that the effects of these compounds on I_K were apparent after two second test pulses to very positive potentials (+60 to +100mV) argues for an action on I_{Ks}.

There have been varying reports on the effects of Ca^{++} on I_{Ks} in cardiac tissue. Tohse (1990) reported that I_{Ks} is increased when intracellular [Ca^{++}] is raised above 10^{-9}M

in guinea-pig ventricular cells, but that there is no shift in the voltage-dependence of the activation curve. In contrast, a positive shift in the voltage-dependence of activation of I_{Ks} was observed by Sanguinetti and Jurkiewicz (1990a) when Ca^{++} was removed from the extracellular bathing medium or when lanthanum (La^{+++}) (Sanguinetti and Jurkiewicz, 1990a), at concentrations which block I_{Kr} and Ca^{++} currents, was added to the external solution. Nisoldipine, at concentrations which block L-type Ca^{++} currents, has no effect on I_{Ks} in guinea-pig ventricular myocytes, and cadmium (Cd^{++}) causes only very small increases in the magnitude of I_{Ks} at positive potentials (+50mV) (Daleau et al., 1998). Finally, decreasing $[K^+]_o$ to 0mM increases the magnitude of I_{Ks}, as would be expected for an increase in driving force, and this effect occurs even in the absence of Ca^{++} in the external solution (Sanguinetti and Jurkiewicz, 1992). These results suggest that Ca^{++} may modulate the activity of I_{Ks} but is not required for channel activation.

Pharmacological Modulation of I_{Ks}

There has been an extensive search for selective blockers of I_{Ks}. The majority of these agents are classified as class III antiarrhythmics since their primary action is to prolong the action potential duration and increase cellular refractoriness. I_{Ks} is insensitive to agents which block I_{Kr} such as E-4031 (Sanguinetti and Jurkiewicz, 1990b), d-sotalol (Sanguinetti and Jurkiewicz, 1990b), and dofetilide (Jurkiewicz and Sanguinetti, 1993). In contrast, azimilide dihydrochloride (NE-10064) is a potent blocker of I_{Ks} in guinea-pig ventricular myocytes and sinoatrial nodal cells with an IC_{50} of 1.9μM and 700nM, respectively (Busch et al., 1994a; Davies et al., 1996b). This compound, however, was recently shown to be non-selective as it can also inhibit I_{Kr}, I_{Ca}, and I_{Na} in both canine and guinea-pig ventricle (Fermini et al., 1995; Yao and Tseng, 1997). Clofilium and triamterene, at concentrations of 10-100μM, inhibit I_{Ks} in guinea pig ventricle, although these compounds also act non-selectively (Li et al., 1996; Daleau and Turgeon, 1994). Recently, two compounds have been identified which appear to act selectively on I_{Ks}. Chromanol 293B, a chromanol derivative, is highly selective for I_{Ks} over I_{Kr} in guinea pig cardiac myocytes with an IC_{50} of 2.1μM (Busch et al., 1996). Furthermore, propenamide

(L735,821), a 1,4 benzodiazepine, is the most potent inhibitor of I_{Ks} described to date with an IC_{50} of 6nM in guinea pig ventricle that is 250 fold more selective than block of I_{Kr} (Salata et al., 1996b). Detailed experiments which investigate the effects of these compounds on other ionic currents are, however, lacking.

Many other non-class III antiarrhythmic and non-antiarrhythmic agents have been shown to act on I_{Ks}, although the majority of these agents are not selective for this channel. The class I antiarrhythmic agents cibenzoline and amiodarone inhibit both I_{Ks} and I_{Kr} in guinea-pig ventricular myocytes, whereas other class I antiarrhythmics such as flecainide (which can block I_{Kr}) and mexiletine have no effect on this current (Balser et al., 1991; Wang et al., 1996). Quinidine decreases the amplitude of I_{Ks} in guinea-pig ventricle with a K_d of 10 to 50μM (Balser et al., 1991; Roden et al., 1988), and propafenone, another widely used class I antiarrythmic, inhibits I_{Ks} in a use-dependent manner, although this compound is more selective for I_{Kr} (Delpón et al., 1995). The general anaesthetics propofol and thiopentone block I_{Ks} but not I_{Kr} in guinea-pig ventricular myocytes (Heath and Terrar, 1996a), whereas the piperidine-containing histamine H_1-receptor antagonist terfenadine, which has previously been shown to cause torsade de pointes in the clinic (Feroze et al., 1996), blocks I_{Ks} in guinea pig ventricular myocytes by approximately 60% at a dose of 10μM. This compound is much more selective for I_{Kr}, however, with an IC_{50} of 50nM (Salata et al., 1995). Chlorpheniramine and pyrilamine, two nonpiperidine-containing histamine H_1-receptor antagonists, also weakly block I_{Ks} (20% at 10μM) and I_{Kr} (IC_{50} 1.1-1.6μM) (Salata et al., 1995), as does cisapride, a gastrointestinal prokinetic agent (Drolet et al., 1998). The diuretic agent indapamide inhibits I_{Ks} but not I_{Kr} in guinea pig ventricular myocytes, with an IC_{50} of 196μM at +10mV (Turgeon et al., 1994). *In vivo* experiments on anaesthetized dogs, however, show that indapamide does not effect action potential duration or effective refractory period in the right or left ventricle, although coinfusion of this compound with dl-sotalol, an I_{Kr} blocker, alters the normal effects of dl-sotalol of prolonging action potential duration and effective refractory period. Indapamide also lowers the threshold for dl-sotalol induced early after depolarizations in dog ventricle, suggesting that

inhibition of I_{Ks} by indapamide can modulate the actions of I_{Kr} blockers (Fiset et al., 1998).

Properties of the Delayed Rectifier K^+ Current in Bullfrog Atrial Myocytes

The action potential of bullfrog atrial myocytes is characterized by a very long plateau phase and a slow rate of repolarization. The complement of ionic currents underlying the action potential is quite simple relative to mammalian heart, and these currents have been well characterized. It includes a large TTX-sensitive Na^+ current (I_{Na}), a calcium current (I_{Ca}), and a small persistent inward current composed of a background calcium current. In addition, these cells express a slow time- and voltage-dependent outward potassium current (I_K) which initiates repolarization, and a time-independent inwardly rectifying potassium current (I_{K1}) responsible for the final third of repolarization (Hume and Giles, 1983; Rasmusson et al., 1990a). This literature review will focus on what is known about the biophysical and pharmacological characteristics of one of these ionic currents, I_K.

Early Studies on Bullfrog Cardiac Myocytes

Early studies of the delayed rectifier in bullfrog heart used the double sucrose gap technique to measure I_K in atrial muscle strips (Brown and Noble, 1969; Ojeda and Rougier, 1974; Brown et al., 1976a; Brown et al., 1976b). This current activated slowly in response to depolarizing voltage steps in the plateau range of the frog atrial action potential, appeared to have an inwardly rectifying current-voltage relationship, and was similar to the delayed rectifier described by Noble and Tsien (1969) in sheep Purkinje fibers. An envelope of tails test suggested the presence of two components of current underlying the bullfrog delayed rectifier with deactivation time constants of 500msec and 5.87 sec at -90mV, neither of which was very K^+ selective (Brown and Noble, 1969). Subsequent experiments separated these components into i_{xfast} and i_{xslow} by virtue of their deactivation kinetics, of which i_{xslow} behaved much like a voltage- and time-dependent Hodgkin-Huxley type current and was believed to contribute to action potential

repolarization (Brown et al., 1976a; Brown et al., 1976b). In contrast, the activation kinetics of i_{xfast} were very slow, leading Brown et al. (1976b) to suggest that this component of current probably plays no role in repolarization.

Biophysical Properties of I_K in Single Cell Preparations

Measurements of the delayed rectifier in single atrial myocytes have revealed some qualitative but not quantitative similarities with the studies described above. Direct comparisons are complicated by the substantial K^+ accumulation that has been shown to occur in multicellular preparations (Brown et al., 1976a; Brown et al., 1976b; Cohen and Kline, 1982). In isolated myocytes two groups have clearly shown that the delayed rectifier is composed of one population of channels in bullfrog atria, suggesting that one or both of the two components of current identified in the multicellular studies were artifacts of the experimental preparation.

Voltage clamp recordings from single bullfrog atrial myocytes have identified large outward currents that reverse at a membrane potential close to that expected by the Nernst equation for a K^+ selective channel. In response to increases in extracellular K^+ concentration the reversal potential for this current changes by 52mV/10 fold change in extracellular K^+ concentration, suggesting that it is K^+ selective. I_K activates in response to depolarizing voltage steps to potentials more positive than -40mV, with full activation occurring at approximately +30mV and a half-maximal activation and slope factor of -15mV and 11.4mV (respectively). This current does not inactivate, reaches steady state only after very long voltage steps (tens of seconds), and its steady state current-voltage relationship is relatively linear. The time course of activation and deactivation of I_K is approximately 1-2 seconds at 0 to +50mV, and 500msec at -90mV (respectively) (Hume et al., 1986; Simmons et al., 1986).

Unlike I_K in guinea pig, canine, rabbit, and human cardiac tissue (as described in the previous section), Hume et al. (1986) and Simmons et al. (1986) reported that I_K in bullfrog consists of only a single component of current, based on an envelope of tails test. The activation of I_K during depolarization exhibits a sigmoid time course of onset and the

deactivating tail currents can be best fit with a single exponential function at potentials negative to -30mV but a biexponential function at more positive potentials (Simmons et al., 1986). Taken together these findings can best be explained by I_K being composed of a single conductance of the Hodgkin-Huxley type in which the gating variable (n) is raised to the power of 2, rather than two distinct conductances.

Attempts to identify the single channel events underlying activation of I_K in bullfrog heart have been difficult. Hume et al. (1986) estimated a very low density of channels in the membrane of bullfrog atrial myocytes (~0.1-0.3 channels/μm^2), perhaps explaining the inability to obtain single channel recordings. Duchatelle-Gourdon and Hartzell (1990), however, took advantage of the positive regulation of I_K by β-adrenergic agonists and were able to record single channel events after intracellular dialysis of bullfrog atrial cells with 30μM cAMP. This approach identified a 20pS channel (at potentials between -20 and -80mV) that was present at a very low frequency (2 out of 40 patches) under control conditions but was observed in 21 of 36 patches after activation with cAMP. The current showed a weakly inwardly rectifying current-voltage relationship, had a mean time-to-first opening of 603msec and an open probability of approximately 0.05. Ensemble average currents closely matched the whole cell macroscopic current, suggesting that the characteristics of this channel mimic I_K.

Modulation of Bullfrog I_K

Similar to I_{Ks} in mammalian tissue, the amplitude of I_K in bullfrog atrial myocytes is enhanced in a concentration-dependent manner by external application of isoprenaline (EC_{50}= 2.3μM; Duchatelle-Gourdon et al., 1989). This increase in I_K can be blocked by the β-adrenergic receptor antagonist propanolol but not by $CdCl_2$, and can be mimicked by external perfusion with forskolin or internal perfusion with cAMP. Isoprenaline speeds up the activation of I_K at potentials positive to -40mV and slows down the deactivation kinetics, in addition to shifting the steady state activation curve in the negative direction (Giles et al., 1989; Duchatelle-Gourdon et al., 1989). Single-channel recordings from cAMP-dialysed myocytes suggest that β-adrenergic stimulation increases I_K by enhancing

open probability, rather than by increasing the unitary conductance of the channel (Duchatelle-Gourdon and Hartzell, 1990).

Contrasting effects on I_K are observed with Mg^{++}. Intracellular dialysis with Mg^{++} decreases the amplitude of I_K in a dose-dependent fashion (IC_{50} 600μM; (Duchatelle-Gourdon et al., 1989; Duchatelle-Gourdon et al., 1991), and high concentrations of Mg^{++} (1mM) appear to result in more rapid run-down of I_K after patch rupture. Furthermore, Mg^{++} slows down the rate of activation at positive potentials (+40mV) but does not effect the time course of deactivation (at -50mV) or voltage-dependence of activation. Thus, Mg^{++} is an important regulator of I_K and physiological changes in the intracellular level of this cation likely influence channel activity.

Acetylcholine (10^{-6} to 10^{-8}M) produces no effect on I_K in bullfrog atrial fibers (Giles and Noble, 1976; Garnier et al., 1978), contrary to the decrease in I_{Ks} observed in guinea-pig sinoatrial cells following cholinergic stimulation (Freeman and Kass, 1995). Furthermore, $LaCl_3$ (10μM) and $CdCl_2$ (100μM), two calcium channel blockers, and PN202-791, a dihydropyridine Ca^{++} channel agonist, are all without effect on I_K, suggesting that changes in intracellular calcium are not responsible for the time-dependence of activation of I_K (Giles et al., 1989; Duchatelle-Gourdon et al., 1989; Hume et al., 1986).

Summary

I_K in bullfrog atrial myocytes is composed of a single conductance, unlike in many mammalian tissues where two components of the delayed rectifier have been reported. The biophysical and pharmacological properties of bullfrog I_K reveal that this current closely resembles I_{Ks} in mammalian tissue, and suggest that the bullfrog heart can be used to advantage for studies of the biophysical and pharmacological characteristics of I_{Ks}. To avoid possible misunderstandings with previous reports on the delayed rectifier in bullfrog cardiac tissue, this current will be referred to as I_K in this dissertation, but in all instances this implies a single component of current closely resembling the previously described I_{Ks}.

Molecular Structure Underlying I_{Ks}

The kinetics of I_{Ks} strongly resemble those of a K^+ current that was first cloned from rat kidney (Takumi et al., 1988), and has since been isolated from numerous other tissues (Folander et al., 1990; Honoré et al., 1991; Murai et al., 1989). This K^+ current, when its RNA is expressed in *Xenopus* oocytes, slowly activates over a time course of many seconds, does not inactivate, and is highly voltage dependent (Takumi et al., 1988; Murai et al., 1989; Folander et al., 1990; Honoré et al., 1991). The transmembrane topology and size of the protein encoding this K^+ channel, however, is different from all other voltage-gated K^+ channels described thus far (see review by Kaczmarek, 1991), in that it is only 129 (mouse, human) or 130 (rat) amino acids long, and has only one putative transmembrane domain (Takumi et al., 1988; Murai et al., 1989; Folander et al., 1990; Honoré et al., 1991). This channel has therefore been called a minimal K channel, or minK.

Distribution of minK

Boyle et al. (1987a) were the first to observe a slowly-activating voltage-dependent outward current (minK-like) in *Xenopus* oocytes following injection of polyadenylated RNA isolated from estrogen-treated rat uterus. Subsequently, minK has been detected in numerous tissues by immunostaining, Northern Blot analysis, *in situ* hybridization, and cloning experiments. These include neonatal rat, neonatal mouse, guinea pig, rabbit and human heart (Folander et al., 1990; Honoré et al., 1991; Varnum et al., 1993; Swanson et al., 1991; Salata et al., 1996a), human T-lymphocytes (Attali et al., 1992), as well as rat kidney, duodenum, stomach, pancreas, inner ear, corneal epithelial cells, retinal large ganglion neurons, and submandibular gland (Takumi et al., 1988; Tsukahara et al., 1995; Sakagami et al., 1991). In the heart, as previously mentioned, minK is thought to underlie the slow component of the delayed rectifier current, whereas in the inner ear it has been suggested that minK may be involved in the transport of K^+

into the fluid medium bathing the hair cell bundles (Marcus and Shen, 1994; Vetter et al., 1996). A putative role for uterine minK in the induction of labour has also been suggested (Boyle et al., 1987b). The functional role of minK in each of the other tissues is not entirely clear.

Structure of MinK

Takumi et al. (1988) were the first to clone the minK gene from rat kidney using expression cloning. Injection of RNA from this tissue into *Xenopus* oocytes resulted in a slowly activating outward current that did not inactivate even after depolarizing voltage pulses for 90 seconds. Sequence analysis demonstrated that this protein consists of 130 amino acids with a total molecular weight of approximately 15 kD. Hydropathy analysis identified a hydrophobic segment 23 amino acids long, which may comprise a single transmembrane domain, surrounded by charged amino acid residues. The amino-terminus of this protein is most likely located at the extracellular surface of the plasma membrane as there are two potential N-glycosylation sites conforming to the Asn-X-Ser/Thr sequence in this region. Epitope-tagging experiments confirm this extracellular location for the amino-terminus (Blumenthal and Kaczmarek, 1994). More detailed results have been obtained using circular dichroism spectroscopy, binding experiments, and fluorescence measurements of 7-nitrobenz-2-oxa-1,3-diazol-4-yl (NBD)-labelled peptides. These experiments suggest that the putative transmembrane region and the amino-terminus of minK are embedded in the lipid membrane, whereas the segment linking these two regions is exposed to the extracellular surface (Ben-Efraim et al., 1994). There is a single cysteine residue at the carboxy-terminus (position 107) of rat kidney minK which Takumi et al. (1988) proposed might be involved in the formation of dimeric or oligomeric structures. The membrane-impermeable methanethiosulfonate derivate MTSES, which covalently binds to cysteine residues, does not alter the activity of minK channels expressed in *Xenopus* oocytes, suggesting that the carboxy-terminus is located on the intracellular side of the membrane (Wang et al., 1996).

K^+ channels resembling rat kidney minK have subsequently been cloned from neonatal rat (Folander et al., 1990), neonatal mouse (Honoré et al., 1991), rabbit (Salata et al., 1996a), and guinea pig (Varnum et al., 1993) heart, rat diethylstilbestrous-primed uterus (Folander et al., 1990; Pragnell et al., 1990), human T-lymphocytes (Attali et al., 1992), and human genomic DNA (Murai et al., 1989). The clones identified from the rat heart and uterus are identical to that isolated from rat kidney, consisting of 130 amino acids and having a hydrophobic region between amino acids 45 and 67. Antisense oligonucleotides directed against the sequence of rat minK blocked the expression of the slowly activating outward K^+ current in *Xenopus* oocytes, suggesting that this gene is critical for the induction of this K^+ current (Folander et al., 1990). Rabbit minK is also 130 amino acids long but differs from the rat clone in that it contains only one N-glycosylation site at the amino-terminus, has two cysteine residues at the carboxy terminus, and shares only 69% homology at the amino acid level (Salata et al., 1996a). The human, mouse and guinea pig proteins, however, are missing one amino acid between residues 29 and 30 (as compared to the rat clone) and guinea pig minK lacks another 4 amino acids at its carboxy-terminus. Neonatal mouse minK is 92.3% homologous with the rat kidney clone (Honoré et al., 1991), whereas the human minK gene bears 76% amino acid homology over the entire sequence, and 96% homology over the central 50 amino acids (including the transmembrane domain and the following carboxy-terminal region). All the minK clones, when expressed in *Xenopus* oocytes, express K^+ currents resembling the rat minK clone (Honoré et al., 1991; Murai et al., 1989), demonstrating that this unique K^+ channel is highly conserved among different species and tissues. Specific differences have, however, been noted with respect to the activation and deactivation kinetics, voltage-dependence, and pharmacological sensitivity of rat, mouse, and human minK, suggesting that the proteins do not behave in an identical manner (Hice et al., 1994). Understanding the differences between the various clones, which vary in their homology to each other, may provide a basis on which to target specific regions of the gene and to analyse further the structure-function relationships of this channel.

Gene Organization of MinK

The human minK gene has been mapped to chromosome 21, position 21q22.1-q22.2 (Malo et al., 1995). The rat and mouse minK gene consists of 2 exons separated by an intron of approximately 10kb. Exon 2 encodes for the entire minK protein-coding sequence, as well as the 3' untranslated region, whereas initiation of the minK mRNA is at two different upstream exons (1a or 1b) corresponding to alternative 5' untranslated sequences (Lesage et al., 1992; Iwai et al., 1990). Two different variants of minK mRNA, alternatively spliced at the 5' end, can therefore be produced. In addition, Northern Blot analysis has revealed the presence of at least two different minK mRNA transcripts in neonatal mouse heart, with a size of approximately 0.9 and 3.4kb. These transcripts differ in their 3' untranslated sequences and are generated from at least 3 different polyadenylation sites (Lesage et al., 1992). Furthermore, multiple transcription start sites have been identified in both the rat and mouse DNA (Lesage et al., 1992; Iwai et al., 1990). Thus, although there is only a single gene encoding minK, there is the possibility of multiple mRNA variants due to alternative splicing at the 5' and 3' ends, and multiple transcription initiation sites.

Pharmacological and Hormonal Regulation of MinK

Honoré et al. (1991) were one of the first groups to investigate specific regulation of minK expressed in *Xenopus* oocytes by pharmacological agents. Clofilium, a class III antiarrhythmic, at concentrations ranging from 10 to 100μM, inhibited neonatal mouse minK whereas other class III antiarrhythmics (sotalol, amiodarone, bretylium tosylate, or tedisamil, at a concentration of 300μM) had no effect. Similar to what has been reported previously by Hausdorff et al. (1991), TEA and barium were both able to block minK, whereas other K^+ channel blockers such as 4-aminopyridine were not. Furthermore, minK was insensitive to dendrotoxin, apamin, β-bungarotoxin, charybdotoxin, quinine and quinidine. Quinidine has, however, recently been reported to block human minK expressed in *Xenopus* oocytes with a Kd of 585μM at +20mV (Yao et al., 1998). It is

possible that the concentrations of quinidine used by Honoré et al. (300μM) were not sufficient to significantly inhibit minK.

The amplitude of minK is enhanced by injection of *Xenopus* oocytes with calcium-calmodulin dependent protein kinase (CaMK) or when the calcium ionophore A23187 is present in the bathing solution. Both of these increases in amplitude are diminished by W7, a calmodulin antagonist (Honoré et al., 1991). Attempts to stimulate the cyclic AMP or cyclic GMP signalling pathways with membrane permeable analogues are without effect on minK, although activators of diacylglycerol (DAG) and protein kinase C (PKC) can significantly block this current. This modulation by PKC and calmodulin is not surprising considering there is a consensus sequence for both CaM-protein kinase II and PKC phosphorylation on mouse heart minK (Honoré et al., 1991). This inhibition by PKC has since been localized to an action at serine 103 in rat kidney minK, as substitution of this residue with alanine abolishes the effect of this kinase on minK (Busch et al., 1992). It is interesting to note that PKC actually enhances guinea pig minK expressed in *Xenopus* oocytes (similar to its effects on I_{Ks} in guinea pig ventricular myocytes; Walsh and Kass, 1991), which may be due to sequence variations between the guinea pig and the rat and mouse clones at cytoplasmic residue 102. Guinea pigs have an asparagine at this residue, whereas rat and mice have a serine. Point mutation of asparagine 102 to serine in the guinea pig minK clone reverses the sensitivity of this current to PKC, providing support for this hypothesis (Varnum et al., 1993; Je Zhang et al., 1994).

The minK protein lacks any consensus phosphorylation sites for protein kinase A (PKA), although Blumenthal and Kaczmarek (1992) have reported that bath application of 8-bromo-cAMP, a membrane permeable analogue of cAMP, increases the amplitude of rat minK expressed in *Xenopus* oocytes. This effect can be mimicked by bath application of forskolin, an activator of adenylate cyclase, whereas progesterone, which transiently decreases intracellular cAMP levels in *Xenopus* oocytes, decreases the amplitude of minK. The modulation of minK by cAMP is in contradiction to the results of Honoré et al. (1991), in which they found no effect on mouse minK after incubation

with either 8-bromo-cAMP or forskolin. The concentrations of 8-bromo-cAMP utilized were the same in both studies, however Honoré et al. did not report the length of time they allowed for incubation. It is therefore difficult to contrast these two studies, in part because they used clones from different species. An enhancement of minK by cAMP, however, is consistent with the effects of this compound on I_{Ks} in guinea pig ventricular myocytes (Sanguinetti et al., 1991; Walsh et al., 1989; Heath and Terrar, 1996a; Walsh and Kass, 1991) and I_K in bullfrog atria (Giles et al., 1989; Duchatelle-Gourdon et al., 1989).

The activity of rat uterine minK is strongly dependent on estrogen levels. Injection of RNA from rats pre-treated with estrogen for 3 days into *Xenopus* oocytes elicits slowly activating minK-like currents (Boyle et al., 1987a; Boyle et al., 1987b). In addition, Northern Blot analysis reveals high levels of minK mRNA in rat uterus in animals that have been pretreated with estrogen, but not in untreated animals. This increase in mRNA expression can occur after only a single estrogen injection 3 to 6 hours before sacrificing the animal and collecting tissue, suggesting that induction of expression can occur very rapidly. MinK 'up-regulation' in rat uterus occurs in the luminal and glandular epithelium of the endometrium, as well as in the myometrium, as revealed by *in situ* hybridization (Pragnell et al., 1990).

The effect of nitric oxide on minK has been investigated by superfusion of *Xenopus* oocytes injected with minK cRNA with the nitroso-donor S-nitroso-cysteine (SNOC; Raber et al., 1995). This compound increases minK current amplitude, an effect which is not dependent on activation of cyclic GMP as the cyclic GMP kinase inhibitor H8, and the guanylate cyclase inhibitor LY-83,583, do not block the enhancement of minK. Furthermore, application of di-butyryl-cyclic GMP, an activator of cyclic GMP dependent kinase, is without effect of minK, in agreement with results described previously by Hausdorff et al. (1991). Mutation of residues previously shown to be involved in phosphorylation and oxidation of minK also does not alter the effect of SNOC on current amplitude; however staurosporine, a nonspecific kinase inhibitor, strongly inhibits minK and prevents the SNOC-mediated increase. Therefore, the

mechanism by which nitric oxide regulates minK is unclear, but likely occurs via a staurosporine-sensitive kinase.

MinK expressed in *Xenopus* oocytes has also been shown to be sensitive to a number of other factors. MinK activation kinetics are enhanced by increases in temperature and intracellular calcium (Busch and Lang, 1993), but its amplitude is diminished by acidification (Yamane et al., 1993). Two general anaesthetics, propofol and thiopentone, which selectively act on I_{Ks} and not I_{Kr} in guinea-pig myocytes (Heath and Terrar, 1996a), have also been shown to block minK expressed in *Xenopus* oocytes with an IC_{50} of 250 and 56μM, respectively (Heath and Terrar, 1997). The class III antiarrhythmic agent azimilide dihydrochloride (NE-10064), at concentrations ranging from 0.3 to 10 uM, potently inhibits rat kidney (Busch et al., 1994a) and rabbit heart (Salata et al., 1996a) minK expressed in *Xenopus* oocytes. This drug was also able to block the slowly activating potassium current at similar concentrations in guinea pig and rabbit ventricular myocytes. (Busch et al., 1994a; Salata et al., 1996a).

Developmental Regulation of MinK

In addition to the widespread tissue distribution of minK, there also appears to be developmental changes in the distribution of this protein, at least in rat and mouse tissues. Northern Blot analysis, in conjunction with functional expression of minK in *Xenopus* oocytes, demonstrated a high level of minK in neonatal mouse heart. This level decreases rapidly in adult animals (Honoré et al., 1991). Felipe et al. (1994) confirmed these results and demonstrated that minK mRNA levels increase gradually between gestational day 15 and 19, sharply rise between gestational day 19 and neonatal day 2, and then decline to undetectable levels in the adult. In rat heart, low levels of minK can be found in neonatal animals, but this signal is virtually undetectable as soon as one week after birth (Honoré et al., 1991). In contrast, distribution of minK RNA in rat and mouse kidney follows an opposite pattern, with high levels of the protein detectable in adult animals which decline to much lower levels in neonate and late-gestational animals (Honoré et al., 1991; Felipe et al., 1994). These changes in minK expression in mouse heart correlate well with the

developmental changes in I_{Ks} current density that occurs in isolated mouse cardiac myocytes (Davies et al., 1996a; Wang et al., 1996b).

Activation and Deactivation of minK

The activation kinetics of minK are strongly dependent on the level of minK channel protein present in *Xenopus* oocytes. Depolarizing shifts in the half-maximal activation of minK have been reported by Cui et al. (1994) in response to increasing concentrations of injected RNA ($V_{1/2}$ of -12.8mV at 0.04pg/nl mRNA, +13.9mV at 10pg/nl mRNA). Furthermore, enhancing the level of minK protein expression by either prolonging incubation time or increasing the amount of RNA injected into a *Xenopus* oocyte, increases the delay in channel activation (ie. activation becomes more sigmoidal) and slows the time course of activation (Blumenthal and Kaczmarek, 1994; Cui et al., 1994). These changes in activation kinetics occur in response to increasing protein synthesis even after minK current amplitude has reached a saturated level (Blumenthal and Kaczmarek, 1994), and suggest that the function of the channel protein is strongly dependent on the interaction of individual minK proteins.

The activation and deactivation kinetics of rat minK expressed in *Xenopus* oocytes have been further investigated by chemical cross-linking experiments (Varnum et al., 1995). Bath application of the chemical cross-linker DTSSP (which acts extracellularly and links two amino groups) increases the rate of activation of minK and shifts the half point of activation to more hyperpolarized potentials, with no effect on the deactivation kinetics of the tail currents. These effects on activation can be partially reversed by addition of the reducing agent DTT to break the "cross-links". These results led the authors to propose a model for activation whereby individual minK monomers aggregate to form a functional potassium channel. This subunit aggregation in the membrane may account for the slow activation kinetics of minK. The authors propose that deactivation however, requires only one subunit to dissociate from the aggregated complex, thereby accounting for the lack of effect of DTSSP on the tail currents (Varnum et al., 1995).

Subunit Stoichiometry

The exact number of individual minK subunits that aggregate to form a functional channel is still under debate. Wang and Goldstein (1995) proposed a model whereby a functional channel in *Xenopus* oocytes is made up of two minK monomers. This conclusion was reached as a result of experiments in which minK was co-expressed in *Xenopus* oocytes with a mutant of minK (D77N). D77N induces no current when expressed on its own, but co-injection of the wild-type and mutant proteins at a 1:1 ratio results in a current approximately one quarter the size of the wild-type current, a decrease which is not due to a decline in the level of wild-type minK protein expression on the oocyte membrane. This depressed current is identical to wild-type channels with respect to its ion selectivity, sensitivity to block by barium, TEA, cesium, and azimilide, and kinetics of activation and deactivation, suggesting that it is made up of only wild-type protein. The most likely interpretation of these results is that incorporation of D77N into minK channel complexes inhibits their function in a dominant lethal manner. Thus, only channel-complexes which form by assembly of pure wild-type minK monomers can produce a functional channel and pass current. Wang and Goldstein (1995) took advantage of this finding by co-expressing D77N and wild-type minK in *Xenopus* oocytes at varying ratios and then using binomial distribution analysis to determine the stoichiometry with which minK subunits coassemble. These experiments yielded a value of two minK monomers per minK channel, a value that was independent of test voltage.

Experiments using a similar approach to that of Wang and Goldstein (1995) were performed by Tzounopoulos et al. (1995a), although an entirely different outcome was reached. Co-expression of wild-type minK with a different mutant of minK, S69A, resulted in a smaller current compared to the wild type current. Increasing the concentration of S69A decreased the wild-type current in a concentration-dependent manner, suggesting that S69A has a dominant negative effect on wild-type minK and that these two proteins coassemble. Binomial distribution analysis following injection of different ratios of S69A and wild-type minK was again used to characterize the subunit stoichiometry of minK. This group reported that at -20mV, a potential at which S69A

activates no current when expressed on its own, 14 minK monomers must combine to form a functional channel. Tzounopoulos et al. (1995a) proposed a model by which 15 monomers first form as five individual trimers, which then assemble in radial symmetry with one monomer from each trimer lining the pore region.

These two sets of experimental data clearly provide two radically different models by which minK monomers assemble. Both experiments assume that assembly of minK subunits occurs completely randomly and that there is no preferential association of different subunits, an assumption which has not been directly tested. These experiments also assume identical levels of synthesis of both wild type and mutant proteins and presuppose that there is no preferred expression of either protein on the surface (tests by Wang and Goldstein (1995), measuring levels of epitope-tagged protein on the surface of the oocyte following injection of varying ratios of D77N and wild-type minK, has verified this assumption). In addition, these experiments presume that only pure wild-type channels can pass current, an assumption that can only be verified by single channel analysis. Finally, these experiments do not consider the possibility of an additional non-minK subunit. Thus, direct comparison of the findings of Wang and Goldstein (1995) and Tzounopoulos et al. (1995a) is difficult until it is clear that all of these assumptions have been met, and determination of the exact number of minK subunits involved in channel formation must await further studies.

Is minK a channel protein or a channel regulator?

The transmembrane topology and size of minK is significantly different from all other voltage-gated K^+ channels described previously in that it is only 129 (mouse, human) or 130 (rat) amino acids in length and has only one putative transmembrane domain (Takumi et al., 1988; Murai et al., 1989; Folander et al., 1990; Honoré et al., 1991). Attempts to express minK in a system other than *Xenopus* oocytes (CHO fibroblast cells, C2C12 skeletal muscle cells, and Jurkat T lymphocyte cells) have been unsuccessful (Lesage et al., 1993), leading to speculation concerning whether minK is itself a channel-forming protein or a regulator of proteins found only in *Xenopus* oocytes.

These findings were complicated by one report demonstrating expression of minK in a human embryonic kidney cell line (HEK293; Freeman and Kass, 1993), although these results have proven difficult to replicate.

Evidence for Regulation of Proteins Endogenous to Xenopus Oocytes

There is abundant evidence supporting a model in which minK forms a functional channel by combining with an endogenous protein in *Xenopus* oocytes. Some of the first clues came from experiments in which the amplitude of the minK current in *Xenopus* oocytes was measured relative to the amount of minK protein expression. Attali et al. (1993) noted that the magnitude of minK current increased in a concentration-dependent manner with injection of minK cRNA at concentrations ranging from 0.03 to 10ng/μl. At concentrations of 1 to 10ng/μl, however, minK current amplitude reached a plateau and then actually decreased in size at levels >10ng/μl. This saturation of the current amplitude is not due to an inability of the oocyte to synthesize additional channel protein, as epitope-tagging experiments revealed that minK protein level increases in a concentration-dependent manner with injections of 100pg to 50ng minK cRNA, despite the current amplitude saturating at a concentration of 1ng (Blumenthal and Kaczmarek, 1994). These data suggest that the minK current is generated by interaction of minK with an oocyte protein that is present in limiting concentrations.

Additional clues that minK requires another protein to form a functional channel comes from attempts to form single channels in planar lipid bilayers. Ben-Efraim et al. (1993, 1994) reported that two truncated mutants of minK, a synthetic peptide encoding the transmembrane region of minK plus 4 or 5 amino acids on either side (residues 41-72) and a 63 amino acid peptide containing residues 1-9 linked to residues 41-94, can induce single channels in planar lipid membranes. Several conductance levels were reported which the authors suggested was due to the formation of aggregates of individual minK monomers within the membrane which can associate and dissociate at different rates. These channels, however, were not K^+ selective and could not distinguish between K^+ or

Na^+, supporting the idea that in order for minK to function as a selective K^+ channel it needs to associate with other factors.

Injection of minK cRNA into *Xenopus* oocytes can enhance expression of an endogenous DIDS-sensitive chloride current (Attali et al., 1993). This chloride current induced by minK is similar to the hyperpolarization-activated chloride current elicited after expression of a variety of small proteins in *Xenopus* oocytes, including the 72 amino acid protein phospholemman found in cardiac sarcolemma (Moorman et al., 1992; Shimbo et al., 1995), the 67 amino acid protein Mat-8 found in human breast tumors (Morrison et al., 1995), and two small (<100 amino acids) viral proteins, NB from influenza B and a synthetic derivative of the influenza A virus M_2 protein, SYN-C (Shimbo et al., 1995). Attali et al. (1995) also reported that injection of the 87 amino acid channel-inducing factor (CHIF) cloned from rat colon in *Xenopus* oocytes, results in expression of a minK-like slowly activating outward current. These results suggest that minK may be a member of a family of small proteins which can activate/regulate proteins endogenous to *Xenopus* oocytes.

Subsequent experiments have investigated the specific region of minK that interacts with the putative endogenous *Xenopus* oocyte proteins. Injection of a small peptide containing only minK residues 68-94 into *Xenopus* oocytes elicits a slowly activating voltage-dependent current with similar biophysical and pharmacological properties to the current produced by wild-type minK. The magnitude of the expressed current is dependent on the concentration of peptide injected and reaches a saturating concentration above 100μM. In contrast, injection of another small protein containing residues 10-43 does not elicit any current, although extracellular superfusion with this peptide elicited a hyperpolarization-activated Cl^- current (as above). This same Cl^- current is activated by external application of an even smaller peptide containing amino acids 31-43, suggesting that this short region is sufficient for channel activation. Thus, it appears that the carboxy-terminal of minK is adequate for activation of a slowly activating K^+ current in *Xenopus* oocytes, whereas the amino-terminus is sufficient for Cl^- channel activation (Ben-Efraim et al., 1996).

Evidence that MinK forms part of a K^+ Channel Complex

Recent evidence, however, has led a different group of researchers to hypothesize that minK actually forms a K^+-selective channel rather than act as a channel regulator. Tzounopoulos et al. (1995b) reported that overexpression of a variety of structurally unrelated proteins in *Xenopus* oocytes, including a non-conducting Shaker-type K^+ channel, a non-conducting inward rectifer K^+ channel, a large amino acid transporter protein, and a dopamine D2 receptor, also increases expression of an endogenous hyperpolarization-activated chloride current, suggesting that regulation of this chloride channel may not be specific to minK and the group of small proteins described above.

Hausdorff et al. (1991) investigated the functional properties of a synthetic minK gene expressed in *Xenopus* oocytes, in order to better understand whether in fact minK encodes for an actual potassium channel or instead expresses a regulator of an endogenous membrane potassium transporter. They reported that barium, cesium and tetraethylammonium (TEA) all block the outward potassium current, although block by TEA is much more weakly voltage-dependent than the block by the other two cations (barium > cesium > TEA). These findings were interpreted to mean that TEA may block on the external surface of a putative pore region, whereas cesium and barium block deeper within the pore. The current induced by the synthetic minK clone is highly selective for potassium, with a selectivity sequence to monovalent cations of $K^+ > Rb^+ > NH_4^+ > Cs^+ >> Na^+, Li^+$. Single amino acid mutations in the putative transmembrane domain of this synthetic gene (changing phenylalanine at amino acid 55 to threonine) changed the relative permeability of the expressed minK current to these monovalent cations, increasing its permeability for NH_4^+ and Cs^+ (Goldstein and Miller, 1991). Thus, the relative selectivity of minK to the various cations, combined with the ability to alter this selectivity by site-specific mutations, suggests that minK currents are mediated by a K^+ channel and not a K^+ transporter (although these results still do not rule out the possibility of minK regulation of an endogenous K^+ channel).

A more complete analysis of the effects of point mutations in the minK gene on current expression has been performed by Takumi et al. (1991). It appears that the entire minK sequence is not essential for expressing minK current in *Xenopus* oocytes. Instead, a 63 amino acid sequence in the central domain (including the transmembrane region) is all that is necessary for eliciting a response, as determined by deletion mutants. Furthermore, substitution of a leucine at position 52 with an isoleucine markedly changes the activation kinetics of minK (activation occurs more rapidly), and substitutions in the cytoplasmic (C-terminal) region immediately following the transmembrane domain also influences channel activity. The functional importance of the membrane spanning region is further verified by a study showing that substitution of phenylalanine at positions 55 or 58 (but not positions 53, 54, 56, or 57) of rat kidney minK with cysteine also largely influences activation gating (Wilson et al., 1994). Combined, these results further support a role of minK as a K^+ channel, or at least a component of one, in oocyte membranes.

Another approach to evaluate whether the transmembrane domain of minK forms part of a K^+ channel pore was described by Wang et al. (1996). This group investigated binding of methanethiosulfonate-ethylsulfonate (MTSES, a membrane-impermeant compound that reacts covalently with exposed cysteine residues) and TEA (an open channel pore blocker) to minK following cysteine mutatagenesis of amino acids thought to be involved in pore formation. MTSES blocked minK current in a voltage-independent manner following replacement of residues 44, 45 or 47 with cysteine. Similar mutations at positions 45, 46, 47, 48, or 55 also decreased the affinity for TEA binding. This TEA binding presumably occurs within the K^+ channel pore, as intracellular injection of KCl inhibited block by extracellularly applied TEA. TEA and MTSES likely compete for binding at position 45, as pre-exposure to TEA of a minK clone containing a cysteine replacement at this position strongly decreased the rate of MTSES block. This change in the rate of block was dependent on concentration of TEA. In addition, prior MTSES modification of cysteine at positions 45 and 47 inhibited the affinity for TEA binding. These results suggest that the binding sites for TEA and MTSES overlap and are on the external surface of the K^+ channel pore, and that the N-terminal end of the transmembrane

domain (residues 44-47) of minK forms part of the K^+ conductance pathway. As with previous studies, these results do not, however, confirm that minK is the only contributor to the pore structure, and subsequent experiments by the same group of researchers (Tai et al., 1997) demonstrated that methanothiosulfonate-ethylammonium (MTSEA) and methanothiosulfonate-ethyltrimethyl ammonium (MTSET), two other positively charged methanothiosulfonate derivates which bind covalently to cysteine residues, can inhibit a cysteine-free mutant of minK and modify its selectivity to monovalent cations. This block is both state- and voltage-dependent, suggesting that minK, although forming part of the pore region, must also be associated with a cysteine-containing protein endogenous to *Xenopus* oocytes.

Coassembly of minK with KvLQT1

The debate surrounding the role of minK was partially settled with the recent publication of two papers demonstrating that minK coassembles with a newly discovered protein, KvLQT1 (Barhanin et al., 1996; Sanguinetti et al., 1996). The KvLQT1 protein was identified by positional cloning to the LQT1 locus and has been reported to be 676 (human; (Yang et al., 1997), 581 (human; Sanguinetti et al., 1996), or 604 (mouse; Barhanin et al., 1996) amino acids long with alternative splice variants at the 5' end (Yang et al., 1997; Lee et al., 1997). This protein has a similar structure to other K^+ channels in that it has 6 transmembrane domains and contains the 'signature' pore sequence for K^+ channels (Wang et al., 1996). Expression of KvLQT1 in either *Xenopus* oocytes (Barhanin et al., 1996; Sanguinetti et al., 1996; Yang et al., 1997; Shalaby et al., 1997), COS cells (Barhanin et al., 1996), or CHO cells (Sanguinetti et al., 1996) induces a current that rapidly activates but does not inwardly rectify at depolarized potentials. This current has a half-maximal activation and slope factor of -11.6mV and 12.6mV, respectively, when transfected into CHO cells (Sanguinetti et al., 1996) or -14.6mV and 13.9mV, respectively, when expressed in *Xenopus* oocytes (Shalaby et al., 1997). Thus, KvLQT1 current characteristics match neither I_{Ks} nor I_{Kr}. However, cotransfection of both KvLQT1 and minK into COS (Barhanin et al., 1996) or CHO cells (Sanguinetti et

al., 1996), both cell lines in which minK expresses no current on its own, induces a current that activates slowly with a sigmoid onset and with a much greater amplitude than KvLQT1 alone. This current has a half-point of activation and slope factor of +7.5mV and 16.5mV, respectively, in CHO cells (Sanguinetti et al., 1996) and +9.2mV and 13.7mV, respectively, in *Xenopus* oocytes (Shalaby et al., 1997). These kinetics strongly resemble those of native I_{Ks} (Sanguinetti and Jurkiewicz, 1994; Kass, 1995). Immunoprecipitation experiments confirm a physical interaction of KvLQT1 and minK in the membrane of Sf9 cells following infection of recombinant tagged KvLQT1 and minK baculoviruses, supporting the idea that the I_{Ks}-like current is formed by assembly of these two proteins (Barhanin et al., 1996). In addition, Northern blot analysis revealed that KvLQT1 mRNA is localized in human adrenal gland, thyroid gland, heart, pancreas, placenta, lung, kidney, stomach, colon, salivary gland, small intestine, trachea, prostate, fetal heart, fetal kidney, and fetal lung (Sanguinetti et al., 1996; Yang et al., 1997), following a similar distribution to minK mRNA. Finally, Sanguinetti et al. (1996) were able to partially clone KvLQT1 from a *Xenopus* oocyte cDNA library, confirming that this protein can be found endogenously in these cells. In combination, this data strongly suggests that minK and KvLQT1 coassemble to produce I_{Ks}.

Mechanism of Coassembly of minK with KvLQT1

The discovery of this protein with which minK coassembles answered a long-standing question in the field of minK research. Nonetheless, these results still did not clarify one of the arguments involving minK; does minK act simply by regulating the activity of KvLQT1, or do minK and KvLQT1 form a hetero-oligomer and both contribute to the pore forming region of the channel? Studies described previously provide strong evidence of an involvement of minK in forming at least part of the pore region. In addition, recent work investigating the mechanism of block of minK by Cd^{++} and Zn^{++} further supports such a role for minK. Tai and Goldstein (1998) demonstrated that minK is unaffected by extracellular or intracellular application of Cd^{++}or Zn^{++}. Serial mutation of individual amino acids in the putative transmembrane domain of minK,

however, identified two amino acids at residues 55 and 56 that were sensitive to blockade by external Cd^{++} and two others, 57 and 59, that were sensitive to internal Cd^{++}. External block by this reagent was voltage-dependent and the magnitude or rate of inhibition decreased when the concentration of K^+ and Rb^+ in the intracellular medium or TEA in the extracellular solution, respectively, was increased. These data suggest that there is a barrier to movement of Cd^{++} between residues 56 and 57, and that Cd^{++} likely blocks minK by blocking within the pore region. Additional evidence demonstrated that residue 57 is also sensitive to blockade by internal but not external Zn^{++}, and that this reagent also blocks minK by occluding the pore. In combination with results showing that mutation of residue 56 increases the permeability of minK to Na^+, this data supports the presence of a selectivity barrier for Cd^{++}, Zn^{++} and Na^+ deep within the pore of the channel, and identifies specific regions of minK that may be involved in pore formation.

Despite this, an entirely different role for minK has been suggested by Romey et al. (1997) as a result of single channel analysis and mutation studies. Single channel analysis of KvLQT1 and/or minK expressed in COS cells revealed that KvLQT1 alone has a single channel conductance of 7.6 pS, whereas both KvLQT1 and minK together have a unitary conductance of 0.6 pS. This finding is unexpected since coexpression of minK with KvLQT1 increases the whole cell current magnitude. Rather, these results suggest that association of minK with KvLQT1 causes a decrease in the single channel conductance that must occur simultaneously with a big increase in the number of functional channels in the membrane. Co-expression of KvLQT1 with mutants of minK in which either a serine has been replaced by a threonine at position 68 in the carboxy-terminus, or the carboxy-terminus has been truncated after residue 80, decreases the magnitude of minK-KvLQT1 currents in *Xenopus* oocytes (Barhanin et al., 1996). In addition, yeast-two hybrid and affinity chromatography assays have demonstrated that the carboxy- and not the amino-terminus of minK interacts specifically with the pore region of KvLQT1 (ie. does not interact with the amino- or carboxy-terminus) (Romey et al., 1997). Incorporating these biochemical and electrophysiological results Romey et al. (1997) proposed a model whereby minK does not form part of the pore but instead binds

to the outer shell of KvLQT1. Upon opening of the KvLQT1 channel the carboxy-terminus of minK flips up into the KvLQT1 pore region and occludes it, thereby decreasing the single channel conductance. The carboxy-terminus then stays bound within the pore and prevents the KvLQT1 channel from closing, resulting in an increase in the number of open channels. This model is clearly in contrast to previous results demonstrating a role for minK in lining the K^+ channel pore, and further experiments must be awaited to clarify this issue.

Clinical Implications

Long QT Syndrome

Romano-Ward long QT syndrome (LQT) is an autosomal-dominant inherited disorder characterized by a prolongation of the QT interval on an electrocardiogram, recurrent syncope, a risk of torsade de pointes, and sudden cardiac death in otherwise healthy people. Five distinct genes have been linked to LQT and their loci have been mapped; LQT1 on chromosome 11p15.5, LQT2 on 7q35-36, LQT3 on 3p21-24, LQT4 on 4q25-27, and LQT5 on 21q22.1-22.2 (see reviews by Keating, 1995; Wilde and Veldkamp, 1997). Of these, mutations in LQT1 account for greater than 50% of this inherited form of LQT (Wang et al., 1996).

LQT is likely caused by mutations in genes that regulate cardiac ion channels, leading to delayed repolarization and torsade de pointes (Keating, 1995). Evidence for this hypothesis comes from genetic testing of members of families affected with LQT. At least three of the five LQT genes encode for K^+ channels, with LQT1 encoding KvLQT1 (Wang et al., 1996), LQT2 encoding HERG (Curran et al., 1995; the protein thought to underlie I_{Kr} (Sanguinetti et al., 1995)), and LQT5 encoding minK (Splawski et al., 1997b) (LQT3 encodes SCN5A, a cardiac Na^+ channel (Wang et al., 1995); LQT4 is unknown). This analysis has revealed several sporadic mutations in both KvLQT1 and minK that could produce LQT. In particular, no less than 29 missense mutations have been identified in the cytoplasmic loops of S2-S3 and S4-S5, the pore region, the S6

transmembrane domain, and the carboxy-terminus of KvLQT1 in Romano-Ward LQT patients (van den Berg et al., 1997; Wollnik et al., 1997; Shalaby et al., 1997; Donger et al., 1997), with the most serious phenotypes occurring with mutations in the pore region and the S4-S5 linker (Donger et al., 1997). Many of these mutations are thought to decrease KvLQT1 activity by a dominant-negative effect, and this mechanism has been confirmed by expression of several of the mutated proteins (A177P, T311I, L272F, G211R, T217I, G219S, and D222N) in *Xenopus* oocytes (Wollnik et al., 1997; Shalaby et al., 1997).

Missense mutations in minK at S74L and D76N have also been identified in two LQT families (Splawski et al., 1997b; Duggal et al., 1998). Synthetic mutation of these residues in the human minK gene, and subsequent coexpression of these mutated proteins in *Xenopus* oocytes with KvLQT1, elicits a current with markedly decreased amplitude, a voltage-dependence of activation relationship that has shifted by 16-19mV to the right, and much faster kinetics of deactivation. The D76N mutation has a dominant-negative effect on minK activity (Splawski et al., 1997b). In combination, these results suggest that mutations in KvLQT1 and/or minK (if these proteins underlie I_{Ks}) would result in decreased activity of I_{Ks}, leading to prolongation of the action potential duration and a resulting predisposition to LQT.

In addition to its role in LQT, mutations in KvLQT1 have also been linked to Jervell and Lange-Nielson syndrome (JLN), an autosomal-recessive inherited disorder characterized by the same symptoms as LQT, as well as congenital bilateral deafness (Neyroud et al., 1997). The JLN gene was recently mapped to the same locus as KvLQT1 and deletions in the carboxy-terminus of this gene, as well as missense mutations at W305S, have been identified in people affected with JLN (Neyroud et al., 1997; Chouabe et al., 1997; Tyson et al., 1997). Furthermore, mutations in minK may also be linked to JLN, as the minK missense mutation D76N, which was identified in several individuals affected with Romano-Ward LQT (Splawski et al., 1997b; see above), has also been localized in one JLN patient (Duggal et al., 1998). In addition, Tyson et al. (1997) have identified mutations in minK at residues 59 and 60 in one JLN-affected family. These

findings are in agreement with the work of Vetter et al. (1996) in which they found that the knockout mouse of minK exhibits degeneration of hair cells in the inner ear and is functionally deaf. Others, however, have reported no mutations in minK in a limited sampling of JLN patients (Tesson et al., 1996).

In combination, these studies demonstrate that mutations in either KvLQT1 or minK can cause Romano-Ward LQT and JLN syndrome, and perhaps other unidentified disorders. It is likely that the particular mutation(s) identified in each individual may well be linked to the different phenotypes of the disorder.

Treatment of Ventricular Tachyarrhythmias

Class III antiarrhythmic drugs increase action potential duration and cellular refractoriness. In an idealised substrate these agents act to prevent ventricular tachyarrhythmias by suppressing the local ectopic events that arise from reentrant circuits. Unfortunately, most antiarrhythmic agents that act predominantly by inhibiting I_{Kr} exhibit reverse use-dependence. That is, under normal conditions these compounds prolong action potential duration but become less effective at increased heart rates. In addition, under bradycardic conditions these agents can excessively prolong action potential duration, leading to early afterdepolarizations and reentrant or focal arrhythmias. Thus, under certain conditions these agents are actually proarrhythmic, and have been described as causing an 'acquired' version of LQT (see review by Sanguinetti and Keating, 1997).

Drugs which target I_{Ks} may prove to be more clinically effective than I_{Kr} blockers for treatment of tachyarrhythmias, as I_{Ks} exhibits residual activation under conditions of rapid pacing (Jurkiewicz and Sanguinetti, 1993). Thus, drugs which block this channel should not exhibit reverse use-dependence and should be most effective under tachycardic conditions. The therapeutic benefits of specifically targeting I_{Ks} has yet to be clinically investigated as there has been only recent development of compounds thought to selectively block this channel in cardiac tissue.

Objectives of this Study

At the time this dissertation was started, it was proposed that minK was the molecular structure underlying I_{Ks} (Kaczmarek and Blumenthal, 1997), although (as described in this literature review) there was a great controversy over whether minK actually formed a functional K^+ channel, or instead acted as a regulator of K^+ channels endogenous to *Xenopus* oocytes. The goal of this study was to carry out a quantitative comparison of the biophysical, pharmacological and molecular properties of I_{Ks} with those of minK, to gain insight into whether minK could be responsible for this K^+ channel. We chose to investigate the properties of I_{Ks} in bullfrog atrium since, as previously described, I_K in this tissue is composed of only a single slowly activating K^+ conductance. The design and objectives of the experiments were as follows: a) To investigate the properties of the delayed rectifier K^+ current in bullfrog atrial myocytes to confirm that the characteristics of this current resemble those of I_{Ks} found in mammalian tissue; b) To compare the properties of I_{Ks} in isolated bullfrog atrial myocytes with minK expressed in *Xenopus* oocytes; c) To provide molecular biological evidence that the proteins proposed to underlie the delayed rectifier K^+ channel are present in bullfrog atrium; and d) To investigate the validity of *Xenopus* oocytes as a model to use for studying K^+ channel function.

CHAPTER 2: MATERIALS AND METHODS

Electrophysiology

Bullfrog Atrial Myocyte Experiments:

Solutions

All of the solutions used in these experiments were made with double-distilled water by diluting concentrated (x10) stock solutions that contained no Ca^{2+} or glucose and were kept at 4°C for not more than three weeks. The composition of the solutions were as follows:

Standard Ringer's solution (in mM): 110 NaCl, 2.5 KCl, 5 $MgCl_2$, 5 HEPES, 10 glucose, 1.8 $CaCl_2$, equilibrated with 100% oxygen. pH was adjusted to 7.35-7.4 with 1M NaOH.

Nominally Ca^{2+}-free Ringer's solution: 110mM NaCl, 2.5mM KCl, 5mM $MgCl_2$, 5mM HEPES, 10mM glucose, 8 μM $CaCl_2$, bubbled with 100% oxygen. pH was adjusted to 7.35-7.4 with 1M NaOH.

Pipette filling solution (in mM): 80 KAsp, 20 KCl, 5 NaCl, 2 MgATP, 1 EGTA, 10 HEPES. pH was adjusted to 7.25 with 1M KOH. pCa was estimated to be >8.

Drugs

All drugs used in either the bullfrog atrial myocyte or *Xenopus* oocyte experiments were added to the recording solution to give the appropriate final concentration (outlined in the text for each particular compound). Clofilium tosylate (RBI) was dissolved in 50% dimethylsulfoxide (DMSO) and 50% Standard Ringer's solution at a concentration of 10mM and stored in aliquots at -20°C. Lanthanum chloride, cadmium chloride and azimilide dihydrochloride (NE-10064; a gift from Norwich-Eaton Pharmaceuticals (Procter and Gamble)) were dissolved in double distilled water at a concentration of 10mM and stored in aliquots at -20°C. E-4031, a gift from Eisai Pharmaceutical (Japan), was dissolved in double-distilled water at a concentration of 10mM and stored at 4°C. MK-499 and propenamide (L 735-821), both gifts from Merck

Pharmaceuticals, were weighed out just before each experiment and dissolved in Standard Ringer's solution or ND96 Buffer (MK-499) or 100% DMSO (propenamide) at a concentration of 10mM. Chromanol 293B was dissolved in 100% DMSO to give a final concentration of 10mM and was stored in aliquots at -20°C. The final concentration of DMSO in the recording chamber was $\leq 0.1\%$.

Cell Isolation Procedure:

Adult bullfrogs (*Rana catesbeiana*, 5-6 inches) were obtained from Amphibians of North America, Charles D. Sullivan Co., Inc., Nashville, Tennessee. They were stored at the Biosciences Animal Care Facility at the University of Calgary, and shipped to the laboratory as needed. After shipping the animals were kept for a maximum of 3 days in the laboratory. Individual bullfrogs were sacrificed by pithing. The heart was quickly removed, placed in nominally Ca^{++}-free Ringer's solution and washed 3-4 times until the atrium was free of blood. The heart was then pinned ventral side up to the bottom of a petri dish which was coated with Sylgard 184 silicone elastomer (Dow-Corning, Midland, Mich.) and filled with nominally Ca^{++}-free Ringer's solution. With the aid of a dissecting microscope (10x magnification) the connective tissue and fat surrounding the atrium was removed. The heart was then turned over to expose its dorsal surface. The left, right, and posterior vena cava and any remaining connective tissue were removed and the atrium was then cut away from the ventricular tissue and the truncus arteriosus. The isolated atrium was subsequently cut open to expose the interatrial septum. This septum was excised to leave only atrial tissue, which was cut into 3-4 pieces measuring approximately 3mm by 7mm each.

These atrial strips were placed in a small Erlenmeyer flask containing 10 ml of nominally Ca^{2+}-free Ringer solution, 2.2-2.7 mg/ml collagenase (type 1A, clostridium histolyticum, 280-400 units/mg; Sigma), and 0.65-0.8 mg/ml bovine pancreatic trypsin (type III, Sigma). The tissue was then gently agitated by triturating the fluid surrounding the tissue using a fire-polished pasteur pipette (bore opening approximately 2mm). The purpose of the trituration was not to mechanically disperse the tissue, but to keep the

tissue circulating in the enzyme solution. After 30-75 minutes single atrial cells were identified under a microscope and the enzyme solution in the Erlenmeyer flask was pipetted off and replaced with 10 ml of nominally Ca^{2+}-free Ringers. Gentle triturating of the fresh solution surrounding the tissue usually provided a high density of single elongated cells (approximately 150-350μM in length and 5-7μM in diameter at the thickest region) after several minutes. These cells were stored in nominally Ca^{2+}-free Ringer's solution and were viable for approximately 6-8 hours.

Recording Chamber and Microelectrodes

The recording chamber consisted of a small 2-tier well cut into a block of Lucite, with a microscope slide glued to the bottom with epoxy. A small aliquot of the cell suspension was placed in the recording chamber and allowed to settle to the bottom. After 10-20 minutes (once the cells had adhered to the bottom of the chamber) solutions were superfused at a rate of 1-2 ml/min by gravity through one end of the bath and removed by suction at the opposite end. A six column perfusion apparatus connected to a remote solenoid driven switching system allowed rapid exchange of bath solutions (20-40 seconds, depending on flow rate).

Microelectrodes were pulled from thin-walled borosilicate glass (1.5mm outer diameter, 1.0mm inner diameter, World Precision Instruments, New Haven CT) using a horizontal puller (David Kopf Instruments, Tujunga, CA). The resistance of the electrodes was between 2 and 5MΩ when filled with pipette solution. The electrodes were mounted in a right-angled microelectrode holder equipped with suction ports and which contained a Ag-AgCl pellet that made contact with the filling solution in the electrode. These electrodes were placed near the atrial cell with the aid of an inverted microscope using a hydraulic micromanipulator (Narishige, MHW-103). The whole-cell patch clamp technique (Hamill, Marty, Neher, Sakmann, and Sigworth, 1981) was used for recording macroscopic K^+ currents. All transmembrane potentials reported in this paper were corrected by adding -10mV to the nominal membrane potential to account for the junction potential between the pipette and bath solutions (Clark et al., 1990).

Electronic circuitry and data acquisition

A List-Medical Electronics (Darmstadt, Germany) type L/M-EPC7 amplifier was used for all experiments. The current transient due to charging/discharging of the cell capacitance was minimized using the compensation dial settings on the amplifier. These values gave estimates of the cell membrane capacitance and the series resistance, of which 40-80% was electronically compensated. Output currents were filtered at a bandwidth of 3kHz.

Rectangular command pulses were generated by applying pulses from a digital pulse generator (World Precision Instruments, New Haven, CT) to a voltage divider circuit which was optically isolated. This generator allowed two separate command steps to be applied in a desired sequence and was also used to select the holding potential (via application of a 5V DC potential to another voltage divider circuit).

Membrane currents and potentials were stored in a Packard Bell 386 computer using an analog-digital converter board (type DT2821F, Data Translation, Inc., Marlborough, MA), and were also simultaneously viewed using a digital storage oscilloscope (Hitachi, VC-6023). Currents were digitized at 100-200Hz. Data acquisition and analysis was achieved using the Cellsoft Program (developed by Mr. Dale Bergman, University of Calgary).

Xenopus Oocyte experiments

Solutions

All solutions were prepared as 20-times stock solutions using double-distilled water and filtered through a 0.22μm pore filter. Experimental solutions were made by appropriate dilutions into double-distilled water. Solution compositions were as follows:

ND96 Buffer without Ca^{2+} (in mM): 96 NaCl, 2 KCl, 1 $MgCl_2$, 5 HEPES, pH was adjusted to 7.5 with 1M NaOH. This solution was used for the enzymatic isolation of oocytes. 1.8 mM Ca^{2+} was added to this solution for experimental recording. In

experiments in which the K^+ concentration was increased to 10mM, NaCl concentration was decreased to 88mM.

ND96 Buffer with Ca^{2+}, Na-pyruvate and penicillin/streptomycin (in mM): 96 NaCl, 2 KCl, 1 $MgCl_2$, 5 HEPES, 2.5 Na-pyruvate, 1.8 $CaCl_2$, 100units/ml penicillin, 100ug/ml streptomycin.

Xenopus Laevis Maintenance

Xenopus Laevis (female, 9cm long) were obtained from Nasco Ltd. (Fort Atkinson, WI). A colony of 10-12 *Xenopus laevis* was maintained in 30 litre (L) holding tanks filled with 15-20L of de-chlorinated tap water (2-4 frogs per tank). The water was kept at 18-19°C and changed every other day after feeding. The *Xenopus* were fed every other day and were allowed as much Nasco frog brittle nuggets as could be consumed in 10-15 minutes (approximately 10-12 nuggets per *Xenopus*). A 12 hour light-dark cycle was maintained.

Isolation of *Xenopus* oocytes

Individual animals were anaesthetized by placing them in a bucket containing 0.2% tricaine (MS-222, Sigma). One or two lobes of the ovary were excised and placed in ND96 buffer without Ca^{2+}, and the muscle layers and skin were then sutured and the animal allowed to recover. Each animal was left for a minimum of 2 months before undergoing another surgery, and was used for oocyte collection 2-4 times before being sacrificed.

The ovarian lobes were teased apart from the superficial connective tissue with sharp forceps (Dumont, No.5) and then torn into small clumps of oocytes. These chunks were washed 1-2 times in ND96 buffer without Ca^{2+} and then placed in a petri dish containing 30mL of 2mg/ml crude bacterial collagenase (type 1A, Sigma). The petri dish was placed on a 3-dimensional platform shaker for 45-60 minutes, at which time the oocyte clumps could be gently teased apart, yielding several free oocytes. The enzyme solution was then replaced with ND96 buffer with Ca^{2+}, Na-pyruvate and

penicillin/streptomycin and the petri dish was returned to the shaker plate for gentle washing of the oocytes (first wash $\leq$ 15 min; subsequent washes 30-40 minutes; total wash time 75-120 minutes depending on the number of free oocytes observed). Stage IV, V and VI de-folliculated oocytes were chosen with well defined animal and vegetal poles. These oocytes were placed in fresh ND96 buffer (with Ca^{2+}, Na-pyruvate and pen/strep) in small plastic agar-coated culture dishes and left to recover overnight at 16-18°C.

The follicular layer was removed from those eggs in which it was still intact by careful manipulation with a fine forceps. At intervals the resting membrane potential of a small sample of eggs (4-5) was recorded prior to injection, to ensure that the oocytes were healthy. Only batches of eggs with resting membrane potentials more negative than -40mV were used for experimentation.

Injection of *Xenopus* oocytes

A pressure micro-injector (PLI-100, Medical Systems, Corp.) was used for oocyte injections. Injection pipettes were pulled on a horizontal pipette puller (David Kopf Instruments) from thin-walled borosilicate glass, 1mm outer diameter (World Precision Instruments). The tips of the microelectrodes were bevelled on a microgrinder (Narashige, MG-4) to give a diameter of 5-10μm. The electrodes were handled at all times with gloves or forceps to prevent any contamination with RNases and were baked after bevelling at 150-200°C for not less than 12 hours to remove residual RNases.

Oocytes were injected with 50nl of 10ng/μl cRNA encoding rat uterine minK (provided by Dr. Kelleen Giffin, Monsanto Ltd., St. Louis, MO) or 10ng/μl cRNA encoding rat Kv1.2 (provided by Dr. David McKinnon, SUNY, Stony Brook, NY), and then placed in individual wells of a 96-well culture dish filled with ND96 buffer with calcium, Na-pyruvate, and penicillin/streptomycin. These oocytes were stored at 16-18°C and the buffer solution was replaced daily.

Removal of Vitelline Layer

When necessary the vitelline layer was removed mechanically using the method of Methfessel et al. (1986). In brief, oocytes were placed into an agar-coated petri dish which was filled with hypertonic solution (containing in mM: 200 K-aspartate, 20 KCl, 1 $MgCl_2$, 10 EGTA, 10 Hepes, pH 7.4, 475mOsm). The eggs were left in this solution for 5-10 minutes at room temperature (20°C). After this time the vitelline membrane separated from the plasma membrane and it could be teased off in its entirety with a pair of fine forceps. The eggs were then transferred to an agar-coated petri dish containing fresh ND-96 solution. This procedure was performed on 2-3 eggs at a time, which were then used as soon as possible for voltage-clamp recordings. Removal of the vitelline membrane was confirmed using both light microscopy and transmission electron microscopy (see Figures 45 and 46).

Two-electrode voltage clamp recordings

Recordings were made 2-4 days after oocyte injection. The recording chamber consisted of a small 2-tier well cut into a block of Lucite, with a microscope slide glued to the underside and a small piece of plastic mesh mounted on the bottom of the chamber. The oocytes were placed on the mesh for recording and were continually perfused at a rate of 1-1.5 ml/min with ND96 containing 1.8mM $CaCl_2$, using a six column perfusion system connected to a remote solenoid driven switching device. The bath solution could be exchanged in 40-60 seconds, depending on flow rate. Unless otherwise stated, all experiments were performed at room temperature (20°C).

Microelectrodes were pulled on a vertical pipette puller (Narishige PE-2) using thin walled borosilicate glass, 1.5mm outer diameter, containing a filament (World Precision Instruments, Sarasota, FL). The resistance of the microelectrodes were 0.3-1.0 MΩ (current-passing) or 0.5-1.5 MΩ (voltage recording) when back-filled with 3M KCl. Currents were recorded with a Dagan TEV-200 amplifier using standard two-microelectrode voltage clamp techniques (Stühmer, 1992). Currents were digitized at 100-1000Hz and filtered at 200Hz (minK) or 1kHz (Kv1.2). The other components of the

electronic circuitry and the data acquisition methodology were the same as described for the bullfrog atrial myocyte experiments.

Data Analysis

All data are reported as mean ± SEM. In both the bullfrog atrial myocyte and *Xenopus* oocyte experiments data analysis was achieved using the Cellsoft Program (developed by Mr. Dale Bergman, University of Calgary). Curve fitting was performed using SigmaPlot v2.0 (Jandel Scientific) and GraphPad Prism v2.01 (GraphPad Software Inc., San Diego, CA). Statistics were done with GraphPad InStat v3.0 (GraphPad Software Inc., San Diego, CA). In *Xenopus* oocyte experiments the % block of the current onset after application of a drug was calculated by estimating the change in the maximum outward current after correction for the initial instantaneous current (ie. current amplitude = peak current - instantaneous current).

Microscopy

Xenopus oocytes were fixed for transmission electron microscopy with Karnovsky's Fixative (2% paraformaldehyde, 2.5% glutaraldehyde with 5mM Ca^{--} in 0.1M cacodylate buffer, pH7.4; Karnovsky, 1965) for at least 2 hours, followed by 1 hour in 1% osmium tetroxide. The eggs were then dehydrated in an ascending ethanol series (50% to 100%) and an ascending combination of Spurr resin (Electron Microscope Sciences, Washington, PA) and 100% alcohol. Oocytes were embedded in Spurr resin and thin sections (2.5μm) were made. Sections were stained with aqueous uranyl acetate and lead citrate (Venable and Coggeshell, 1965) and examined in a Hitachi H7000 (30,000x) electron microscope. Sections examined by light microscopy were stained with hematoxylin and eosin and examined under a Leitz Orthoplan microscope (Ernest Leitz Canada Ltd., Midland, Ontario).

In Situ Hybridization

Reagents

All stock solutions were prepared with diethylpyrocarbonate (DEPC)-treated water and were diluted as needed during the course of the experiment from stock solutions. The composition of the various solutions were as follows:

Phosphate Buffered Saline (PBS): 140mM NaCl, 2.7mM KCl, 10mM Na_2HPO_4, 1.8mM KH_2PO_4 (pH 7.4).

SSC: 150mM sodium chloride and 15mM sodium citrate (pH 7.0).

TEA Buffer: 9% sodium chloride in 1M triethanolamine (Sigma).

Denhardt's solution: 0.02% Ficoll, 0.02% polyvinylpyrrolidone, 10mg/ml RNase-free bovine serum albumin

Buffer 1: 100mM Tris-HCl and 150mM sodium chloride (pH7.5).

Buffer 2: 100mM Tris-HCl, 100mM sodium chloride, and 50mM magnesium chloride (pH 9.5).

Blocking Buffer: Buffer 1 containing 1% normal sheep serum and 0.3% Triton X-100.

PVA solution: 10% polyvinyl alcohol in Buffer 2.

Washing Buffer: 100mM maleic acid and 150mM sodium chloride (pH 7.5); 0.3% Tween20.

Maleic Acid Buffer: 100mM maleic acid and 150mM sodium chloride (pH 7.5).

Blocking Solution: Maleic acid buffer plus 1% blocking reagent (Boehringer Mannheim).

Detection Buffer: 100mM Tris-HCl and 100mM sodium chloride (pH 9.5).

TE Buffer: 10mM Tris-HCl and 0.1mM EDTA (pH 8.0).

Tris-EDTA buffer: 10mM Tris-HCl and 1mM Na_2EDTA (pH 8.0).

Preparation of Probes and Labelling

Oligonucleotide probes (see below) of 50 nucleotides in length were designed to target the KvLQT1 sequence. The KvLQT1 probe was targeted to the 3' end of the

known bullfrog cardiac sequence (cloned by Mr. Robert Winkfein in the University of Calgary MRC Molecular Biology Core Facility), corresponding to nucleotides 1120-1169 (see Figure 33). The probes were analysed using Gene Runner (version 3.0, Hastings Software) to ensure no extensive secondary structure existed. The specificity of the probe was also investigated by searching the GenBank database using BLAST, and the probes were considered acceptable if no other ion channels appeared in the first 50 matches of the search for either the antisense or sense probes. Oligonucleotide probes were synthesized and purified by gel electrophoresis in the University of Calgary DNA Synthesis Facility. They were then 3' end-labelled with digoxigenin-11-ddUTP and terminal transferase using the Boehringer-Mannheim DIG oligonucleotide 3'-end labelling kit (Boehringer-Mannheim Co., Indiana, USA, catalogue number 1362372). This kit incorporates one DIG-ddUTP molecule into the 3' end of each oligonucleotide, and is advantageous as it avoids many of the hazards involved with radioactive labelling, without compromising the sensitivity of the probe.

KvLQT1 sense probe 5'CAGATTCCAGCTGCAGCATCTCTCATACAGACAGCGTGGAGGTGTTATGC 3'

Estimating the Yield of DIG-labelled Oligonucleotide Probe

The yield of incorporated DIG-label was determined according to a protocol supplied by Boehringer-Mannheim (Nonradioactive *in situ* hybridization application manual, edition 2). An aliquot of each of the labelled antisense and sense oligonucleotide probes were diluted to a concentration of 2.5pmol/μl. Serial dilutions of these labelled probes and a control DIG-labelled probe (2.5pmol/μl, Boehringer-Mannheim) were then made to give aliquots with a final concentration of 50, 10, 2, 0.4, or 0.08 fmol/μl. 1μl of each of these samples was blotted onto a piece of nylon membrane in descending concentration and the membrane was baked at 65°C for 3 hours to fix the nucleic acids. The membrane was rinsed quickly in washing buffer, incubated in blocking solution for 30 minutes at room temperature with occasional gentle agitation, incubated in anti-DIG-alkaline phosphatase (1:5000 dilution in blocking solution) solution for 30 minutes, and

then washed twice with washing buffer for 15 minutes each. The membrane was left to equilibrate in detection buffer for two minutes, followed by incubation in the dark in freshly prepared colour substrate solution containing 45µl NBT (75mg/ml nitroblue tetrazolium salt in 70% dimethylformamide) and 35µl BCIP (50mg/ml 5-bromo-4-chloro-3-indolyl phosphate, toluidinium salt in dimethylformamide) in 10ml Detection Buffer. The reaction was left to proceed until the colour precipitate developed to an optimal intensity (2-3 hours). The reaction was then stopped by washing the membrane with TE buffer. The concentration of the probes were determined by comparing the intensity of the signal of labelled probe to that of the control probe.

Tissue Preparation

Adult bullfrogs (5-6 inches) were sacrificed by pithing. The heart was quickly removed, rinsed in cold PBS to remove the blood, and frozen in isopentane. Longitudinal sections (6-10µm thick) were cut on a cryostat and placed on glass slides. The prepared slides were stored at -70°C until use.

Prehybridization

In situ hybridization was performed based on a modification of the technique described by Molecular Techniques (Laval, Quebec) for *in situ* hybridization using oligonucleotides. The slides were removed from the freezer and allowed to air dry before use (10-15min). Sections were fixed in 4% paraformaldehyde in PBS for one hour at room temperature, washed three times with PBS, permeabilized in PBS containing 0.4% Triton X-100 for 30 minutes, and then washed an additional two times with PBS and two times with DEPC-treated water. The slides were then treated with 0.1M triethanolamine (TEA; pH 8.0) for 5 minutes, followed by treatment with 0.1M TEA containing 0.25% (v/v) acetic anhydride (added immediately before use) for 10 minutes. The sections were washed two times with 2x SSC, dehydrated through a series of graded ethanol (50%, 70%, 80%, 90%, 95%, 100%, 100% ethanol in DEPC-treated water), and then allowed to air dry.

Hybridization

50µl of hybridization mix was applied on top of each tissue section and then covered with a coverslip. The slides were incubated in a humid chamber at 42°C for 18-20 hours. The hybridization mixture contained the following: 50% formamide, 3x SSC, 1x Denhardt's solution, 0.2mg/ml yeast tRNA, 50mM sodium phosphate buffer (pH 7.4), 20mM DTT, 10% dextran sulfate, and 500pmol/ml labeled oligonucleotide probe.

Posthybridization

The coverslips were removed by immersing the slides in 2x SSC for 5-10 minutes. The sections were then washed at room temperature with 2x SSC for 20 minutes, 1x SSC for 20 minutes, 0.5x SSC for 20 minutes, and then at 50°C with 0.5x SSC for 60 minutes. A further wash was performed at room temperature in 0.5x SSC for 10 minutes.

Immunological Detection

Sections were washed 3 times in Buffer 1 and then incubated with anti-DIG-alkaline phosphatase conjugated antibody diluted at 1:1000 in blocking buffer for 5 hours at room temperature in a humid container. The slides were subsequently washed 2 times in Buffer 1, once in Buffer 2, and then 50µl of chromagen solution containing 45µl of NBT, 35µl of BCIP, and 2.4mg levamisole per 10ml of PVA solution was applied to each tissue section in the dark. Incubation was allowed to proceed until a colour reaction was observed (5-18 hours). The reaction was then stopped by washing in Tris-EDTA buffer for 10-30 minutes. Sections were rapidly dehydrated in graded ethanol (50%, 70%, 80%, 90%, 95%, 100%, 100% ethanol in DEPC-treated water), and then mounted in an aqueous mounting medium.

CHAPTER 3:

ELECTROPHYSIOLOGICAL AND PHARMACOLOGICAL PROPERTIES OF THE DELAYED RECTIFIER IN BULLFROG ATRIAL MYOCYTES

Introduction

The characteristics of the delayed rectifier K^+ current in amphibian heart have been studied in detail in both multicellular and single cell preparations. There have been disagreements regarding the biophysical characteristics of this current and, in particular, there have been discrepancies with respect to whether this current is comprised of more than one component, the voltage range over which the current(s) activate(s), the activation kinetics, and the ionic selectivity (see Introduction of this dissertation for review). The time and voltage dependent characteristics of the delayed rectifier K^+ current in isolated bullfrog atrial myocytes have been extensively characterised by Hume et al. (1986) and Simmons et al. (1986). These groups described the presence of a single Hodgkin-Huxley like conductance that is strongly selective for K^+ ions, and has activation and deactivation kinetics consistent with this current playing a major role in action potential repolarization. The studies described in this chapter, therefore, were designed to investigate the characteristics of the delayed rectifier in bullfrog atrium, and to test whether we could confirm the findings of Hume and Giles (1986) and Simmons et al. (1986) regarding the existence of only a single K^+ conductance underlying the delayed rectifier, I_K. We also investigated the effects of several relatively new compounds that have been shown to inhibit I_{Ks} or I_{Kr} in mammalian cardiac tissue, on the bullfrog delayed rectifier.

Results

Cell Morphology and Electrical Properties

The morphological characteristics of isolated single bullfrog atrial cells have been described previously. These myocytes are elongate and spindle shaped with a length of approximately 150-350μm (average of 284μm; Hume and Giles, 1983) and a diameter of 5-7μm at their thickest region near the nucleus and about 2μm at the ends (Hume and Giles, 1983; Simmons et al., 1986). These cells remain relaxed and quiescent in normal Ringer's solution containing 2.5mM calcium. An example of a typical cell used for these

electrophysiological recordings is shown in Figure 1. These cells were very similar morphologically to those previously described, having regular, well-defined striations, a single nucleus found in the thickest region of the cell, and being relaxed and quiescent.

The electrical properties of myocytes isolated from bullfrog atria have also been well characterized. In our experiments a random sampling of the resting membrane potential yielded a value of -90.9 ± 0.5mV (n=70). Cell capacitance was 57.6 ± 2.3pF (n=36), and input resistance was 332.4 ± 39.3 MΩ (n=17). These values correlate well with those previously reported by Hume and Giles (1983; resting membrane potential = -89.6mV, cell capacitance= 76pF, and input resistance= 289.3MΩ) and Simmons et al. (1986; cell capacitance= 64pF). An example of an action potential recorded from a single bullfrog atrial myocyte is shown in Figure 2. This action potential had a duration of 580msec and amplitude of 131.1mV (peak at +38.4mV), which are very similar to values reported earlier by other investigators (Hume and Giles, 1983; action potential duration= 772.5 ± 43.4 msec, action potential amplitude=131.6 ± 2.6mV).

General Characteristics of the Delayed Rectifier Current

Figure 3 consists of representative traces of the time and voltage-dependent outward current recorded from a single bullfrog atrial myocyte. Depolarizing voltage steps from -50 to +50mV were applied for 30sec from a holding potential of -90mV, and tail currents were measured at -70mV. Each depolarization activated a slow outward current that increased in magnitude as voltage became more positive. This current reached steady state after about 20 seconds and did not inactivate, even during very long voltage pulses (greater than 30 seconds). The onset of this current had a sigmoid time-course. This sigmoidicity was less pronounced at more positive potentials.

Note also in Figure 3 that a fast inward Na^+ current (I_{Na}) and a small L-type Ca^{++} current (I_{Ca}) are activated by the depolarizing voltage steps. Previous reports have demonstrated that I_{Na} reaches a peak of approximately 1.5-2.0 nA (at -10mV) and turns off within 5msec (Clark and Giles, 1987; Hume and Giles, 1983), whereas I_{Ca} has a maximum amplitude of approximately 200pA (at +10mV) and decays within 250msec

Figure 1: Photomicrograph of a single bullfrog atrial myocyte under phase contrast, isolated using the procedure described in Chapter 2. Magnification = 440x.

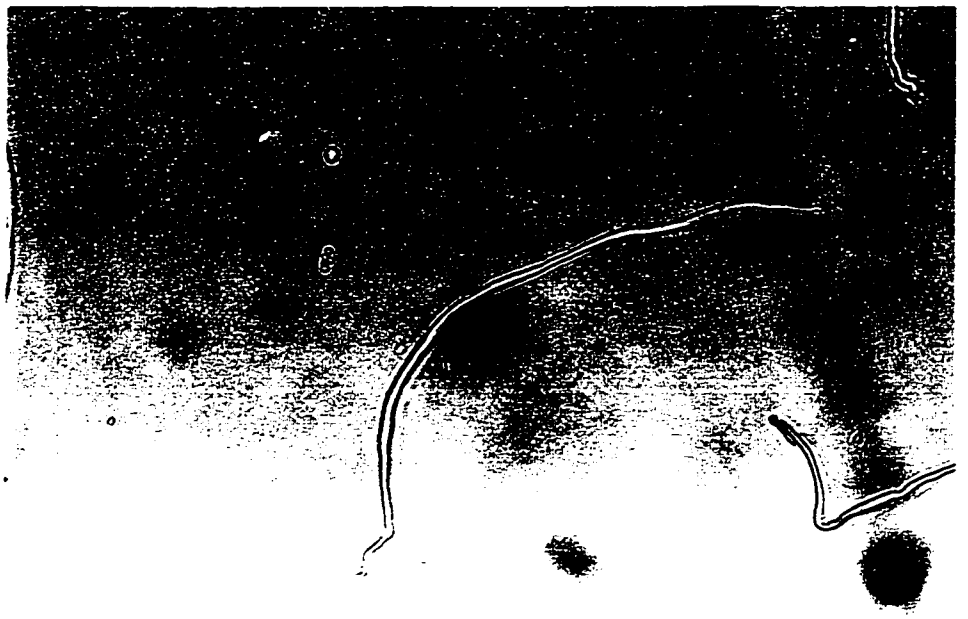

Figure 2: An action potential recorded at room temperature (20°C) from a bullfrog atrial myocyte in response to a depolarizing current pulse of 500pA for 3msec, applied every 10sec. The zero reference for voltage is shown by the horizontal line.

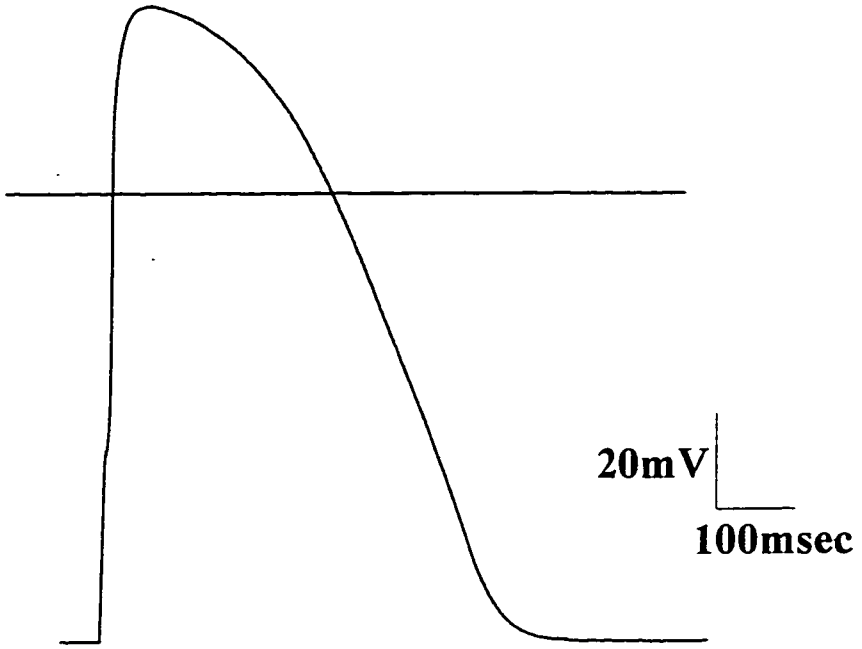
20mV
100msec

Figure 3: Representative recording of the time- and voltage-dependent outward current in a single bullfrog atrial myocyte. Current traces were elicited (activated) by 30 second depolarizing voltage steps from a holding potential of -90mV to -50 to +50mV in 10mV increments. Tail currents were measured at -70mV. The outward current activates slowly and with a sigmoid time course. Note also the inward Na^{+} and Ca^{++} currents (downward spikes) that activate quickly relative to I_K and then inactivate.

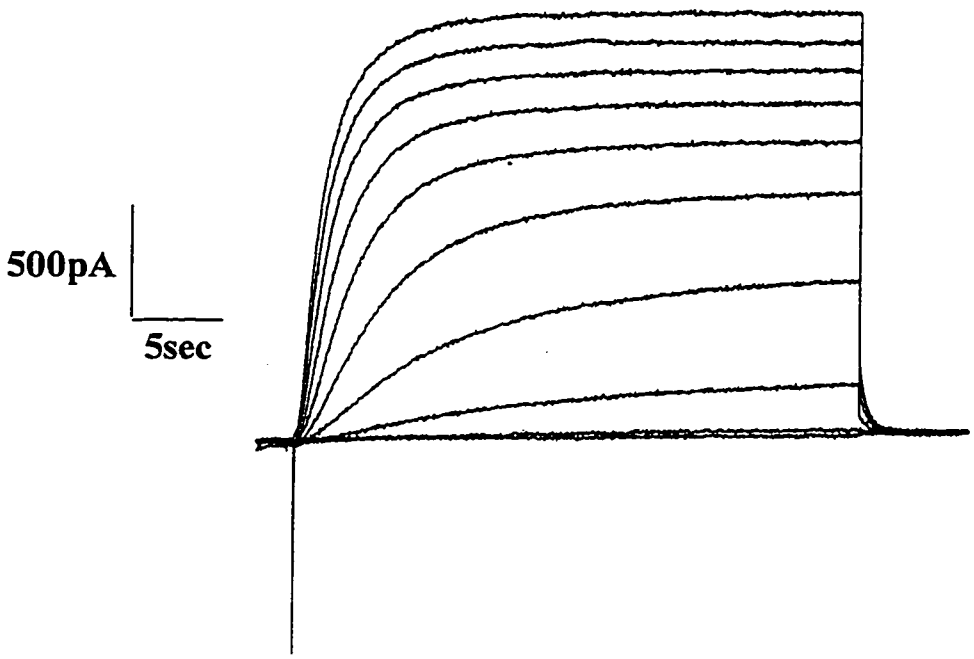
500pA
5sec

(Hume and Giles, 1983; Giles et al., 1989). Therefore, neither I_{Na} and I_{Ca} significantly overlap with the onset of the time- and voltage-dependent outward current and, unless otherwise stated, no attempt was made to inhibit these currents in the experiments reported here.

Reversal Potential

The ion selectivity of the slow outward current was investigated to determine whether this current is K^+ selective. Reversal potential measurements were made using a conventional two-pulse protocol. Depolarizing pulses from a holding potential of -90mV to +50mV were applied, followed by repolarizing pulses in the range -60 to -120mV for 8sec. The membrane potential at which there was no net tail current was defined as the reversal potential, and this value was determined by interpolation. Figure 4A illustrates an example of typical currents recorded using this protocol in 2.5mM external KCl. The average reversal potential was -93.8 ± 0.6mV (n=14), which is very close to that predicted by the Nernst equation for a K^+ selective current (-95.5mV; $[K^+]_i$ = 110mM, T = 20°C).The effect of increasing the K^+ concentration in the external medium bathing the cells is illustrated in Figure 4B. The points were best fit with a straight line with a slope of 50.1mV/10-fold change in $[K^+]_o$. These results strongly suggest that the slow outward current is selective for K^+, and it will therefore be referred to as I_K.

Steady State Voltage Dependence

The steady-state voltage dependence of I_K is shown in Figure 5. Long prepulses (30sec) from a holding potential of -90mV were applied in order to be certain that I_K had reached steady state. The peak amplitude of the tail current (measured at -70mV) was used as a measure of the extent of activation of I_K. Representative tail currents are shown in Figure 5A, taken from the same cell as in Figure 3. The activation kinetics of I_K were described by a single voltage- and time-dependent gating variable (n), based on conventional Hodgkin-Huxley theory ($I_K = nI_{K\infty}$, where n is the activation variable and $I_{K\infty}$ is the fully activated current) (Hodgkin and Huxley, 1952). The sigmoidicity in the

Figure 4: Reversal potential of the time- and voltage-dependent outward current and dependence on $[K^+]_o$. **A)** Representative current traces used to measure the reversal potential of the slow outward current. Cells were held at -90mV and then depolarized to +50mV for 3 seconds. Tail currents were measured at membrane potentials between -60 and -120mV. The reversal potential in this cell was -93mV, very close to the value expected by the Nernst equation for a K^+ selective current. **B)** Summary of the dependence of the reversal potential on $[K^+]_o$. Data are shown as mean ± SEM and n values are indicated beside each point. The data were best fit with a straight line having a slope of 50.1mV/10 fold change in $[K^+]_o$, suggesting that this current is strongly K^+ selective.

A

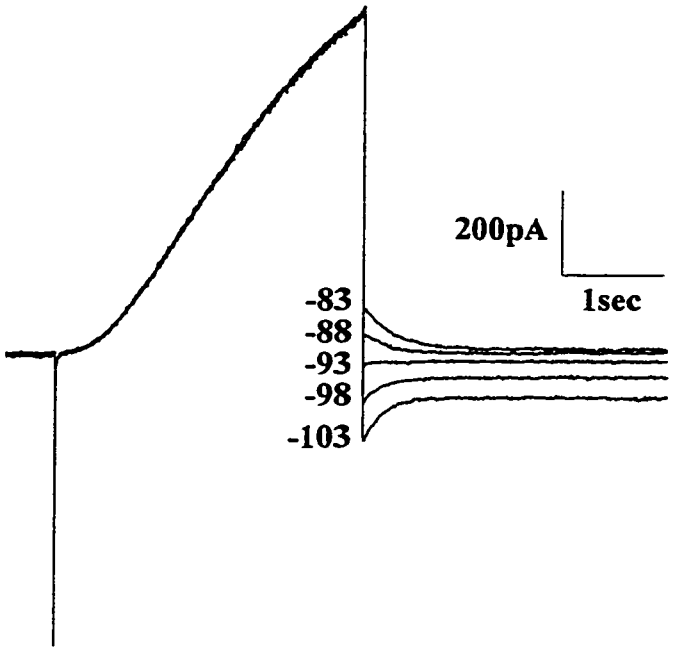
200pA
1sec
-83
-88
-93
-98
-103

B

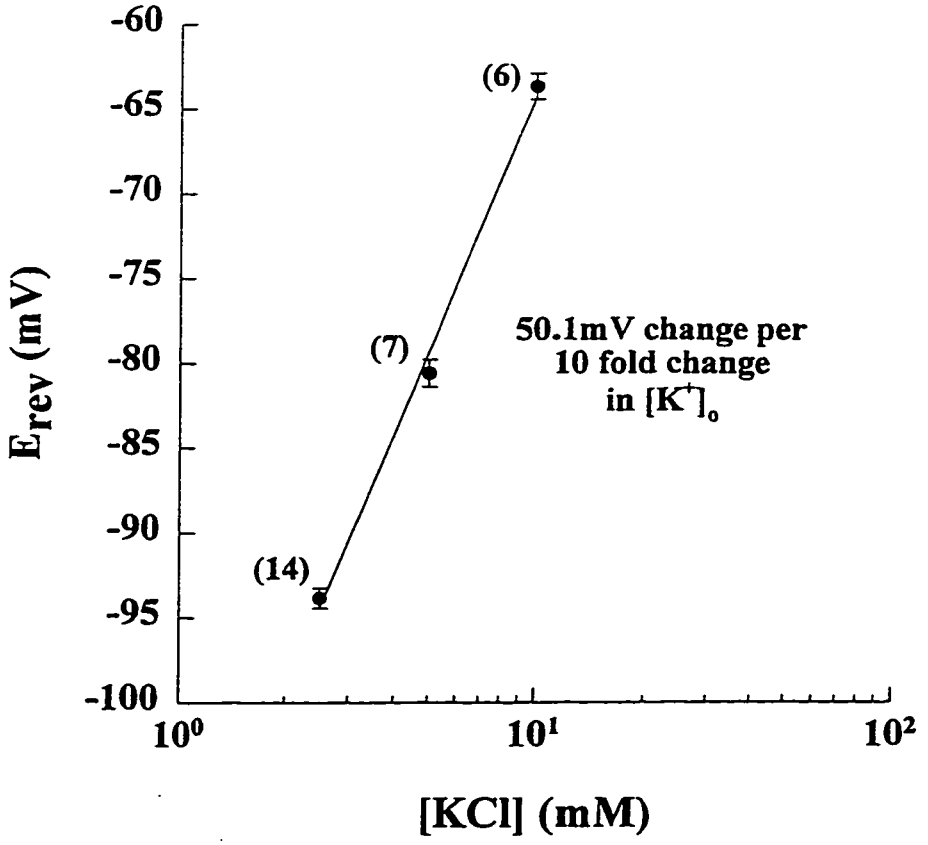
-60
-65
-70
-75
-80
-85
-90
-95
-100
E_{rev} (mV)
(6)
(7)
(14)
50.1mV change per
10 fold change
in $[K^+]_o$
10^0
10^1
10^2
[KCl] (mM)

Figure 5: Steady-state activation relationship for I_K. **A)** Representative tail currents used to measure steady-state activation, taken from the same cell and following the same protocol as in Figure 3. **B)** Steady-state activation curve (n_∞). Data are given as mean ± SEM (n=8). n_∞ values were calculated as described in the text and fitted to a Boltzmann distribution (see text). Values for $V_{1/2}$, the half-activation potential and K, the slope factor, are reported on the graph. Where error bars cannot be seen it is because they are too small to be resolved.

A

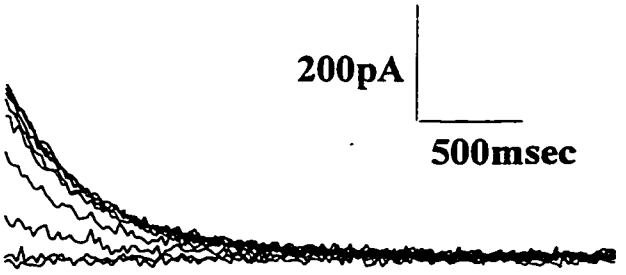
200pA
500msec

B

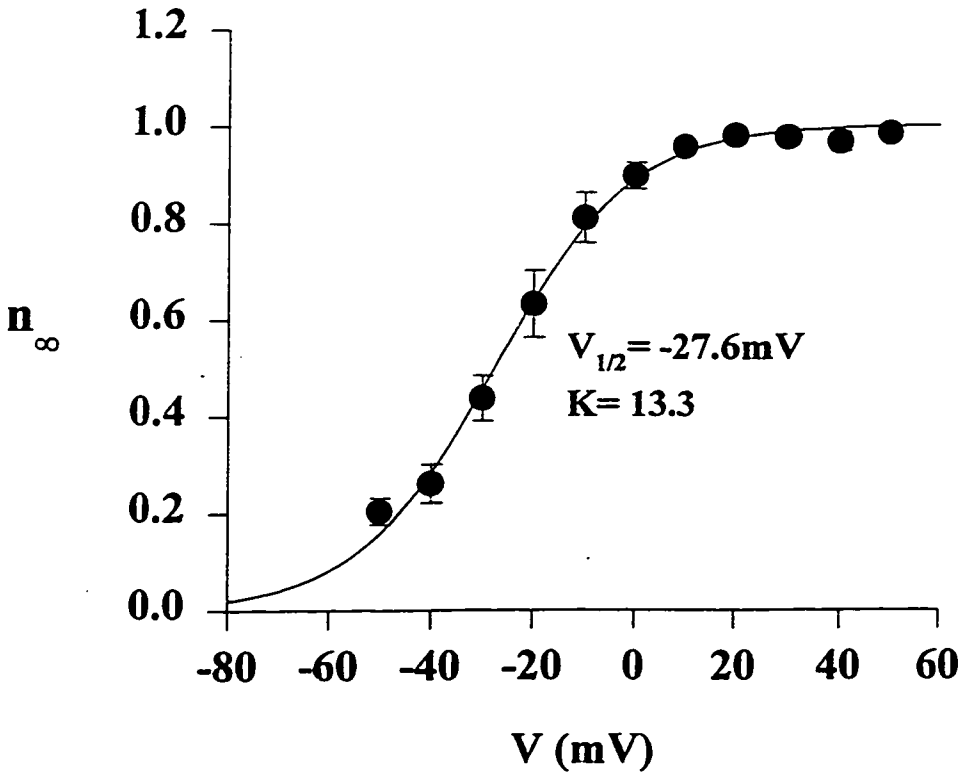
1.2
1.0
0.8
0.6
0.4
0.2
0.0
n∞
V1/2= -27.6mV
K= 13.3
-80
-60
-40
-20
0
20
40
60
V (mV)

onset kinetics, however, required that the activation kinetics be fitted by raising n to the power of 2, as described by Rasmusson et al. in their mathematical models of the delayed rectifier in bullfrog cardiac pacemaker (Rasmusson et al., 1990b) and atrial (Rasmusson et al., 1990a) cells. The steady-state activation (n_{∞}) values were therefore calculated by normalizing the tail current amplitudes relative to the maximum value and then accounting for this second-power relationship (see Hume et al., 1986). The equation used to calculate n_{∞} values was:

$$n_{\infty} = [I_{K\_tail} / I_{K\_tail.max}]^{1/2}$$

This data was fit with a Boltzmann function:

$$n_{\infty} = 1/(1+\exp(V_{1/2}-V_m)/K),$$

(where K=slope factor) which determined the half point of activation and slope factor to be -27.6mV and 13.3, respectively. These values are similar to those reported previously for bullfrog atrial myocytes ($V_{1/2}$ = -15mV, K = 11.36) (Hume et al., 1986). Note that the threshold for activation of I_K is approximately -50mV and the currents fully activate at +20 to +30mV.

Effects of Calcium Channel Blockers

As mentioned previously, bullfrog atrial myocytes express an L-type Ca^{++} current (I_{Ca}) that activates at approximately -30mV, reaches its peak between 0 and +10mV, and reverses at about +60mV. This current activates quickly and inactivates after pulses 250msec in length (Hume and Giles, 1983). The possibility that the sigmoid time-course of activation of I_K is controlled by an increase in intracellular calcium due to activation of I_{Ca} was investigated by measuring the effect of cadmium chloride ($CdCl_2$), a calcium channel blocker, on I_K. Neither bath application of 100μM $CdCl_2$ in combination with 100nM TTX (to block I_{Na}; n=3), nor 100μM $CdCl_2$ alone (n=4) changed the magnitude of I_K onset or tail current. An example of the effects of both $CdCl_2$ and TTX on a single cell is shown in Figure 6. These results confirm that activation of I_K is not dependent on influx of calcium into the cell as a result of activation of I_{Ca}.

Figure 6: Effect of $CdCl_2$ on I_K. **A)** Raw current traces elicited in response to 5 sec depolarizing voltage steps from a holding potential of -90mV to between -20 and +30mV in 10mV increments. Tail currents were recorded at -70mV. Current traces measured in normal Ringer's solution (control) and after the addition of 100μM $CdCl_2$ and 100nM TTX to the Ringer's solution are shown. **B)** Summary of the data illustrated in **A**. Closed symbols represent the peak of the current onset and open symbols depict the peak values of the current tails. Circles = control; squares = in presence of $CdCl_2$ and TTX. Note that there was very little change in the magnitude of I_K.

A

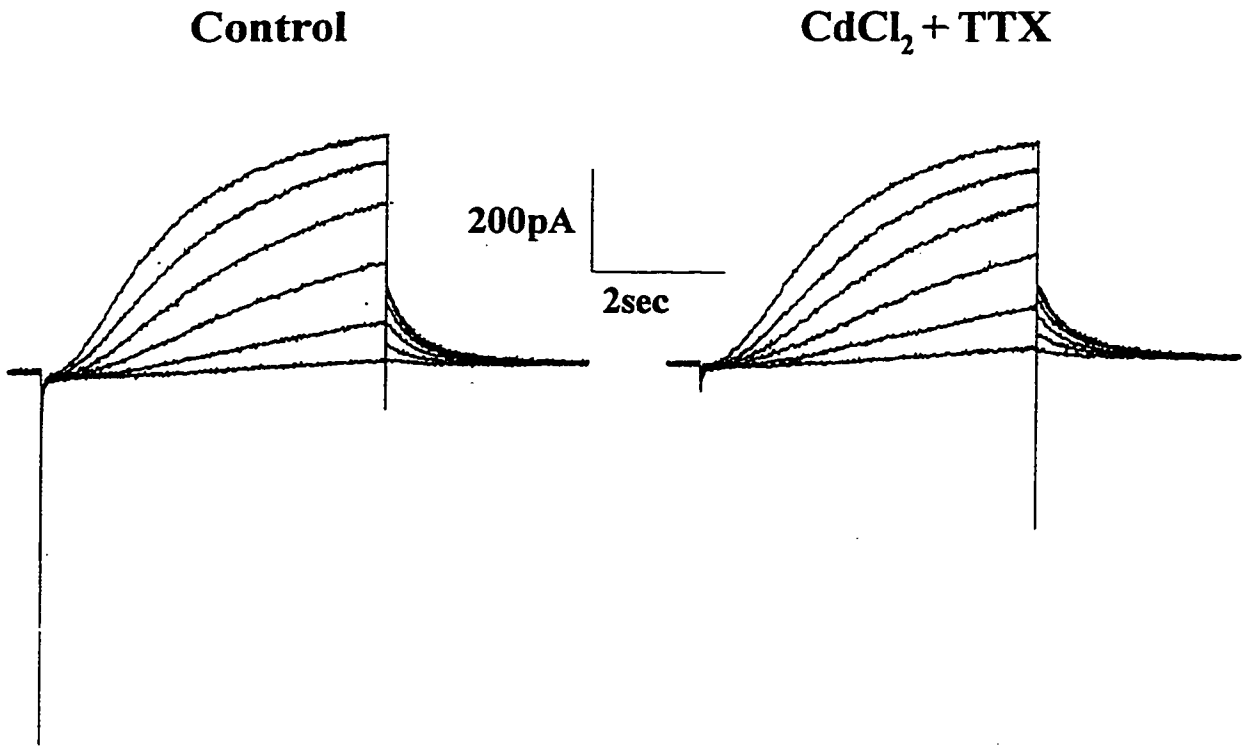
Control
CdCl2 + TTX
200pA
2sec

B

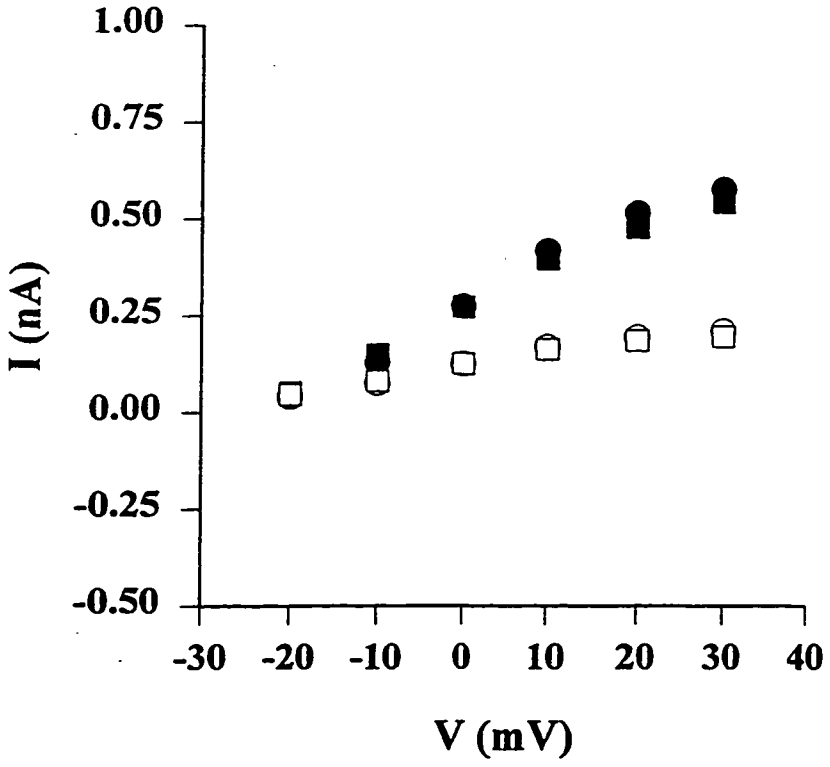
1.00
0.75
0.50
0.25
0.00
-0.25
-0.50
I (nA)
-30
-20
-10
0
10
20
30
40
V (mV)

Quasi-Instantaneous Current-Voltage Relationship

The fully-activated quasi-instantaneous current-voltage relationship provides a measure of the maximum current which can be generated by I_K over a selected range of potentials. The raw traces in Figure 7A depict representative current traces used to make these measurements. These traces were recorded from a single cell superfused with either 2.5 or 5mM extracellular KCl. Cells were held at -90mV and then depolarized to +30mV for 20 seconds to fully activate I_K. Tail currents were measured at voltages ranging from +20 to -120mV in 10mV increments. The bath solution was then replaced with Normal Ringer's solution containing 5mM KCl and the protocol was repeated. Figure 7B illustrates the quasi-instantaneous current-voltage relationship for I_K. Each point represents data averaged from 4-6 cells. The initial amplitude of the tail current immediately following the decay of the capacity transient was plotted as a function of voltage for all data points ranging from +30mV to -40mV. For those voltage steps more negative than -40mV it was necessary to eliminate the contribution of the inward rectifier K^+ current by subtracting the steady-state component of the tail current (taken at the end of the 15second pulse) from the peak. This value was then plotted as a function of voltage. The data were expressed as current density to account for variations in cell size. These results suggest that the ion transfer relationship of I_K is very nearly linear (ohmic) in the range of -120 to -50mV, however, a small degree of inward rectification can be seen at voltages positive to -40mV. Increasing the concentration of K^+ in the external bathing medium caused this I-V curve to shift to the right but did not significantly change its shape.

Envelope of Tails

One of the fundamental assumptions of many of the experiments described in this dissertation is that I_K in bullfrog atrium is composed of only one conductance, unlike other delayed rectifier K^+ channels found in mammalian tissue which consist of a slowly and a rapidly activating component (see Introduction for review). Hume and Giles (1986) and Simmons et al. (1986) have previously presented evidence for the presence of only a

Figure 7: Fully activated quasi-instantaneous current-voltage relationship for I_K. **A)** Representative current traces of I_K measured at two different extracellular K^+ concentrations in response to 20 second depolarizing pulses from a holding potential of -90mV to +30mV. Tail currents were measured at +20 to -120mV in 10mV increments. **B)** Summary of quasi-instantaneous I-V curve data. These values were calculated as described in the text and were normalized to account for cell capacitance. Data show mean ± SEM for 4-6 cells (2.5mM KCl) or 3-4 cells (5mM KCl) for all points.

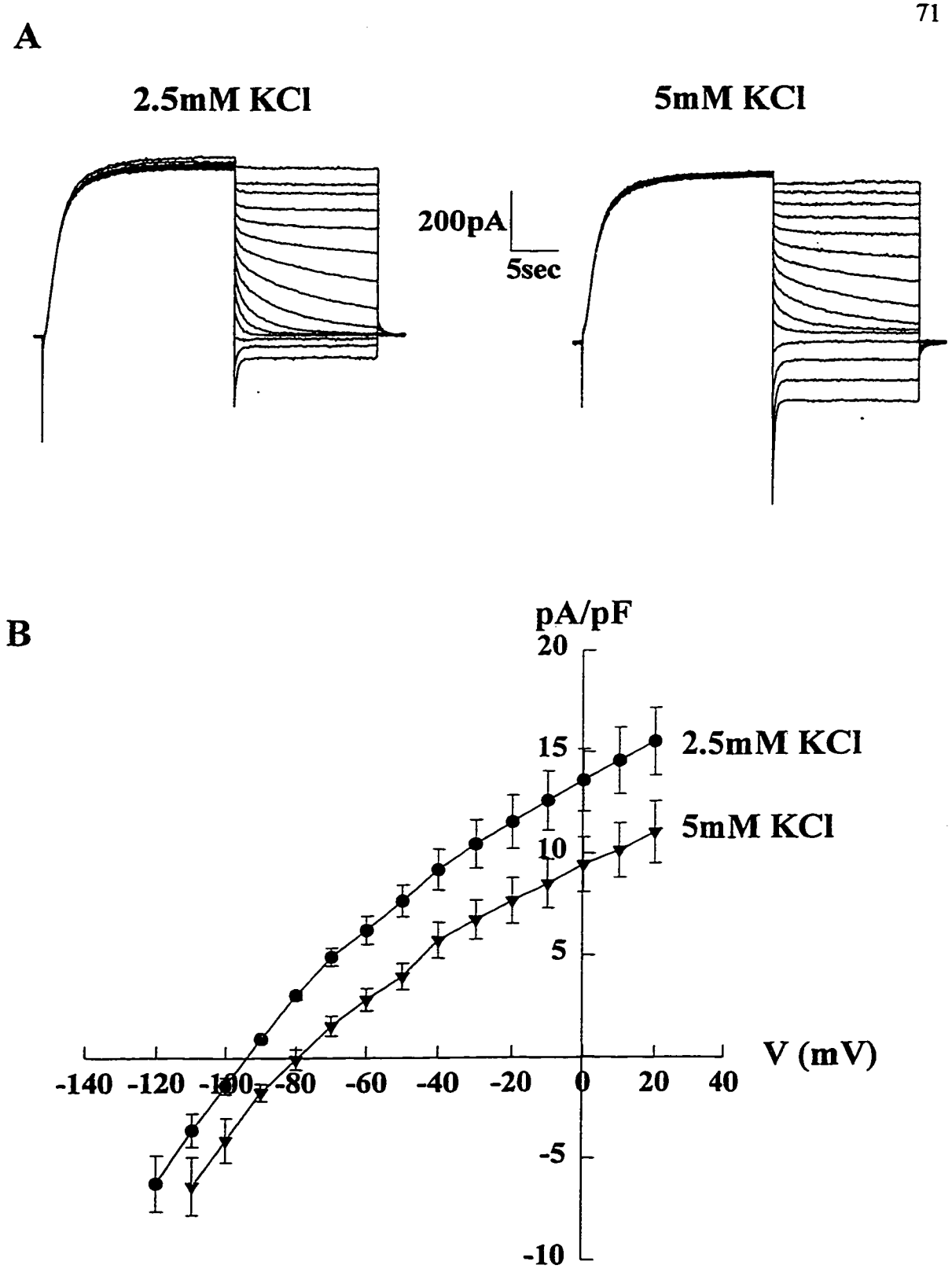
A
2.5mM KCl
5mM KCl
200pA
5sec
B
pA/pF
20
15
10
5
-5
-10
2.5mM KCl
5mM KCl
V (mV)
-140 -120 -100 -80 -60 -40 -20 0 20 40

single conductance underlying bullfrog I_K by using an envelope of tails test. We set out to determine whether we could corroborate these findings, and therefore utilize the same framework of analysis for the experiments outlined here. Figure 8A shows superimposed current traces obtained by applying depolarizing voltage steps to +30mV from a holding potential of -90mV for 1, 2, 3, 5, or 10. Current tails were recorded at -70mV. In order to establish whether I_K consists of a single component two criteria must be met. The first is that the time course of the initial tail current amplitudes (the envelope) must match that of the current onset (that is, the tail current amplitude does not change instantaneously as a function of time). In order to evaluate this, the peak amplitude of each current tail was plotted and the current onset was scaled in order to compare the time course. Figure 8B demonstrates that for the cell shown in Figure 8A this requirement is obeyed; there is a very close fit between the time course of the onset and tail currents. The ratio of I_{Ktail} to I_K (Sanguinetti and Jurkiewicz, 1990b; Sanguinetti and Jurkiewicz, 1991) was also calculated. Figure 8D shows summary data (n=6) for the I_{Ktail} / I_K ratio at a potential of -70mV, plotted as a function of pulse duration. This value stays constant regardless of pulse length, with a mean ratio of 0.310 ± 0.004, providing strong evidence that I_K is comprised of only a single population of channels.

The second criterion that must be met is that the time course of decay of the current tail must remain constant, regardless of the amplitude of the tail current. Figure 8C shows that over a range of tail amplitudes from 112 to 436 pA the deactivation tails from the myocyte shown in Figure 8A could be best fit with a single exponential function, thereby satisfying the envelope of tails test. Occasionally a double exponential provided a better fit (approximately 20%), although all data are reported using a single exponential function. Table 1 summarizes the time constant of decay of the deactivation tails as a function of pulse duration and potential for a total of 14 cells. Note that at -70 and -60mV the time constant of decay after a 1sec prepulse is smaller (ie. faster) than the other pulse durations. This was consistent between experiments and is similar to a previous report (Simmons et al., 1986).

Figure 8: Envelope of tails test for I_K in bullfrog atrium. **A)** Superimposed I_K current onsets recorded in response to 1, 2, 3, 5, or 10 second depolarizing voltage steps to +30mV from a holding potential of -90mV. Tail currents were measured at -70mV. **B)** Comparison of envelope of peak tail amplitudes with the time course of current onset. Peak amplitudes of the five tail currents shown in **A** were plotted as a function of time, as shown by the closed circles. The solid line represents the current onset that has been scaled by a factor of 3.1. Note that the time course of the envelope of tails matches closely with that of the scaled current onset. **C)** Letters **a** to **e** correspond to the current tails labelled in panel **A**. Solid lines show single exponential fits to each current tail. τ_n values for each trace are (a) 1 sec = 516msec, (b) 2 sec = 626msec, (c) 3sec = 667msec, (d) 5sec = 685 msec, and (e) 10sec = 683 msec. **D)** Ratio of the amplitude of I_{Ktail} (measured at -70mV) to I_K (n=6 for each point), plotted as a function of pulse duration. Where standard error bars cannot be seen it is because they are too small to be resolved. The solid line indicates the mean value of all 6 time points ($I_{Ktail}/I_K = 0.310$).

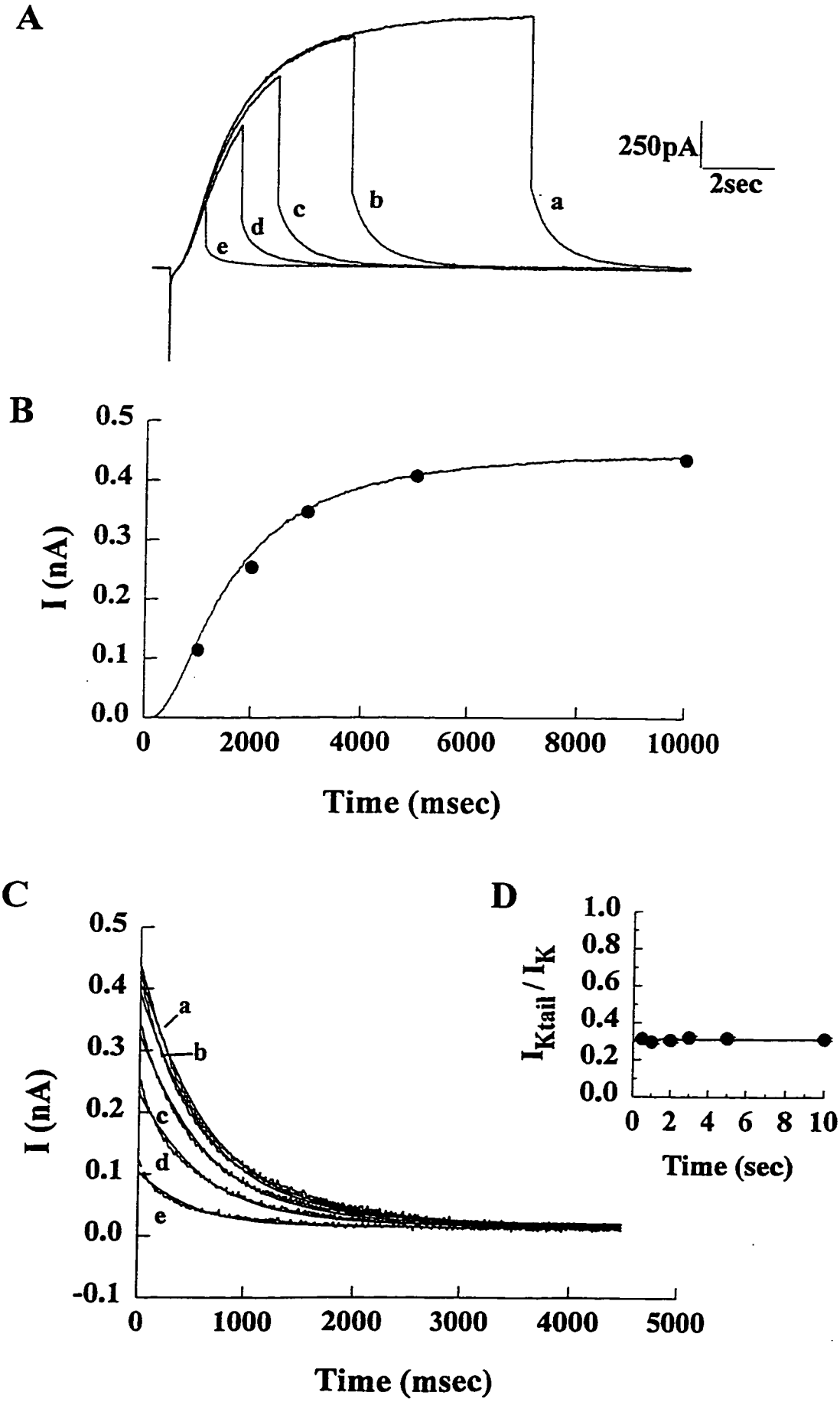
A
250pA
2sec
a
b
c
d
e
B
I (nA)
0.5
0.4
0.3
0.2
0.1
0.0
0
2000
4000
6000
8000
10000
Time (msec)
C
I (nA)
0.5
0.4
0.3
0.2
0.1
0.0
-0.1
0
1000
2000
3000
4000
5000
Time (msec)
D
I_{Ktail} / I_K
1.0
0.8
0.6
0.4
0.2
0.0
0
2
4
6
8
10
Time (sec)

Table 1: Summary τ_n values for envelope of tails test of I_K showing the effect of changing the prepulse duration and the membrane potential (P2) at which the current tails were measured. * indicates $p<0.05$ compared with τ_n measured after 1 sec depolarizing voltage pulse at each potential, as determined by a two-tailed paired Student's t-test.

Table 1: Summary Time Constants of I_K Tails at 3 Different Membrane Potentials

	P2 Membrane Voltage		
Duration of Activating Voltage Step	**-80mv (n=5)**	**-70mV (n=6)**	**-60mv (n=3)**
1sec	--	545.6 ± 46.3	1277.5 ± 69.6
2sec	--	654.3 ± 77.3*	1459.0 ± 65.7
3sec	--	708.7 ± 50.7*	1493.1 ± 53.6
5sec	433.8 ± 31.2	715.0 ± 55.7*	1540.7 ± 61.4
10sec	437.8 ± 30.9	696.0 ± 45.1*	1599.0 ± 61.2*
20sec	430.2 ± 32.6	--	1592.4 ± 94.8*

All current tails were fitted to a single exponential function. Data represent mean ± SEM (in msec).

Kinetics of I_K

The kinetics of activation and deactivation of I_K are shown in Figure 9. As described previously, the onset of activation of I_K is best fit by an exponential function raised to the second power. Therefore, at voltages positive to -50mV (the potential at which I_K begins to activate) onset currents elicited by long voltage pulses (30sec) were fitted with the equation:

$$I_K = I_{K\infty} [1-\exp(-t/\tau_n)]^2$$

where $I_{K\infty}$ is the fully activated current and τ_n is the time constant of activation. At potentials negative to the activation threshold current tails elicited by a two-pulse protocol (test pulse +50mV for 3sec, second pulse -50 to -120mV in 5mV increments) were fitted with a single exponential function:

$$I_K = I_{Ko}[\exp(-t/\tau_n)]^2$$

where I_{Ko} is the value of the I_K tail at t=0.

Based on a knowledge of the steady-state activation and time constant values, manipulation of the equations:

$$n_\infty = \alpha_n/(\alpha_n + \beta_n)$$

$$\tau_n = 1/(\alpha_n + \beta_n)$$

allowed us to determine the voltage dependence of opening (α_n) and closing (β_n) of I_K. The data in Figure 9 was curve-fit with the resultant equations

$$\alpha_n = \frac{0.0128\,(Vm + 28.49)}{1-\exp[-0.0803(V_m + 28.49)]}$$

and

$$\beta_n = 0.2679 \exp[-0.0259(V_m + 28.49)],$$

as shown by the dashed lines. These results suggest that I_K activates with a time constant of approximately 650msec at +30mV and decays with a time constant of approximately

1sec at -60mV, consistent with I_K contributing to action potential repolarization (see Discussion).

K^+ Accumulation

Simmons et al. (1986) reported the presence of numerous small caveolae on the surface of bullfrog atrial myocytes. It is possible that K^+ ions could accumulate in these caveolae during the prolonged activation of I_K and thereby change the reversal potential. The extent of accumulation was therefore evaluated using the same protocol described previously for measuring the reversal potential, except that the test pulse to +50mV was applied for 1, 5, 10, or 20 sec. Raw current traces recorded in response to a 1sec or 10sec test pulse are illustrated in Figure 10A. Note that the reversal potential remained at approximately -94mV regardless of pulse duration. Figure 10B summarizes the effect of varying pulse duration on reversal potential in 3 different experiments. In all such experiments increasing pulse duration did not significantly change the reversal potential. These findings show that K^+ accumulation is not a significant problem on the surface of isolated bullfrog atrial myocytes.

Effect of Class III Antiarrhythmics

Clofilium tosylate and azimilide, two new agents being evaluated as class III antiarrhythmics, have been previously shown to inhibit the slowly activating delayed rectifier K^+ current in mammalian tissue (Li et al., 1996; Arena and Kass, 1988; Busch et al., 1994a). We therefore investigated whether these compounds could also inhibit I_K in bullfrog atrial cells. Figure 11A shows the effect of 50μM clofilium on I_K. At this concentration clofilium blocked the current onset by 47.5 ± 4.2% (n=3), which is similar to results previously reported in guinea pig ventricular myocytes (Li et al., 1996). Block by clofilium was irreversible; there was virtually no recovery in the current amplitude after 10 minutes of drug washout. Clofilium also significantly inhibited I_{Ca} at this concentration, although an exact measurement of the magnitude of block is difficult due to contamination of the records with I_{Na}. Figure 11B illustrates the effect of 10μM

Figure 9: Kinetics of I_K as a function of membrane potential. I_K current onsets (-40 to +50mV) and current tails (-120 to -50mV) were curve fit to obtain the time constant (τ) of activation and deactivation, as described in the text. Data are shown as mean ± SEM of 4-5 cells (current onsets) or 4-6 cells (current tails) for each point. Dashed lines represent the opening (α) and closing (β) rate constants (see text for further explanation).

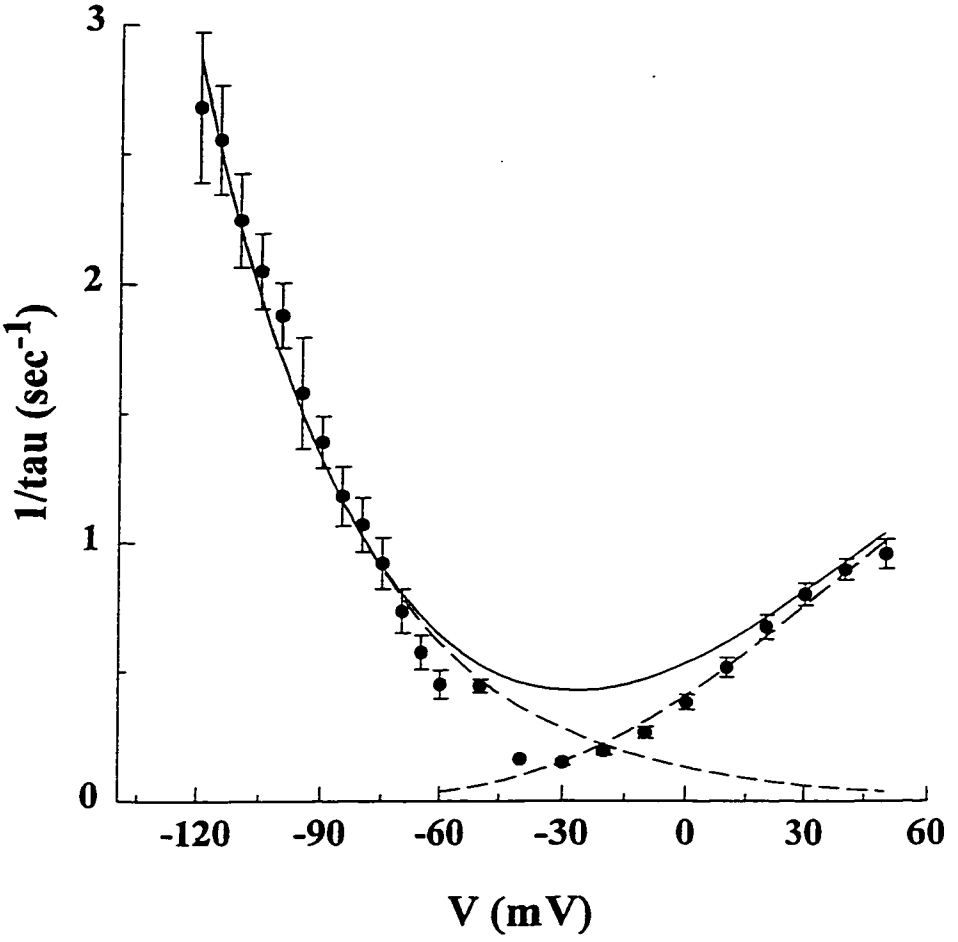
3
2
1
0
1/tau (sec-1)
-120
-90
-60
-30
0
30
60
V (mV)

Figure 10: Test for K^+ accumulation in bullfrog atrial myocytes. A voltage protocol similar to that described in Figure 4 was applied, except that the duration of the test pulse was varied to 1, 5, 10, or 20 seconds. The superimposed current traces show the reversal potential after a 1 (**A**) or 10 (**B**) second test pulse in the same cell. Note the reversal potential does not change, regardless of pulse duration. **C**) Summary data describing the lack of effect of changing pulse duration on reversal potential (n=3). These results suggest that no K^+ accumulation occurs on the surface of bullfrog atrial myocytes.

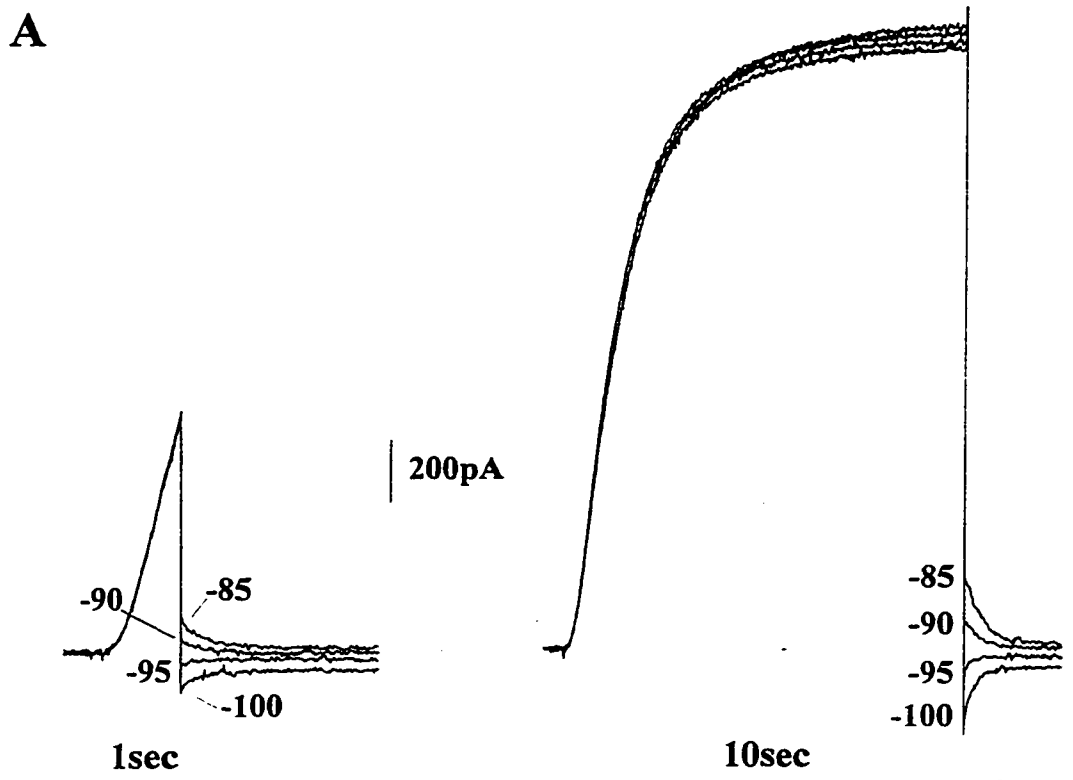
A
200pA
-90
-85
-95
-100
1sec
-85
-90
-95
-100
10sec

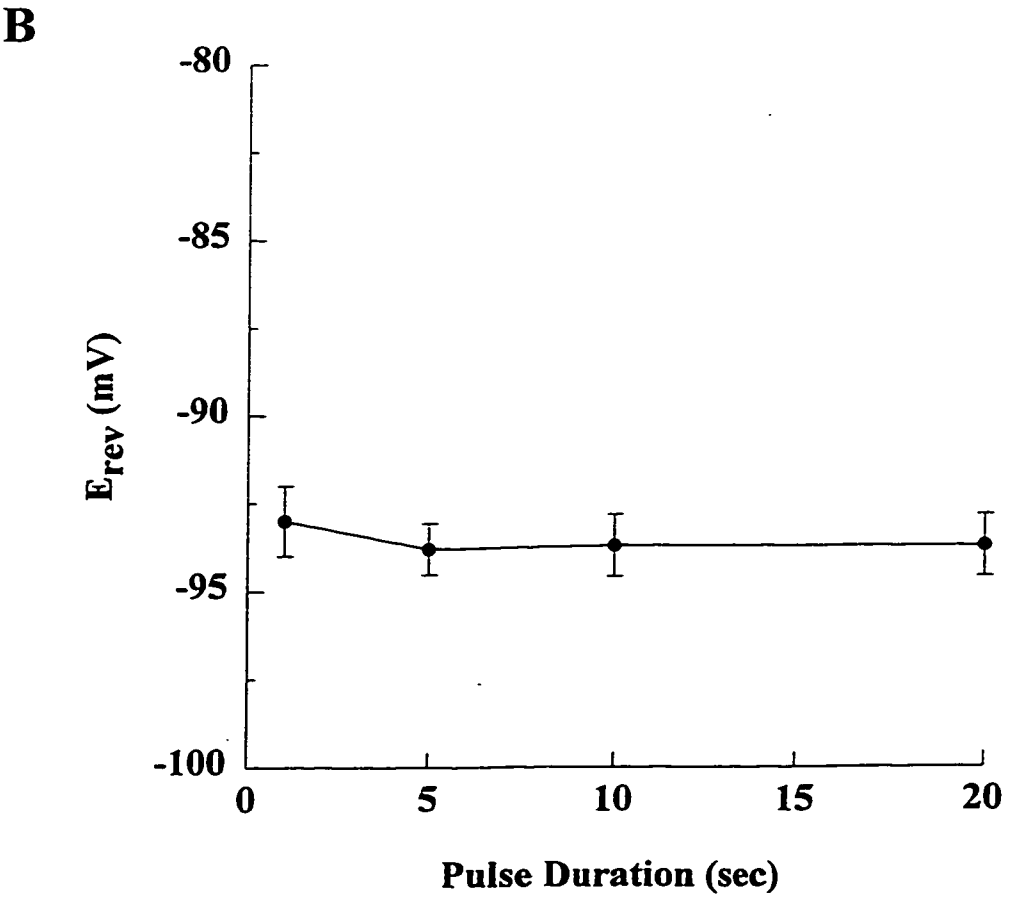
B
-80
-85
-90
-95
-100
E_{rev} (mV)
0
5
10
15
20
Pulse Duration (sec)

Figure 11: Effect of bath application of clofilium tosylate and azimilide on I_K. In both **A** and **B** 3 second depolarizing voltage steps to +30mV from a holding potential of -90mV were applied. **A)** Clofilium (50μM) blocked I_K by about 50% and there was virtually no recovery of this inhibitory response, even after washout of the drug for 8 minutes. Clofilium also inhibited I_{Ca} at this concentration. **B)** Azimilide (10μM) diminished the amplitude of I_K current onset and tail by approximately 50%. The current recovered partially after washout of azimilide. Small inhibitory effects were also observed on I_{Ca} (data not shown).

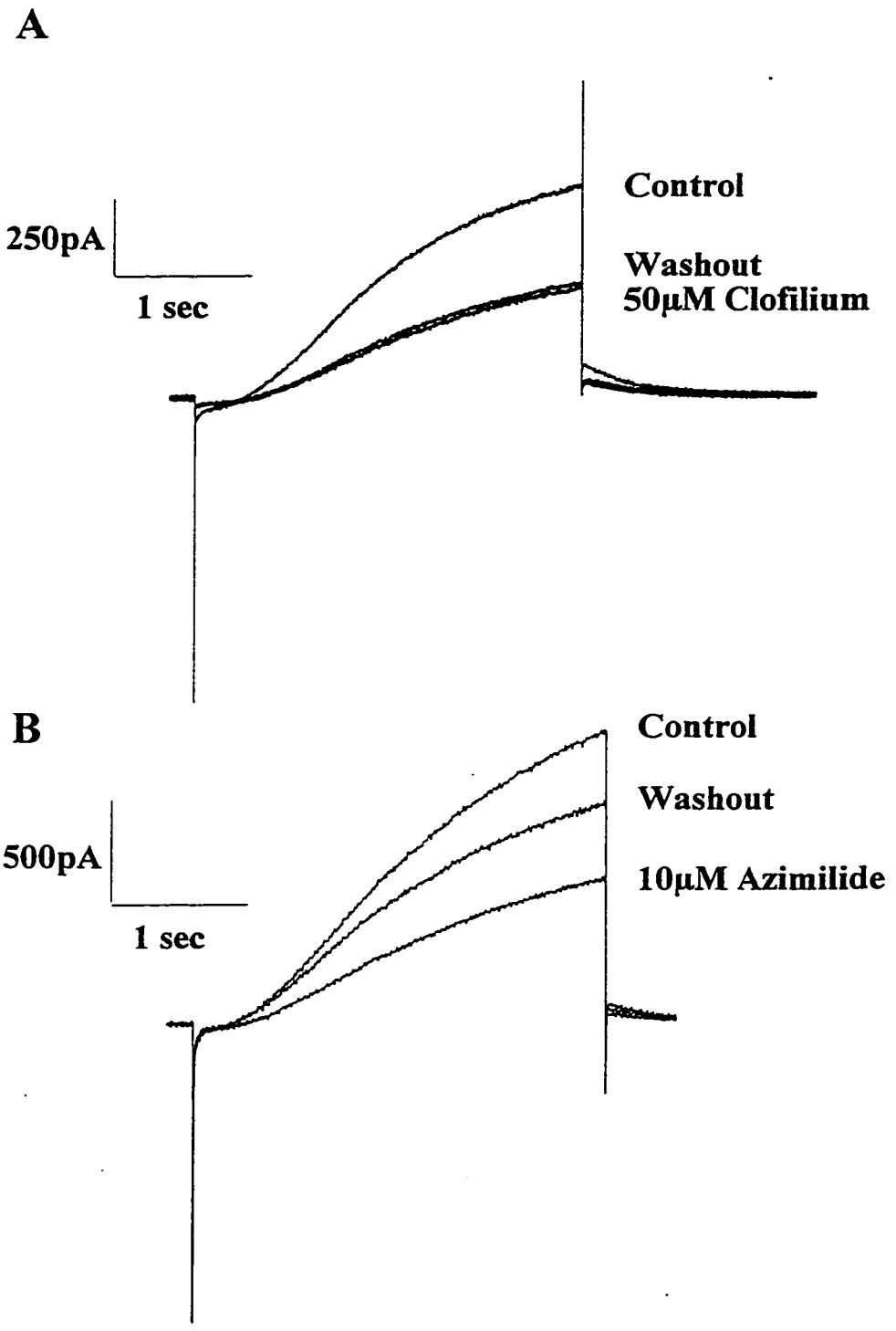
A
250pA
1 sec
Control
Washout
50μM Clofilium
B
500pA
1 sec
Control
Washout
10μM Azimilide

Figure 12: Effect of bath application of inhibitors of I_{Kr} on I_K in bullfrog atrial myocytes. Superfusion of bullfrog atrial myocytes with 10μM E-4031 (**A**), 1μM dofetilide (**B**), or 1μM MK-499 (**C**), was without significant effect on I_K. Current traces were elicited by a 5 sec depolarizing voltage step from a holding potential of -90mV to +30mV (**A, C**) or +40mV (**B**).

A

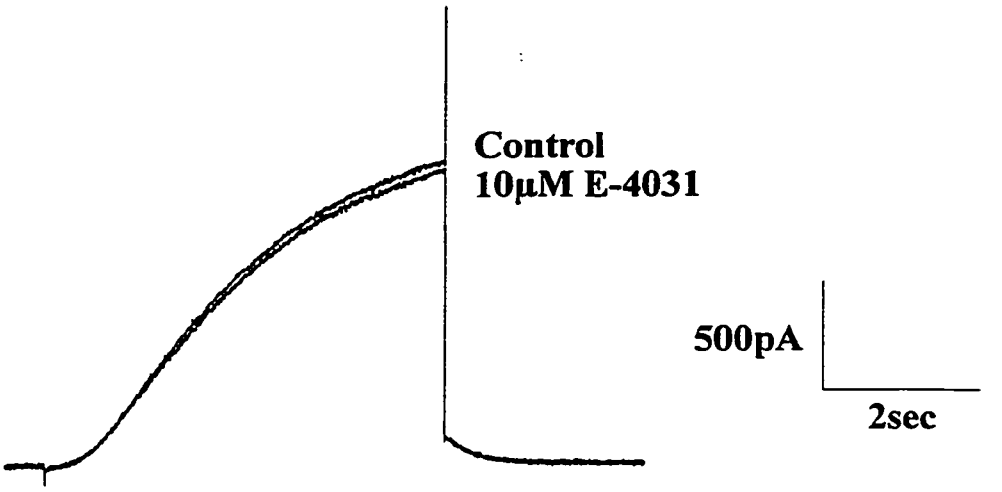
Control
10μM E-4031
500pA
2sec

B

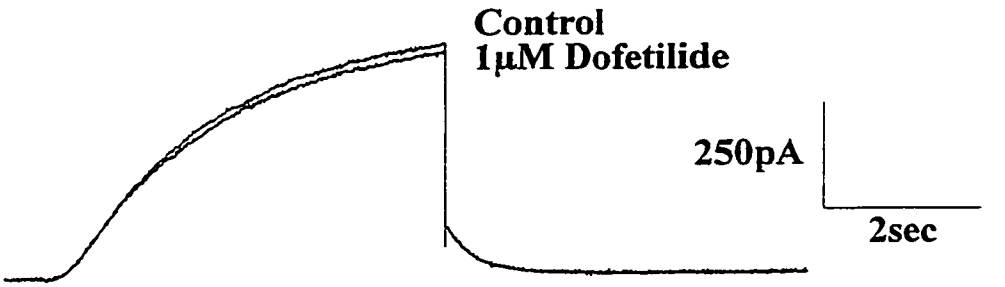
Control
1μM Dofetilide
250pA
2sec

C

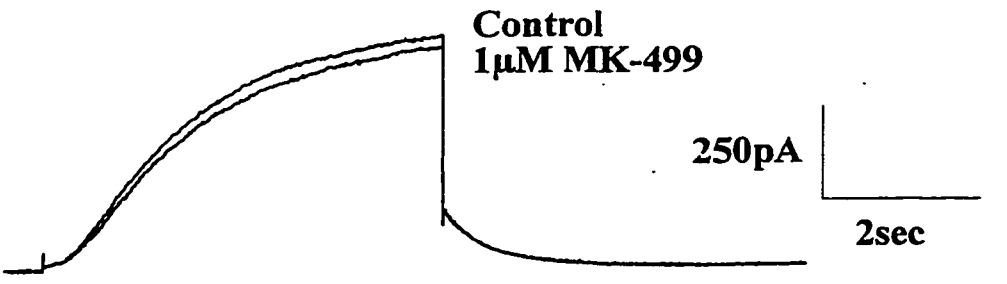
Control
1μM MK-499
250pA
2sec

azimilide on I_K. At this concentration azimilide decreased the magnitude of I_K by 48.7 ± 3.7% (n=7). The inhibition by azimilide was partially reversible upon washout, although we did not observe complete recovery of the response in any of our experiments. Azimilide also partially inhibited I_{Ca}, although this effect is difficult to distinguish at the time scale shown in Figure 11B. The mechanism and concentration-dependence by which azimilide blocks I_K, and also a more direct look at the effects of azimilide on I_{Ca}, is discussed in detail in Chapter 4 of this dissertation.

E-4031, a class III antiarrhythmic agent which blocks the rapid component of the delayed rectifier in guinea pig ventricular myocytes (IC_{50} of 397nM; (Sanguinetti and Jurkiewicz, 1990), was without significant effect on I_K at a concentration of 1 (n=3) or 10 (n=2) μM. Furthermore, MK-499 and dofetilide, two other compounds which also inhibit I_{Kr} (IC_{50} 43.9nM and 31.5nM, respectively) (Lynch et al., 1994; Jurkiewicz and Sanguinetti, 1993a), did not significantly inhibit I_K at a concentration of 1μM. Representative results showing the effect of these agents on I_K are shown in Figures 12A, B, and C.

Discussion

These experiments have described the characteristics of the time- and voltage-dependent K^+ current in bullfrog atrial myocytes. Consistent with previously published reports on bullfrog I_K (Hume et al., 1986; Simmons et al., 1986), our data show that this current is comprised of a single Hodgkin-Huxley like conductance with an activation variable (n) raised to the power of two. This current is carried mainly by K^+ ions and has a linear fully-activated quasi-instantaneous current-voltage relationship with a small degree of inward rectification. The kinetics of activation and deactivation of this K^+ current are consistent with it playing a major role in action potential repolarization. We also show that I_K is inhibited by clofilium and azimilide, two agents which block I_{Ks} in mammalian tissue, but is not significantly affected by application of three compounds known to inhibit I_{Kr}, E-4031, dofetilide, and MK-499. These results are consistent with

the delayed rectifier in bullfrog atrium being comprised of a single population of channels resembling I_{Ks}.

Early studies on the delayed rectifier in multicellular trabeculae dissected from bullfrog atria were hindered by accumulation of K^+ ions during the long voltage clamp steps used to measure this current (Brown et al., 1976a; Brown et al., 1976b). This phenomena can significantly alter the characteristics of, in particular, the inward rectifier K^+ current, and can lead to errors in data interpretation and analysis. In agreement with previous reports (Hume et al., 1986; Simmons et al., 1986), we have shown that there is no significant shift in the reversal potential of I_K with increasing pulse duration, proving that there is no substantial accumulation of K^+ on the surface of bullfrog atrial myocytes. This preparation can therefore be used for quantitative study of the characteristics of I_K.

I_K activates with a characteristic sigmoid time course which becomes less pronounced at more depolarized voltage steps. One potential explanation for this sigmoidicity is that activation of I_K is controlled by increases in intracellular calcium; that is, this conductance may actually be a Ca^{++}-activated K^+ current. Inhibition of I_{Ca} with $CdCl_2$, however, did not significantly affect I_K, suggesting that influx of Ca^{++} into the cell is not required for I_K activation. Similar results were found by Simmons et al. (1986) after block of I_K with $CdCl_2$, and also by Hume and Giles (1986) after inhibition of I_K with $LaCl_3$. In addition, the recordings reported in this study were made with 1mM EGTA in the pipette solution and therefore with very low levels of free intracellular Ca^{++} (estimated pCa>8), further suggesting that activation of I_K is not Ca^{++}-dependent.

Instead, the sigmoid time course of I_K activation can be best described by a single conductance with an activation variable raised to the power of two. Attempts were also made to fit the current onset traces with a n^3 model, but consistently a n^2 model gave better results. In addition, our envelope of tails test supports previous reports (Hume et al., 1986; Simmons et al., 1986) describing only a single conductance underlying I_K. We have shown that the time course of deactivation of I_K can be best fit with a single exponential function, and the time course of the initial tail current amplitudes closely matches that of the current onset. Furthermore, the ratio of I_{Ktail} to I_K is constant regardless

of pulse duration. This method of analysis has previously been used to separate two components of current, I_{Ks} and I_{Kr}, in guinea pig ventricular (Sanguinetti and Jurkiewicz, 1990b) and atrial (Sanguinetti and Jurkiewicz, 1991) myocytes. Surprisingly, although the envelope of tails test was satisfied for all the criteria listed above, the time course of decay of I_K at short pulse durations (1sec) was significantly faster than the longer pulse lengths. This result was very reproducible and has been previously reported by Simmons et al. (1986) in bullfrog atrial myocytes. It is possible that this change in the decay rate could represent the presence of another, previously unidentified, current in bullfrog atria that activates in response to short depolarizing voltage pulses. The fact that the ratio of I_{Ktail} to I_K does not change with pulse durations ranging from 0.5-10 sec, however, suggests that this current does not substantially contribute to the outward current and does not significantly effect our analysis of I_K.

In summary, the results presented here suggest that I_K in bullfrog atria, in agreement with previous reports (Hume et al., 1986; Simmons et al., 1986), is composed of a single conductance which closely resembles I_{Ks} in mammalian cardiac tissue. This preparation can therefore be used to advantage for studies of the molecular, electrophysiological and pharmacological properties of I_{Ks}.

CHAPTER 4:

COMPARISON OF I_K IN BULLFROG ATRIA TO RAT UTERINE MINK EXPRESSED IN *XENOPUS* OOCYTES

Introduction

As described in Chapter 1 of this dissertation, expression of minK in *Xenopus* oocytes induces a slowly activating, time- and voltage-dependent K^+ current that qualitatively resembles I_{Ks} identified in some tissues in mammalian heart and I_K in bullfrog cardiac tissue. These findings have led to the proposal that minK encodes for I_{Ks}, although there has been no detailed quantitative comparison of minK expressed in *Xenopus* oocytes with I_{Ks} in native tissue. In the previous chapter, evidence was presented showing that I_K in bullfrog atrial myocytes expresses only a single component of the delayed rectifier that resembles I_{Ks}. In this study we have compared the biophysical and pharmacological properties of bullfrog I_K with those of rat uterine minK expressed in *Xenopus* oocytes, in an attempt to determine whether an amphibian isoform of minK could underlie this native delayed rectifier K^+ current. Our results demonstrate close similarities between the electrophysiological properties of minK and I_K in bullfrog atrial myocytes, and very similar responses to two pharmacological agents known to inhibit I_{Ks} (Busch et al., 1994a; Salata et al., 1996b), azimilide and propenamide (L735-821).

Results

Unless otherwise stated, in all electrophysiological experiments on bullfrog atrial myocytes the holding potential was -90mV, and in *Xenopus* oocytes the holding potential was -80mV. All experiments were performed at room temperature (20°C). Data are reported as mean ± SEM.

Biophysical Characteristics

Comparison of Current Waveforms

Figure 13 illustrates representative traces of I_K recorded from bullfrog atrial myocytes (A) and minK recorded from *Xenopus* oocytes (B). Depolarizing voltage steps from -50 to +50mV were applied to the myocytes for 30 sec and tail currents were measured at -70mV. Oocytes were stepped from -60 to +40mV for 30 sec and tail

currents were measured at -60mV. Voltage steps were elicited every 50 sec. Activation of both I_K and minK results in a very slow outward K^+ current that increases in magnitude and activates more quickly as voltage becomes more positive. Note, however, that although I_K reaches a plateau by the end of the 30 sec depolarizing steps, minK continues to rise, ie. it does not saturate under these conditions (see Discussion).

Steady State Voltage Dependence

The 'steady-state' voltage dependence of I_K and minK activation are shown in Figures 14A and 14B, respectively. The peak amplitude of the tail currents after 30 sec depolarizing voltage pulses (representative traces shown in Figure 13) was chosen as a measure of the 'steady state' activation of I_K and minK. The 'steady state' activation variable (n_∞) was calculated as previously described (see Chapter 3). These calculations were based on the assumption that both I_K and minK could be described by a single gating variable (n) raised to the power of 2. The data were fit with a Boltzmann function from which the half point of activation and slope factor were determined to be, respectively, -27.6mV and 13.3 for I_K, and -22.6mV and 15.1 for minK. Note that the threshold for activation of both K^+ currents is approximately -50mV and the currents appear to fully activate at +20 to +30mV. It is important to note that, in the case of minK, measurement of the steady-state voltage relationship is not possible because this current does not saturate even after voltage pulses up to 60 sec in length. We therefore arbitrarily chose to measure the voltage dependence of activation of minK after a 30sec depolarizing voltage step, as previous measurements for I_K had been taken at this time frame (see Figure 5, Chapter 3). Thus, the curve shown in Figure 14B for minK is an isochronal activation relationship.

Current-Voltage Relationship

Accurate calculation of the fully-activated quasi-instantaneous I-V curve from tail current amplitudes, as described for I_K in Chapter 3, requires that the test pulse be long enough to allow the onset current to reach steady state. As stated previously, minK does

Figure 13: Representative traces of I_K (**A**) and minK (**B**) recorded in response to 30 second depolarizing voltage steps from the holding potential in the range -50 to +50mV (I_K) or -60 to +40mV (minK) in 10mV increments. Tail currents were measured at -70mV (I_K) or -60mV (minK).

A **Bullfrog I_K**

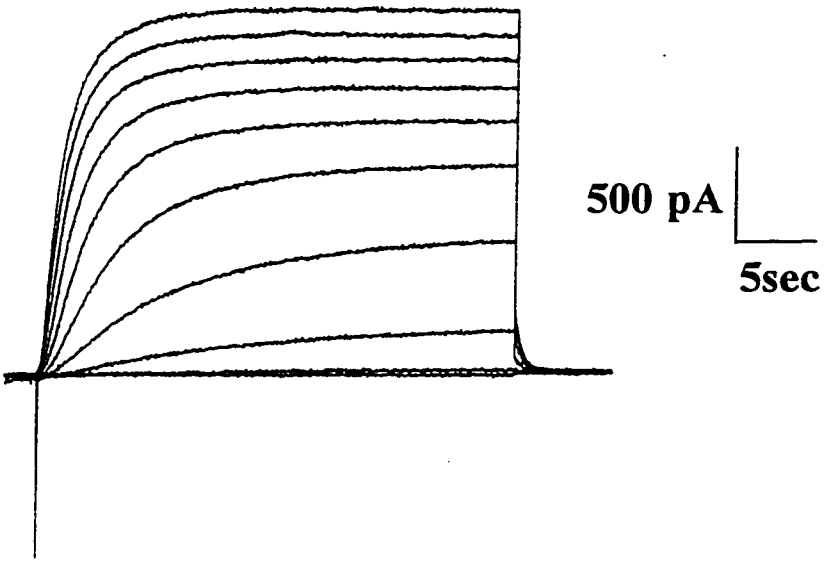

B **Rat uterine minK**

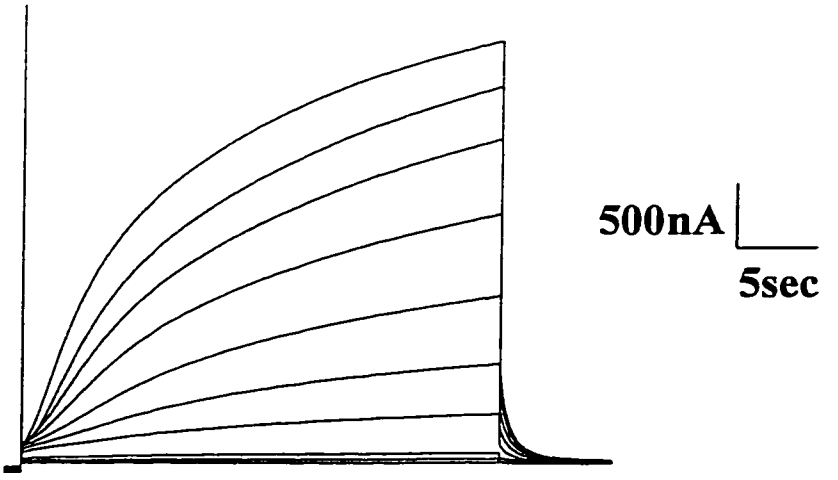

Figure 14: Steady-state activation curves (n_∞) for I_K (n=8) and minK (n=6). Data are presented as mean ± SEM. n_∞ values were calculated by normalizing the tail current amplitudes to the maximum value and then accounting for the second-power relationship of the gating variable n, as described in the text. Data points were fitted to a Boltzmann distribution. Values for $V_{1/2}$, the half-activation potential and K, the slope factor, are reported in each panel of the Figure. Where error bars cannot be seen it is because they are too small to be resolved.

A

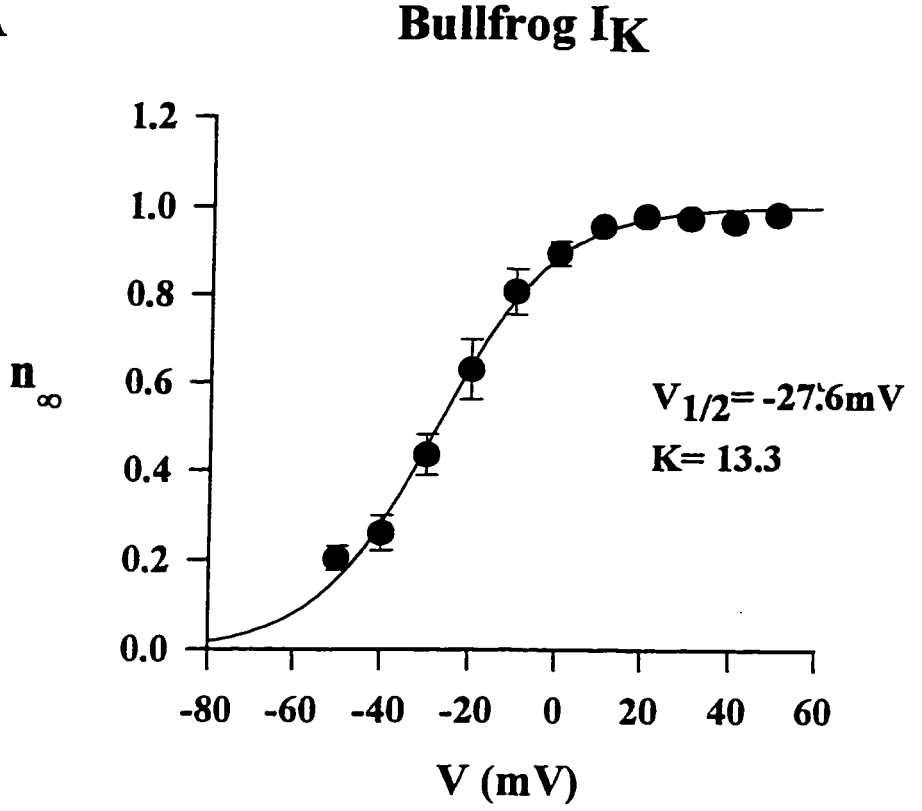
Bullfrog I_K
1.2
1.0
0.8
0.6
0.4
0.2
0.0
n_∞
$V_{1/2}$= -27.6mV
K= 13.3
-80 -60 -40 -20 0 20 40 60
V (mV)

B

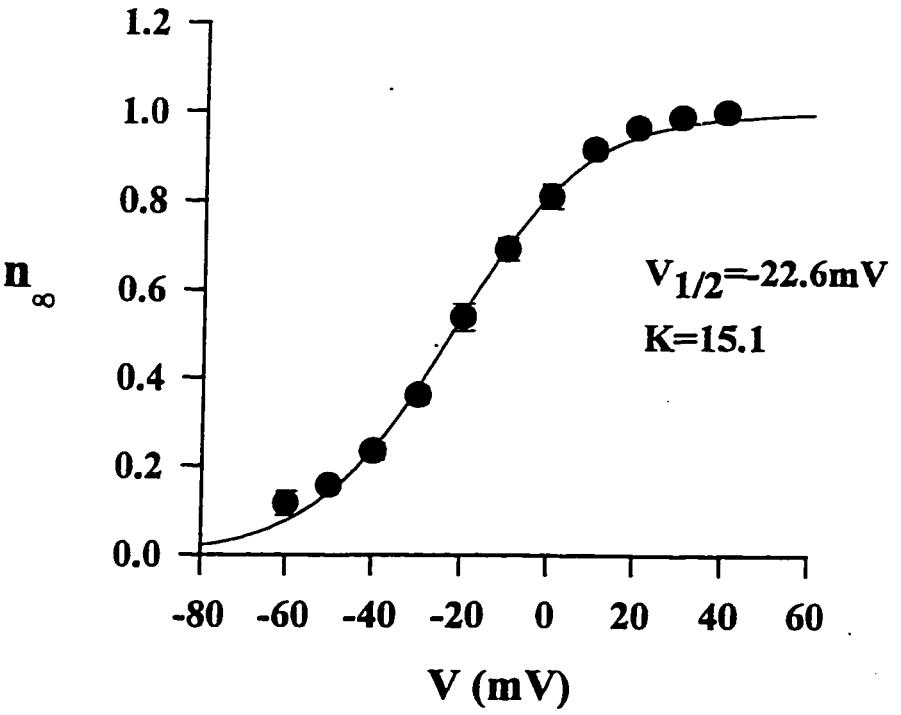
Rat uterine minK
1.2
1.0
0.8
0.6
0.4
0.2
0.0
n_∞
$V_{1/2}$=-22.6mV
K=15.1
-80 -60 -40 -20 0 20 40 60
V (mV)

not appear to reach steady state, therefore it is difficult to make a quantitative comparison of this characteristic for these two K^+ currents. Instead, we chose to plot the I-V curve by measuring the peak of the current onset after 30 sec depolarizing steps from -60 to +40mV (I_K) or -50 to +50mV (minK). Figure 15 illustrates this isochronal I-V relationship for both I_K (A) and minK (B). Note that the shape of the I-V curve and the threshold for activation for both currents are similar, suggesting I_K and minK share similar ion transfer characteristics.

K^+ Selectivity

The K^+ selectivity of I_K and minK was compared by measuring the reversal potential of the two currents following selected changes in $[K^+]_o$, using a conventional two-pulse protocol. Depolarizing pulses to +50mV (I_K) or +20mV (minK) were applied for 3sec (I_K) or 1sec (minK), followed by repolarizing pulses to potentials near the calculated reversal potential. The membrane potential at which there was no net tail current was defined as the reversal potential, and this value was determined by interpolation. The reversal potential for I_K in 2.5mM external KCl was -93.8 ± 0.6mV (n=14) and for minK in 2mM KCl was -103.3 ± 1.7mV (n=3). These values are very close to that predicted by the Nernst equation for a K^+ selective current (predicted values: I_K -95.5mV, when $[K^+]_i$ = 110mM and T = 20°C; minK -106.3mV when $[K^+]_i$ = 135mM and T=20°C). Figure 16 summarizes the shift in reversal potential when the concentration of K^+ bathing the cells is increased. The data were fit with a best fit straight line which gave a slope of 56.4mV (minK) or 50.1mV (I_K) /10 fold change in $[K^+]_o$. These results indicate that both I_K and minK are K^+ selective currents.

Pharmacology

Concentration Dependence of Azimilide Block

The top panels in Figure 17 show representative traces of I_K and minK recorded under control conditions (**C**), following steady-state block due to 10μM azimilide (**D**), and after washout of the drug (**W**). These currents were elicited in response to 3 sec (I_K)

Figure 15: Isochronal (30sec) I-V relationship for I_K (**A**) and minK (**B**). Data show mean ± SEM for 8 cells each. The values represent the maximum outward current during a 30 sec depolarizing pulse to the membrane voltages indicated.

A

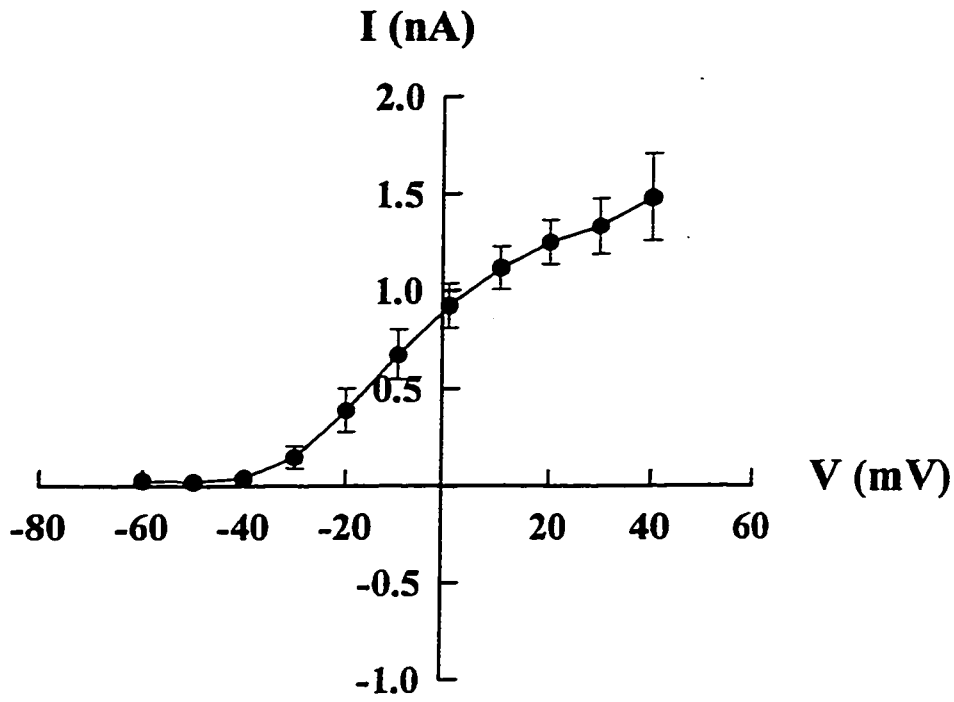
Bullfrog I_K
I (nA)
2.0
1.5
1.0
0.5
-0.5
-1.0
V (mV)
-80
-60
-40
-20
20
40
60

B

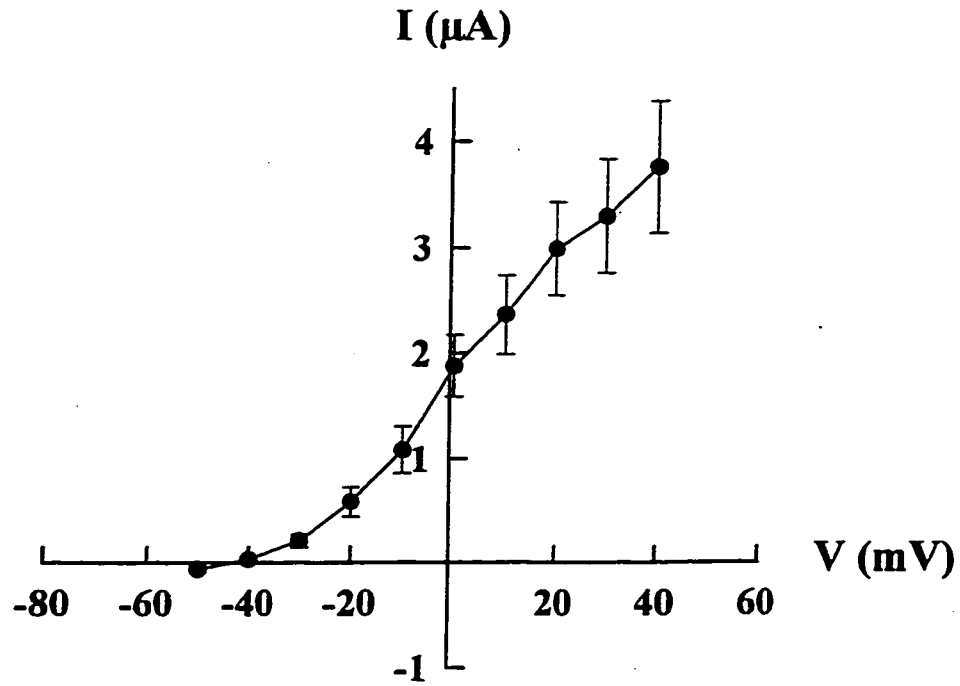
Rat uterine minK
I (μA)
4
3
2
1
-1
V (mV)
-80
-60
-40
-20
20
40
60

Figure 16: Measurements of selectivity of I_K and minK. Reversal potential was measured following 3 second (I_K) or 1 second (minK) depolarizing voltage steps to +30 (I_K) or +20mV (minK). These values were plotted as a function of extracellular [K^+] and fit with a straight line giving a slope of 50.1 mV (I_K) or 56.4mV (minK) /10 fold change in $[K^+]_o$. n values for I_K data points were 14, 7, and 8 at 2.5, 5, and 10mM KCl respectively, and for minK were 3, 5, and 5 for 2, 5, and 10mM KCl respectively.

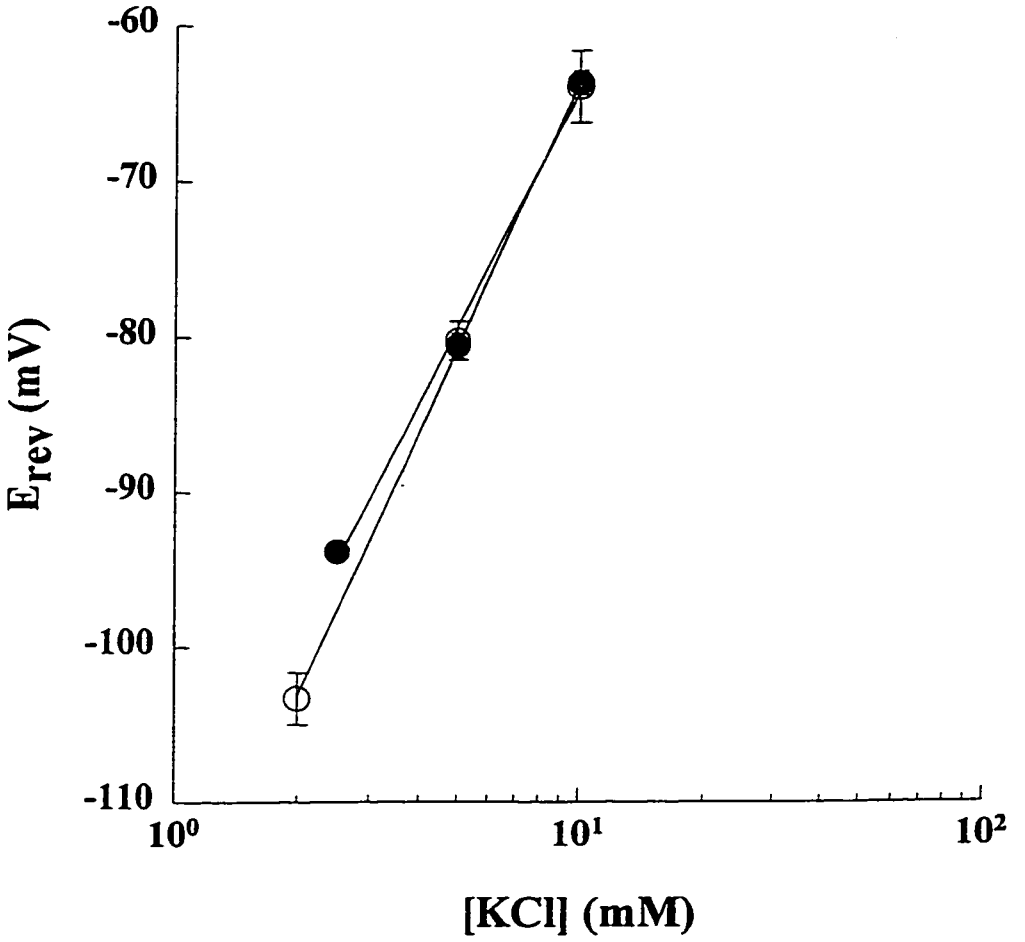

○ minK; Slope = 56.4 mV/10 fold change in $[K^+]_o$

● I_K; Slope= 50.1 mV/10 fold change in $[K^+]_o$

or 5 sec (minK) depolarizing steps to +30mV (I_K) or +20mV (minK). Development of azimilide block occurred shortly after exchange of the bath solution with drug-containing superfusate and was complete after 2-3 min (I_K) or 5-6 min (minK). This variability in the time course of drug block may be due to the different lipid composition of the plasma membrane of the myocytes vs the oocytes. The effects of azimilide on both I_K and minK were reversible, although complete recovery of the inhibitory response was not obtained in any of our experiments. Davies et al. (1996b) have also reported difficulty in completely reversing the effects of this drug.

The lower panel in Figure 17 summarizes the concentration-dependence of azimilide-induced block for I_K and minK. The % block was calculated by normalizing the conductance at the peak of the current onset to that measured under control conditions for a 3 sec (I_K) or 5 sec (minK) depolarizing step to +30mV (I_K) or +20mV (minK). These values were measured after steady-state block had developed following the administration of azimilide (0.5-500μM). In the case of minK, the % block was calculated after the peak current was adjusted to account for instantaneous endogenous currents (see Materials and Methods). Only those experiments which lasted long enough for steady-state block to be reached and partial washout of the drug response to be observed were included in the analysis. Data points were fitted by the function:

$$\%\text{block} = a/(1+(Kd/[\text{azimilide}])^{n_H})$$

where a=maximal block and n_H= Hill coefficient. Azimilide blocked I_K with a Kd of 11.2 ± 2.8μM and minK with a Kd of 7.2 ± 1.9μM when the Hill coefficient was set to 1. When the Hill coefficient was not constrained these values were 9.2 ± 0.6μM (n_H = 1.47 ± 0.12) and 6.6 ± 1.8μM (n_H = 1.17 ± 0.36), respectively. Maximal block in both preparations was observed at approximately 200μM, although the magnitude of block was greater in the myocytes (92.1 ± 1.2%) than the oocytes (83.9 ± 3.1%). This likely partially reflects the inability of azimilide to completely block time-dependent background currents which are endogenous to the *Xenopus* oocyte (see below).

Figure 17: Effect of bath application of azimilide (10μM) on I_K and minK. **A)** Representative current traces recorded under control conditions (**C**), in the presence of drug (**D**), and following washout (**W**). Azimilide decreased the amplitude of the current in response to depolarizing voltage steps to +30mV (I_K) or +20mV (minK) from a holding potential of -90mV (I_K) or -80mV (minK). The currents recovered partially upon washout. **B)** Summary of the concentration-dependence of azimilide-induced block of I_K (open circles, dashed line) and minK (closed circles, solid line). Data represent the % block of the maximum outward current at the end of a 3 second (I_K) or 5 second (minK) depolarizing pulse to +30mV (I_K) or +20mV (minK), relative to control. Values are expressed as mean ± SEM, with a minimum of n=3 for all points. The experimental data were fit with a Hill equation (n_H=1), as described in the text.

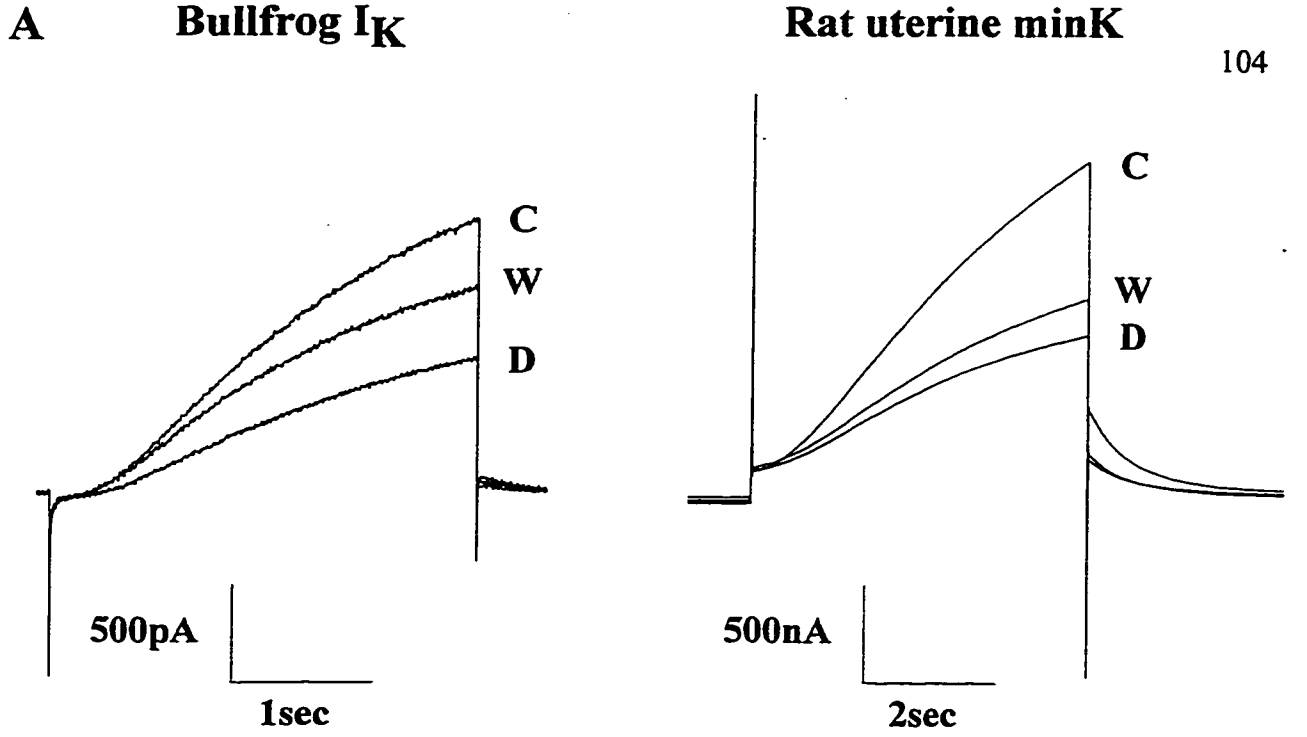
A
Bullfrog I_K
Rat uterine minK
C
W
D
500pA
1sec
C
W
D
500nA
2sec

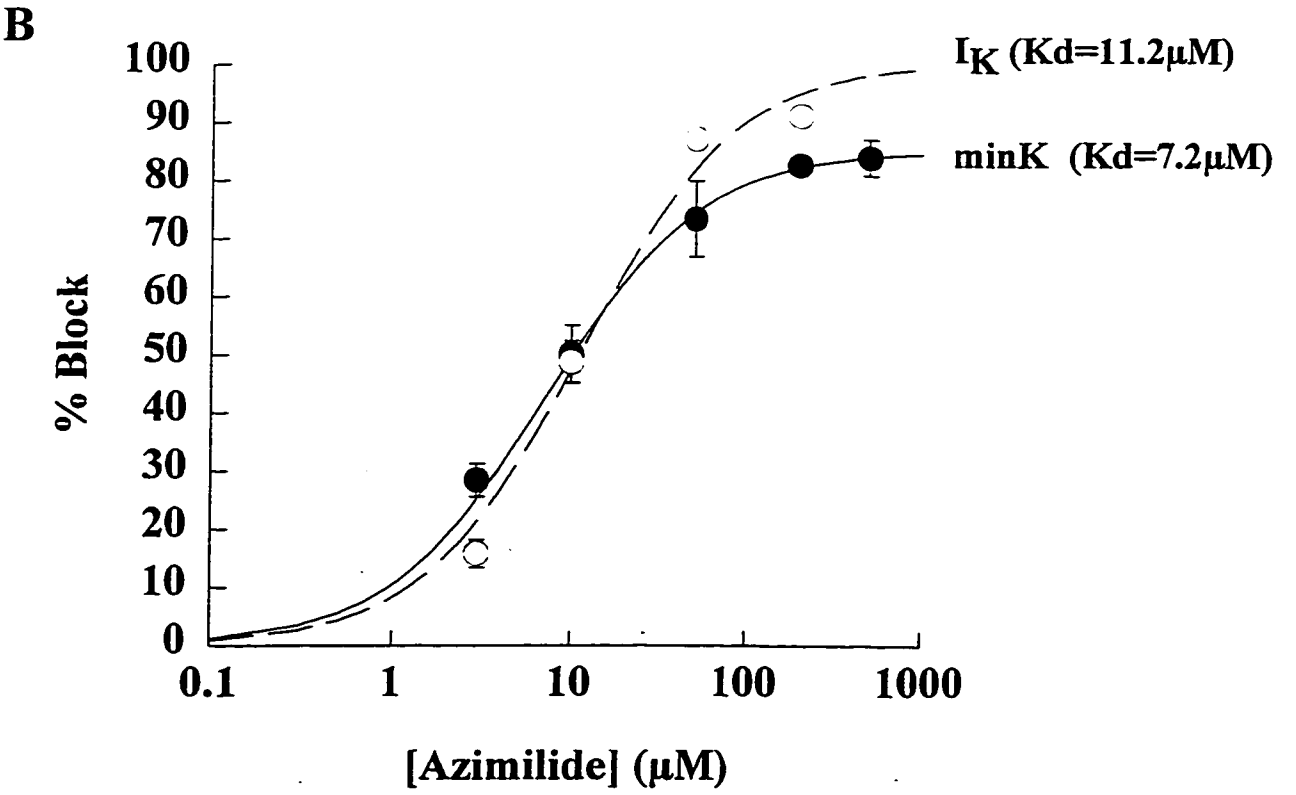
B
100
90
80
70
60
50
40
30
20
10
0
% Block
0.1
1
10
100
1000
[Azimilide] (μM)
I_K (Kd=11.2μM)
minK (Kd=7.2μM)

Selectivity of Azimilide-Induced Block

Azimilide is a potent blocker of I_K and minK; however, it can also inhibit Na^+, Ca^{2+}, and other K^+ currents (Fermini et al., 1995; Yao and Tseng, 1997). We examined the selectivity of this drug in our experimental system by measuring the effects of azimilide on the other major repolarizing current in bullfrog atrial myocytes, the inward rectifier K^+ current (I_{K1}). Three second hyperpolarizing voltage steps from the holding potential to -100 to -130mV were applied in 10mV increments. An example of the effects of 10μM azimilide on I_{K1} recorded from a single atrial myocyte is illustrated in Figure 18A. There is only a very small effect of azimilide on I_{K1} at this concentration. The current-voltage relationship under control conditions and after perfusion with azimilide, for the same cell as shown in part A, is shown in Figure 18B.

Figure 19 illustrates the concentration and voltage-dependence of the effects of azimilide on I_{K1}. 10μM azimilide inhibited I_{K1} measured at -110mV by 9.1 ± 3.0% (n=5) and by 8.4 ± 2.1% (n=5) at -130mV. This change is statistically significant only at -130mV (p=0.042, Student's paired 2-tailed t-test). At higher concentrations, however, azimilide had more substantial effects on I_{K1}. For instance, at 50μM azimilide inhibited I_{K1} by 14.0 ± 3.9% (n=2, -120mV) and at 200μM azimilide attenuated I_{K1} by 29.5 ± 3.6% (n=2, -120mV). Block of I_{K1} by azimilide at a concentration of either 10 or 50μM was not voltage dependent. These results are in agreement with those of Fermini et al. (1995) in which azimilide at concentrations ≤10μM had no effect on I_{K1} in guinea pig ventricular myocytes.

Azimilide (3-200μM) also had inhibitory effects on I_{Ca} in bullfrog atrial mycoytes at test potentials in the range of -30 to +30mV. Although these effects were not systematically investigated in this study, Figure 20 shows recordings from two different atrial myocytes illustrating the effects of azimilide on I_{Ca}. In these cells the peak inward current (after the fast Na^+ current) was inhibited by 29.2% following application of 10μM azimilide (Figure 20A) and by 95.6% in response to 200μM azimilide (Figure 20B). This

Figure 18: Effect of bath application of azimilide on the inwardly rectifying K^+ current, I_{K1}, in a single bullfrog atrial myocyte. (**A**) Raw current traces in control conditions and after application of 10μM azimilide. 3 second hyperpolarizing pulses from a holding potential of -90mV to -100 to -130mV in 10mV increments were applied. Currents were filtered at 200Hz. (**B**) Summary of the data from the same cell as in (**A**). Solid circles represent the current magnitude under control conditions and squares represent the current magnitude after application of azimilide.

A

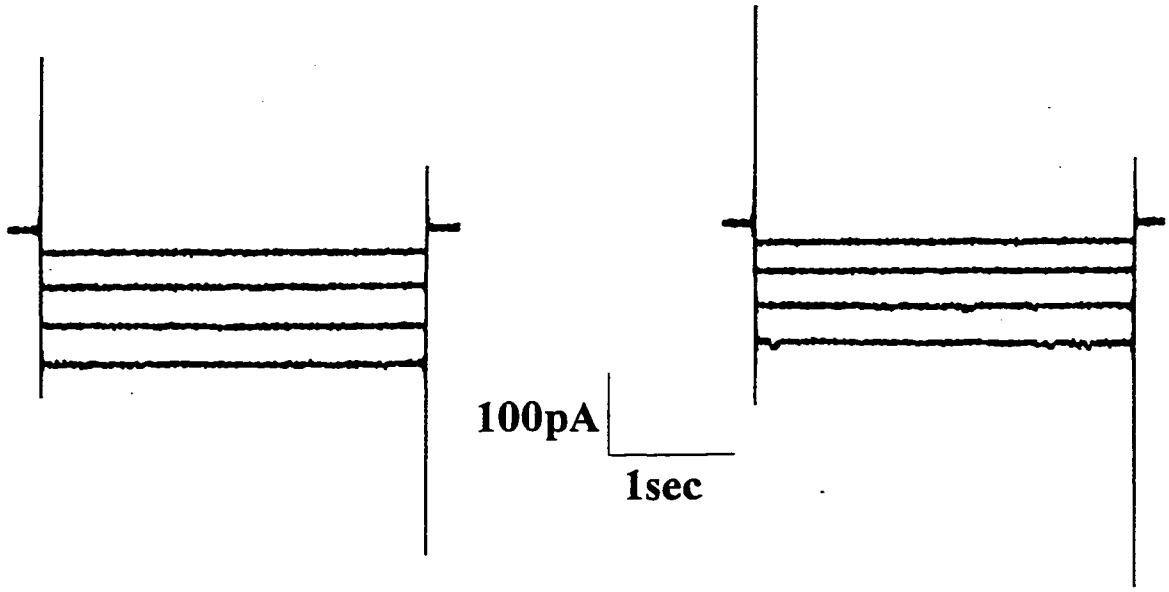
Control
10μM Azimilide
100pA
1sec

B

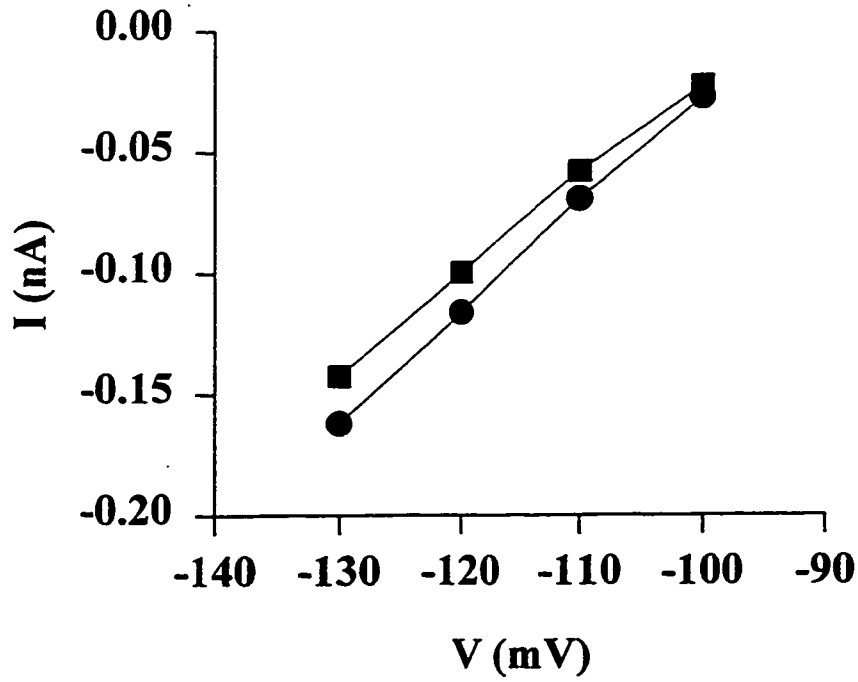
0.00
-0.05
-0.10
-0.15
-0.20
I (nA)
-140
-130
-120
-110
-100
-90
V (mV)

Figure 19: Concentration- and voltage-dependence of azimilide-induced block of I_{K1}. Data represent the % block of the current onset, relative to control at the end of a 3 second hyperpolarizing pulse to the membrane potentials indicated. Values are expressed as mean ± SEM. n values are reported on the graph.

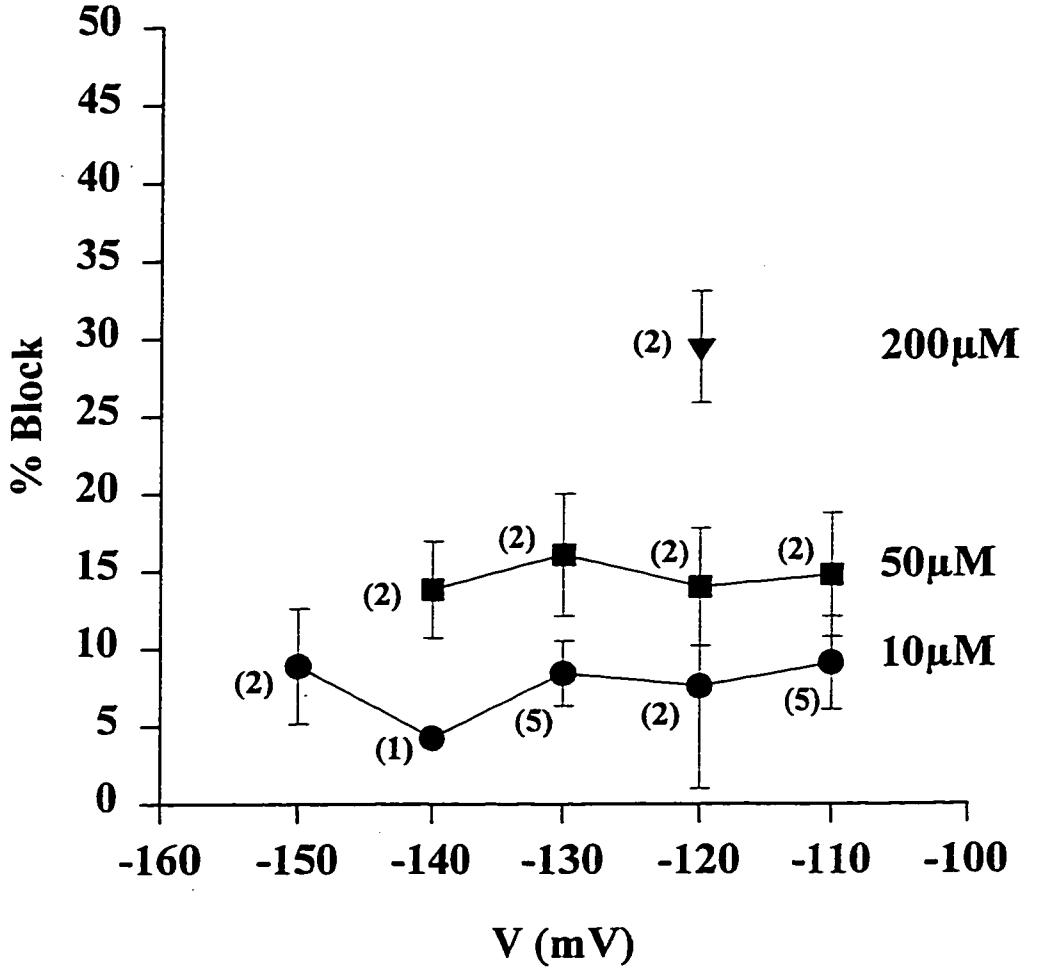
50
45
40
35
30
25
20
15
10
5
0
% Block
(2)
200µM
(2)
(2)
(2)
(2)
50µM
(2)
10µM
(1)
(5)
(2)
(5)
-160
-150
-140
-130
-120
-110
-100
V (mV)

Figure 20: Effect of bath application of azimilide on I_K and I_{Ca} in two different bullfrog atrial myocytes. Raw current traces in control conditions and after application of 10μM (**A**) or 200μM (**B**) azimilide are shown. 5 second depolarizing pulses from a holding potential of -90mV to +30mV were applied. Tail currents were measured at -80mV (**A**) or -70mV (**B**). The insets at the right show the initial inward current at increased scale to facilitate observation of I_{Ca}. I_{Na} can be seen in panel **A** but not panel **B** because the recordings were taken at a faster sampling rate (333Hz in A vs 200Hz in B).

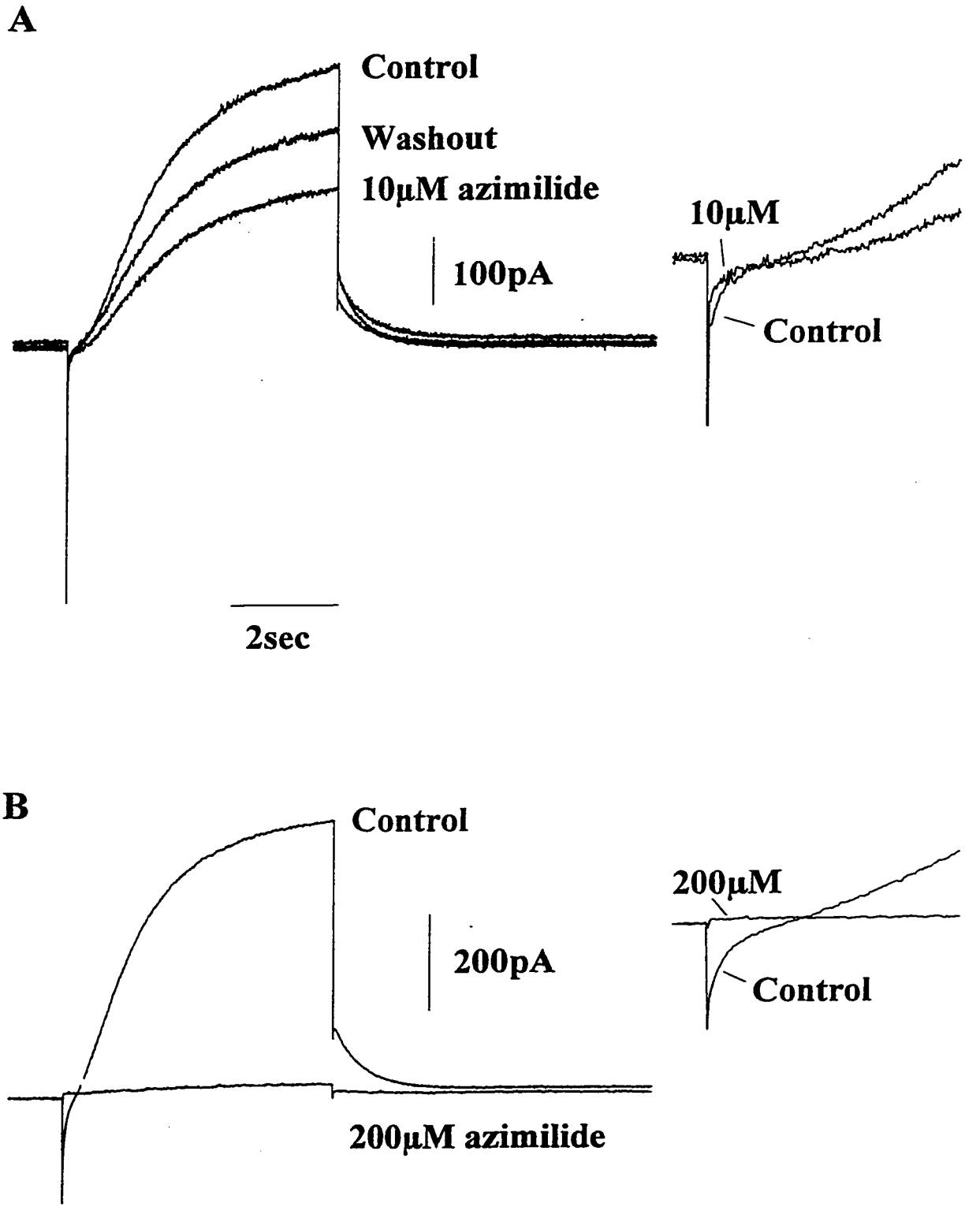
A
Control
Washout
10μM azimilide
100pA
2sec
10μM
Control
B
Control
200pA
200μM azimilide
200μM
Control

effect on I_{Ca} should not influence the block of I_K by azimilide, as activation of I_K is not dependent on influx of Ca^{++} resulting from activation of I_{Ca} (see Figure 6, Chapter 3).

The selectivity of azimilide-induced block in *Xenopus* oocytes was also investigated. Busch et al. (1994a) have previously reported that azimilide at concentrations up to 20μM is without effect on three potassium channel clones, RBK1, RBK2, and RGK5, expressed in *Xenopus* oocytes. We examined the effect of azimilide on endogenous oocyte currents in our experimental system. Figure 21A illustrates typical current traces recorded from uninjected *Xenopus* oocytes under control conditions and after perfusion with 10μM azimilide. These currents were elicited in response to 5 second depolarizing voltage steps from a holding potential of -80mV to -40 to +30mV in 10mV increments. Our results demonstrate that at a concentration of 10μM azimilide is without significant effect on these endogenous currents; however, when the concentration is increased to 50μM azimilide inhibits the endogenous currents by 18.5 ± 5.9% at +20mV (n=3), as summarized in Figure 21B. For all subsequent experiments testing the mechanism of block of azimilide (see below) we therefore used a dose of 10μM to eliminate the possibility of non-selective inhibition of other currents in both bullfrog atrial myocytes and *Xenopus* oocytes.

Voltage-Dependence of Azimilide Block

Azimilide has previously been reported to block I_{Ks} in guinea-pig ventricular myocytes in a voltage-dependent (Fermini et al., 1995) or -independent manner (Davies et al., 1996b); and to inhibit human minK expressed in *Xenopus* oocytes in a voltage-dependent manner (Busch et al., 1994). We therefore investigated whether any significant voltage-dependence of azimilide-induced block of I_K and minK could be observed in our experimental system. Cells were depolarized from the holding potential to -10, +10, +30 and +50mV for 3 sec (I_K) or -20, 0, +20, and +40mV for 5 sec (minK). Each cell was then depolarized repetitively to +30mV (I_K) or +20mV (minK) while 10μM azimilide was added to the bath solution superfusing the cells. Once steady-state block was achieved the same voltage protocol was applied and the magnitude of inhibition of azimilide on the

Figure 21: Effect of azimilide on endogenous currents in *Xenopus* oocytes. (**A**) Raw current traces in control conditions and after application of 10μM azimilide in an uninjected *Xenopus* oocyte. Five second depolarizing pulses from a holding potential of -80mV to the range -40 to +30mV were applied in 10mV increments. (**B**) Concentration- and voltage-dependence of azimilide-induced block of the endogenous currents. Data represent the % block of the maximum outward current relative to control at the end of a 5 second depolarizing pulse to the membrane potentials indicated. The 10μM data (n=1) is from the same cell shown in the upper panel, whereas the 50μM data is summarized from 3 cells. Values are expressed as mean ± SEM.

A

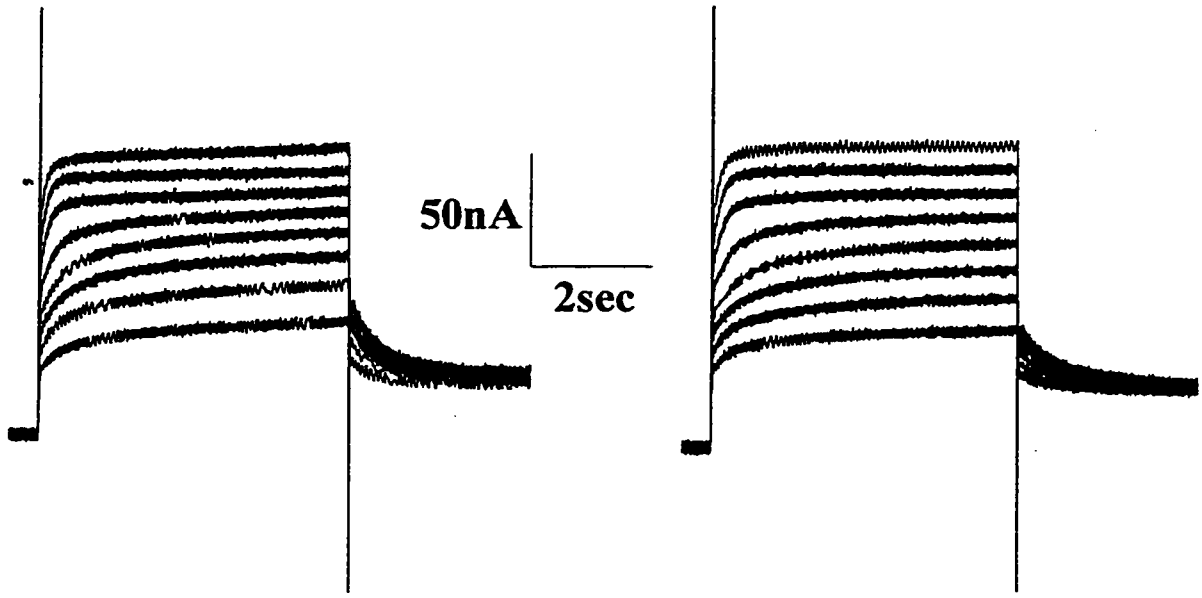
Control
10μM Azimilide
50nA
2sec

B

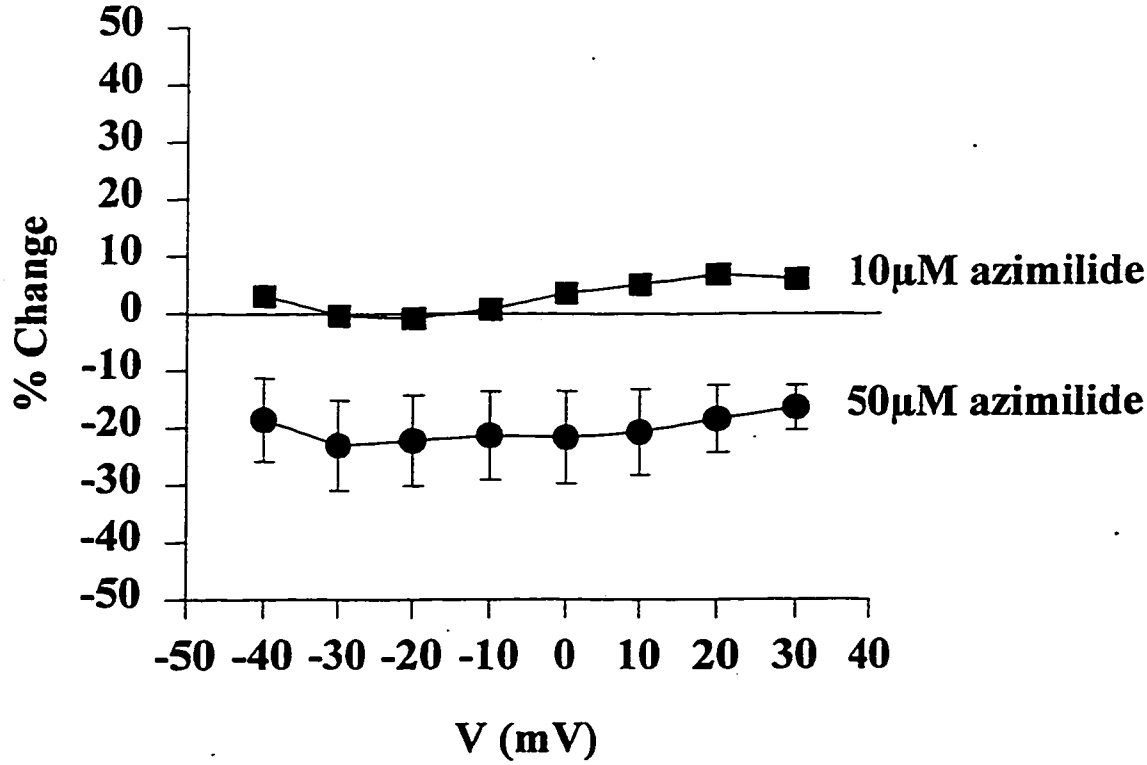
50
40
30
20
10
0
-10
-20
-30
-40
-50
% Change
-50 -40 -30 -20 -10 0 10 20 30 40
V (mV)
10μM azimilide
50μM azimilide

peak of the current onset was plotted as a function of voltage. A summary of the results from these experiments in bullfrog atrial myocytes is shown in Figure 22A. Note that there is virtually no change in the amount of inhibition induced by 10μM azimilide as voltage becomes more positive. The % block at -10mV was 43.6 ± 0.7% (n=2), +10mV was 45.6 ± 2.3% (n=4), +30mV was 48.0 ± 3.6% (n=7) and +50mV was 43.1 ± 2.4% (n=4). These results suggest that azimilide block of I_K is voltage-independent.

Figure 22B (closed symbols) summarizes the voltage-dependence of azimilide-induced block of minK measured using the protocol as described above. The voltage dependence of inhibition of 50 and 200μM azimilide is also shown. At a concentration of 10μM (n=5) azimilide-induced block of minK is not voltage-dependent (44.1 ± 6.6% block at -20mV; 46.7 ± 3.5% block at +40mV). When the concentration of azimilide is increased to 50 (n=4) or 200 (n=2) μM there appears to be a small decrease in the magnitude of inhibition at depolarized potentials (50μM: 70.3 ± 13.9% block at -20mV; 67.2 ± 6.6% block at +40mV. 200μM: 84.2 ± 2.0% block at -20mV; 76.1 ± 3.6% block at +40mV), although none of the differences between any of the potentials within each group was considered statistically significant ($p>0.1$ for all points, Student's paired t-test). These results suggest that azimilide block of minK is not voltage-dependent, as we reported for azimilide-induced block of I_K.

As indicated previously, there is a discrepancy in the literature regarding whether azimilide block of I_{Ks} is voltage-dependent. Our results demonstrate virtually no voltage-dependence of block with I_K or minK. It seemed possible that our protocol for measuring voltage-dependence was influencing the pattern of results or the interpretation of our results. That is, it is possible that by repetitive pulsing to a single potential during drug perfusion that we were "conditioning" the magnitude of azimilide-induced block at all potentials to that which is observed at this single (selected) potential. For example, this "conditioning" effect might occur for a drug that dissociates very slowly from its binding site (as we observed with azimilide; see below), with the consequence that drug binding following depolarizing voltage steps to potentials other than the "conditioning" potential would not be in equilibrium. To investigate this possibility we performed a second series

Figure 22: Voltage-dependence of azimilide-induced block of I_K (**A**) and minK (**B**). Data represented by the closed symbols were obtained in response to depolarizing voltage steps to (**A**) -10, +10, +30, or +50mV for 3sec, or (**B**) -20, 0, +20, or +40mV for 5sec, under control conditions and in the presence of steady-state block with 10μM azimilide (pulse rate= 0.05Hz). The open symbols depict data obtained by examining the amount of azimilide-induced inhibition while pulsing to a single potential (see text for full details). All points are expressed as mean ± SEM and represent the % block of the maximum outward current.

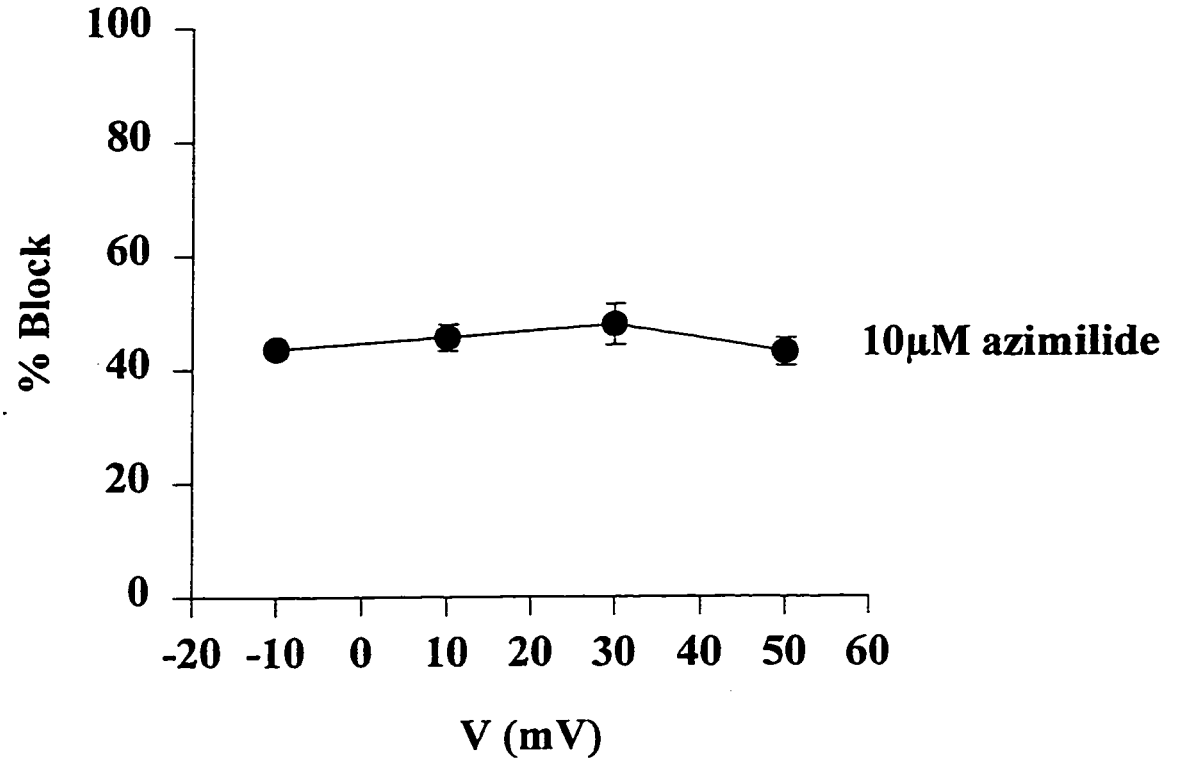
A
Bullfrog I_K
100
80
60
40
20
0
% Block
-20 -10 0 10 20 30 40 50 60
V (mV)
10μM azimilide

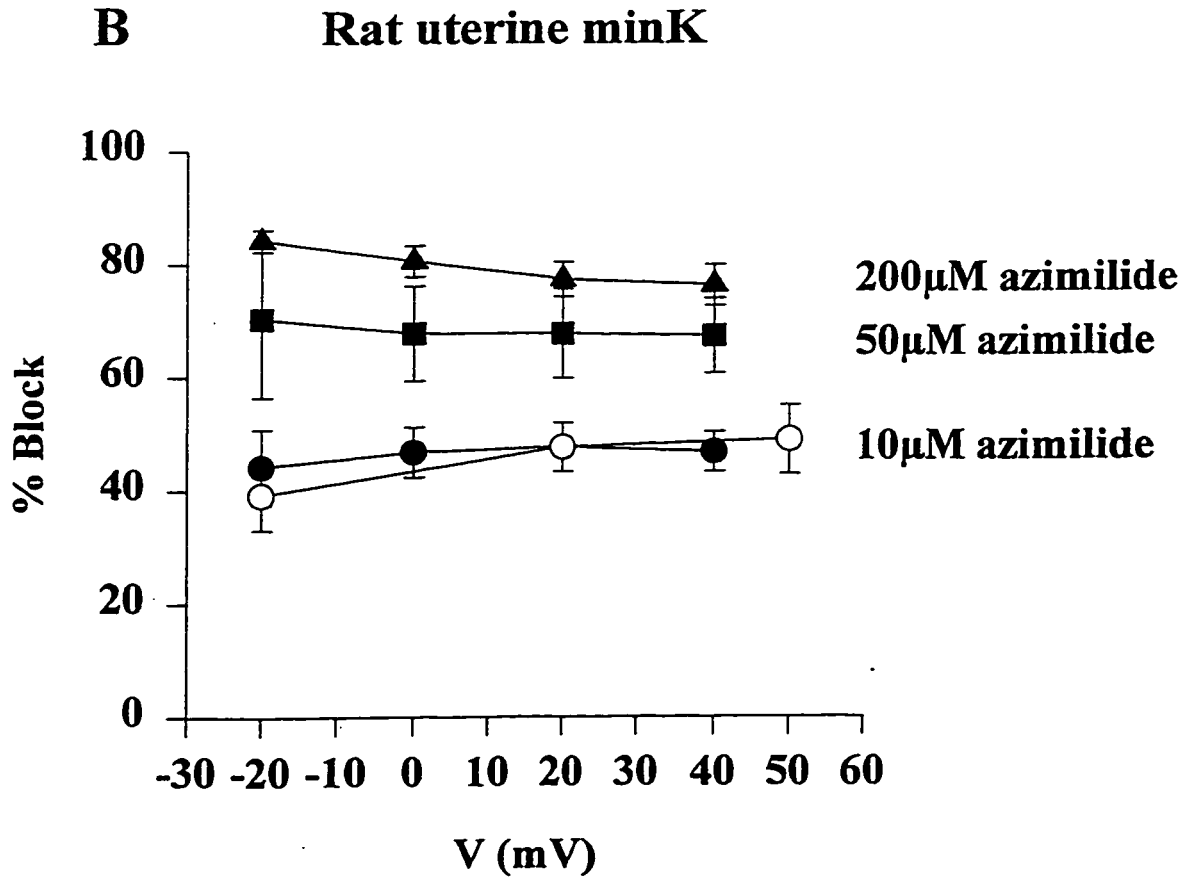
B
Rat uterine minK
100
80
60
40
20
0
% Block
-30 -20 -10 0 10 20 30 40 50 60
V (mV)
200μM azimilide
50μM azimilide
10μM azimilide

of experiments in which the oocyte was pulsed to only a single potential (-20, +20, or +50mV) under control conditions, and both during perfusion of 10μM azimilide and upon washout. The % block was then measured after steady-state inhibition was achieved. The results of these experiments are shown as the open circles in Figure 22B. Again, there is no significant change in the magnitude of block as the test voltage becomes more positive (-20mV: 39.1 ± 6.1% (n=5); +20mV: 47.5 ± 4.3% (n=4); +50mV: 48.9 ± 6.1% (n=3); p=0.33, -20mV vs +50mV, Student's unpaired two-tailed t-test), further supporting our initial data set which suggested that azimilide-induced inhibition of minK is not voltage-dependent.

Mechanism of Azimilide Block

Our assumption/expectation was that if minK underlies I_K then the process of azimilide-induced block of both these currents must be very similar. We therefore investigated the mechanism of azimilide-induced block of both I_K and minK. The activation kinetics of minK are very difficult to describe accurately since the current never reaches steady-state during very long depolarizing voltage pulses. The effect of azimilide on the activation kinetics of minK and I_K therefore was limited to a description of the changes in the time course of these two currents. Figure 23 shows superimposed current traces of I_K and minK recorded in response to depolarizing voltage steps to +30mV (I_K) or +20mV (minK). Recordings are shown both before and after application of 10μM azimilide. To illustrate the effects of azimilide on the time course of activation, the current trace recorded in the presence of drug was scaled to match the peak current under control conditions. The results show that azimilide has no effect on the activation kinetics of either I_K or minK. The effect of azimilide on the deactivation kinetics of I_K and minK was measured by analysing tail currents recorded after 5 sec test pulses to +30mV (I_K) or +20mV (minK) under control conditions and following superfusion of 10μM azimilide. The deactivation tails for both I_K and minK were best fit with a single exponential function. At a potential of -80mV the time constants of deactivation (τ_{deact}) for I_K were 447.0 ± 26.8 msec under control conditions (n=6) and 490.2 ± 43.3 msec after

Figure 23: Effect of azimilide on activation kinetics of I_K and minK. Depolarizing voltage steps to +30mV (I_K) or +20mV (minK) were applied from a holding potential of -90mV (I_K) or -80mV (minK). Current traces were recorded under control conditions and after application of 10μM azimilide. Currents recorded in the presence of drug (*) have been scaled to match the peak outward current under control conditions (o).

A **Bullfrog I_K**

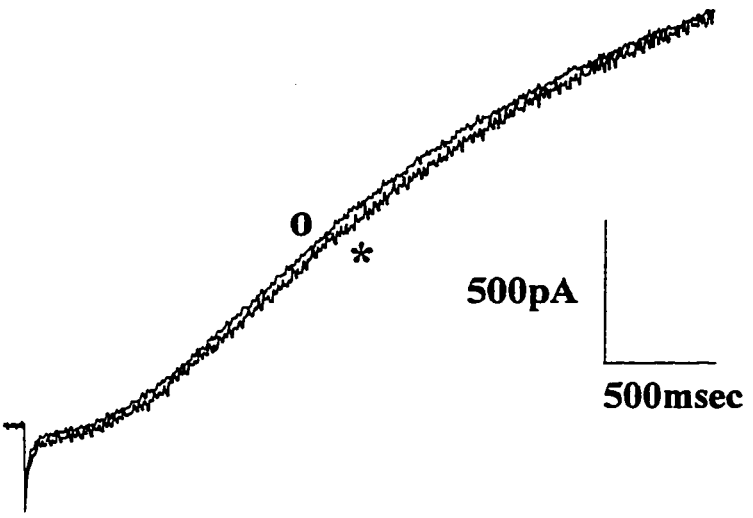

B **Rat uterine minK**

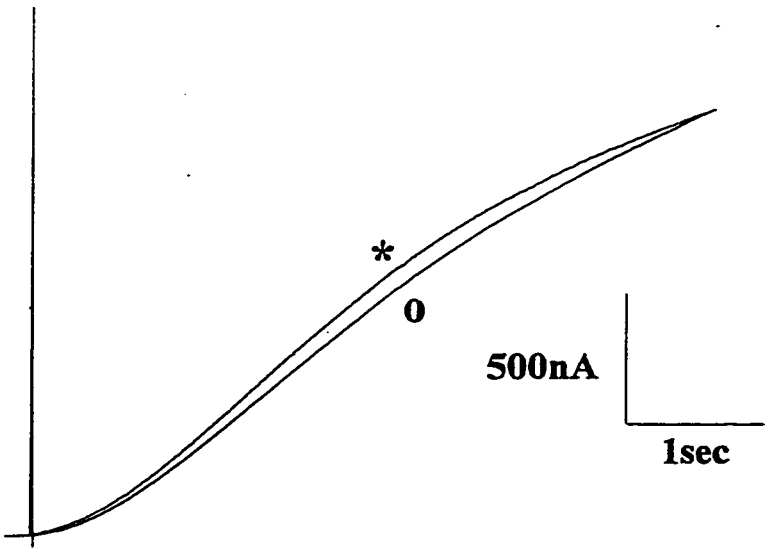

application of 10μM azimilde (n=6). These values were not significantly different (p= 0.21; Student's paired two-tailed t-test). The τ_{deact} for minK at -60mV were 860.5 ± 75.7 msec (control; n=13) and 884.4 ± 75.3 msec (10μM azimilide; n=13; p=0.19 vs control). Thus, azimilide did not significantly change the activation or deactivation kinetics of I_K or minK.

Azimilide has previously been shown to block I_{Ks} in canine ventricular myocytes (Yao and Tseng, 1997) and human minK expressed in *Xenopus* oocytes (Busch et al., 1994), in a use-dependent manner. We therefore investigated the possibility of a use-dependent mechanism of block of I_K by azimilide. Five second voltage steps to +30mV were applied in the form of trains at 0.05Hz. The pulses were then stopped and azimilide was superfused for 6 minutes to allow time for complete exchange of the bath solution and for steady-state block to be reached (recall that maximum steady-state block can be achieved after 2-3 minutes in the presence of azimilide). After this time, voltage steps were again applied and the peak of the current onset and tail current were measured. Figure 24 illustrates data obtained following this protocol from a single bullfrog atrial myocyte. Panel A shows representative current traces and panel B depicts the peak of the onset and tail currents plotted as a function of time. In every experiment a measurable reduction of the current was observed during the first pulse after drug application (26.7 ± 2.3%, n=3). This was followed by a progressive increase in block with each subsequent voltage pulse (additional 16.5 ± 2.9%, n=3).

The time-dependent pattern of azimilide-induced block of minK was also investigated. Figure 25A illustrates the currents elicited by 5sec depolarizing voltage steps to +20mV at 0.05Hz in a *Xenopus* oocyte. A similar protocol to that described for Figure 24 was applied, except that the administration of voltage steps was halted for 2 minutes following the first 4 pulses after drug application to investigate whether there was any recovery of the use-dependent block. A summary of the effects on the peak of the current onset and tail current is shown in Figure 25B. The inhibition of minK was similar to that observed with I_K: there was a block during the first pulse after drug application of 39.8 ± 2.6% (n=4), followed by additional use-dependent block of 13.4 ±

Figure 24: Mechanism of azimilide-induced block of I_K. (**A**) Representative current traces from a single myocyte showing I_K in control conditions, as well as individual current records after a 6 minute superfusion of 10μM azimilide. The cell was held at -90mV and stepped to +30mV at 0.05Hz. (**B**) Summary of the maximum outward current onsets and tail currents vs time, measured from the same cell as in the upper panel.

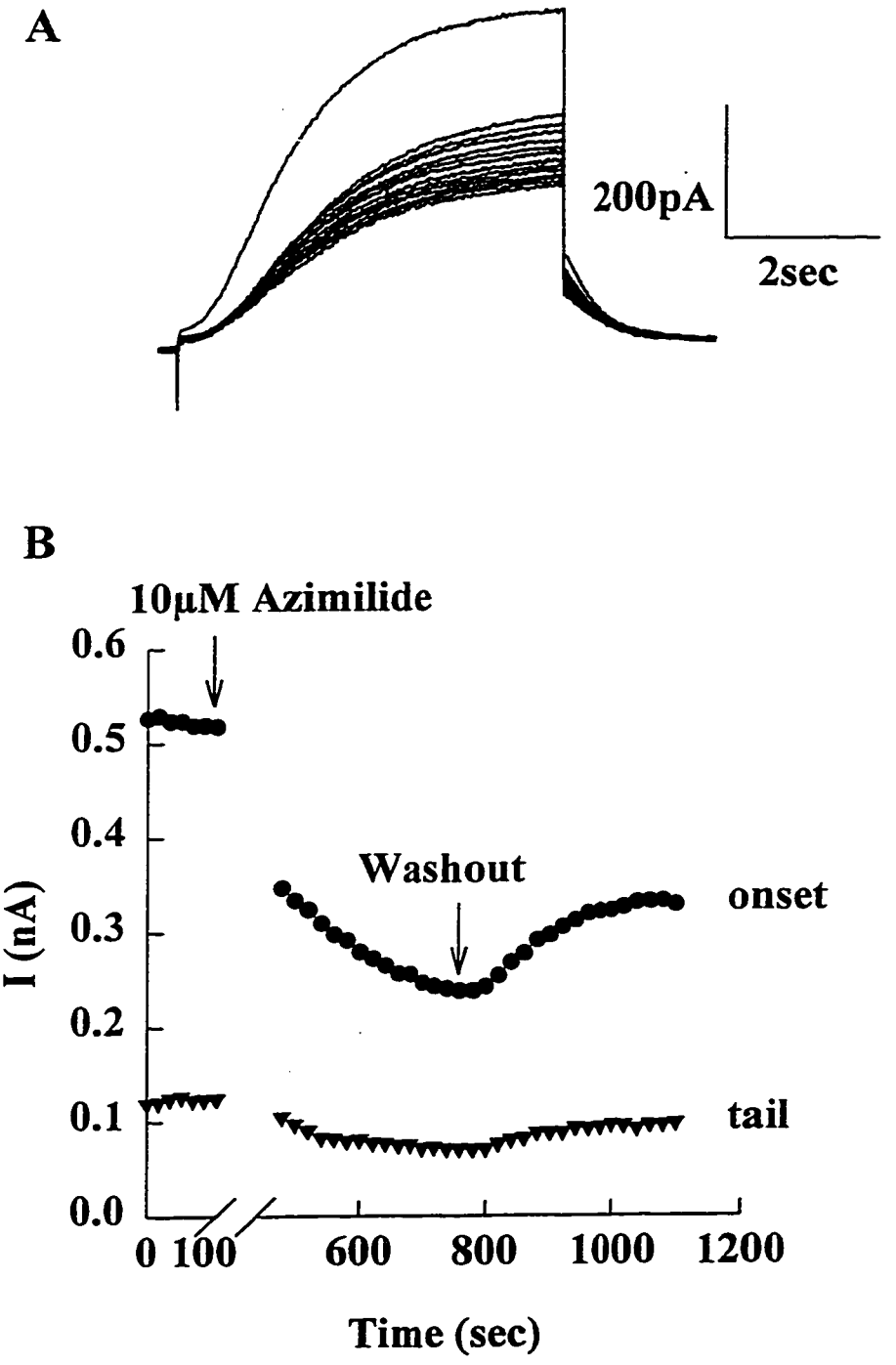
A
200pA
2sec
B
10μM Azimilide
0.6
0.5
0.4
0.3
0.2
0.1
0.0
I (nA)
Washout
onset
tail
0 100
600
800
1000
1200
Time (sec)

Figure 25: Mechanism of azimilide-induced block of minK. **A)** Representative current minK records obtained in control conditions, and after a 6 minute superfusion of 10μM azimilide, are superimposed. A 2 minute pause (interruption) from pulsing in the continued presence of the drug occurred after the first 4 depolarizing voltage steps. Thereafter, the voltage steps were again applied at the same frequency (0.05Hz). The cell was held at -80mV and stepped to +20mV. **B)** Summary of the peak of the current onsets and tail currents vs time, measured from the same cell as in the upper panel.

A

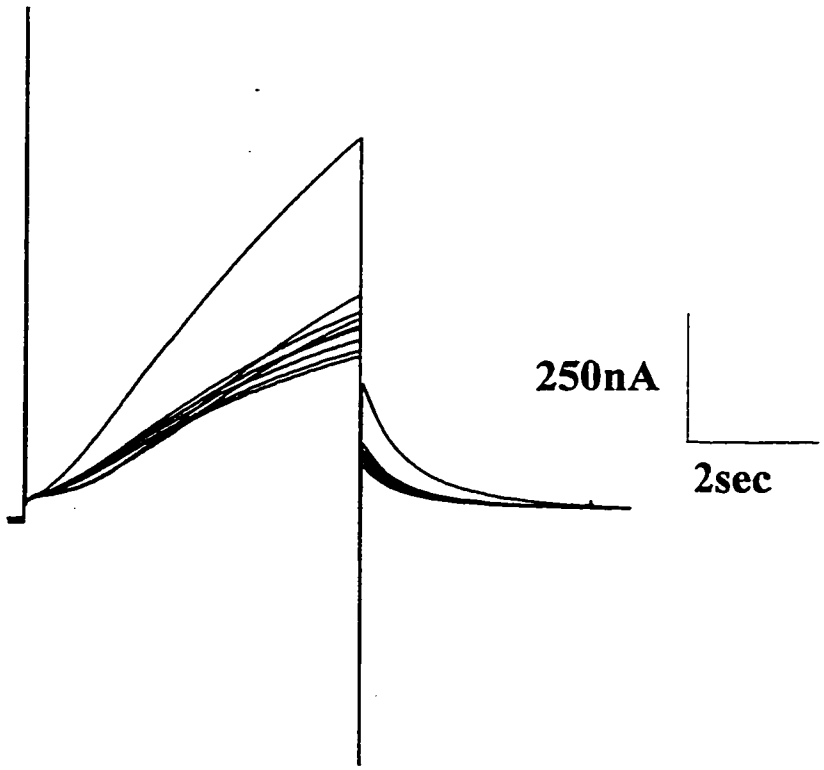
250nA
2sec

B

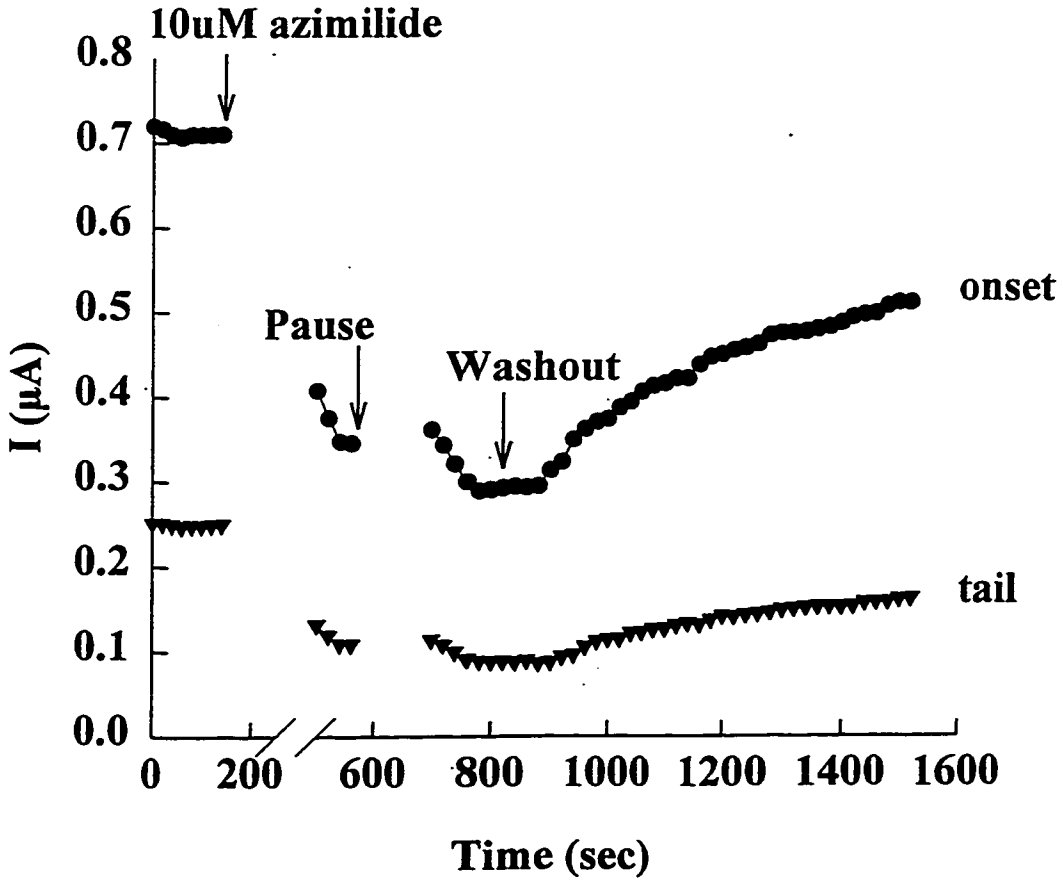
10uM azimilide
0.8
0.7
0.6
0.5
0.4
0.3
0.2
0.1
0.0
I (μA)
Pause
Washout
onset
tail
0
200
600
800
1000
1200
1400
1600
Time (sec)

1.3% (n=4). At a dose of 50μM azimilide, these values were 61.1 ± 5.8% (n=3) after the initial pulse, and an additional total of 8.4 ± 3.2% (n=3) induced by subsequent voltage pulses.

As shown in Figure 25B, a 2 minute halt of the depolarizing pulses in the continued presence of azimilide resulted in only a slight recovery of the use-dependent block, suggesting that the 'off-rate' of drug block is very slow. Increasing the frequency of pulsing to 0.083Hz did not change the rate of use-dependent block, as shown in Figure 26, although there was an increase in the magnitude of the use-dependent component of block (block after first voltage pulse= 39.7 ± 7.6%, additional use-dependent block= 25.9 ± 2.6%; n=5). The magnitude of block was not effected by changing the holding potential to -60mV, as the initial block after application of 10μM azimilide was 45.0 ± 3.9% (n=8) at this holding potential, and the use-dependent block measured 12.3 ± 3.5% (n=8, data not shown). These values are similar to those obtained under identical conditions at a holding potential of -80mV.

These findings suggest that azimilide blocks both I_K and minK predominantly in the closed state, but there is also a component of use-dependent inhibition. Changes in holding potential from -80mV to -60mV do not significantly change the levels of closed-state and use-dependent block, and unbinding of the drug must be very slow. A summary of the mechanism of azimilide-induced block of I_K and minK is shown in Figure 27.

Concentration- and Voltage-Dependence of Propenamide Block

The effect of propenamide (Salata et al., 1996b), a novel class III antiarrhythmic, on I_K and minK was also investigated in a small number of cells. Previous reports have suggested that this compound blocks I_{Ks} at very low (nM) concentrations (Salata et al., 1996b). Figure 28A illustrates the effects of 100 and 200nM propenamide on I_K recorded from a single bullfrog atrial myocyte, in response to a depolarizing voltage step to +30mV for 5 seconds. Tail currents were measured at -80mV. Propenamide reversibly inhibited I_K and the development of steady-state block was achieved after approximately 10 minutes of drug application. Propenamide, however, also appeared to inhibit I_{Ca}

Figure 26: Mechanism of azimilide-induced block of minK. **A)** Representative current traces recorded from a *Xenopus* oocyte when using the same protocol as described for Figure 25, except that the pulsing frequency was 0.083Hz. These records are from a different oocyte than in Figure 25. **B)** Summary of the changes in maximum outward current and tail currents vs time, measured from the same cell as in the upper panel.

A

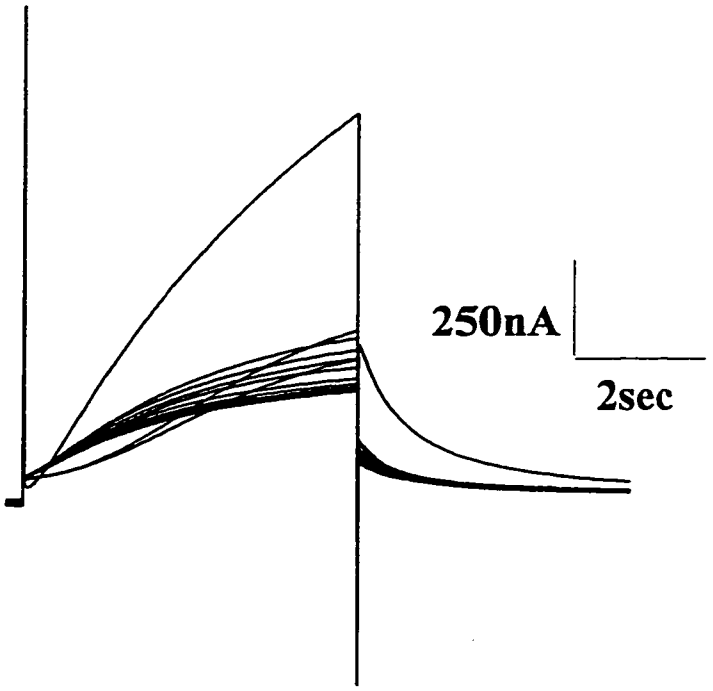
250nA
2sec

B

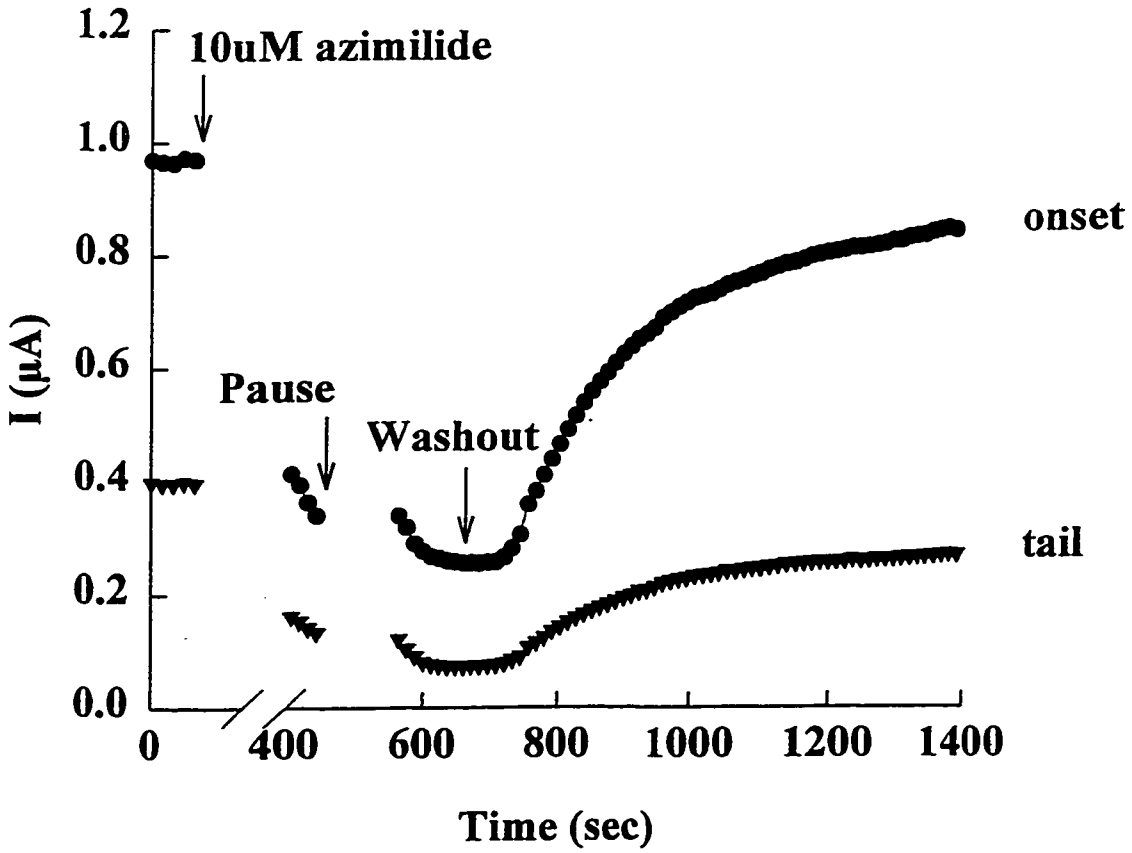
1.2
1.0
0.8
0.6
0.4
0.2
0.0
I (μA)
10uM azimilide
Pause
Washout
onset
tail
0
400
600
800
1000
1200
1400
Time (sec)

Figure 27: Summary of the mechanism of azimilide-induced block of I_K and minK. Open bars represent the % block during the first voltage clamp depolarization after drug superfusion (closed-state block) and the solid bars depict the additional % block that developed upon repetitive pulsing (use-dependent inhibition). More details of the protocol are given in the text. Values are expressed as mean ± SEM.

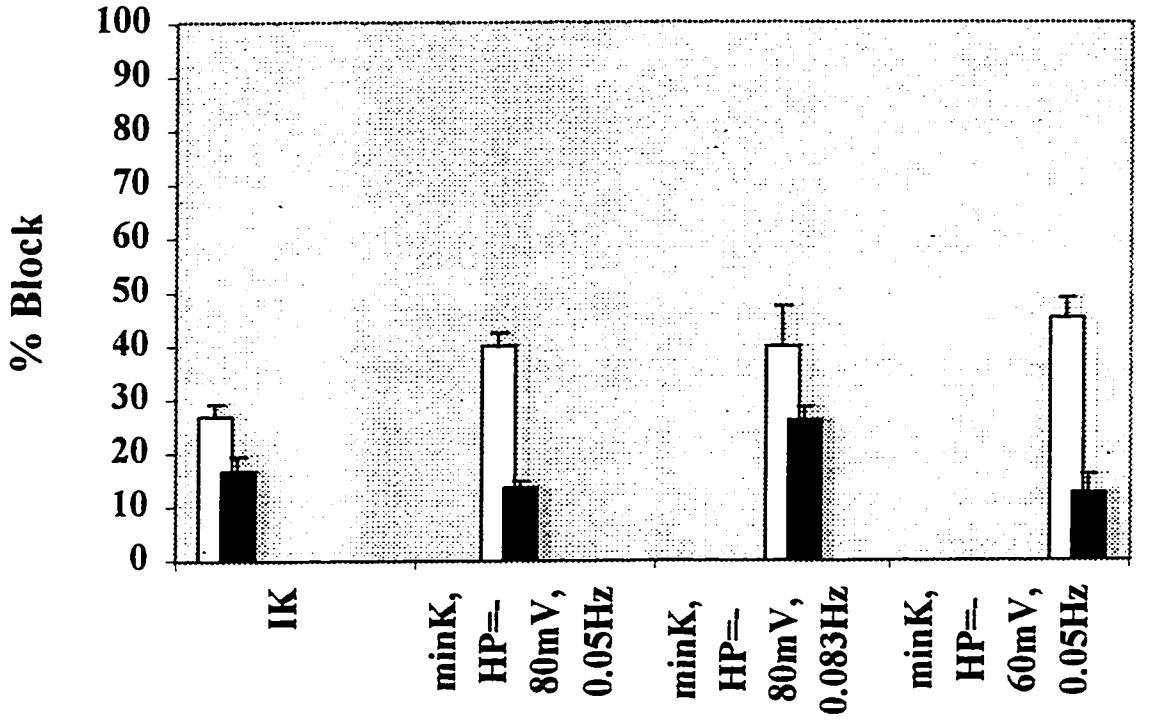
% Block
100
90
80
70
60
50
40
30
20
10
0
IK
minK, HP=_ 80mV, 0.05Hz
minK, HP=_ 80mV, 0.083Hz
minK, HP=_ 60mV, 0.05Hz

Figure 28: Effect of bath application of propenamide on I_K. **A)** Representative current traces recorded from a single bullfrog atrial myocyte under control conditions and following bath perfusion of 100nM or 200nM propenamide. Propenamide decreased the amplitude of the current in response to 5 second depolarizing voltage steps to +30mV from a holding potential of -90mV (pulse rate= 0.05Hz). **B)** Concentration-dependence of propenamide-induced block of I_K (100nM, n=2; 200nM, n=1). **C)** Voltage-dependence of propenamide-induced block of I_K. n values are the same as in panel **B**. Data were obtained by applying depolarizing voltage steps to -30, -10, +10, +30 for 5sec under control conditions and after steady-state block with 10μM azimilide was achieved. All data in panels **B** and **C** are mean ± SEM and represent the % block of the maximum outward current relative to control.

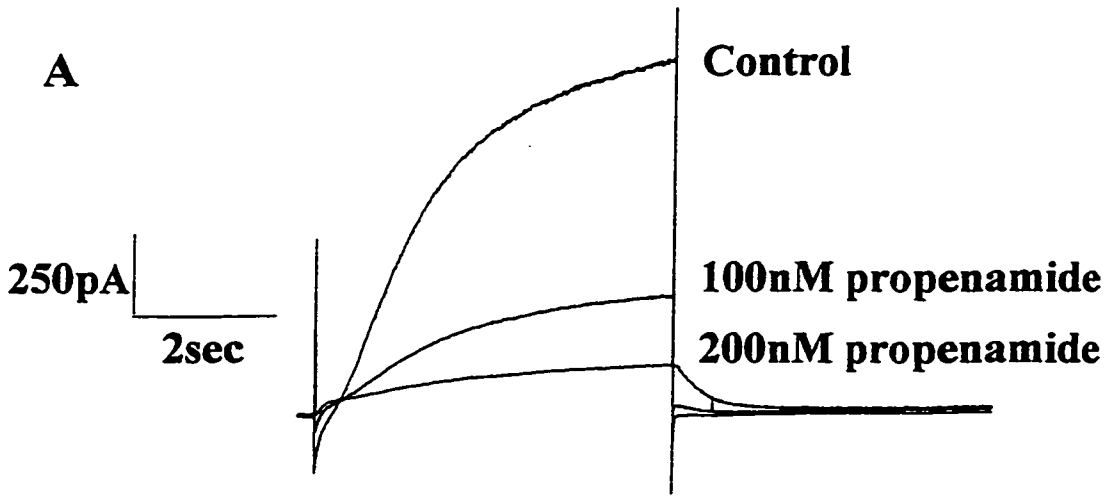
A
Control
250pA
2sec
100nM propenamide
200nM propenamide

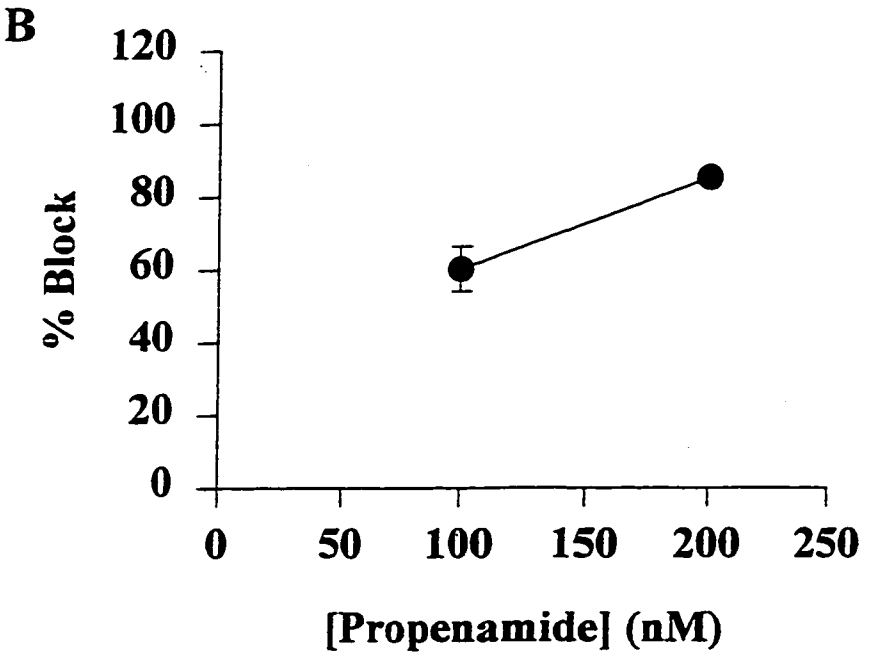
B
% Block
120
100
80
60
40
20
0
0
50
100
150
200
250
[Propenamide] (nM)

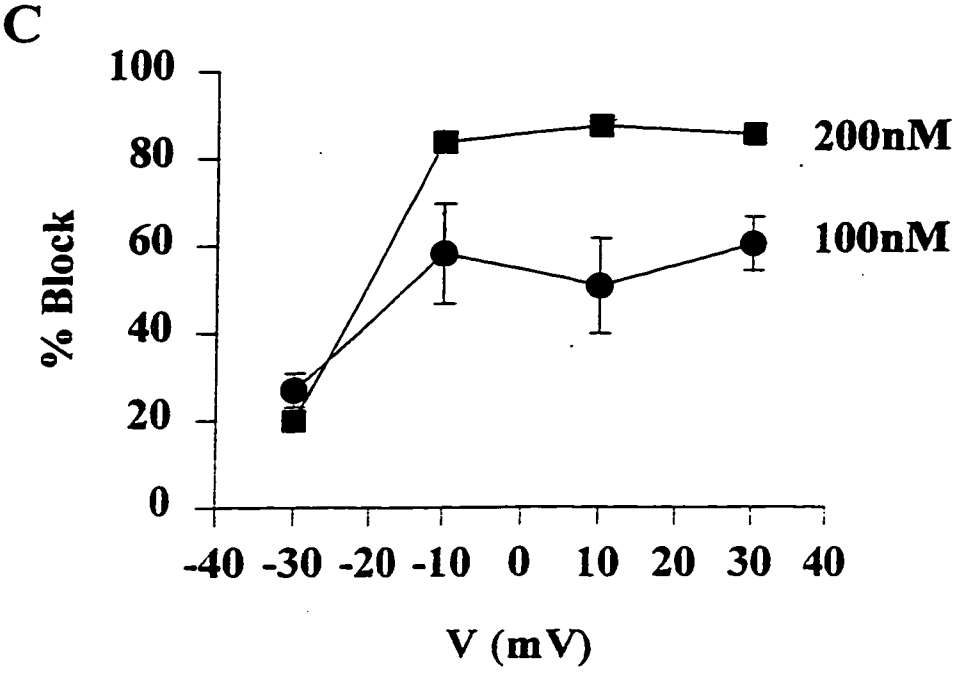
C
% Block
100
80
60
40
20
0
200nM
100nM
-40
-30
-20
-10
0
10
20
30
40
V (mV)

(66.0% block of peak inward current at a dose of 100nM). Figure 28B summarizes the effect of propenamide on I_K at two different concentrations. Propenamide blocked I_K by 60.3 ± 6.1% (n=2) at a dose of 100nM and by 85.4% (n=1) at a dose of 200nM, with an estimated K_d of approximately 60nM. Figure 28C shows the magnitude of propenamide-induced block of the current onset as a function of voltage. Currents were elicited using the same protocol as was described previously for determining the voltage-dependence of azimilide inhibition (see Figure 22), except that the test pulses were 5 seconds in duration. Note that the amount of inhibition increases as the test potential becomes more positive. At a concentration of 100nM this difference between -30mV (26.9 ± 3.9% block) and +30mV (60.3 ± 6.1% block) is statistically significant (p=0.043, Student's paired t-test, n=2).

Figure 29A illustrates the effect of 500nM propenamide on minK expressed in a single *Xenopus* oocyte. The oocyte was held at -80mV and then depolarized to +20mV for 5 seconds. Tail currents were measured at -70mV. Propenamide inhibited minK in a concentration-dependent manner, as shown in Figure 29B. Steady-state block was achieved after 12-14 minutes of drug application. At a concentration of 200nM propenamide blocked minK by 60.8 ± 5.2% (n=6), with an estimated K_d of approximately 150nM. The voltage-dependence of propenamide-induced block is depicted in Figure 29C. These values were obtained using the same protocol as previously described to test the voltage-dependence of azimilide block of minK, except that block was measured at -20, -10, 0, +10, and +20mV. At a concentration of 100nM propenamide there was a statistically significant (p=0.006) increase in the magnitude of inhibition between -20mV (12.9 ± 7.6%, n=5) and +20mV (32.1 ± 5.6%, n=4), somewhat similar to that observed in studies of I_K in atrial myocytes. At 500nM propenamide there is also a trend for the % block to increase at positive potentials. % block was 57.7 ± 2.2% at -20mV, 69.5 ± 1.1% at 0mV, and 71.8 ± 2.2% at +20mV. The difference between -20mV and 0mV is statistically significantly (p=0.035, Student's paired t-test, n=3).

Figure 29: Effect of bath application of propenamide on minK. **A)** Representative current traces recorded from a single *Xenopus* oocyte under control conditions and following superfusion with 500nM propenamide. Propenamide decreased the amplitude of the current in response to 5 second depolarizing voltage steps to +20mV from a holding potential of -80mV. **B)** Concentration-dependence of propenamide-induced block of minK (100nM, n=4; 200nM, n=6; 500nM, n=3). **C)** Voltage-dependence of propenamide-induced block of minK (100nM, n=4; 500nM, n=3). Data were obtained by applying depolarizing voltage steps to -20, -10, 0, +10, +20 for 5sec under control conditions and after steady-state block with 10μM azimilide had developed. All data in panels **B** and **C** are mean ± SEM and represent the % block of the maximum outward current relative to control. Where error bars cannot be seen it is because they are too small to be resolved.

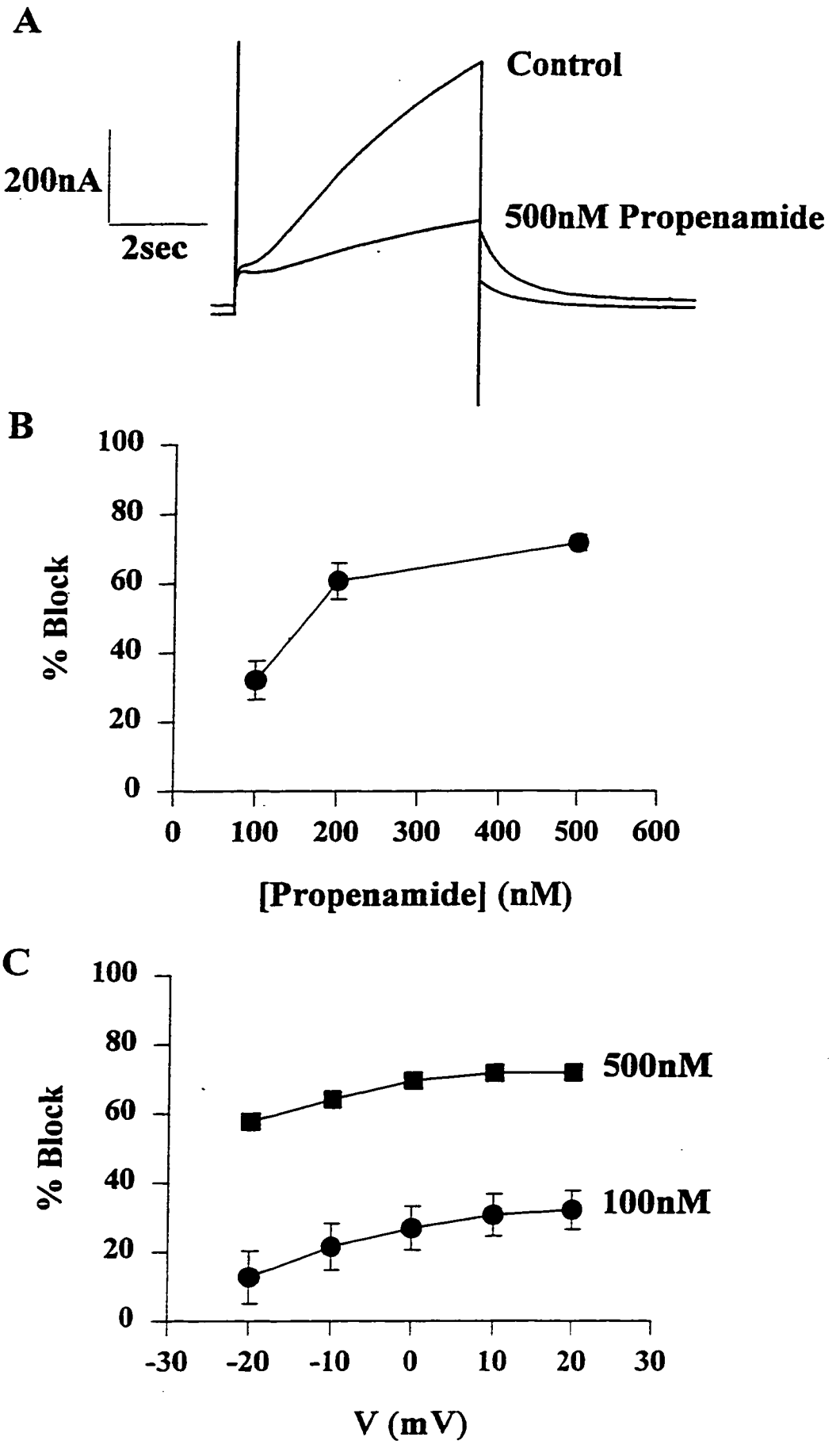
A
Control
200nA
2sec
500nM Propenamide
B
100
80
60
40
20
0
% Block
0
100
200
300
400
500
600
[Propenamide] (nM)
C
100
80
60
40
20
0
% Block
500nM
100nM
-30
-20
-10
0
10
20
30
V (mV)

Mechanism of Propenamide Block

To our knowledge there are no published reports investigating the mechanism by which propenamide inhibits minK. We therefore investigated the effects of propenamide on the activation and deactivation kinetics of this current. Propenamide was without effect on the time course of minK activation. This was measured by scaling the current traces recorded following propenamide perfusion to the peak current recorded under control conditions. Five second depolarizing voltage steps to +20mV were applied. As can be seen in Figure 30, 500nM propenamide had no effect on the time course of activation of minK. Unlike azimilide, however, 200nM propenamide slowed the τ_{deact} of minK from 704.6 ± 39.9 msec to 797.2 ± 19.6 msec (n=6), at a potential of -70mV. This difference was statistically significant ($p<0.05$; Student's paired two-tailed t-test).

The possibility of a use-dependent mechanism of block of minK by propenamide was also investigated. Depolarizing voltage steps to +20mV for 5 seconds were applied every 20 seconds until a stable baseline was reached. The oocyte was then held at -80mV and the voltage clamp depolarizations were stopped while the bath solution was switched to ND96 solution containing 200nM propenamide. The oocyte was allowed to equilibrate in the presence of drug for 10-14 minutes (depending on flow rate) before the voltage clamp steps were again applied. Figure 31 illustrates data obtained from a single *Xenopus* oocyte using this protocol. Panel A depicts representative current traces and the panel B shows the maximum onset and tail currents plotted as a function of time. An initial reduction of the current was observed on the first pulse after drug application (42.2 ± 9.2%, n=4), followed by an increased block with each subsequent voltage pulse (additional 20.0 ± 3.1%, n=4), a similar effect to that which was observed with azimilide.

Effect of Chromanol 293B on minK

Chromanol 293B has recently been shown to inhibit I_{Ks} in guinea pig myocytes with an IC_{50} of 2.1μM (Busch et al., 1996), and rat or guinea pig minK expressed in *Xenopus* oocytes with an IC_{50} of 6-7μM (Suessbrich et al., 1996; Busch et al., 1996). This compound is without effect on I_{Kr} or I_{Ca} in guinea pig ventricular myocytes, and at

Figure 30: Effect of propenamide on activation kinetics of minK. Depolarizing voltage steps to +20mV were applied from a holding potential of -80mV (minK). Current traces were recorded under control conditions and after application of 500nM propenamide. Currents recorded in the presence of drug (*) have been scaled to match the peak outward current under control conditions (o).

Rat uterine minK

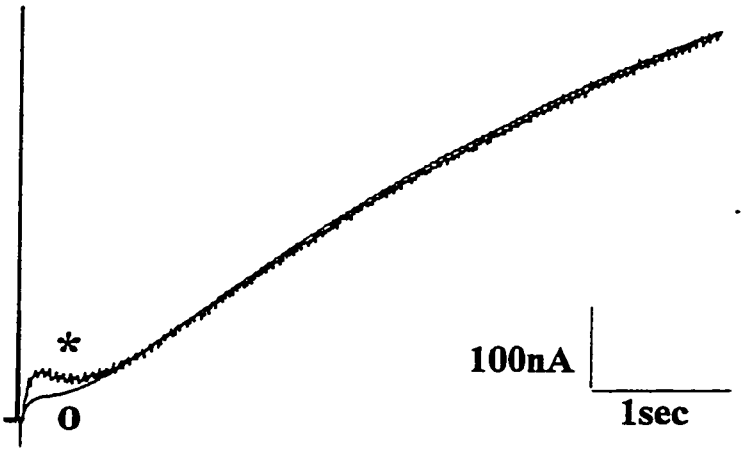

Figure 31: Mechanism of propenamide-induced block of minK. A) Representative current traces recorded from a *Xenopus* oocyte showing minK in control conditions followed by individual pulses after a 14 minute period of superfusion with 200nM propenamide. The cell was held at -80mV and stepped to +20mV at 0.05Hz. **B)** Summary of the maximum outward currents and tail currents vs time, measured from the same cell as in the upper panel.

A

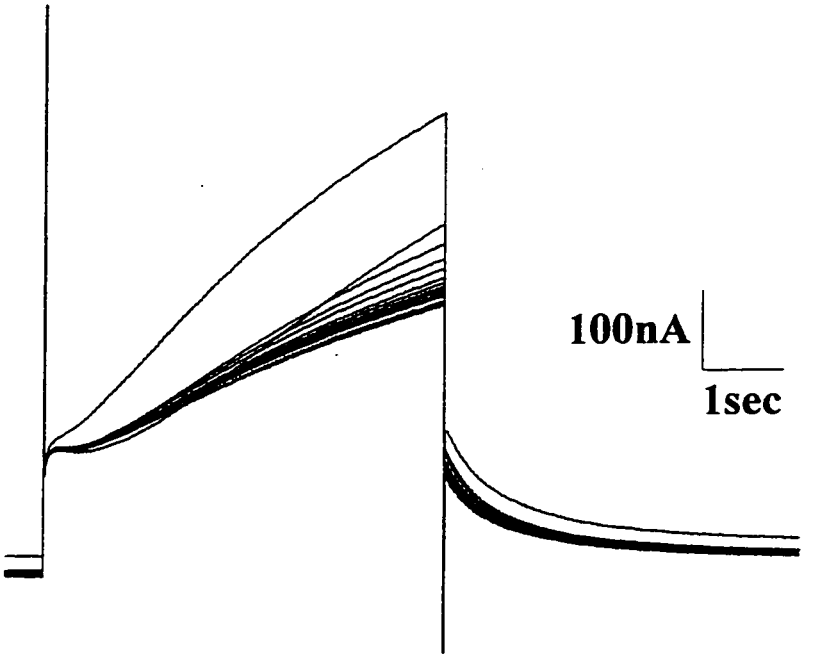
100nA
1sec

B

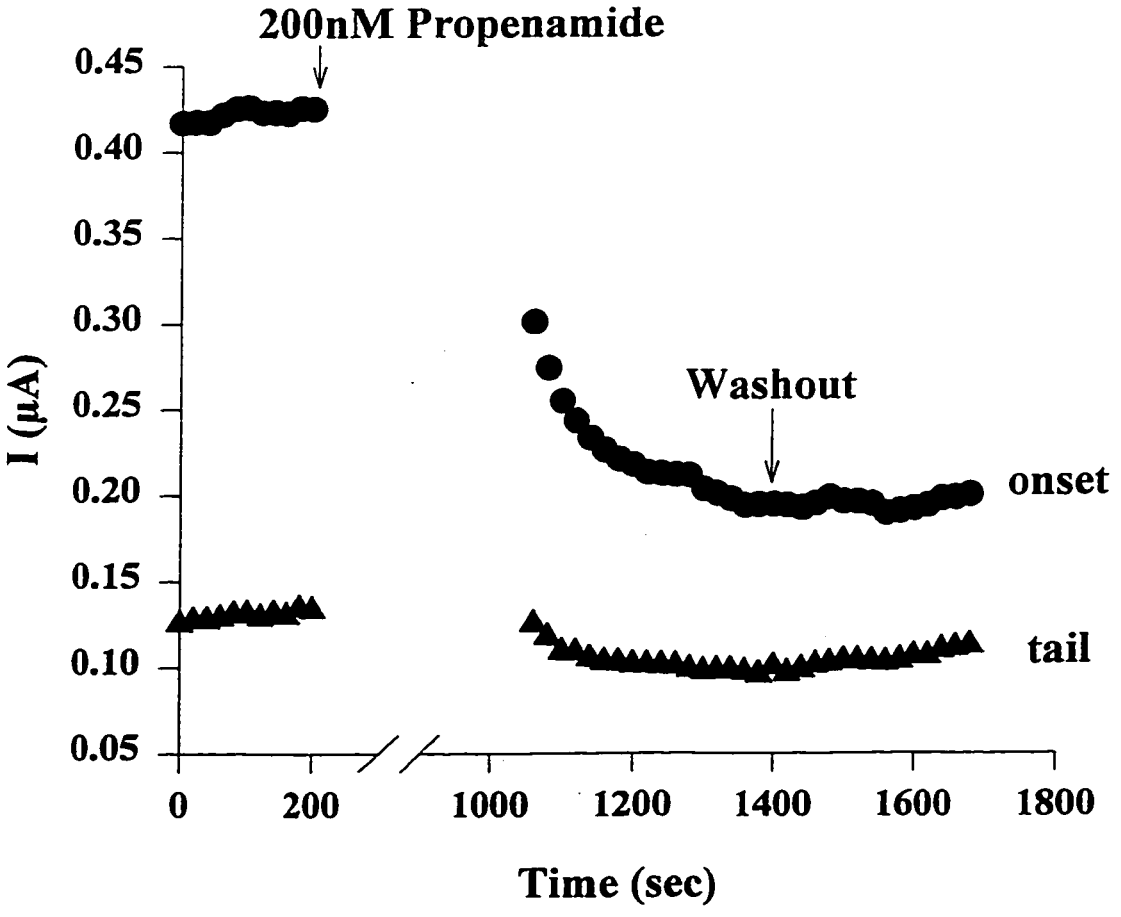
200nM Propenamide
0.45
0.40
0.35
0.30
0.25
0.20
0.15
0.10
0.05
I (μA)
Washout
onset
tail
0
200
1000
1200
1400
1600
1800
Time (sec)

Figure 32: Effect of chromanol 293B on minK. Representative current traces recorded from a single *Xenopus* oocyte under control conditions and following bath superfusion of 10μM chromanol 293B. 293B decreased the amplitude of the current in response to 5 second depolarizing voltage steps to +20mV from a holding potential of -80mV. This effect was reversible upon washout.

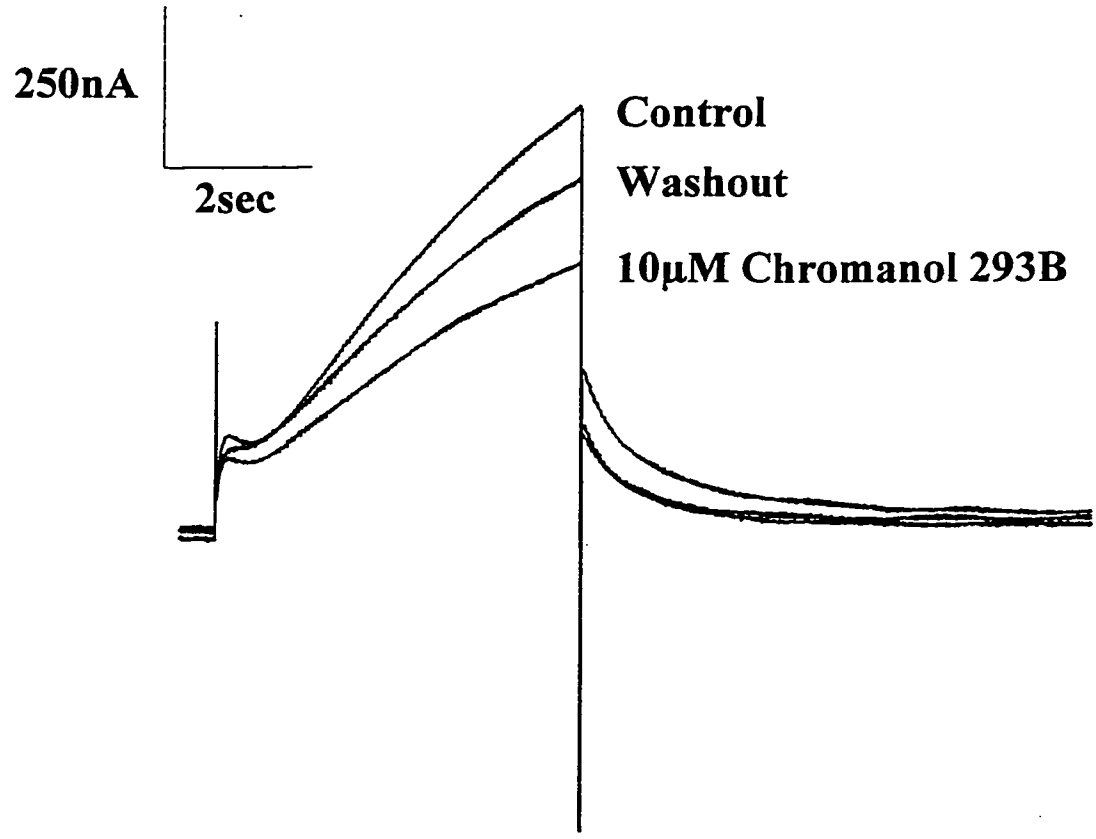
250nA
2sec
Control
Washout
10μM Chromanol 293B

concentrations that block I_{Ks} it has no effect on HERG, $K_v1.1$, or $K_{ir}2.1$ expressed in *Xenopus* oocytes (Busch et al., 1996; Suessbrich et al., 1996). Dr. Giles' laboratory received a sample of this compound from Hoescht Pharmaceuticals just before I concluded my experimental work in his laboratory. The effect of chromanol 293B was therefore tested on only one oocyte expressing minK, as illustrated in Figure 32. Following a depolarizing pulse to +20mV for 5 seconds 10μM 293B inhibited rat uterine minK by 36.4%. Steady-state block was achieved after 9 minutes and this effect was reversible after 8 minutes of washout.

Discussion

Biophysical Characteristics

Our results demonstrate close similarities in a number of biophysical properties of I_K in bullfrog atrial myocytes and minK expressed in *Xenopus* oocytes. We have found that minK and I_K have similar steady-state activation characteristics, current-voltage relationships, and selectivity for K^+. Taken together these findings suggest a significant role for this protein in I_K expression/function. In chapter 3 of this dissertation we compared the characteristics of I_K measured in this study to earlier reports in the literature, and demonstrated that our data is very similar to the results others have described. Furthermore, our steady-state activation values for minK of a $V_{1/2}$ of -22.6mV and a slope of 15.1 correspond well with previous findings of -8.2mV and 10.6 reported for rat minK expressed in *Xenopus* oocytes (as calculated from isochronal activation curves; Hice et al., 1994). K^+ selectivities yielding slopes of 52 (Barhanin et al., 1996), 58 (Goldstein and Miller, 1991), 59 (Takumi et al., 1988) and 52 (Folander et al., 1990) mV per 10 fold change in extracellular $[K^+]$ have been published for minK, similar to the value of 56.4mV per 10 fold change reported here. In addition, the outwardly-rectifying shape of the current-voltage relationship at potentials positive to -50mV, measured at the peak of the current onset, matches well with previous reports (Sanguinetti et al., 1996;

Wilson et al., 1994; Folander et al., 1990; Honoré et al., 1991; Honoré et al., 1992; and others).

However, despite the many similarities between the biophysical properties of I_K and minK, there are quite obvious differences in the time-course of the current waveforms. In particular, I_K activates slowly with a sigmoid onset and reaches steady-state after depolarizing voltage pulses 20-30 seconds in length. MinK also activates slowly and with a sigmoid time course, however, it does not reach steady-state even after very long pulses. As discussed in Chapter 1, one plausible explanation for the slow activation kinetics and sigmoidicity is the requirement for subunit assembly prior to and/or during activation. Alternatively, the observed differences may be due to different temperature sensitivities or intracellular regulation of the two currents, or microanatomical differences between *Xenopus* oocytes and bullfrog atrial myocytes. This latter possibility is discussed further in Chapter 6 of this dissertation.

Pharmacological Characteristics

In addition to similar biophysical characteristics, this study also demonstrates virtually identical pharmacological properties of I_K and minK. We describe the first report of inhibition of bullfrog I_K by azimilide and propenamide, and show that minK and I_K are blocked by these compounds with a similar concentration- and voltage-dependence. Importantly, we also show that block by azimilide is selective for I_K and minK at the concentrations used in this study.

Mechanism of Azimilide Block

Azimilide was the first class III antiarrhythmic agent to be discovered which had a substantial inhibitory effect on I_{Ks} (see review by Salata and Brooks, 1997). This compound was originally thought to selectively act on I_{Ks} (Busch et al., 1994a), but has recently been shown to inhibit I_{Kr}, I_{Ca} and I_{Na} (Fermini et al., 1995; Yao and Tseng, 1997). Moreover, azimilide blocks I_{Kr} at approximately 10 fold lower concentrations than I_{Ks} in guinea pig ventricular myocytes (Fermini et al., 1995). We have found that azimilide

blocks minK with a K_d of 7.2μM and I_K with a K_d of 11.2μM.These results correspond well with the values of 1.8 (Busch et al., 1994a) and 5.4μM (Busch et al., 1994) previously reported for rat and human minK expressed in *Xenopus* oocytes, respectively; and also the values of 1.9 and 1.8μM published for I_{Ks} in guinea pig and canine ventricular myocytes (Yao and Tseng, 1997).

Davies et al. (1996b) found no change in the magnitude of azimilide-induced block of I_{Ks} in guinea pig ventricle or sinoatrial node with changes in holding potential between -100 and -30mV. Furthermore, block by azimilide was not dependent on the test potential. In contrast, Fermini et al. (1995) and Yao and Tseng (1997) described an increased block of I_{Ks} in guinea pig or canine ventricular myocytes at more positive test potentials (Fermini et al.: 24% block at +20mV vs 44% at +80mV), and Busch et al. (1994) reported small increases (46% vs 35%) in the magnitude of block of human minK expressed in *Xenopus* oocytes at +40mV vs -20mV. In this study we show that changing holding potential from -80 to -60mV does not alter the magnitude of azimilide-induced block of minK, and also that the extent of inhibition of minK and I_K by azimilide is not strongly voltage-dependent. These results are therefore in closer agreement with the findings of Davies et al. (1996b).

A consistent finding in our experiments which supports a role for minK underlying I_K is that azimilide blocks both of these currents with the same potency and, quite likely, by the same mechanism. Azimilide-induced inhibition was apparent within the first 100-200msec (minK) or 300-400msec (I_K) following a depolarizing voltage step, despite only minimal current activation at this time. No evidence of open channel block was observed even after long (20 second) voltage pulses (data not shown). These results can be interpreted to mean that either azimilide does not require channel opening to exert its inhibitory effects on I_K and minK, ie. that it binds to the channel in the closed state, or that the rate of drug binding is very fast. Our data demonstrating that azimilide does not change the activation kinetics of I_K or minK does not differentiate between either of these two types of block, but does suggest that azimilide does not influence channel gating. The fact that azimilide inhibits I_K and minK in a voltage-independent manner, and also that

there was no change in the deactivation kinetics of both currents following azimilide superfusion, argues against open channel block. That is, if azimilide bound only to the open state of the channel a slowing of the decay of the tail currents should have been observed, since a fraction of the channels would have to pass from an open blocked state to an open unblocked state before closing.

In experiments studying the mechanism of azimilide-induced block we consistently observed an initial decrease of both I_K and minK onset and tail currents on the first pulse following drug perfusion (27% block for I_K; 40% for minK), accompanied by an addditional inhibition of the current with each subsequent voltage pulse until steady-state block was reached (additional 16% block for I_K, 13% for minK). These results confirm that the majority of azimilide-induced block of I_K and minK is in the closed state, but also suggests that there is a use-dependent component of inhibition. Increasing the pulse frequency from 0.05Hz (5 second pulse once every 20 seconds) to 0.083Hz (5 second pulse once every 12 seconds) resulted in a small increase in the total block of minK (~53% to 66%), and this change was due entirely to an increase in the use-dependent component of block. There was virtually no recovery of block when the depolarizing pulses were halted for two minutes following the first 4 voltage steps after drug superfusion, suggesting that the off-rate of the drug must be very slow. Our inability to achieve complete washout of azimilide (ie. inhibition was not completely reversible), and the observation that the deactivation kinetics of I_K and minK are not affected by this compound, also suggest a slow off-rate. Furthermore, changing the holding potential from -80 to -60mV did not significantly change the level of closed-state and use-dependent block, supporting our previous findings that there is virtually no voltage-dependence of azimilide-induced inhibition.

In combination, these results suggest that azimilide binds to I_K and minK predominantly in the closed state. Channel opening, however, appears to facilitate further drug block. This effect could occur if the conformational changes in the channel during opening increases the affinity or the availability of the binding site. This site, however, likely is not modulated significantly by imposed changes in the electric field across the

channel as block by azimilide shows virtually no voltage dependence. Busch et al. (1994) also observed a small (10-30%) closed-state block of human minK expressed in *Xenopus* oocytes, followed by a second component of inhibition that was strongly use-dependent and only weakly voltage-dependent (see their Figure 3). Unlike our results, however, Busch et al. reported that azimilide decreased the 'fast' time constant of activation of minK (although they were unable to adequately fit the slow component of activation) and increased the deactivation time constant, suggesting that azimilide was acting as an open channel blocker. Yao and Tseng (1997) have also described open channel block of I_{Ks} by azimilide in canine ventricular myocytes. It is unclear why our results are so different from those of Busch et al. (1994) and Yao and Tseng (1997). The concentrations of azimilide and the recording conditions were similar in all studies. It is possible that the effects of azimilide in canine ventricular myocytes could have been contaminated by actions of this compound on other currents in this tissue (azimilide was shown to block I_{Kr}, I_{Ca}, and I_{Na} at similar concentrations; Yao and Tseng (1997). Alternatively, the variability could be due to alternate azimilide binding sites specific to the different species used in these studies.

Mechanism of Propenamide Block

Propenamide is a new benzodiazepine compound which has been reported to be a selective blocker of I_{Ks} at low (nM) concentrations (Salata et al., 1996b). This compound blocks I_{Ks} in guinea pig ventricle and minK expressed in *Xenopus* oocytes with an IC_{50} of 6nM (Salata et al., 1996b) and 5nM (Richard Swanson, personal communication), respectively. In this study we report a Kd of approximately 60nM for I_K and 150nM for minK (approximations: we did not do complete concentration-dependence curves), values which are 10-30 fold higher than those reported previously. The reason for this discrepancy is unclear. Propenamide is a highly lipophilic compound which takes a long time (10 minutes) to achieve steady-state block. The difference between efficacy of block of I_K in bullfrog compared to guinea pig I_{Ks} may be based on species differences. However, this possibility does not explain why the K_d for block of minK expressed in

Xenopus oocytes is also much higher (25x) compared to earlier reports. Propenamide is insoluble in aqueous solutions and therefore needs to be dissolved in 100% dimethylsulfoxide before dilution into perfusion solution. Furthermore, this compound is somewhat unstable and small aliquots need to be prepared daily (Joseph Salata, Merck Ltd., personal communication). Although we followed the preparation instructions, it is possible that there was either some precipitation of propenamide in the perfusion solution or some degradation of propenamide occurred either in transit or during preparation of solutions. None of these possibilities can be entirely ruled out until more data are available and we, or others, gain more information about the binding site for propenamide.

The magnitude of propenamide-induced inhibition of I_K and minK increases at positive potentials. These results are in agreement with the findings of Salata et al. (1996b) demonstrating that this compound blocks I_{Ks} in guinea pig ventricular myocytes in a voltage-dependent manner. Furthermore, we have obtained data illustrating that there are two-separate components of propenamide-induced block of minK; an initial closed-state inhibition accounting for approximately 2/3 of the total block; and a use-dependent component which is responsible for 1/3 of the total inhibition. Salata et al. (1996b) reported an increased rate of propenamide-induced block of guinea pig I_{Ks} when prepulse frequency was increased from 0.5 to 4Hz, also suggesting block is use-dependent. Propenamide did not change the kinetics of activation of minK, but increased the time constant of deactivation by approximately 14%. Based on these findings one can speculate that propenamide binds to and blocks the channel predominantly in the closed state, and changes that occur during channel opening (ie. conformational shifts or changes in the electric field) facilitate an increased magnitude of inhibition. The fact that block is voltage-dependent, and also that there is a slowing of the decay of deactivation, suggests that there may also be a small component of open channel block. This component must be very small, however, as propenamide does not change the activation kinetics of minK. Since this compound his highly lipophilic there is no way to predict from this data whether the binding site is intracellular or extracellular.

Summary and Limitations

Despite the many similarities between the two currents investigated here, caution must be used when comparing characteristics of a mammalian clone injected into an amphibian expression system with a native amphibian K^+ channel. Originally we had wanted to perform a direct comparison of minK isolated from bullfrog atrial myocytes to bullfrog I_K in order to circumvent many of the problems involved with comparing different species (ie. temperature differences, structural changes, sequence variability). Numerous attempts to clone minK from bullfrog heart, however, were unsuccessful, leading us to perform the experiments using the rat minK clone described in these studies.

These results are the first describing a detailed semi-quantitative comparison of minK expressed in *Xenopus* oocytes to I_K in bullfrog atrial myocytes. We show that these currents have similar biophysical and pharmacological properties, suggesting that minK is at least part of the molecular structure underlying I_K. These data do not rule out the possibility that minK interacts with another subunit such as KvLQT1, as it is possible that all the pharmacological data reported in this study are due to actions of these compounds on KvLQT1 endogenous to *Xenopus* oocytes and present in bullfrog atria, rather than on minK. Indeed, recent reports have shown that azimilide (Busch et al., 1997) and chromanol 293B (Busch et al., 1997; Loussouarn et al., 1997) can inhibit KvLQT1 expressed in *Xenopus* oocytes. A preliminary investigation of the molecular components underlying bullfrog I_K is the subject of the following chapter.

CHAPTER 5:

MOLECULAR STRUCTURES UNDERLYING I_K IN BULLFROG ATRIA

Introduction

In Chapter 4 we have shown that expression of minK in *Xenopus* oocytes results in a K^+ current with very similar biophysical and pharmacological properties as I_K in bullfrog atria. However, as described in the Introduction, minK likely does not form a channel on its own, but instead coassembles with the KvLQT1 isoform which is endogenous in *Xenopus* oocytes (Sanguinetti et al., 1996). KvLQT1 is also present in mouse (Barhanin et al., 1996) and human (Wang et al., 1996; Sanguinetti et al., 1996) hearts. Coexpression of KvLQT1 and minK in either *Xenopus* oocytes or mammalian cell lines (Barhanin et al., 1996; Sanguinetti et al., 1996) results in a current with very similar selectivity, kinetics, and voltage-dependence to I_{Ks} in mammalian heart. Therefore, it has been proposed that this I_{Ks} current is encoded by a mixture of minK and KvLQT1, although the subunit stoichiometry, and the exact role of minK, is still unclear (Kaczmarek and Blumenthal, 1997).

Our pharmacological and biophysical data reported in Chapter 4 illustrate a number of impressive similarities between I_K and minK, but do not directly address the possibility that minK may interact with KvLQT1 endogenous to *Xenopus* oocytes. It is possible that azimilide and propenamide, which we demonstrated inhibit both minK and I_K, act on a KvLQT1 subunit rather than minK. In an attempt to gain further insight into the molecular structures underlying I_K in bullfrog heart, we have attempted to obtain molecular biological evidence that the proteins proposed to underlie the slowly activating delayed rectifier K^+ channel (minK and KvLQT1) are present in bullfrog atrium.

Results

Identification of MinK in Bullfrog Heart

We have tried to identify minK in bullfrog heart using a number of different approaches, including screening of a bullfrog heart cDNA library, reverse transcriptase polymerase chain reaction (RT-PCR), Northern Blot analysis, and injection of bullfrog heart poly(A)$^+$ RNA (20ng) into *Xenopus* oocytes. Unfortunately, none of these have

yielded positive results. Our rationale for most of these tests was based on targeting minK using primers/probes designed from knowledge of the conserved regions of identified mammalian minK sequences. Using this rationale to design channel-specific primers we were able to identify KvLQT1 (see below) and also small (~150bp) fragments of two inward rectifier-type K^+ channels in bullfrog heart by RT-PCR. These fragments show 94% and 92% amino acid identity to GIRK1 (which encodes an acetylcholine-activated K^+ channel) identified in human brain (Chan et al., 1996) and rat atrium (Dascal et al., 1993), and an adenosine triphosphate-sensitive K^+ channel in human heart (Sakura et al., 1995), respectively. These results suggest that, for at least some K^+ channels, the amino acid sequence is highly conserved among amphibians and mammals. Nonetheless, we were unable to identify minK in bullfrog cardiac tissue, suggesting either that the sequence of minK in bullfrog heart is highly diverged from that of mammalian tissue, or that minK is not present in bullfrog heart.

Identification of KvLQT1 in Bullfrog Heart

Molecular Cloning of KvLQT1

As part of this research project, KvLQT1 cDNA from bullfrog heart was identified and cloned by our colleague, Robert Winkfein, in the Medical Research Council Group Molecular Biology Core Facilities at the University of Calgary. A 3'RACE protocol was first employed to amplify a portion of bullfrog KvLQT1. Three distinct PCR products were identified from the 3'RACE experiment, of which two represented different splice variants of bullfrog KvLQT1, and one appeared to be a PCR artifact. A combination of standard RT-PCR and 5'RACE was employed to determine the complete nucleotide sequences of the two splice variants. The nucleotide and deduced amino acid sequences of these two variants are shown in Figure 33. These variants are 2114nt (splice variant A) and 1544nt (splice variant B) in length, and share complete identity at the 5' end but diverge at the 3' end following amino acid 414. The longest open reading frames encode two proteins of 654 (variant A) and 487 amino acids (variant

Figure 33: Nucleotide and deduced amino acid sequences of each splice variant of bullfrog KvLQT1. Nucleotides and amino acids are numbered consecutively at the right. Both splice variants diverge following amino acid 414. Underlined amino acids represent the putative transmembrane domains and pore region, and underlined nucleotides represent consensus polyadenylation signals in the 3' untranslated regions. Potential N-linked glycosylation sites are indicated by the arrows (▼).

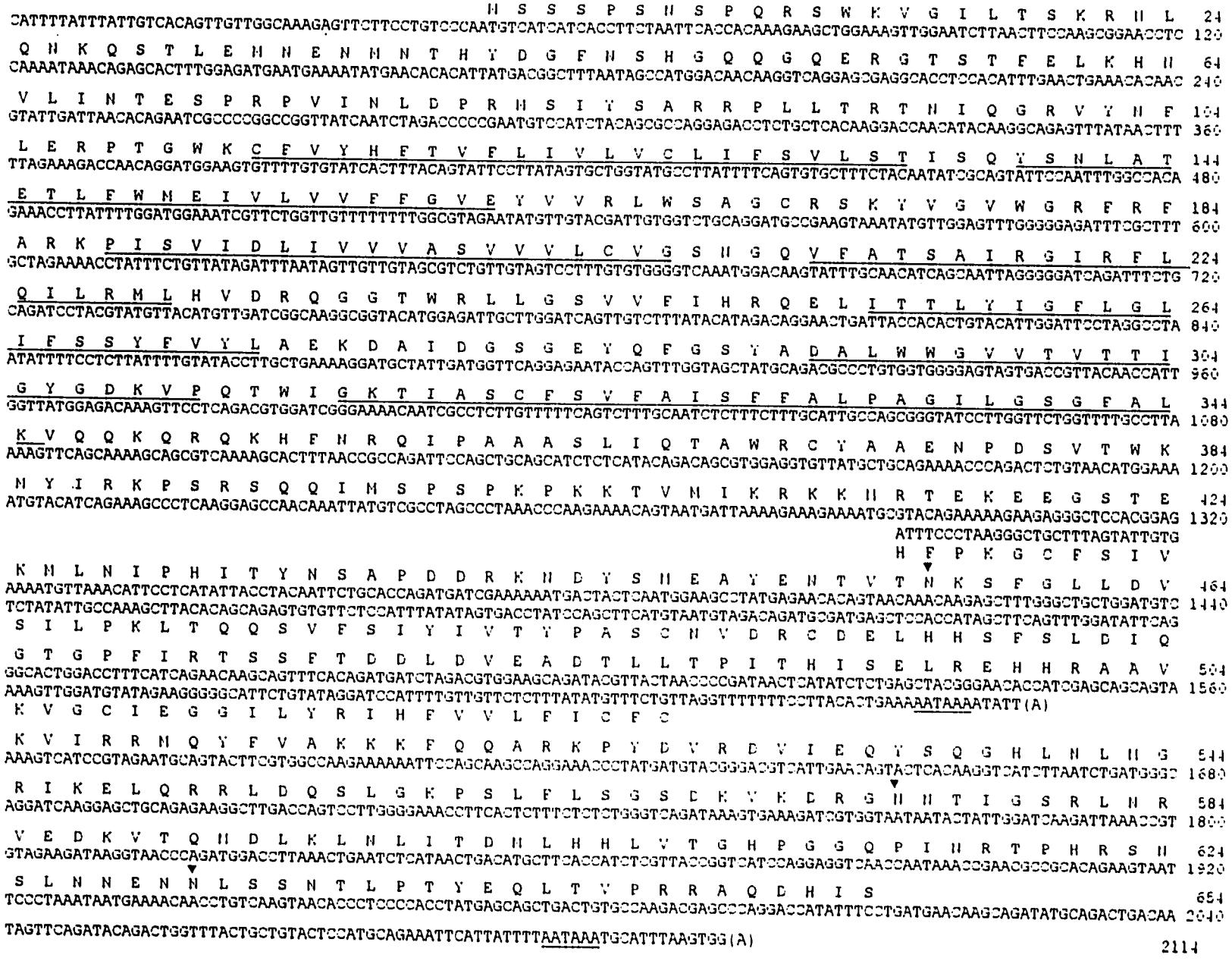

154

B), with a 5' untranslated region of 48bp and a 3' untranslated region of 104bp (variant A) or 35bp (variant B). Hydropathy analysis (Figure 34) of the putative proteins predicts that both variants have a topology similar to other voltage-gated K^+ channels, with 6 transmembrane domains and a cytoplasmic carboxy-terminus. Splice variant B, however, also possesses a stretch of approximately 18 amino acids at the carboxy-terminus that are strongly hydrophobic, perhaps representing another transmembrane domain.

Figure 35 shows the sequence alignment of splice variant A with KvLQT1 isolated from human heart (Splawski et al., 1997a; GenBank accession number U89364), mouse heart (Barhanin et al., 1996; GenBank accession number U70068), and *Xenopus* oocytes (Sanguinetti et al., 1996; GenBank accession number U71076). Splice variant A has 68% identity and 76% similarity at the amino acid level with the human cardiac KvLQT1 sequence, with the majority of divergence occurring at the 5' end. In the putative transmembrane domains and pore region the bullfrog and human sequences share 95% identity and 97% amino acid similarity. Furthermore, in the 401 amino acids that are known for the sequence of KvLQT1 in *Xenopus* oocytes, bullfrog and *Xenopus* KvLQT1 have 85% identity and 88% similarity. Thus, bullfrog KvLQT1 shares a high degree of homology with KvLQT1 isolated from other species.

There are three methionine residues in bullfrog KvLQT1 at positions 1, 33 and 37, that represent putative translation start sites. At positions 1 and 33, but not 37, there are also corresponding methionines in the *Xenopus* oocyte sequence. We have therefore assumed (but have no functional evidence to prove) that the first methionine represents the translational start site. One consensus polyadenylation signal is present in each splice variant upstream of the poly $(A)^+$ tail in the 3' untranslated region, and three potential N-linked glycosylation sites are located at residues 456, 575, and 631 in splice variant A. One potential cAMP- and cGMP-dependent protein kinase phosphorylation site is present at amino acid 388 in both variants A and B, and 12 potential protein kinase C (PKC) phosphorylation sites are located at positions 12, 19, 20, 71, 86, 238, 382, and 400 corresponding to both variants A and B, with additional sites at residues 416, 423, 455,

Figure 34: Hydropathy plot of splice variants A (**A**) and B (**B**) of bullfrog KvLQT1, calculated according to Kyte and Doolittle (1982), using a window of 9 amino acids.

A

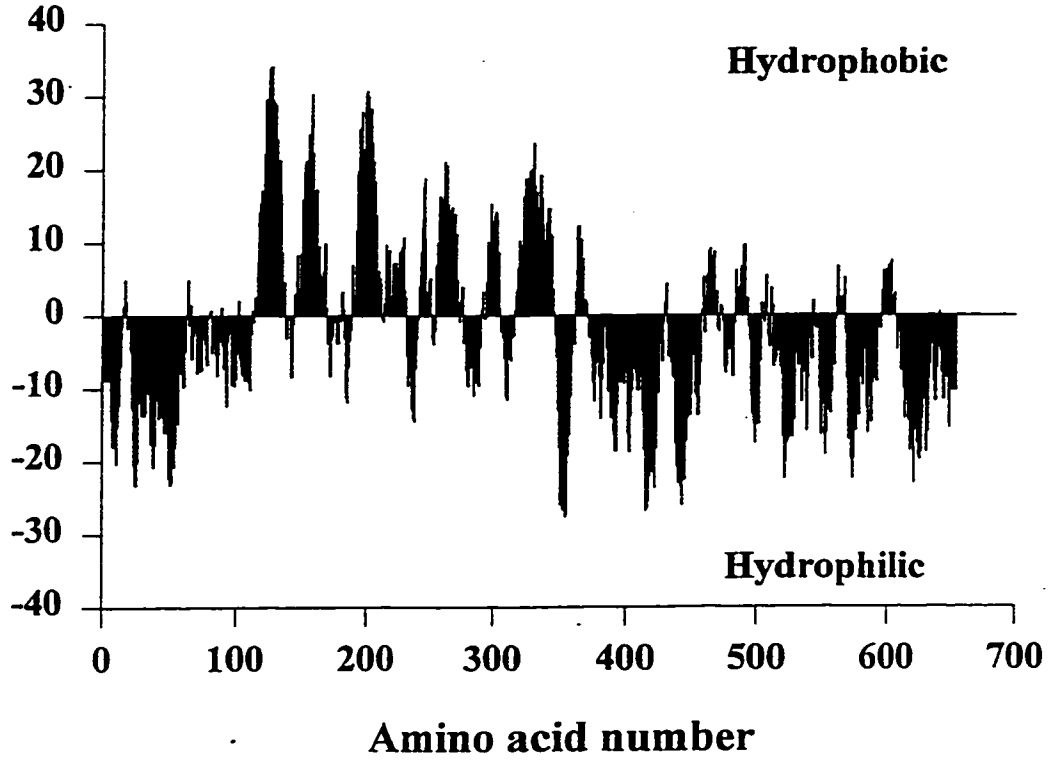
40
30
20
10
0
-10
-20
-30
-40
Hydrophobic
Hydrophilic
0
100
200
300
400
500
600
700
Amino acid number

B

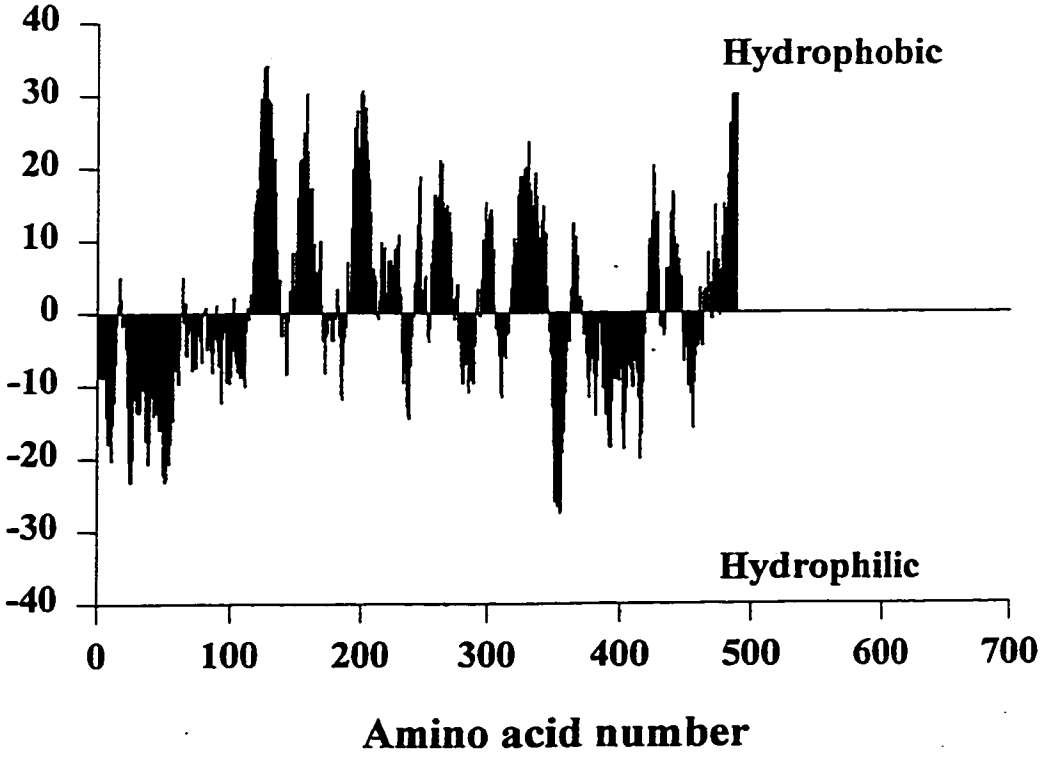
40
30
20
10
0
-10
-20
-30
-40
Hydrophobic
Hydrophilic
0
100
200
300
400
500
600
700
Amino acid number

Figure 35: Amino-acid sequence alignment of bullfrog KvLQT1 with human, mouse, and *Xenopus* oocyte KvLQT1 (see text for references). Amino acids are numbered consecutively on the left. Horizontal bars denote the six putative transmembrane domains (**S1** to **S6**) and the pore region (**P**). Dotted lines indicate a gap in the sequence, and dashed lines represent regions where no corresponding sequence is available.

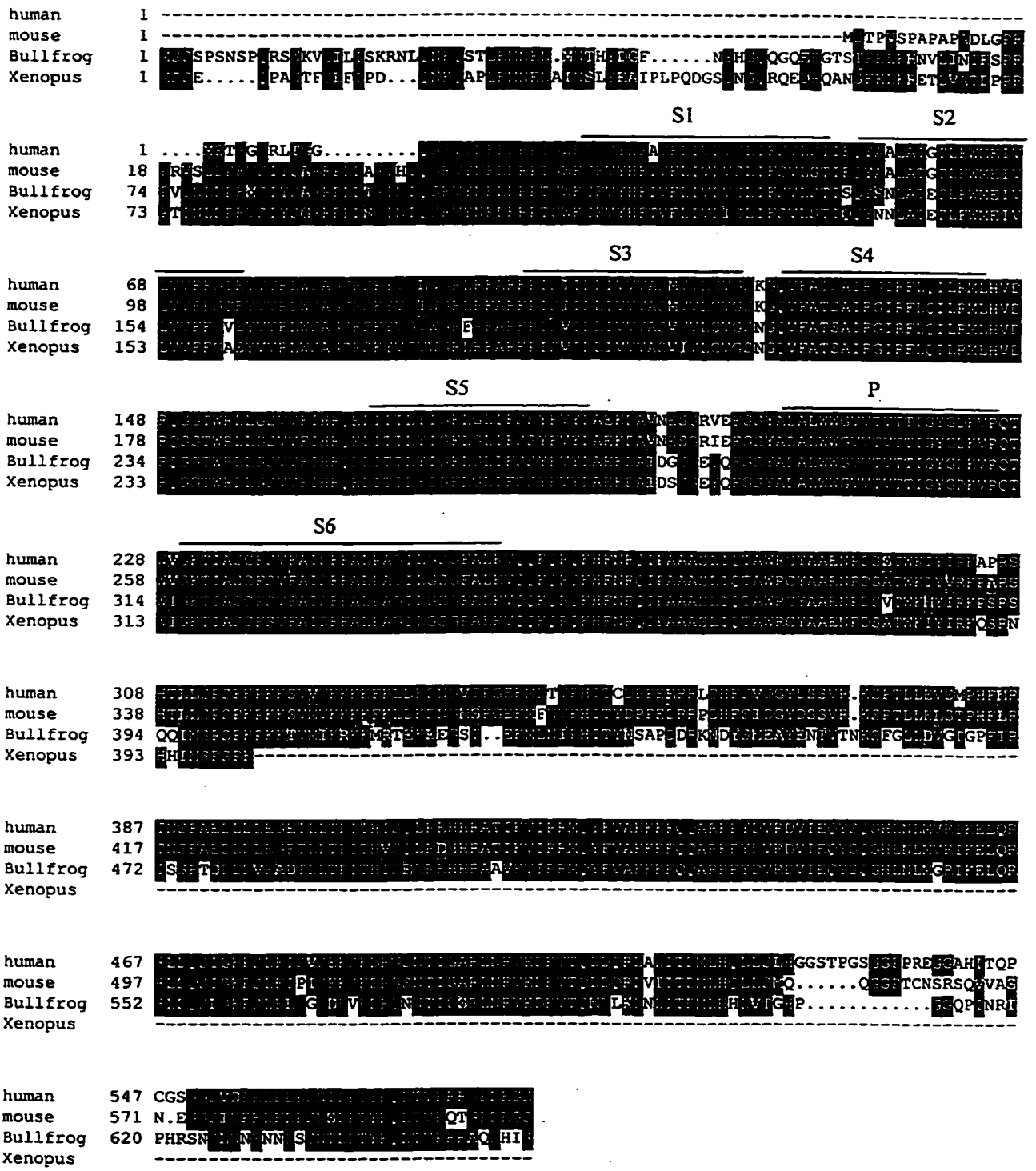
human 1
mouse 1
Bullfrog 1
Xenopus 1
S1
S2
human 1
mouse 18
Bullfrog 74
Xenopus 73
S3
S4
human 68
mouse 98
Bullfrog 154
Xenopus 153
S5
P
human 148
mouse 178
Bullfrog 234
Xenopus 233
S6
human 228
mouse 258
Bullfrog 314
Xenopus 313
human 308
mouse 338
Bullfrog 394
Xenopus 393
human 387
mouse 417
Bullfrog 472
Xenopus
human 467
mouse 497
Bullfrog 552
Xenopus
human 547
mouse 571
Bullfrog 620
Xenopus

and 567 in splice variant A. The phosphorylation sites at amino acids 238, 382, and 400 are also conserved in the human sequence.

In Situ Hybridization

The expression of KvLQT1 in bullfrog heart was also investigated using *in situ* hybridization. We used non-radioactive digoxigenin (DIG)-labelled oligonucleotide probes in attempts to localize KvLQT1 mRNA transcripts in frozen tissue slices from bullfrog heart. The probes were designed based on a conserved region in both 3' splice variants of bullfrog KvLQT1, as described in the Materials and Methods (Chapter 2). In all experiments the corresponding sense probe was also included as a negative control to determine the specificity of the hybridization reaction. DIG-labelled probes were incubated with an anti-DIG-alkaline phosphatase conjugated antibody, and then detected colorimetrically with a mixture of NBT and BCIP. The incubation time in the detection solution was optimized to maximize the intensity of the signal but to minimize non-specific background activity. Figures 36 and 37 illustrate the pattern of KvLQT1 mRNA transcript expression in bullfrog atria at two different magnifications. In panels A and B (of both Figures 36 and 37) atrial tissue sections were hybridized with the KvLQT1 antisense or sense probe, respectively, and incubated in detection solution for 17 hours. Note the strong hybridization signal in panel A, supporting the presence of KvLQT1 in bullfrog heart. The intensity of staining is much weaker in panel B, suggesting that our results represent specific hybridization of the antisense probe to KvLQT1 mRNA. Although it is not possible to more specifically localize the anatomical correlates of this staining, note the darker staining in the nuclei of the muscle fibers that are shown in cross-section. Additional control experiments (to test background levels of staining generated by the anti-DIG antibody and/or the NBT and BCIP substrates), in which hybridization occurred without the addition of oligonucleotide probe, or the anti-DIG antibody was omitted, both gave negative results (data not shown), further suggesting that the hybridization signal seen in Figures 36 and 37 results from specific binding of the antisense probe to its target.

Figure 36: *In situ* hybridization analysis of KvLQT1 in tissue sections from bullfrog atrium. Serial sections of atrial tissue were hybridized with antisense (**A**) or sense (**B**) DIG-labelled oligonucleotide probes targeted against bullfrog KvLQT1. Note that virtually no hybridization is evident in the section treated with the sense DIG-labelled probe. Both photomicrographs were taken at the same exposure (1/30sec). Magnification = 176x.

A

B

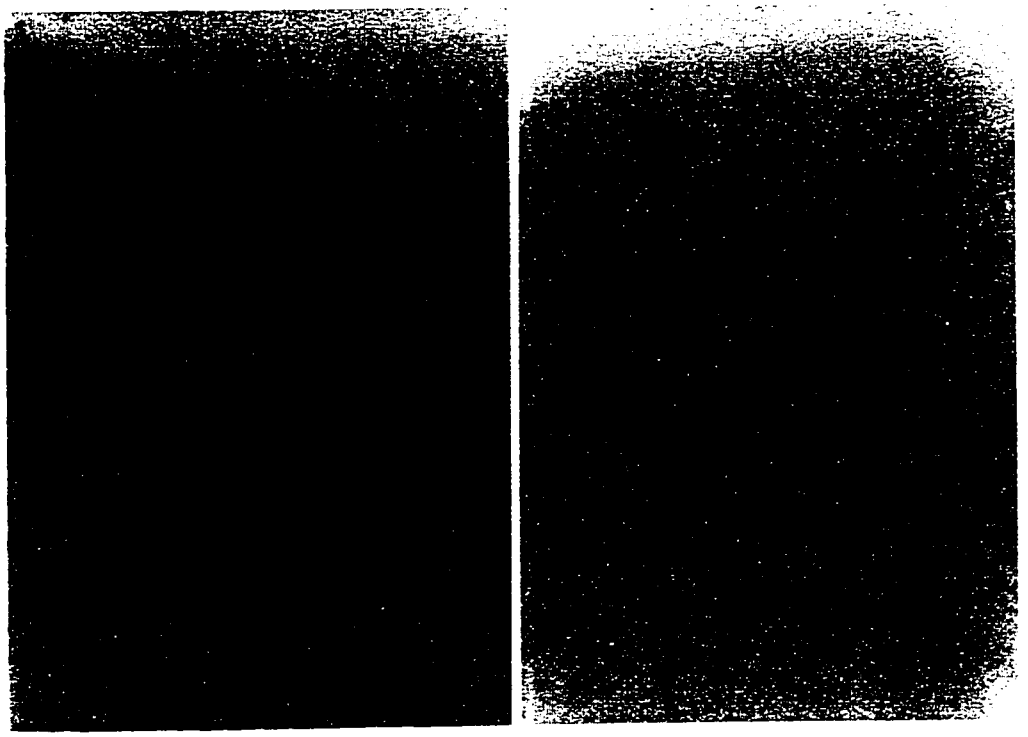

Figure 37: *In situ* hybridization analysis of KvLQT1 in tissue sections from bullfrog atrium. Serial sections of atrial tissue were hybridized with antisense (**A**) or sense (**B**) DIG-labelled oligonucleotide probes targeted against bullfrog KvLQT1. Both photomicrographs were taken at the same exposure (1/8sec). Magnification = 352x.

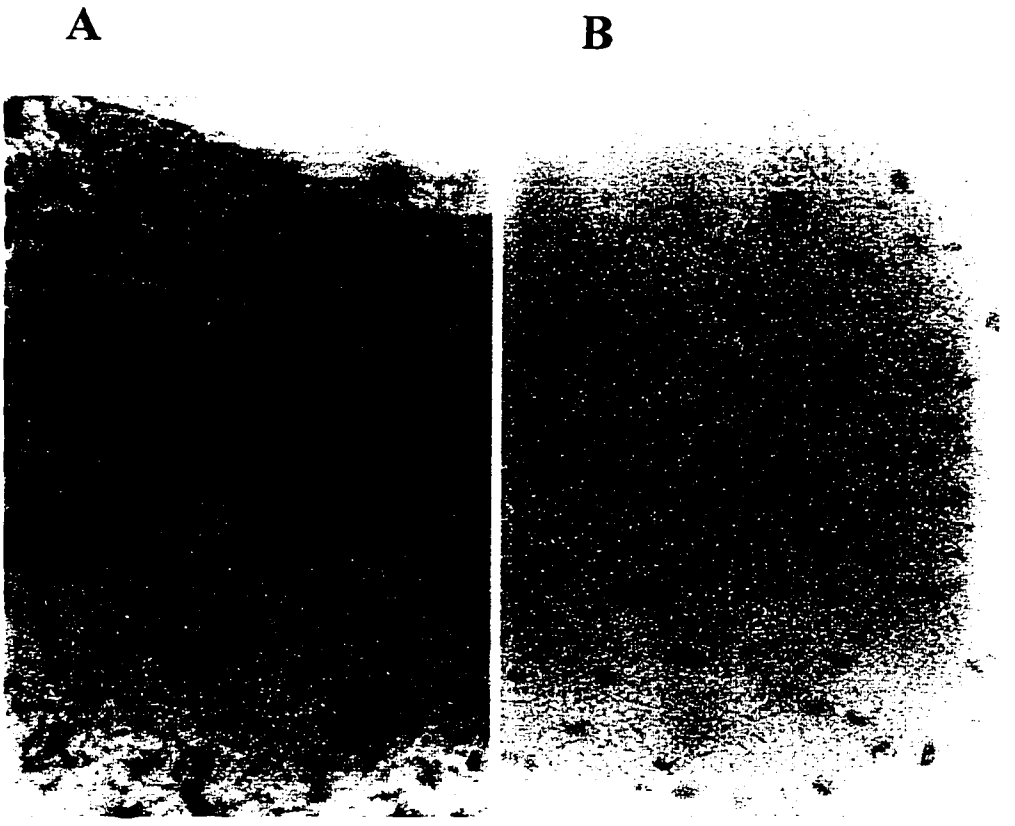
A
B

Discussion

The aim of this study was to obtain molecular biological evidence which would provide a test of the hypothesis that the proteins KvLQT1 and minK, which underlie I_{Ks}, are present in bullfrog atrium. Our results demonstrate expression of KvLQT1 in bullfrog cardiac tissue, but we have been unable to identify minK in bullfrog heart. We have cloned two potential splice variants (A and B) of KvLQT1, and shown that each sequence diverges in the putative carboxy-terminus. Splice variant A shares the highest degree of homology with KvLQT1 isolated from other species, although both variants are virtually identical to human KvLQT1 within both the putative transmembrane segments and pore domain, suggesting that these regions are highly conserved between species. The open reading frame of splice variant A predicts a protein of 654 amino acid sequence, which is somewhat larger than the 604 amino acid sequence which has been described for mouse heart KvLQT1 (Barhanin et al., 1996), and 581 amino acids reported for human cardiac KvLQT1 (Wang et al., 1996; Sanguinetti et al., 1996), but similar to the 676 amino acids described by Yang et al. (1997) for another splice variant of KvLQT1 in human heart. These differences between the bullfrog, mouse, and human clones are predominantly due to variations in the length of the amino-terminus. Hydropathy analysis predicts that bullfrog KvLQT1 may have a topology similar to other known K^+ channels, with 6 transmembrane regions and a pore domain. However, a potentially novel and interesting finding of this study is that splice variant B also has an additional region of approximately 18 amino acids at the carboxy-terminus. This region consists of strongly hydrophobic amino acids, and may represent another transmembrane domain.

Despite several reports describing multiple 5' splice variants of KvLQT1 (Yang et al., 1997; Lee et al., 1997; Jiang et al., 1997), to our knowledge this is the first report of 3' splice variants of KvLQT1. The functional characteristics of these two 3' splice variants are not yet known, since we have not attempted any rigorous functional expression experiments of either splice variant in *Xenopus* oocytes (variant A has been cloned but did not express in *Xenopus* oocytes). Our initial negative results, ie. inability

to get functional expression of bullfrog KvLQT1, may be due to mutations introduced into the sequence during multiple rounds of PCR amplification. Comparison of the clone sequence to the sequence derived from PCR products indicates that seven amino acid substitutions were introduced during the cloning process of variant A. These include the following changes: Pro to His (aa72), Val to Thr (aa191), Ile to Thr (aa226), Lys to Ile (aa317), Asn to Lys (aa456), Asp to Gly (aa593) and Thr to Ala (aa600). Interestingly, residues 191, 226, and 317 are located in the regions containing the putative transmembrane segments (191 is in the S3 domain; 226 is in the S4 domain; and 317 is in the S6 domain). Therefore, we suspect, but cannot be certain, that the lack of functional expression of bullfrog KvLQT1 is due to one or more of these mutations, and at present we are in the process of correcting these missense errors.

It is also unclear at this time which of the two 3' splice variants is the major isoform of bullfrog KvLQT1, although the fact that splice variant A shares such a high degree of homology with the human and mouse sequences suggest that this isoform likely represents the full-length clone. Ongoing Northern Blot analysis and/or RNase Protection Assay may allow us to determine the tissue distribution and/or the relative abundance of these two mRNA transcripts in bullfrog, and thus provide insight into the significance of each isoform.

Our *in situ* hybridization experiments provide quite strong evidence for the expression of KvLQT1 in bullfrog heart. We observed specific hybridization of the KvLQT1 antisense oligonucleotide probe to KvLQT1 mRNA in bullfrog cardiac slices, with the strongest signal being localized in the nuclei of the muscle fibers. Several control experiments including hybridization with the sense probe, hybridization without any probe, and exclusion of the anti-DIG antibody, all produced negative results, providing support for the specificity of our detection signal.

In summary, the results presented in this chapter provide evidence for the presence of KvLQT1 in bullfrog heart, but suggest that minK may not be present in this tissue. The possible consequences of these findings are discussed in Chapter 7.

CHAPTER 6:

K^+ ACCUMULATION DURING ACTIVATION OF K^+ CURRENTS EXPRESSED IN *XENOPUS* OOCYTES

Introduction

Accumulation of K^+ in restricted extracellular spaces, and the resulting modulation of electrophysiological responses in various tissues, has been well described. Frankenhaeuser and Hodgkin (1956) were the first to demonstrate the consequences of an increase in the concentration of external K^+ ($[K^+]_o$) in response to a train of action potentials in squid giant axons. More recently it has been reported that increasing external K^+ also can slow the time constant of removal of sodium inactivation and speed the development of inactivation in squid giant axons (Gillespie and Meves, 1981). The activity of various K^+ currents in frog atria (Noble, 1976; Brown et al., 1980), frog ventricle (Cleemann and Morad, 1979), *Xenopus* axons (Safronov and Vogel, 1995), and squid axons (Clay, 1986), is modulated by external K^+. In addition, changes in $[K^+]_o$ which occur during depolarizing voltage clamp steps have been described in numerous experimental preparations, including frog skeletal muscle (Almers, 1972), frog axon (Dubois and Bergman, 1975), squid axon (Adelman et al., 1973), and sheep cardiac Purkinje fibers (Baumgarten and Isenberg, 1977). A similar phenomenon has been described during the cardiac action potential in frog ventricular strips (Kline and Morad, 1976; Kline and Morad, 1978), canine Purkinje fibers (Kline and Kupersmith, 1982), snail visceral ganglion cells (Neher and Lux, 1973), and when rabbit atrium is driven at high rates (Kunze, 1977). Furthermore, increases in $[K^+]_o$ have been measured during repetitive firing of Purkinje cells in guinea pig hippocampal slices (Nicholson and Hounsgaard, 1983). The changes in $[K^+]_o$ in many of these tissues result from the extensive infolding of the plasma membrane. These 'clefts' or cavaeolae hinder diffusion of K^+ ions from the cell surface into the bulk solution, thereby resulting in localized increases of K^+ ions in the extracellular space. This phenomenon has been discussed in several comprehensive reviews (Attwell et al., 1979; Cohen and Kline, 1982).

As described in the Introduction, minK is a small 129-130 amino acid protein which is thought to coassemble with KvLQT1, and to be responsible for I_{Ks} which has been identified in a number of mammalian and amphibian cardiac tissues. When injected

into *Xenopus* oocytes, minK expresses a slowly activating K^+ current that does not reach steady-state, even in response to large depolarizing voltage clamp steps lasting longer than 30 seconds (see Chapter 4). The process underlying this very slow activation is not well understood. One suggestion is that many minK subunits must combine to form a functional channel and that this results in the slow activation kinetics (see Introduction; also review by Kaczmarek and Blumenthal, 1997). There is no direct evidence, however, concerning whether this is the mechanism responsible for the very slow increase in current amplitude observed at depolarized membrane voltages.

I_K in isolated bullfrog atrial myocytes exhibits many of the same characteristics as minK expressed in *Xenopus* oocytes (see Chapter 4). However, in single myocytes from bullfrog hearts I_K, unlike minK, reaches steady-state after approximately 20-25 seconds at eg. +30mV. This is not usually true, however, in multicellular atrial trabeculae preparations from bullfrog in which I_K does not saturate, and in which K^+ accumulation in restricted spaces is known to alter the current kinetics (Brown et al., 1976a; Brown et al., 1976b). It is possible that the difference between the activation kinetics of minK and I_K may be due to microanatomical differences between bullfrog atrial myocytes and *Xenopus* oocytes. The surface microanatomy of a *Xenopus* oocyte is quite complex. The plasma membrane is extensively fenestrated with macrovilli and microvilli, and it lies in series with a fibrous vitelline layer and an outer follicular membrane (Dumont and Brummett, 1978). Although the follicular membrane is usually removed by mechanical or enzymatic techniques prior to injection of cRNA (Stühmer, 1992), the presence of microvilli on the plasma membrane increases the surface area of the oocyte by as much as 3-10 times (personal calculations), and could form a significant barrier for diffusion.

As part of our analysis of minK recordings in *Xenopus* oocytes (see Chapter 4), we reasoned that K^+ ions accumulating in these extracellular fenestrations could cause a depolarizing shift in the reversal potential for a K^+ current, due to K^+ accumulation during the voltage clamp step. This change in electrochemical driving force could result in the outward K^+ current not reaching steady-state (similar to that observed in multicellular bullfrog atrial preparations); in fact, it may slowly increase if the ion transfer (current-

voltage) relationship showed inward rectification and/or was strongly dependent on the extracellular concentration of K^+ (Cohen and Kline, 1982). To examine this possibility, experiments were performed in which the effect of increasing voltage clamp step duration and magnitude on reversal potential in *Xenopus* oocytes injected with rat uterine minK was investigated. We observed that as either pulse duration or the magnitude was increased, reproducible depolarizing shifts in reversal potential occurred, consistent with there being K^+ accumulation on the extracellular surface of the oocyte.

To address the possibility that the observed changes were specific for minK, the influence of K^+ accumulation during voltage clamp experiments in *Xenopus* oocytes was studied using two different K^+ channel clones, rat uterine minK and RBK2 (Kv1.2). A depolarizing shift in reversal potential with increasing duration of a voltage clamp step was observed in studies of both K^+ channel subtypes expressed in *Xenopus* oocytes. Furthermore, depolarizing shifts in reversal potential were still observed after mechanical removal of the vitelline membrane. Our results are interpreted in terms of accumulation of K^+ occurring in subsurface "crypts" in the microvilli layer as well as in an unstirred fluid layer surrounding the cell. A simple mathematical model, based on known microanatomy and restricted diffusion, which can account for this K^+ accumulation was developed. These results and calculations provide a basis for determining the circumstances under which *Xenopus* oocytes can be used reliably as an expression system for studying K^+ channel voltage-dependence and selectivity.

Results

K^+ Accumulation in Oocytes Injected with Rat Kv1.2

RBK2 (Kv1.2), a K^+ channel clone that generates a rapidly activating, non-inactivating K^+ current when expressed in *Xenopus* oocytes, was chosen to investigate the phenomenon of K^+ accumulation. This clone was selected, in part, because the relatively slow (in comparison to other Shaker-like K^+ channel subtypes) decay of its tail currents allows accurate measurements of the reversal potential (E_{rev}). Figure 38 illustrates the effect of increasing pulse duration on E_{rev} in a single oocyte expressing Kv1.2. The superfusion solution was cooled to 17 (±1) °C to further slow the time constant of decay of the tail currents. All oocytes were held at -80mV and voltage steps to +20mV were applied for 100, 250, 500, 1000, or 2000msec at a rate of 0.05Hz. Each test pulse was followed by a second voltage step to selected membrane potentials near the estimated E_{rev} for a K^+ selective current. The membrane potential at which the tail currents showed no change was defined as the E_{rev} and was obtained by interpolation. E_{rev} following a 100msec pulse was -96.9 ± 1.0mV, very close to that predicted by the Nernst equation for a K^+ selective current. However, with longer pulse lengths a depolarizing shift in E_{rev} was consistently observed. E_{rev} following a 500msec pulse was -92.2 ± 0.8mV and following a 2000msec pulse it was -86.8 ± 2.1mV (n=7-13). These changes in E_{rev} can be used to give an estimate of the amount of K^+ ions that accumulated on the extracellular surface of the egg. Figure 39 summarizes these calculated changes in $[K^+]_o$ with increasing pulse duration. The intracellular K^+ concentration was assumed to be constant and equal to 135mM (temperature= 17°C), and $[K^+]_o$ was calculated using the Nernst equation. At the end of a 2000msec pulse $[K^+]_o$ increased from 2.0mM to 4.3mM. If intracellular K^+ depletion, rather than extracellular K^+ accumulation, was responsible for the depolarizing shifts in E_{rev} then for an equivalent change in E_{rev} $[K^+]_i$ would have had to change from 135mM to 64.5mM. Shifts of this magnitude are unlikely in such a big cell with an intracellular K^+ concentration of 90-150mM (Dascal, 1987). Thus, it was concluded that

Figure 38: Representative current traces obtained when Kv1.2 is expressed in a *Xenopus* oocyte. The oocyte was held at -80mV and pulsed to +20mV for 100, 250 or 1000 msec. Current tails were recorded at membrane potentials near E_K. Right panels show expanded current tails with the respective membrane potentials listed at the side. Note the depolarizing shift in E_{rev} with increasing pulse duration.

100msec pulse

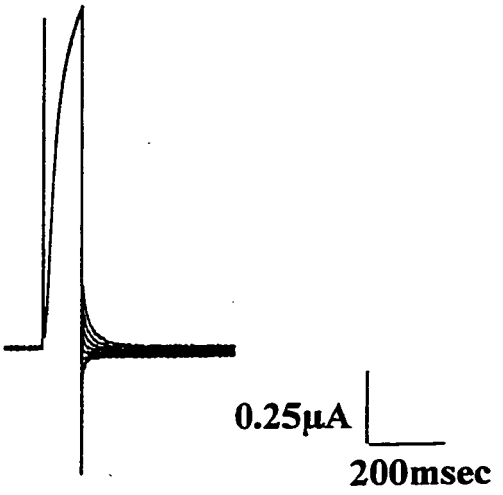

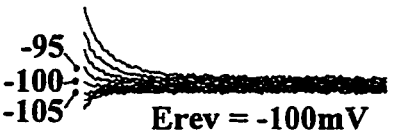

250msec pulse

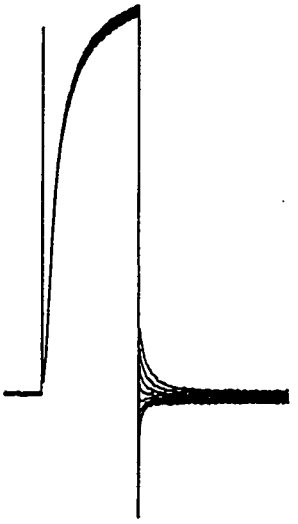

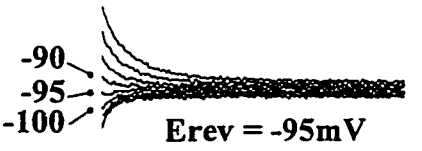

1 second pulse

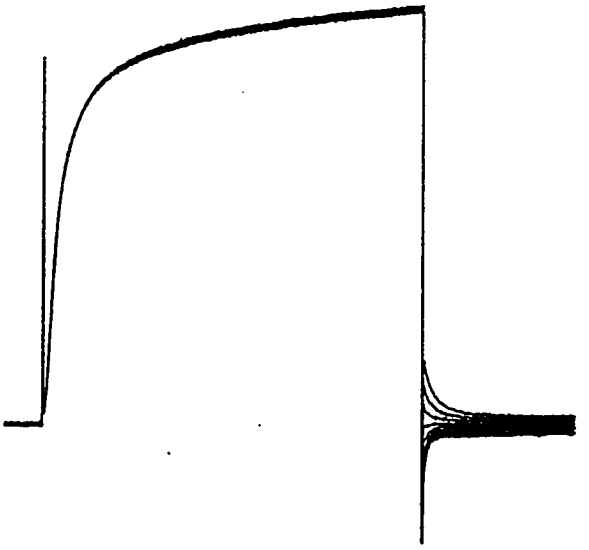

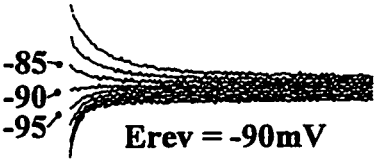

Figure 39: Change in $[K^+]_o$ as a function of voltage clamp duration in oocytes expressing Kv1.2 (n=7-13). $[K^+]_o$ was calculated as described in the text.

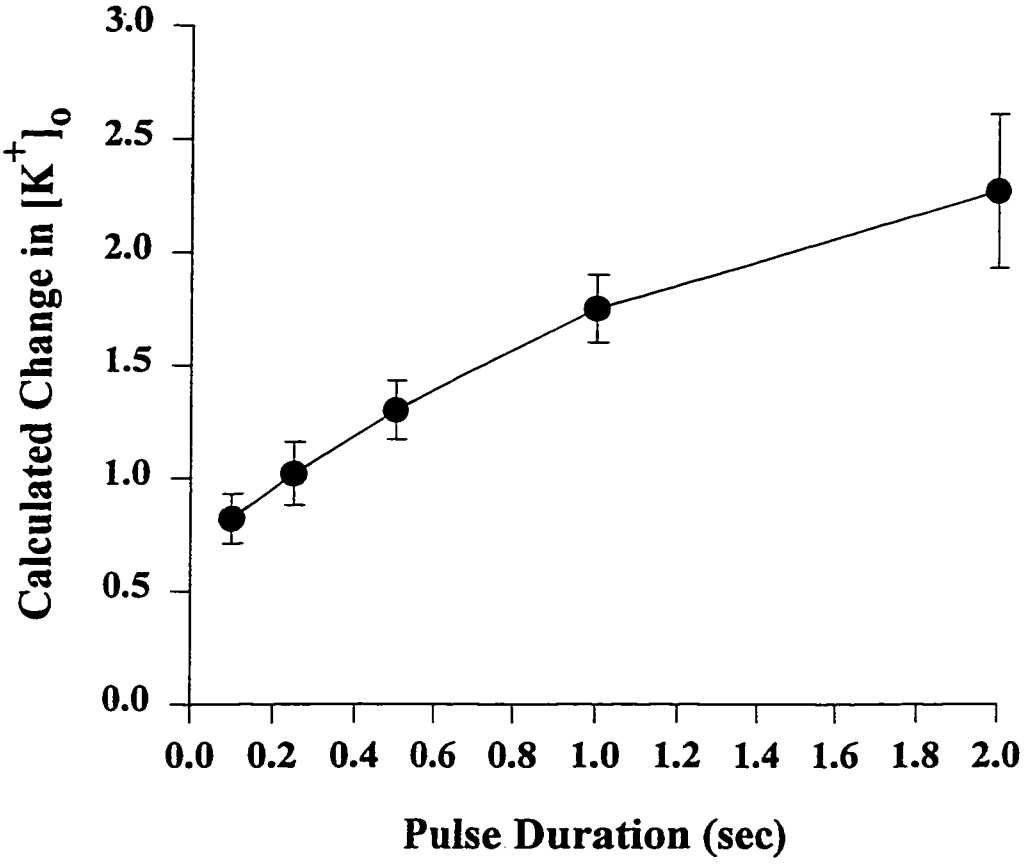
Calculated Change in $[K^+]_o$
3.0
2.5
2.0
1.5
1.0
0.5
0.0
0.0 0.2 0.4 0.6 0.8 1.0 1.2 1.4 1.6 1.8 2.0
Pulse Duration (sec)

the observed shifts in E_{rev} were due to accumulation of K^+ near the external surface of the oocyte (see Discussion for further comments).

K^+ Accumulation in Oocytes Injected with Rat Uterine MinK

As described in Chapter 4, minK generates a slowly activating, non-inactivating K^+ current when expressed in *Xenopus* oocytes. Experiments were performed to examine whether K^+ accumulation also occurred during activation of minK. *Xenopus* oocytes injected with rat uterine minK were held at -80mV and depolarized to +20mV for 1, 2, 3, 5, 10 or 20 sec every 50sec. E_{rev} was then measured as described above for the Kv1.2 experiments. Figure 40 illustrates the effect of increasing pulse duration on E_{rev}, measured using this protocol. A depolarizing shift in E_{rev} was observed with longer voltage pulses. In a series of experiments these values were measured to be -103.3 ± 1.7mV for a 1sec voltage step, -96.6 ± 1.5mV for a 5sec step, and -89.7 ± 1.7mV for a 20sec step (n=3-6).

To rule out the possibility that the depolarizing shifts in E_{rev} were simply an artifact of the repetitive voltage pulse protocol used to measure E_{rev}, we performed a second series of tests where E_{rev} was measured using ramp voltage pulses. In these experiments each depolarizing pulse to +20mV was followed by a 500msec ramp from -70mV to -120mV. An identical control ramp was applied from -70mV to -120mV without any prepulse. The currents elicited by these ramps were waveform subtracted and the voltage at which these currents intersected the zero level was taken as the E_{rev}. This subtraction procedure eliminated the contribution of currents endogenous to the oocyte from the E_{rev} values. Figure 41 illustrates the effect of increasing pulse duration on E_{rev} measured using this ramp protocol in a different oocyte from that shown in Figure 40. A similar depolarizing shift in E_{rev} was observed when pulse duration was increased (Summary data: 1sec pulse: E_{rev}= -104.3 ± 1.7mV; 5sec pulse: E_{rev}= -101.8 ± 0.5mV; 20sec pulse: E_{rev}= -96.8 ± 0.5mV; n=5-16 for all points). The changes in $[K^+]_o$ corresponding to these E_{rev} shifts for both batches of minK eggs, calculated as described above in the Kv1.2 experiments (except temperature= 20°C), is shown in Figure 42. Note that the changes in $[K^+]_o$ with increasing pulse duration in the ramp experiments are

Figure 40: Representative current traces of rat uterine minK expressed in a *Xenopus* oocyte. The egg was held at -80mV and pulsed to +20mV for 3, 5, or 10sec. Current tails were recorded at membrane potentials near E_K. Right panels show expanded current tails expanded with the respective membrane potentials listed at the side. Note the depolarizing shift in E_{rev} with increasing pulse duration.

3 second pulse

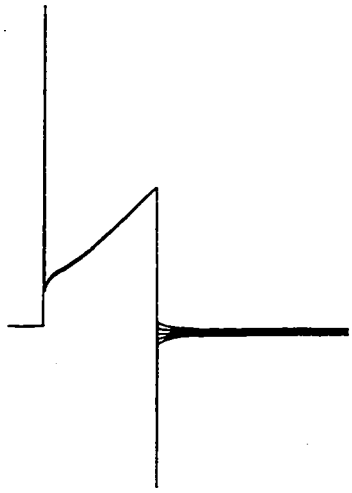

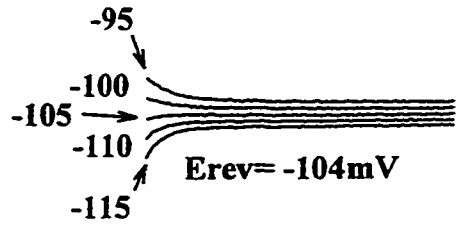

5 second pulse

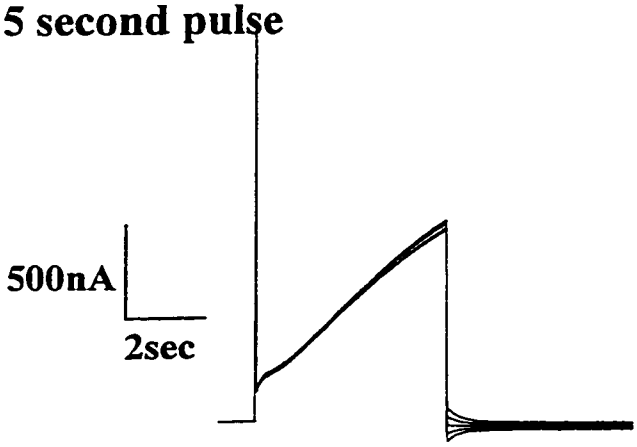

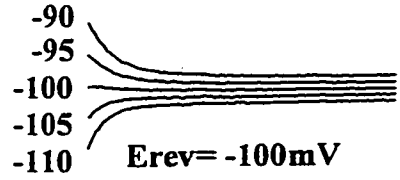

10 second pulse

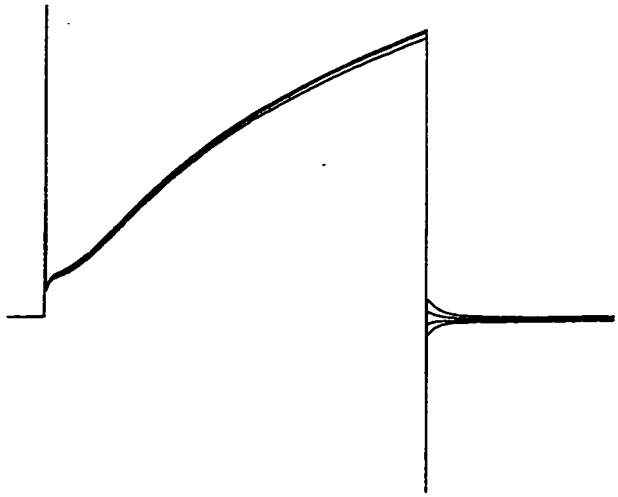

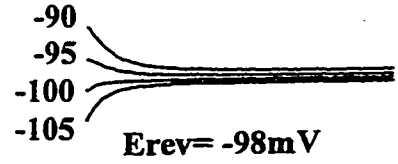

Figure 41: **A)** Representative current traces of rat uterine minK expressed in a *Xenopus* oocyte. The egg was held at -80mV and pulsed to +20mV for 1,3, 5, 10, or 20sec. Current tails were measured by applying ramp voltage waveforms from -70 to -120mV for 500msec, immediately after the depolarizing voltage steps. Capacity transients have been removed. **B)** Current-voltage relationship obtained after 3, 10, and 20sec pulses from the cell shown in the upper panel. Traces are marked as **c**, **b**, and **a**, respectively. Note the depolarizing shifts in E_{rev} with increasing pulse duration.

A

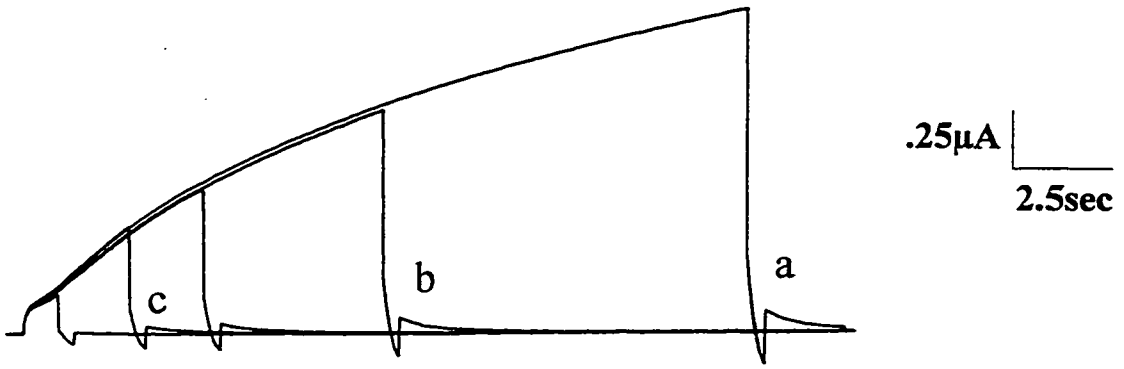
.25µA
2.5sec
a
b
c

B

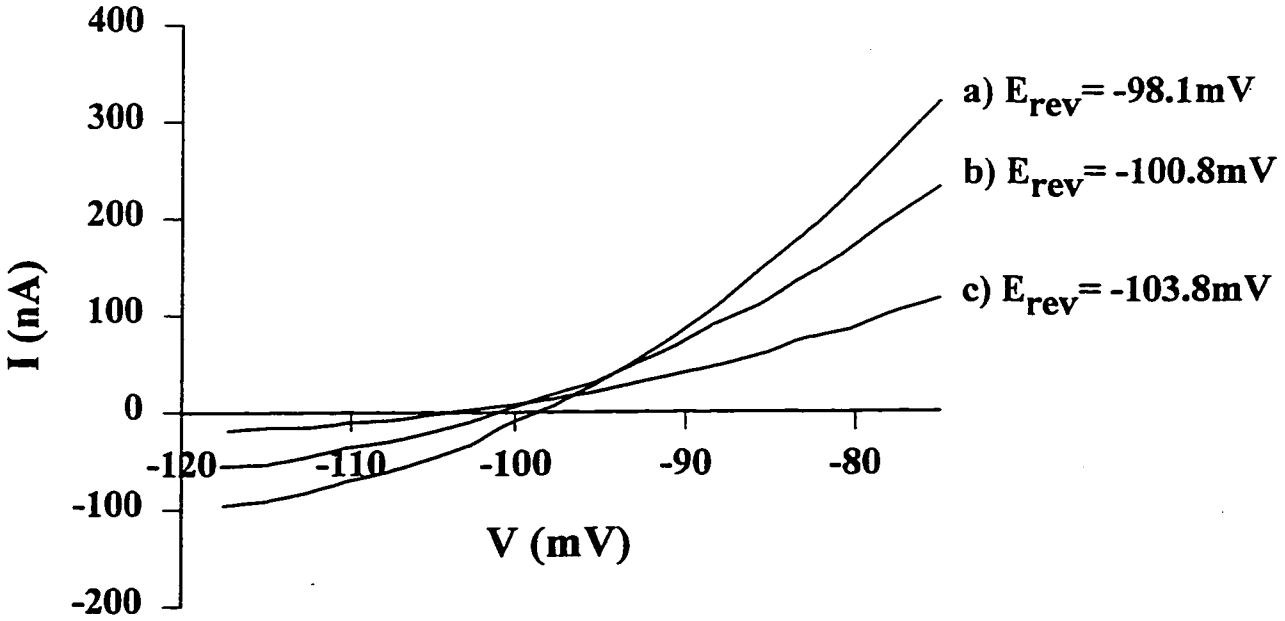
400
300
200
100
0
-100
-200
I (nA)
-120
-110
-100
-90
-80
V (mV)
a) E_{rev}= -98.1mV
b) E_{rev}= -100.8mV
c) E_{rev}= -103.8mV

Figure 42: Change in $[K^+]_o$ as a function of pulse duration for normal eggs expressing rat uterine minK, measured using either a rectangular voltage step (closed circles, n=3-6) or ramp voltage waveform (closed squares, n=5-16) protocol. $[K^+]_o$ was calculated as described in the text.

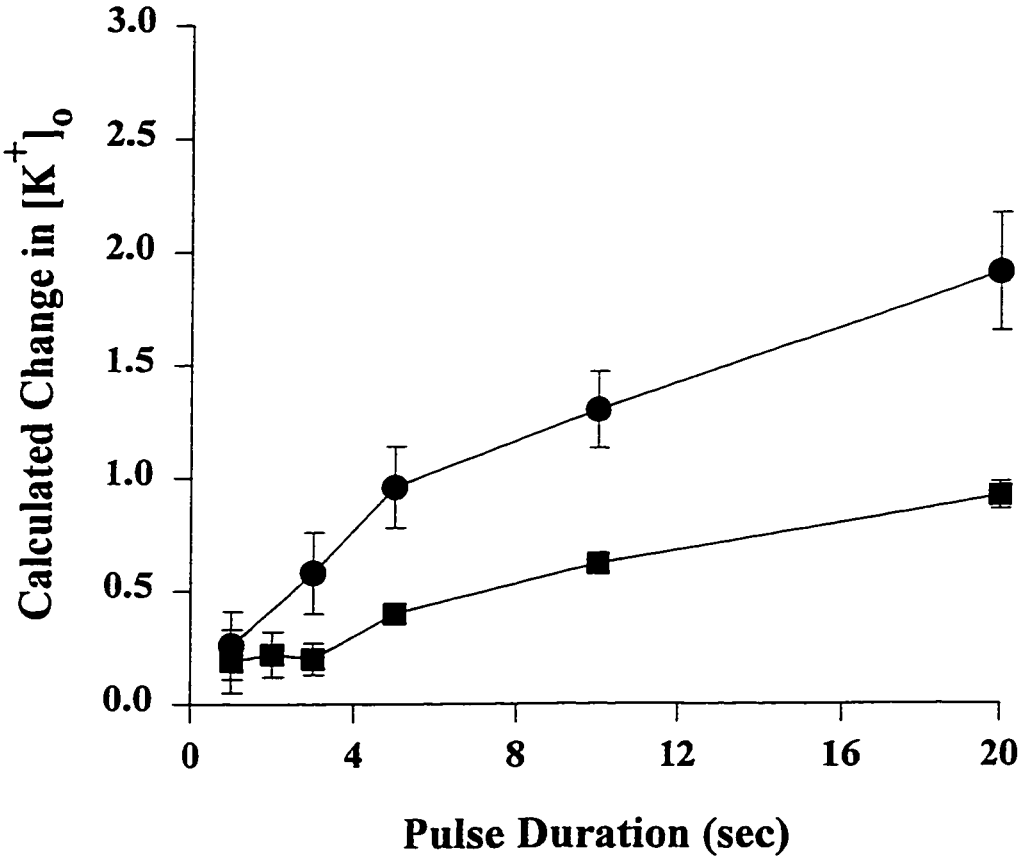
3.0
2.5
2.0
1.5
1.0
0.5
0.0
Calculated Change in $[K^+]_o$
0
4
8
12
16
20
Pulse Duration (sec)

smaller than those measured using the rectangular step voltage clamp commands. These differences are due in part to the larger current magnitudes in the rectangular step experiments. This difference will be addressed in more detail in the following section.

These results strongly suggest that K^+ accumulates on the extracellular surface of the oocyte as the length of the voltage pulse increases. Similarly, K^+ accumulation should be enhanced if the length of the pulse duration is kept constant but the magnitude of the current pulse is increased. Figure 43 illustrates the results of a single experiment in which an oocyte injected with minK was held at -80mV and then depolarized to -20mV, 0mV, or +20mV for 20sec. E_{rev} was measured using the ramp voltage protocol. As expected, positive shifts in E_{rev} were observed when pulse magnitude was increased, with E_{rev} changing from -104.7 ± 1.8mV at -20mV, to -100.8 ± 1.3 at 0mV, and -97.6 ± 1.1mV at +20mV (n=13).

Volume of the K^+ Accumulation Space

The changes in E_{rev} and the magnitude of the current of each pulse can be used to estimate the volume of space in which K^+ must accumulate on the extracellular surface of the oocyte, a measure that standardizes the changes in $[K^+]_o$ relative to the efflux of K^+ for each current pulse. To calculate this volume, $[K^+]_o$ for each pulse was determined as described previously. The current change during the depolarizing step was then integrated and converted to moles of K^+ flux, utilizing Faraday's constant (96, 487 coulombs/mole for a monovalent ion):

$$\#\ \text{moles} = (\int I \bullet dt)/96{,}487).$$

The volume of the space in which the K^+ accumulation occurs was then estimated using the equation:

$$\text{Volume} = \#\text{moles}/[\Delta K^+]_o.$$

Figure 44A provides a summary of this calculated volume of the accumulation space vs pulse duration for oocytes injected with Kv1.2 (see the closed circles). This calculated volume is very small for oocytes injected with Kv1.2; for a 100msec pulse the accumulation volume was calculated to be 5.0 ± 1.2 nl, or less than 1% of the total

Figure 43: **A)** Representative current traces of rat uterine minK expressed in a *Xenopus* oocyte. The egg was held at -80mV and pulsed to -20mV, 0mV, or +20mV for 20sec. Deactivating K^+ currents were recorded by applying ramp voltage waveforms from -70 to -120mV for 500msec, immediately following the depolarizing voltage steps. **B)** Current-voltage relationship obtained after the -20mV, 0mV, and +20mV pulses in the same oocyte as shown in the upper panel. Traces are marked as **c**, **b**, and **a** respectively. Note the depolarizing shifts in E_{rev} with increasing pulse magnitude.

A

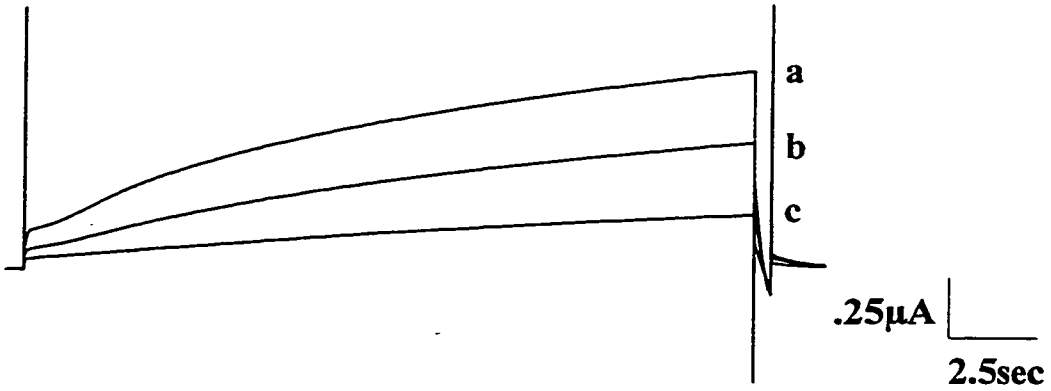
a
b
c
.25µA
2.5sec

B

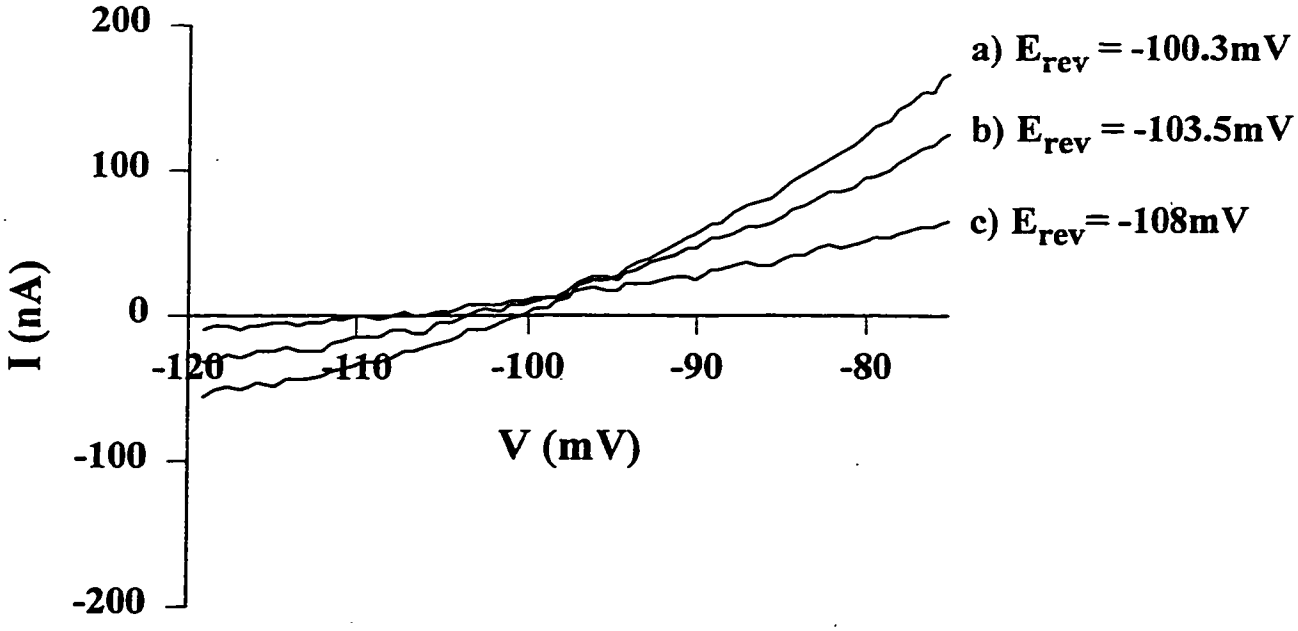
200
100
0
-100
-200
I (nA)
-120
-110
-100
-90
-80
V (mV)
a) E_{rev} = -100.3mV
b) E_{rev} = -103.5mV
c) E_{rev} = -108mV

volume of the egg (assuming egg diameter=1mm), and for a 2000msec pulse the accumulation volume was 45.6 ± 5.2nl (8.7% of the total egg volume). Figure 44B summarizes the calculated volume of the accumulation space vs pulse duration for oocytes injected with minK for both the square (closed circles) and ramp (closed squares) voltage protocols. In contrast, the volume of the accumulation space is much larger for eggs injected with minK [Square steps: 5sec pulse= 33.1 ± 8.6nl (%egg volume= 6.3%), 20sec pulse= 131.0 ± 18.5nl (%egg volume= 25%), n=5-6; Ramp steps: 5sec pulse= 55.1 ± 13.2nl (% egg volume= 10.5%), 20sec pulse= 202.0 ± 20.5nl (% egg volume= 38.5%), n=16]. This difference between minK and Kv1.2 could arise from the distinct activation kinetics of the two currents. This will be addressed in more detail in the Discussion of this Chapter. The apparent differences between the accumulation volumes measured using either the ramp or square step protocols (especially at the longer pulse durations) are not statistically significant ($p>0.05$, Student's unpaired two-tailed t-test).

K^+ Accumulation in Devitellinized Eggs

The vitelline membrane is a fibrous layer that helps to maintain the structural integrity of the oocyte (see Figure 45). Since this layer is approximately 2μm thick it could act as a significant barrier for K^+ ions diffusing away from the microvilli. We therefore examined whether the presence of the vitelline membrane influenced the extent of K^+ accumulation by repeating E_{rev} measurements in the absence of this membrane in eggs injected with minK or Kv1.2. Under these conditions significant depolarizing shifts in E_{rev} were still observed with increasing pulse duration after activation of either K^+ current, suggesting that accumulation of external K^+ does not occur in the space delimited by the vitelline membrane. E_{rev} measurements for oocytes injected with minK were -104.3 ± 1.2mV for a 3sec pulse, -98.2 ± 1.2mV for a 5sec pulse, and -90.1 ± 1.0mV for a 20sec pulse using the square voltage step protocol (n=7-8). In experiments using the ramp voltage step protocol, E_{rev} for a 3sec pulse was -97.2 ± 1.6mV, for a 5sec pulse was -93.3 ± 2.1mV, and for a 20sec pulse was -87.1 ± 2.0mV (n=9). E_{rev} measurements for eggs injected with Kv1.2 were -94.2 ± 0.6mV for a 100msec pulse, -89.5 ± 0.5mV for a

Figure 44: Calculated apparent volume of the K^+ accumulation space as a function of pulse duration for normal (closed symbols) and devitellinized (open symbols) eggs expressing Kv1.2 (**A**) or rat uterine minK (**B**). Also shown are data comparing square voltage steps (circles) and ramp (squares) voltage waveforms in normal and devitellinized eggs expressing rat uterine minK. Volumes were calculated as described in the text.

A

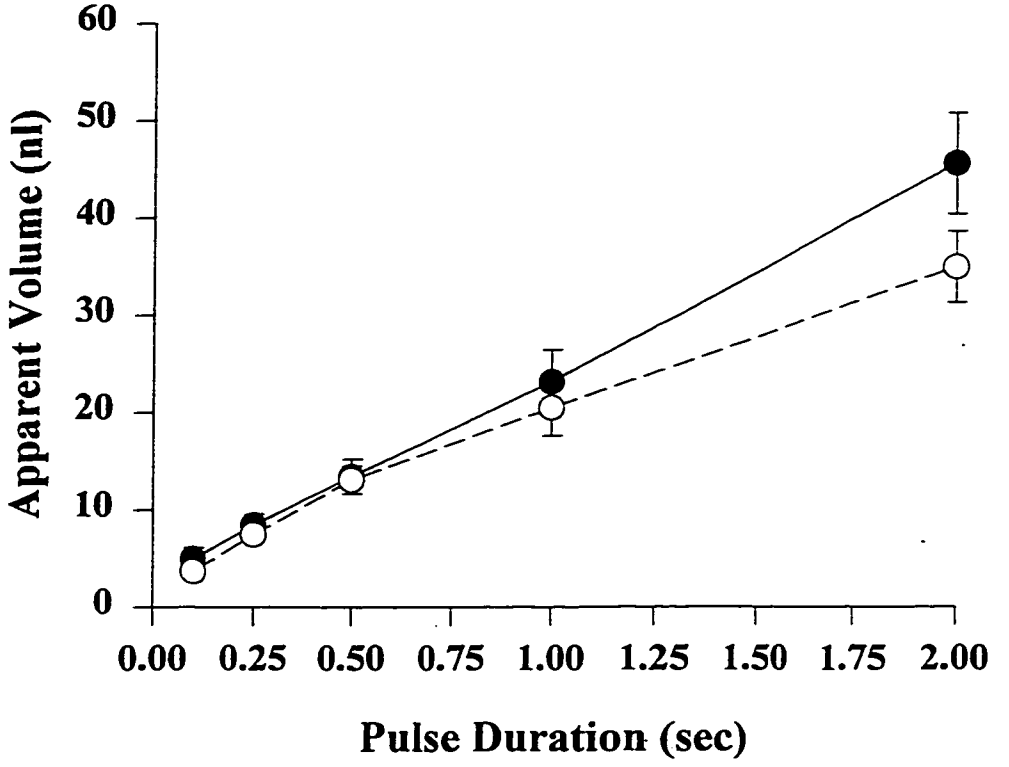
60
50
40
30
20
10
0
Apparent Volume (nl)
0.00
0.25
0.50
0.75
1.00
1.25
1.50
1.75
2.00
Pulse Duration (sec)

B

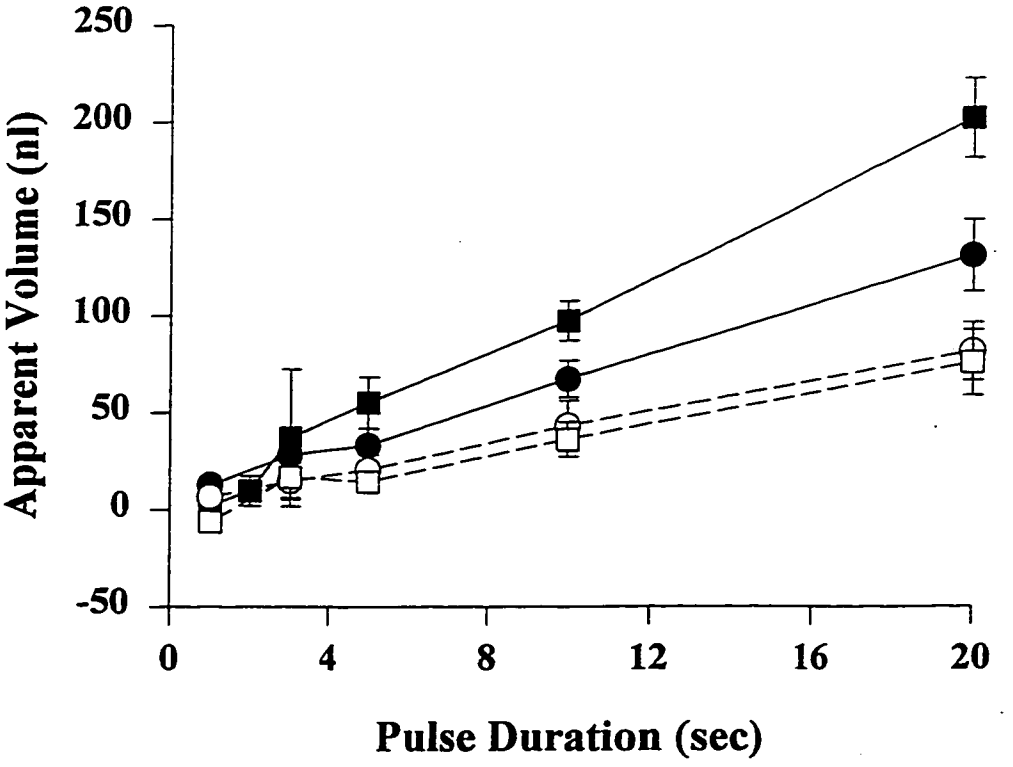
250
200
150
100
50
0
-50
Apparent Volume (nl)
0
4
8
12
16
20
Pulse Duration (sec)

500msec pulse, and -84.5 ± 0.8mV for a 2000msec pulse (n=3). Complete removal of the vitelline layer was confirmed using both light microscopy and transmission electron microscopy (see Figures 45 and 46).

To evaluate further whether the vitelline membrane may contribute to the process of K^+ accumulation on the oocyte surface, we calculated the volume of the accumulation space for the devitellinized eggs and compared it to the data obtained when the vitelline membrane was intact. This comparison is illustrated in Figures 44A (Kv1.2, open circles) and 44B (minK, open symbols). Somewhat surprisingly, the accumulation volume remained very nearly the same for eggs injected with Kv1.2 (2000msec pulse= 35.0 ± 3.7nl or 15.0% of total egg volume). Moreover, the volume appeared to decrease at longer pulse durations in devitellinized oocytes injected with minK (Square steps: 20sec pulse= 81.6 ± 14.9nl or 15.5% of the total egg volume; Ramp steps: 20sec pulse= 75.8 ± 16.9nl or 14.5% of the total egg volume) as compared to normal oocytes. In the experimental data based on the ramp waveforms this difference was statistically significant ($p<0.001$). It is unclear why the accumulation volumes are smaller in the devitellinized eggs, but several possibilities are outlined in the Discussion.

Effect of $[K^+]_o$ on K^+ Accumulation

The effect of changing $[K^+]$ in the external bathing solution was examined to determine whether raising $[K^+]_o$ could reduce the depolarizing shifts in E_{rev} observed with increasing pulse duration. At a concentration of 10mM $[K^+]_o$ in oocytes injected with Kv1.2, a shift in E_{rev} of only +3.7mV was measured between the 100msec pulse (-63.3 ± 1.8mV) compared to the 2000msec pulse (-59.6 ± 1.3mV, n=3). This shift is small compared with the 10.1mV change measured under identical conditions in 2mM $[K^+]_o$. Moreover, when changes in integrated current size between the 2mM and 10mM $[K^+]_o$ groups are accounted for by calculating the volume of the accumulation space there is no significant difference between the two data sets, as shown in Figure 47A. These results suggest that increasing the concentration of K^+ in the external bathing medium diminishes the magnitude of the depolarizing shifts in E_{rev} which occurs with increasing pulse

Figure 45: Transmission electron micrograph of the surface of a *Xenopus* oocyte. The panel on the left illustrates a normal oocyte (magnification 13500x) from which the follicular layer had been removed during the isolation procedure. The fibrous vitelline layer (VT) can be seen in series with microvilli (MV) which project from the surface of the oocyte. The panel on the right shows an oocyte (magnification 13500x) in which the vitelline layer has been removed, as described in the Materials and Methods.

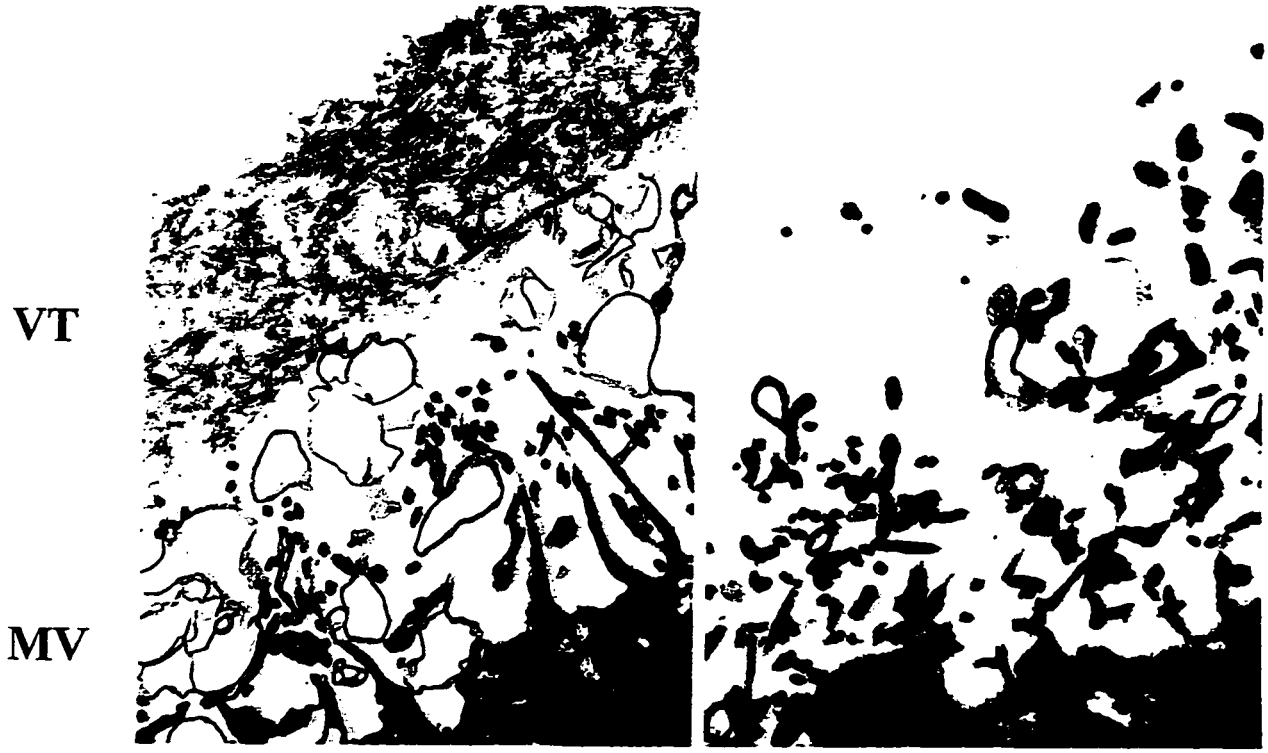
VT
MV

Figure 46: Light micrograph of the surface of a *Xenopus* oocyte stained with haematoxylin and eosin. The upper panel illustrates a normal egg (275x magnification) from which the follicular layer had been removed during the oocyte isolation procedure. The vitelline membrane, which appears as a light line enveloping the oocyte, is labelled by the arrow. The lower panel depicts a devitellinized egg (275x magnification).

Figure 47: Calculated apparent volume of the K^+ accumulation space as a function of pulse duration in different external K^+ concentrations for normal eggs expressing Kv1.2 (**A**) or rat uterine minK (**B**). E_{rev} values used to calculate the volumes in panel **B** were obtained using ramp voltage waveforms. Volumes were calculated as described in the text.

A

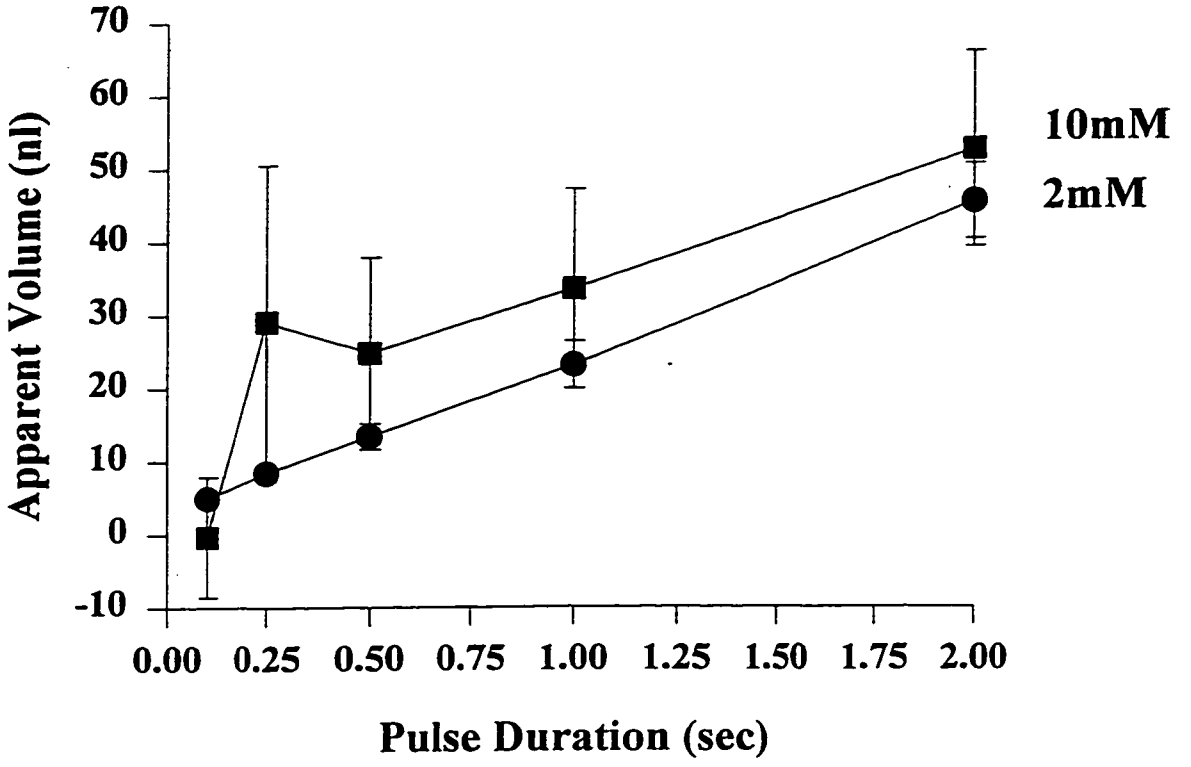
70
60
50
40
30
20
10
0
-10
Apparent Volume (nl)
0.00
0.25
0.50
0.75
1.00
1.25
1.50
1.75
2.00
Pulse Duration (sec)
10mM
2mM

B

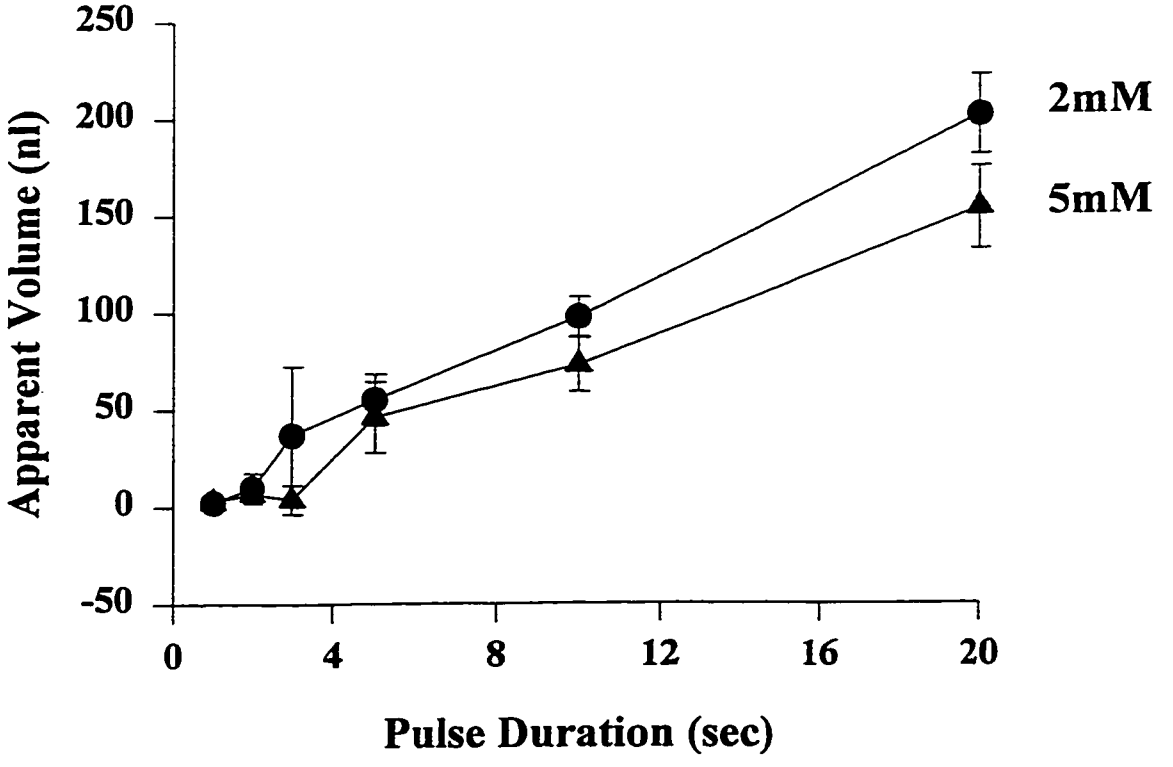
250
200
150
100
50
0
-50
Apparent Volume (nl)
0
4
8
12
16
20
Pulse Duration (sec)
2mM
5mM

durations, but this decrease is not simply due to changes in the size of the charge movement.

In minK injected oocytes $[K^+]_o$ was increased to 5mM and ramp steps from -50 to -100mV were used to measure E_{rev} after varying pulse lengths. In 5mM $[K^+]_o$, E_{rev} for a 1sec pulse was -80.3 ± 1.2mV (n=5) and for a 20sec pulse was -77.2 ± 0.6 mV (n=7), a total change of 3.1mV. This shift was smaller than the shift (7.5mV) measured under identical conditions in 2mM $[K^+]_o$. Decreases in the size of the current integral cannot account for these differences since there is no significant difference in the volume of the accumulation space between the 2mM and 5mM $[K^+]_o$ groups (see Figure 47B).

Discussion

Our initial reason for investigating whether K^+ accumulation occurred on the surface of *Xenopus* oocytes was to gain insight into the causes(s) for the continued slow increase in the amplitude of minK during prolonged depolarizing voltage pulses. A K^+ current having an inwardly rectifying current-voltage relationship can, in response to elevating $[K^+]_o$ (on the surface of the oocyte), increase the magnitude of current at a given potential (Cohen and Kline, 1982). This phenomenon could account for the non-saturating characteristics of minK. Initial experiments which investigated this possibility, however, suggested that it is unlikely that K^+ accumulation contributes to the non-saturating kinetics of minK, since increasing $[K^+]_o$ from 2mM to 20 or 50mM decreased current magnitude (as would be expected for a current following a Goldman-Hodgkin-Katz scheme), but the current still did not reach steady-state even after long (30sec) depolarizing voltage steps (data not shown). These experiments do not, however, entirely eliminate a role for K^+ accumulation. In practise, however, it is very difficult to further define this phenomenon since the exact shape of the fully activated current-voltage relationship for minK is not known (minK does not reach steady state and it has been difficult to obtain single-channel recordings of this current). Isochronal current-voltage curves for minK have revealed an outwardly rectifying relationship (see Chapter 4), although these recordings are contaminated with currents endogenous to *Xenopus* oocytes

and leak currents. Interestingly, Blumenthal and Kaczmarek (1993) have described a strongly inwardly-rectifying instantaneous current-voltage relationship for both rat and human minK expressed in *Xenopus* oocytes when the contribution of endogenous currents and leak currents are taken into consideration. It is unclear, however, whether the shape of this relationship was dependent on $[K^+]_o$.

Our data demonstrate that efflux of K^+, during activation of either Kv1.2 or minK expressed in *Xenopus* oocytes, causes significant and reproducible depolarizing shifts in E_{rev}. These changes are observed after either prolonged activation of minK or Kv1.2, or when the magnitude of the current is increased. We propose that accumulation of K^+ on the extracellular surface of the oocyte during activation of these K^+ currents decreases the K^+ gradient across the cell membrane, resulting in variations in E_{rev}. Depletion of K^+ near the intracellular surface of the cell could have a similar effect on the K^+ gradient, but the magnitude of these changes would have to be enormous in order to explain the shifts in E_{rev} observed in these experiments. Although we cannot rule out the possibility that intracellular depletion makes some contribution to these changes, it seems unlikely that it plays a major role, considering the size of the oocyte and the estimated intracellular $[K^+]$ of 90-150mM (Dascal, 1987). Our results showing smaller shifts in E_{rev} when the concentration of K^+ in the extracellular bathing medium is increased, support the hypothesis of K^+ accumulation on the surface of the oocyte. All of our calculations therefore assume that the major contributor to the changes in E_{rev} is extracellular K^+ accumulation. Accordingly, we have developed a mathematical model (see Appendix 1) based on K^+ accumulation in a restricted space and an unstirred layer on the surface of the oocyte.

The possibility that accumulation of K^+ occurs on the surface of a *Xenopus* oocyte is consistent with the microanatomy of the oocytes. Dumont and Brummett (1978) described an outer follicular layer (which is removed during oocyte isolation) enclosing a fibrous vitelline envelope. Underneath the vitelline membrane are long microvilli that extend from the surface of the egg to the vitelline layer, as well as elaborate and deep crypts that give rise to a fenestrated surface of the oocyte. Stage IV eggs are heavily and

deeply invaginated, whereas during stage V and VI the microvilli become shorter and broader and the surface becomes less contoured (Dumont and Brummett, 1978). The electron microscopy shown in Figure 45 was performed on eggs in stages V or VI. From these we calculated that the microvilli can increase the surface area of the oocyte anywhere from 3 to 10 times. It is conceivable that this number may be increased in stage IV eggs. In the experiments reported here we used eggs from stages IV-VI.

Electron micrographs show that the vitelline membrane is a dense mat of intricately woven fibers (Dumont and Brummett, 1978) and our measurements estimate that this layer is approximately 2μm thick. This structure therefore seems the most likely structure responsible for restricting diffusion of K^+. However, mechanical removal of the vitelline membrane did not diminish the extent of K^+ accumulation. In fact, dissecting off this layer actually decreased the volume of the apparent accumulation space, suggesting that perhaps more K^+ accumulation occurred on the surface of these eggs. It is possible that the physical process of removing the vitelline membrane by first placing the egg in a hypertonic solution may cause the egg to shrink, and that it does not completely recover upon return to a isotonic solution. The shrinking of the eggs may cause the microvilli and 'crypts' on the surface of the egg to become more densely packed, leading to a more tortuous diffusion pathway. The process of devitellinization appears not to change the capacitance of the eggs, since this value was measured to be 198.5 ± 4.5nF (n=8) for normal eggs and 198.5 ± 6.2nF (n=10) for devitellinized eggs (capacitance of the oocyte is estimated to be 31nF for an ideal sphere with a radius of 0.5mm, assuming a capacitance of 1μF/cm^2). Alternatively, it is feasible that the apparent greater K^+ accumulation in the devitellinized eggs is due to variability in surface anatomy between these particular eggs and the normal eggs injected with minK, as there was no change in the accumulation volume after devitellinization in eggs injected with Kv1.2.

It is very difficult to obtain direct evidence for other anatomical locations where accumulation of K^+ ions could occur. Our estimates of the oocyte surface from electron micrographs suggest that the microvilli layer alone is not thick (or dense) enough to account for the K^+ accumulation observed. However, in the mathematical model outlined

in Appendix 1 we provide evidence that this layer, in conjunction with the presence of deep 'crypts' or caveolae on the surface of the oocyte and an unstirred layer surrounding the egg, is sufficient to account for the accumulation described in these experiments.

Several useful insights can be gained from these findings. It is apparent that caution must be exercised when interpreting results from *Xenopus* oocyte recordings. The magnitude of K^+ accumulation is exaggerated with increasing current magnitude and also when long pulse durations are needed. In our experiments K^+ accumulation was detected in Kv1.2 injected eggs even after voltage pulses of 250msec in duration, suggesting that this phenomena is not solely an artifact associated with the long voltage pulses needed to activate slow K^+ currents. Secondly, the possibility of accumulation must especially be taken into consideration when recording from currents that are sensitive to $[K^+]_o$, as changes in $[K^+]_o$ over the length of the voltage pulse may alter the shape of the current waveform. Thirdly, electron microscopy measurements suggest that enhanced K^+ accumulation may occur in less mature (stage IV) oocytes. Therefore, caution should be taken to use stage V and VI oocytes when recording from K^+ channels in *Xenopus* oocytes. Finally, these results suggest that all previous selectivity measurements in *Xenopus* oocytes are suspect.

Our mathematical model (Appendix 1) provides a framework for evaluating whether the presence of an unstirred layer on the surface of the oocyte can contribute to the observed K^+ accumulation. Our findings are not surprising considering the size of the oocyte and the fluid dynamics associated with adequately perfusing a cell of its size. It is unlikely that the presence of an unstirred layer and the inability to rapidly superfuse the surface of the egg is a feature unique to our experimental set-up. Results dictated by an unstirred layer on the surface of the oocyte have also been reported by Girard and Clapham (1994). They demonstrated that simply lifting the oocyte off from the bottom of the recording chamber onto a polyethylene mesh increased almost six fold the magnitude of intracellular Ca^{++} transients elicited in response to activation of m3 ACh receptors expressed in *Xenopus* oocytes (in our experiments the oocyte sat on a mesh platform raised up from the bottom of the recording chamber). These results suggest that the fluid

dynamics surrounding the oocyte, and the extent of superfusion of these cells, can be a significant problem and this factor should also be taken into consideration when recording from *Xenopus* oocytes.

The presence of an unstirred layer may also explain the apparent differences in accumulation volume measured during activation of either Kv1.2 or minK. Recall that these volumes were much smaller for eggs injected with Kv1.2 than with minK. As described in the mathematical model (see Figure 50), the unstirred layer makes a much greater contribution to accumulation in currents that activate slowly, as K^+ ions have more time to diffuse into the surrounding medium over the length of the voltage pulse. Minimizing the thickness of the unstirred layer (by improving superfusion of the cells) would therefore substantially decrease the amount of accumulation observed after activation of these currents. The relative importance of the unstirred fluid layer is much less for rapidly activating currents such as Kv1.2, since most of the accumulation likely occurs in the deep crypts on the surface of the oocyte. These results and calculations provide a basis for determining the circumstances under which *Xenopus* oocytes can be used reliably as an expression system for studying K^+ channel function.

CHAPTER 7: GENERAL DISCUSSION

Discussion

There has been widespread recent interest in identifying and understanding the molecular structures underlying I_{Ks}. Mutations in minK and KvLQT1 have been linked to the development of two inherited forms of LQT; Romano-Ward syndrome (characterized by torsade de pointes leading to sudden cardiac death) and Jervell and Lange-Nielson syndrome (characterized by similar symptoms, in addition to congenital bilateral deafness). Pharmacological agents that target I_{Ks} are currently being developed in the hope that they may prove to be clinically effective in the treatment of ventricular tachyarrhythmias (see Introduction for review). Detailed knowledge of the protein(s) that contribute to I_{Ks} is essential to improve the design and development of drugs targeting this channel.

At the time that this dissertation was started, it was proposed that minK was the molecular structure underlying I_{Ks}, although there was a great controversy over whether minK actually formed a functional K^+ channel, or instead acted as a regulator of K^+ channels endogenous to *Xenopus* oocytes (see Introduction; also, Kaczmarek and Blumenthal, 1997). The goal of this study was therefore to perform a detailed comparison of the properties of minK expressed in *Xenopus* oocytes to I_K in bullfrog atrium, to gain insight into whether minK could be responsible for this K^+ channel. As described previously (Hume et al., 1986; Simmons et al., 1986), and confirmed in Chapter 3 of this dissertation, bullfrog I_K consists of only an I_{Ks}-like current, unlike many mammalian species (see Introduction). We therefore chose the bullfrog heart as a model for studying the properties of I_{Ks} in isolation; that is, without the need to separate I_{Ks} from I_{Kr} by pharmacological or electrophysiological manipulations.

Originally we had intended to make a quantitative comparison between I_K in bullfrog atrium and minK cloned from bullfrog heart. Our rationale was that expression of an amphibian clone in an amphibian expression system, and the subsequent comparison of this clone to an amphibian channel, would circumvent problems associated with temperature variability, and/or sequence and structural changes. However, as

mentioned in Chapters 4 and 5, numerous attempts to clone minK, or to provide evidence for the presence of this protein in bullfrog heart, have been unsuccessful. Thus, our experiments in Chapter 4 compared the properties of bullfrog I_K to rat uterine minK expressed in *Xenopus* oocytes. These experiments identified very close similarities between the biophysical and pharmacological properties of these two currents. One interpretation of these results is that minK (presumably due to coassembly with KvLQT1 endogenous to *Xenopus* oocytes) forms at least part of the molecular structure underlying bullfrog I_K. Our pharmacological data, showing a very similar concentration-dependence (azimilide: Kd of 7.2μM and 11.2μM for minK and I_K, respectively), voltage-dependence, and mechanism of block of I_K and minK by azimilide and propenamide, do not, however, preclude an action of these compounds at another subunit, such as KvLQT1. As mentioned in Chapter 4, both azimilide (Busch et al., 1997) and chromanol 293B (Busch et al., 1997) have recently been shown to inhibit KvLQT1 expressed in *Xenopus* oocytes.

We have put considerable effort into trying to identify minK and KvLQT1 in bullfrog heart. We have cloned KvLQT1 from this tissue and have shown that the amino acid sequence shares a high degree of homology with human KvLQT1. Our *in situ* hybridization results provide further evidence for the expression of KvLQT1 in this tissue. Unfortunately, at this time we have been unable to functionally express bullfrog KvLQT1 in *Xenopus* oocytes, and an understanding of how the characteristics of this clone compares with published mouse (Barhanin et al., 1996) and human (Sanguinetti et al., 1996) KvLQT1 must await future experiments.

Our efforts to identify the minK transcript in bullfrog heart, despite numerous attempts using various approaches (see Chapter 5), have been unsuccessful. These negative results do not necessarily mean that minK is not expressed in bullfrog heart, as it is possible that bullfrog minK is highly diverged from the known mammalian minK sequences. Nonetheless, it is tempting to explore the hypothesis that if minK is not present in bullfrog heart I_K in bullfrog may then be encoded by KvLQT1 alone, or KvLQT1 may coassemble with another as-yet-unidentified protein. This latter hypothesis

may be plausible. MinK is a member of a family of small proteins, including CHIF, Mat-8, and phospholemman (Attali et al., 1995; Moorman et al., 1992; Morrison et al., 1995), which are thought to interact with ion channels endogenous to *Xenopus* oocytes (see Introduction). CHIF, an 87 amino acid protein which shows no sequence homology to minK but has a similar secondary structure, induces a minK-like current when expressed in *Xenopus* oocytes (Attali et al., 1995), presumably by coassembling with KvLQT1 endogenous to *Xenopus* oocytes. Furthermore, minK has recently been shown to increase the magnitude of HERG (which encodes I_{Kr}; Sanguinetti et al., 1995) expressed in CHO cells and to shift its voltage dependence of activation to the left (McDonald et al., 1997). In addition, an antisense oligonucleotide targeted against minK has been shown to decrease the current density of I_{Kr} in an atrial tumour cell line (Yang et al., 1995). Thus, this family of small proteins may interact with numerous ion channels and modify their function, and it would be interesting to determine if any of these other proteins (in particular, CHIF) are expressed in bullfrog heart.

KvLQT1 expressed alone has a similar pharmacological profile to mammalian I_{Ks} and bullfrog I_K. This channel is inhibited by chromanol 293B, azimilide, and 17-β-oestradiol with IC_{50}'s of 41, 77, and >50μM, respectively (Busch et al., 1997), by application of 10μM clofilium or 10mM TEA (Yang et al., 1997), and by activation of PKC with phorbol-12-myristate-13-acetate (Barhanin et al., 1996). KvLQT1 is enhanced by raising internal Ca^{++} concentrations with intracellular injection of inositol triphosphate (Barhanin et al., 1996), or by increasing cAMP levels with bath application of 10μM forskolin and 100μM isobutylmethylxanthine (Yang et al., 1997). Furthermore, 10μM E-4031 and 1μM dofetilide are without effect on KvLQT1 (Yang et al., 1997), similar to the effects of these compounds on I_{Ks} in guinea pig ventricular myocytes (Sanguinetti and Jurkiewicz, 1990b; Jurkiewicz and Sanguinetti, 1993), and I_K in bullfrog atrium (see Chapter 3). However, despite these pharmacological similarities, the time course of activation of human and mouse KvLQT1 expressed either in *Xenopus* oocytes or mammalian cell lines is much faster than mammalian I_{Ks} or bullfrog I_K (Barhanin et al., 1996; Sanguinetti et al., 1996; Yang et al., 1997), suggesting that this protein alone is

unlikely to encode these native channels. The functional characteristics of bullfrog KvLQT1 are unknown, however, and it is possible that the kinetics of bullfrog KvLQT1 may be slower than the mammalian clones due to differences in temperature, intracellular regulation, and/or sequence variations. Bullfrog KvLQT1 is highly homologous (95% identity) to human KvLQT1 through the transmembrane regions and pore domain, but diverges in the amino-terminus and shares only 68% identity across the full-length protein. Furthermore, we have identified two alternative 3' splice variants of bullfrog KvLQT1, of which splice variant B possesses a unique carboxy-terminus with a strongly hydrophobic region at the end. Thus, it may be plausible to predict that the characteristics of bullfrog KvLQT1 differ from mammalian KvLQT1. An understanding of the role of bullfrog KvLQT1, and whether it requires coassembly with minK (or another small protein) to mimic the properties of I_K, awaits the examination of the biophysical and pharmacological characteristics of bullfrog KvLQT1. The results of these experiments could have interesting consequences for the understanding of how minK and KvLQT1 coassemble in mammalian heart; that is, whether minK is required to form part of the pore of a KvLQT1-minK complex channel (Tai and Goldstein, 1998), or whether minK acts simply as a regulator of KvLQT1 (Romey et al., 1997).

Limitations

One limitation of this study, as mentioned at the end of Chapter 4, is that we have compared an amphibian K^+ channel to a mammalian minK clone, for reasons described previously. Species differences in the voltage dependence of activation, activation kinetics, and sensitivity to lanthanum have been reported when rat, mouse, or human minK are expressed in *Xenopus* oocytes (Hice et al., 1994). Thus, it is possible that bullfrog minK and/or KvLQT1 have different biophysical and pharmacological properties, and are regulated in a different manner, from their mammalian counterparts. Despite these potential variations, we have shown that bullfrog I_K is very similar to rat uterine minK expressed in *Xenopus* oocytes. Whether these similarities result from activation of minK and/or KvLQT1 in bullfrog heart remains to be determined.

The other major limitation of this study, in light of the results presented in Chapter 6, is that the expression system we have used for studying the characteristics of minK is *Xenopus* oocytes. This system is widely used due to its relative simplicity for screening large number of oocytes but, as we have shown, can be compromised by accumulation of K^+ and poor superfusion on the surface of the oocyte. Accumulation of K^+ can significantly alter the outcome of electrophysiological studies and change the characteristics of the current under study (Cohen and Kline, 1982). For example, K^+ accumulation on the surface of a cell can convert an inward rectifier-type K^+ current from a time-independent to a time-dependent current (Cohen and Kline, 1982). Therefore, caution must be taken when interpreting data obtained from expression of K^+ channels in *Xenopus* oocytes. When this dissertation was started, analysis of the properties of minK were limited to this expression system and, for reasons described previously, we wanted to use an amphibian expression system to study the characteristics of the bullfrog delayed rectifier channel. However, the properties of minK can now be studied by coexpression of minK and KvLQT1 in mammalian cell lines (Barhanin et al., 1996; Sanguinetti et al., 1996).

Future Experiments

There are many interesting and important experiments yet to be performed. As mentioned previously, an investigation of the biophysical and pharmacological properties of bullfrog KvLQT1 is required before we can make any conclusions about the molecular components underlying I_K in bullfrog atrium. The outcome of these experiments will give insight into whether minK, or another protein, are required for coassembly with KvLQT1 in this tissue, and perhaps help to determine the role that minK plays in mammalian tissue. The results in Chapter 4 described a similar concentration- and voltage-dependence of block of I_K and minK by azimilide and propenamide. However, with the available data we are unable to determine the exact mechanism of block by these two compounds. It will be important to test the effects of azimilide and propenamide on bullfrog KvLQT1, to determine whether the observed effects are due to actions on this

subunit. In addition, we have identified two different 3' splice variants of bullfrog KvLQT1. It will be interesting to determine if both of these variants produce functional channels when expressed in *Xenopus* oocytes, and also to compare the characteristics of the two variants. Furthermore, an investigation of the tissue distribution of these two splice variants by RNase protection assay, and a comparison of their relative abundance in the various tissues, will provide some of the data needed to determine the role of each splice variant. Finally, depending on the outcome of these bullfrog KvLQT1 experiments, it will be interesting to look for the presence of other small regulatory proteins (such as CHIF) in bullfrog heart.

References

Adelman, W.J., Jr., Palti, Y., and Senft, J.P. (1973). Potassium ion accumulation in a periaxonal space and its effect on the measurement of membrane potassium ion conductance. J. Membr. Biol. *13*, 387-410.

Almers, W. (1972). Potassium conductance change in skeletal muscle and the potassium concentration in the transverse tubules. J. Physiol. (London) *225*, 33-56.

Anumonwo, J.M., Freeman, L.C., Kwok, W.M., and Kass, R.S. (1992). Delayed rectification in single cells isolated from guinea pig sinoatrial node. Am. J. Physiol. *262*, H921-H925.

Arena, J.P. and Kass, R.S. (1988). Block of heart potassium channels by clofilium and its tertiary analogs: relationship between drug structure and type of channel blocked. Mol. Pharmacol. *34*, 60-66.

Attali, B., Guillemare, E., Lesage, F., Honoré, E., Romey, G., Lazdunski, M., and Barhanin, J. (1993). The protein IsK is a dual activator of K^+ and Cl^- channels. Nature *365*, 850-852.

Attali, B., Latter, H., Rachamim, N., and Garty, H. (1995). A corticosteroid-induced gene expressing an "IsK-like" K^+ channel activity in *Xenopus* oocytes. Proc. Natl. Acad. Sci. USA *92*, 6092-6096.

Attali, B., Romey, G., Honoré, E., Schmid-Alliana, A., Mattei, M.-G., Lesage, F., Ricard, P., Barhanin, J., and Lazdunski, M. (1992). Cloning, functional expression, and regulation of two K^+ channels in human T-lymphocytes. J. Biol. Chem. *267*, 8650-8657.

Attwell, D., Eisner, D., and Cohen, I. (1979). Voltage clamp and tracer flux data: effects of a restricted extra-cellular space. Quart. Rev. Biophys. *12*, 213-261.

Attwell, D.E. and Cohen, I. (1977). The voltage clamp of multicellular preparations. Prog. Biophys. Mol. Biol. *31*, 201-245.

Balser, J.R., Bennett, P.B., Hondeghem, L.M., and Roden, D.M. (1991). Suppression of time-dependent outward current in guinea pig ventricular myocytes. Actions of quinidine and amiodarone. Circ. Res. *69*, 519-529.

Barhanin, J., Lesage, F., Guillemare, E., Fink, M., Lazdunski, M., and Romey, G. (1996). KvLQT1 and IsK (minK) proteins associate to form the IKs cardiac potassium current. Nature *384*, 78-80.

Barry, P.H. (1984). Slow potential changes due to transport number effects in cells with unstirred membrane invaginations or dendrites. J. Membr. Biol. *82*, 221-239.

Barry, P.H. and Diamond, J.M. (1984). Effects of unstirred layers on membrane phenomena. Physiol. Rev. *64*, 763-872.

Baumgarten, C.M. and Isenberg, G. (1977). Depletion and accumulation of potassium in the extracellular clefts of cardiac Purkinje fibers during voltage clamp hyperpolarization and depolarization. Pflügers Arch. *368*, 19-31.

Ben-Efraim, I., Bach, D., and Shai, Y. (1993). Spectroscopic and functional characterization of the putative transmembrane segment of the minK potassium channel. Biochem. *32*, 2371-2377.

Ben-Efraim, I., Shai, Y., and Attali, B. (1996). Cytoplasmic and extracellular IsK peptides activate endogenous K^+ and Cl^- channels in *Xenopus* oocytes. Evidence for regulatory function. J. Biol. Chem. *271*, 8768-8771.

Ben-Efraim, I., Strahilevitz, J., Bach, D., and Shai, Y. (1994). Secondary structure and membrane localization of synthetic segments and a truncated form of the IsK (minK) protein. Biochem. *33*, 6966-6973.

Bennett, P.B., McKinney, L.C., Kass, R.S., and Begenisich, T. (1985). Delayed rectification in the calf cardiac Purkinje fiber. Evidence for multiple state kinetics. Biophys. J. *48*, 553-567.

Blumenthal, E.M. and Kaczmarek, L.K. (1992). Modulation by cAMP of a slowly activating potassium channel expressed in *Xenopus* oocytes. J. Neurosci. *12*,290-296.

Blumenthal, E.M. and Kaczmarek, L.K. (1993). Inward rectification of the MinK potassium channel. J. Membr. Biol. *136*, 23-29.

Blumenthal, E.M. and Kaczmarek, L.K. (1994). The minK potassium channel exists in functional and nonfunctional forms when expressed in the plasma membrane of *Xenopus* oocytes. J. Neurosci. *14*, 3097-3105.

Boyle, M.B., Azhderian, E.M., MacLuskey, N.J., Naftolin, F., and Kaczmarek, L.K. (1987a). *Xenopus* oocytes injected with rat uterine RNA express very slowly activating potassium currents. Science *235*, 1221-1224.

Boyle, M.B., MacLuskey, N.J., Naftolin, F., Kaczmarek, L.K. (1987b). Hormonal regulation of K^+-channel messenger RNA in rat myometrium during oestrus cycle and in pregnancy. Nature *330*, 373-375.

Brown, A.M. (1997). Cardiac potassium channels in health and disease. Trends Cardiovasc. Med. *7*, 118-124.

Brown, H., DiFrancesco, D., Noble, D., and Noble, S. (1980). The contribution of potassium accumulation to outward currents in frog atrium. J. Physiol. (London) *306*, 127-149.

Brown, H.F., Clark, A., and Noble, S. (1976a). Identification of the pace-maker in frog atrium. J. Physiol. (London) *258*, 521-545.

Brown, H.F., Clark, A., and Noble, S. (1976b). Analysis of pace-maker and repolarization currents in frog atrial muscle. J. Physiol. (London) *258*, 547-577.

Brown, H.F., Giles, W., and Noble, S.J. (1977). Membrane currents underlying activity in frog sinus venosus. J. Physiol. (London) *271*, 783-816.

Brown, H.F. and Noble, S.J. (1969). Membrane currents underlying delayed rectification and pace-maker activity in frog atrial muscle. J. Physiol. (London) *204*, 717-736.

Busch, A.E., Busch, G.L., Ford, E., Suessbrich, H., Lang, H.-J., Greger, R., Kunzelmann, K., Attali, B., and Stühmer, W. (1997). The role of the IsK protein in the specific pharmacological properties of the IsK channel complex. Brit. J. Pharmacol. *122*, 187-189.

Busch, A.E., Herzer, T., Takumi, T., Krippeit-Drews, P., Waldegger, S., and Lang, F. (1994). Blockade of human IsK channels expressed in *Xenopus* oocytes by the novel class III antiarrhythmic NE-10064. Eur. J. Pharmacol. *264*, 33-37.

Busch, A.E. and Lang, F. (1993). Effects of $[Ca^{2+}]_i$ and temperature on minK channels expressed in *Xenopus* oocytes. FEBS Lett. *334*, 221-224.

Busch, A.E., Malloy, K., Groh, W.J., Varnum, M.D., Adelman, J.P., and Maylie, J. (1994a). The novel class III antiarrhythmics NE-10064 and NE-10133 inhibit IsK channels expressed in *Xenopus* oocytes and IKs in guinea pig cardiac myocytes. Biochem. Biophys. Res. Commun. *202*, 265-270.

Busch, A.E., Suessbrich, H., Waldegger, S., Sailer, E., Greger, R., Lang, H.-J., Lang, F., Gibson, K.J., and Maylie, J.G. (1996). Inhibition of IKs in guinea pig cardiac myocytes and guinea pig IsK channels by the chromanol 293B. Pflügers Arch. *432*, 1094-1096.

Busch, A.E., Varnum, M.D., North, R.A., and Adelman, J.P. (1992). An amino acid mutation in a potassium channel that prevents inhibition by protein kinase C. Science *255*, 1705-1707.

Chan, K.W., Langan, M.N., Sui, J.L., Kozak, J.A., Pabon, A., Ladias, J.A., and Logothetis, D.E. (1996). A recombinant inwardly rectifying potassium channel coupled to GTP-binding proteins. J. Gen. Physiol. *107*, 381-397.

Chouabe, C., Neyroud, N., Guicheney, P., Lazdunski, M., Romey, G., and Barhanin, J. (1997). Properties of KvLQT1 K^+ channel mutations in Romano-Ward and Jervell and Lange-Nielsen inherited cardiac arrhythmias. EMBO J. *16*, 5472-5479.

Clapham, D.E. and Logothetis, D.E. (1988). Delayed rectifier K^+ current in embryonic chick heart ventricle. Am. J. Physiol. *254*, H192-H197.

Clark, R.B. and Giles, W. (1987). Sodium current in single cells from bullfrog atrium: Voltage dependence and ion transfer properties. J. Physiol. (London) *391*. 235-265.

Clark, R.B., Tse, A., and Giles, W.R. (1990). Electrophysiology of parasympathetic neurones isolated from the interatrial septum of bull-frog heart. J.Physiol. (London) *427*, 89-125.

Clay, J.R. (1986). Potassium ion accumulation slows the closing rate of potassium channels in squid axons. Biophys.J. *50*,197-200.

Cleemann, L. and Morad, M. (1979). Potassium currents in frog ventricular muscle: Evidence from voltage clamp currents and extracellular K^+ accumulation. J. Physiol. (London) *286*. 113-143.

Cohen, I. and Kline, R. (1982). K^+ fluctuations in the extracellular spaces of cardiac muscle: Evidence from the voltage clamp and extracellular K^+ selective microelectrodes. Circ. Res. *50*. 1-16.

Cui, J., Kline, R.P., Pennefather, P., and Cohen, I.S. (1994). Gating of IsK expressed in *Xenopus* oocytes depends on the amount of mRNA injected. J. Gen. Physiol. *104*. 87-105.

Curran, M.E., Splawski, I., Timothy, K.W., Vincent, G.M., Green, E., and Keating, M.T. (1995). A molecular basis for cardiac arrhythmia: HERG mutations cause long-QT syndrome. Cell *80*, 705-803.

Daleau, P., Khalifa, M., and Turgeon, J. (1998). Effects of cadmium and nisoldipine on the delayed rectifier potassium current in guinea pig ventricular myocytes. J. Pharm. Exp. Ther. *281*, 826-833.

Daleau, P. and Turgeon, J. (1994). Triamterene inhibits the delayed rectifier potassium current (IK) in guinea pig ventricular myocytes. Circ. Res. *74*, 1114-1120.

Dascal, N. (1987). The use of *Xenopus* oocytes for the study of ion channels. CRC Crit. Rev. Biochem. *22*, 317-387.

Dascal, N., Schreibmayer, W., Lim, N.F., Wang, W., Chavkin, C., Dimagno, L., Labarca, C., Kieffer, B.L., Gaveriaux-Ruff, C., Trollinger, D., Lester, H.A., and Davidson, N. (1993). Atrial G-protein-activated K^+ channel: expression cloning and molecular properties. Proc. Natl. Acad. Sci.USA *90*, 10235-10239.

Davies, M.P., An, R.H., Doevendans, P., Kubalak, S., Chein, K.R., and Kass, R.S. (1996a). Developmental changes in ionic channel activity in the embryonic murine heart. Circ. Res. *78*, 15-25.

Davies, M.P., Freeman, L.C., and Kass, R.S. (1996b). Dual action of the noval class III antiarrhythmic drug NE-10064 on delayed potassium channel currents in guinea pig ventricular and sinoatrial node cells. J. Pharmacol. Exp. Ther. *276*, 1149-1154.

Delpón, E., Valenzuela, C., Perez, O., Casis, O., and Tamargo, J. (1995). Propafenone preferentially blocks the rapidly activating component of delayed rectifier K^+ current in guinea pig ventricular myocytes. Circ. Res. *76*, 223-235.

Donger, C., Denjoy, I., Berthet, M., Neyroud, N., Cruaud, C., Bennaceur, M., Chivoret, G., Schwartz, K., Coumel, P., and Guicheney, P. (1997). KvLQT1 C-terminal missense mutation causes a forme fruste long-QT syndrome. Circulation *96*, 2778-2781.

Drolet, B., Khalifa, M., Daleau, P., Hamelin, B.A., and Turgeon, J. (1998). Block of the rapid component of the delayed rectifier potassium current by the prokinetic agent cisapride underlies drug-related lengthening of the QT interval. Circulation *97*, 204-210.

Dubois, J.M. and Bergman, C. (1975). Potassium accumulation in the perinodal space of frog myelinated axons. Pflügers Arch. *358* , 111-124.

Duchatelle-Gourdon, I. and Hartzell, H.C. (1990). Single delayed rectifier channels in frog atrial cells. Effects of beta-adrenergic stimulation. Biophys. J. *57*, 903-909.

Duchatelle-Gourdon, I., Hartzell, H.C., and Lagrutta, A.A. (1989). Modulation of the delayed rectifier potassium current in frog cardiomyocytes by β-adrenergic agonists and magnesium. J. Physiol. (London) *415*, 251-274.

Duchatelle-Gourdon, I., Lagrutta, A.A., and Hartzell, H.C. (1991). Effects of Mg^{2+} on basal and beta-adrenergic-stimulated delayed rectifier potassium current in frog atrial myocytes. J. Physiol. (London) *435*, 333-347.

Duggal, P., Vesely, M.R., Wattanasirichaigoon, D., Villafane, J., Kaushik, V., and Beggs, A.H. (1998). Mutation of the gene for IsK associated with both Jervell and Lange-Nielsen and Romano-Ward forms of Long-QT syndrome. Circulation *97*, 142-146.

Dumont, J.N. and Brummett, A.R. (1978). Oogenesis in *Xenopus laevis* (Daudin): V. Relationships between developing oocytes and their investing follicular tissues. J. Morphol. *155*, 73-98.

Felipe, A., Knittle, T.J., Doyle, K.L., Snyders, D.J., and Tamkun, M.M. (1994). Differential expression of IsK mRNAs in mouse tissue during development and pregnancy. Am. J. Physiol. *267*, C700-C705.

Fermini, B., Jurkiewicz, N.K., Jow, B., Guinosso, P.J., Jr., Baskin, E.P., Lynch, J.J., Jr., and Salata, J.J. (1995). Use-dependent effects of the class III antiarrhythmic agent NE-10064 (azimilide) on cardiac repolarization: block of delayed rectifier potassium and L-type calcium currents. J. Cardiovasc. Pharmacol. *26*, 259-271.

Feroze, H., Suri, R., and Silverman, D.I. (1996). Torsades de pointes from terfenadine and sotalol given in combination. Pacing Clin. Electrophysiol. *10*, 1519-1521.

Firek, L. and Giles, W.R. (1995). Outward currents underlying repolarization in human atrial myocytes. Cardiovasc. Res. *30*, 31-38.

Fiset, C., Drolet, B., Hamelin, B.A., and Turgeon, J. (1998). Block of IKs by the diuretic agent indapamide modulates cardiac electrophysiological effects of the class III antiarrhythmic drug *dl*-sotalol. J. Pharmacol. Exp. Ther. *283*, 148-156.

Folander, K., Smith, J.S., Antanavage, J., Bennett, C., Stein, R.B., and Swanson, R. (1990). Cloning and expression of the delayed-rectifier IsK channel from neonatal rat heart and diethylstilbestrol-primed rat uterus. Proc. Natl. Acad. Sci. USA *87*, 2975-2979.

Follmer, C.H. and Colatsky, T.J. (1990). Block of delayed rectifier potassium current, IK, by flecainide and E-4031 in cat ventricular myocytes. Circulation *82*, 289-293.

Frankenhaeuser, B. and Hodgkin, A.L. (1956). The after-effects of impulses in the giant nerve fibres of *Loligo*. J. Physiol.(London) *131*, 341-376.

Freeman, L.C. and Kass, R.S. (1993). Expression of a minimal K^+ channel protein in mammalian cells and immunolocalization in guinea pig heart. Circ. Res. *73*, 968-973.

Freeman, L.C. and Kass, R.S. (1995). Cholinergic inhibition of slow delayed-rectifier K^+ current in guinea pig sino-atrial node is not mediated by muscarinic receptors. Mol. Pharmacol. *47*, 1248-1254.

Furukawa, T., Kimura, S., Furukawa, N., Bassett, A.L., and Myerburg, R.J. (1992). Potassium rectifier currents differ in myocytes of endocardial and epicardial origin. Circ. Res. *70*, 91-103.

Garnier, D., Nargeot, J., Ojeda, C., and Rougier, O. (1978). The action of acetylcholine on background conductance in frog atrial trabeculae. J. Physiol. (London) *274*, 381-396.

Giles, W., Nakajima, T., Ono, K., and Shibata, E.F. (1989). Modulation of the delayed rectifier K^+ current by isoprenaline in bull-frog atrial myocytes. J. Physiol. (London) *415*, 233-249.

Giles, W. and Noble, S.J. (1976). Changes in membrane currents in bullfrog atrium produced by acetylcholine. J. Physiol. (London) *261*, 103-123.

Giles, W.R. and Imaizumi, Y. (1988). Comparison of potassium currents in rabbit atrial and ventricular cells. J. Physiol. (London) *405:123-45*, 123-145.

Giles, W.R. and Shibata, E.F. (1985). Voltage clamp of bull-frog cardiac pace-maker cells: a quantitative analysis of potassium currents. J. Physiol. (London) *368:265-92*, 265-292.

Gillespie, J.I. and Meves, H. (1981). The effects of external potassium on the removal of sodium inactivation in squid giant axons. J. Physiol. (London) *315*, 493-514.

Gintant, G.A. (1995). Regional differences in IK density in canine left ventricle: role of IKs in electrical heterogeneity. Am. J. Physiol. *268*, H604-H613.

Gintant, G.A. (1996). Two components of delayed rectifier current in canine atrium and ventricle. Does IKs play a role in the reverse rate dependence of class III agents? Circ. Res. *78*, 26-37.

Girard, S. and Clapham, D.E. (1994). Simultaneous near ultraviolet and visible excitation confocal microscopy of calcium transients in *Xenopus* oocytes. Methods in Cell Biol. *40*, 263-272.

Goldstein, S.A.N. and Miller, C. (1991). Site-specific mutations in a minimal voltage-dependent K^+ channel alter ion selectivity and open-channel block. Neuron *7*, 403-408.

Hausdorff, S.F., Goldstein, S.A.N., Rushin, E.E., and Miller, C. (1991). Functional characterization of a minimal K^+ channel expressed from a synthetic gene. Biochem. *30*, 3341-3346.

Heath, B.M. and Terrar, D.A. (1996a). Separation of the components of the delayed rectifier potassium current using selective blockers of IKr and IKs in guinea-pig isolated ventricular myocytes. Exp. Physiol. *81*, 587-603.

Heath, B.M. and Terrar, D.A. (1996b). The deactivation kinetics of the delayed rectifier components IKr and IKs in guinea-pig isolated ventricular myocytes. Exp. Physiol. *81*, 605-621.

Heath, B.M. and Terrar, D.A. (1997). Block by propofol and thiopentone of the minK current (IsK) expressed in *Xenopus oocytes*. Naunyn-Schmiedeberg's Arch.Pharmacol. *356*, 404-409.

Hice, R.E., Folander, K., Salata, J.J., Smith, J.S., Sanguinetti, M.C., and Swanson, R. (1994). Species variants of the IsK protein: differences in kinetics, voltage dependence, and La^{3+} block of the currents expressed in *Xenopus* oocytes. Pflügers Arch. *426*, 139-145.

Hodgkin, A.L. and Huxley, A.F. (1952). A quantitative description of membrane current and its application to conduction and excitation in nerve. J. Physiol. (London) *117*, 500-544.

Hondeghem, L.M. (1992). Development of class III antiarrhythmic agents. J. Cardiovasc. Pharmacol. *20(suppl.2)*, S17-S22.

Honoré, E., Attali, B., Lesage, F., Barhanin, J., and Lazdunski, M. (1992). Receptor-mediated regulation of IsK, a very slowly activating, voltage-dependent K^+ channel in *Xenopus* oocytes. Biochem. Biophys. Res. Comm. *184*, 1135-1141.

Honoré, E., Attali, B., Romey, G., Heurteaux, C., Ricard, P., Lesage, F., Lazdunski, M., and Barhanin, J. (1991). Cloning, expression, pharmacology and regulation of a delayed rectifier K^+ channel in mouse heart. EMBO J. *10*, 2805-2811.

Horie, M., Hayashi, S., and Kawai, C. (1990). Two types of delayed rectifying K^+ channels in atrial cells of guinea pig heart. Jap. J. Physiol. *40*, 479-490.

Howarth, F.C., Levi, A.J., and Hancox, J.C. (1996). Characteristics of the delayed rectifier K^+ current compared in myocytes isolated from the atrioventricular node and ventricle of the rabbit heart. Pflügers Arch. *431*, 713-722.

Hume, J.R. and Giles, W. (1983). Ionic currents in single isolated bullfrog atrial cells. J. Gen. Physiol. *81*, 153-194.

Hume, J.R., Giles, W., Robinson, K., Shibata, E.F., Nathan, R.D., Kanai, K., and Rasmusson, R. (1986). A time- and voltage-dependent K^+ current in single cardiac cells from bullfrog atrium. J. Gen. Physiol. *88*, 777-798.

Iwai, M., Masu, M., Tsuchida, K., Mori, T., Ohkubo, H., and Nakanishi, S. (1990). Characterization of gene organization and generation of heterogeneous mRNA species of rat IsK protein. J. Biochem. *108*, 200-206.

Je Zhang, Z., Jurkiewicz, N.K., Folander, K., Lazarides, E., Salata, J.J., and Swanson, R. (1994). K^+ currents expressed from the guinea pig cardiac IsK protein are enhanced by activators of protein kinase C. Proc. Natl. Acad. Sci. USA *91*, 1766-1770.

Jiang, M., Tseng-Crank, J., and Tseng, G.-N. (1997). Suppression of slow delayed rectifier current by a truncated isoform of KvLQT1 cloned from normal human heart. J. Biol. Chem. *272*, 24109-24112.

Johnson, E.A. and Lieberman, M. (1971). Heart: excitation and contraction. Annu. Rev. Physiol. *33*, 479-532.

Jurkiewicz, N.K. and Sanguinetti, M.C. (1993). Rate-dependent prolongation of cardiac action potentials by a methanesulfonanilide class III antiarrhythmic agent. Circ. Res. *72*, 75-83.

Kaczmarek, L.K. (1991). Voltage-dependent potassium channels: minK and Shaker families. New Biol. *3*, 315-323.

Kaczmarek, L.K. and Blumenthal, E.M. (1997). Properties and regulation of the minK potassium channel protein. Physiol. Rev. *77*, 627-641.

Karnovsky, M. (1965). A formaldehyde-glutaraldehyde fixative of high osmolarity for use in electron microscopy. J. Cell Biol. *27*, 137A-138A.

Kass, R.S. (1995). Delayed potassium channels in the heart: cellular, molecular, and regulatory properties. In Cardiac Electrophysiology. From Cell to Bedside. D.P. Zipes and J. Jalife, eds. (Philadelphia: W.B.Saunders Co.), pp. 74-82.

Keating, M.T. (1995). Genetic approaches to cardiovascular disease: Supravalvular aortic stenosis, Williams syndrome, and long-QT syndrome. Circulation *92*, 142-147.

Kline, R. and Morad, M. (1976). Potassium efflux and accumulation in heart muscle: Evidence from K^+ electrode experiments. Biophys. J. *16*, 367-372.

Kline, R.P. and Kupersmith, J. (1982). Effects of extracellular potassium accumulation and sodium pump activation on automatic canine purkinje fibres. J. Physiol. (London) *324*, 507-533.

Kline, R.P. and Morad, M. (1978). Potassium efflux in heart muscle during activity: extracellular accumulation and its implications. J. Physiol. (London) *280*, 537-558.

Kokubun, S., Nishimura, M., Noma, A., and Irisawa, H. (1982). Membrane currents in the rabbit atrioventricular node cell. Pflügers Arch. *393*, 15-22.

Kunze, D.L. (1977). Rate-dependent changes in extracellular potassium in the rabbit atrium. Circ. Res. *41*, 122-127.

Kyte, J. and Doolittle, R.F. (1982). A simple method for displaying the hydropathic character of a protein. J. Mol. Biol. *157*, 105-132.

Lee, M.P., Hu, R.-J., Johnson, L.A., and Feinberg, A.P. (1997). Human KvLQT1 gene shows tissue-specific imprinting and encompasses Beckwith-Wiedemann syndrome chromosomal rearrangements. Nat. Genet. *15*, 181-185.

Lesage, F., Attali, B., Lakey, J., Honoré, E., Romey, G., Faurobert, E., Lazdunski, M., and Barhanin, J. (1993). Are *Xenopus* oocytes unique in displaying functional IsK channel heterologous expression? Receptors Channels *1*, 143-152.

Lesage, F., Attali, B., Lazdunski, M., and Barhanin, J. (1992). IsK, a slowly activating voltage-sensitive K^+ channel. Characterization of multiple cDNAs and gene organization in the mouse. FEBS Lett. *301*, 168-172.

Li, Q., Himmel, H.M., and Ravens, U. (1996). Selectivity of class-III antiarrhythmic action of clofilium in guinea pig ventricular myocytes. J. Cardiovasc. Pharmacol. *27*, 401-410.

Lide, D.R. (1992). CRC Handbook of Chemistry and Physics (Cleveland, Ohio: CRC Press).

Liu, D.W. and Antzelevitch, C. (1995). Characteristics of the delayed rectifier current (IKr and IKs) in canine ventricular epicardial, midmyocardial, and endocardial myocytes. A weaker IKs contributes to the longer action potential of the M cell. Circ. Res. *76*, 351-365.

Liu, D.W., Gintant, G.A., and Antzelevitch, C. (1993). Ionic basis for electrophysiological distinctions amoung epicardial, midmyocardial, and endocardial myocytes from free wall of the canine left ventricle. Circ. Res. *72*, 671-687.

Loussouarn, G., Charpentier, F., Mohammad-Panah, R., Kunzelmann, K., Baró, I., and Escande, D. (1997). KvLQT1 potassium channel but not IsK is the molecular target for *trans*-6-Cyano-4-(*N*-ethylsulfonyl-*N*-methylamino)-3-hydroxy-2,2-dimethyl-chromane. Mol. Pharmacol. *52*, 1131-1136.

Lynch, J.J.J., Wallace, A.A., Stupienski, R.F., Baskin, E.P., Beare, C.M., Appleby, S.D., Salata, J.J., Jurkiewicz, N.K., Sanguinetti, M.C., Stein, R.B., Gehret, J.R., Kothstein, T., Claremon, D.A., Elliot, J.M., Butchier, J.W., Remy, D.C., and Baldwin, J.J. (1994). Cardiac electrophysiologic and antiarrhythmic actions of two long-acting spirobenzopyran piperidine class III agents, L-702,958 and L-706,000 [MK-499]. J. Pharmacol. Exp. Ther. *269*, 541-554.

Malo, M.S., Srivastava, K., and Ingram, V.M. (1995). Gene assignment by polymerase chain reaction: localization of the human potassium channel IsK gene to the Down's syndrome region of chromosome 21q22.1-q22.2. Gene *159*, 273-275.

Marcus, D.C. and Shen, Z. (1994). Slowly activating voltage-dependent K^+ conductance is apical pathway for K^+ secretion in vestibular dark cells. Am. J. Physiol. *267*, C857-C864.

Matsuura, H., Ehara, T., and Imoto, Y. (1987). An analysis of the delayed outward current in single ventricular cells of the guinea-pig. Pflügers Arch. *410*, 596-603.

McDonald, T.F. and Trautwein, W. (1978). The potassium current underlying delayed rectification in cat ventricular muscle. J. Physiol. (London) *274*, 217-246.

McDonald, T.V., Yu, Z., Ming, Z., Palma, E., Meyers, M.B., Wang, K.-W., Goldstein, S.A.N., and Fishman, G.I. (1997). A minK-HERG complex regulates the cardiac potassium current IKr. Nature *388*, 289-292.

Methfessel, C., Witzemann, V., Takahashi, T., Mishina, M., Numa, S., and Sakmann, B. (1986). Patch clamp measurements on *Xenopus laevis* oocytes: currents through endogenous channels and implanted acetylcholine receptor and sodium channels. Pflügers Arch. *407*, 577-588.

Moorman, J.R., Palmer, C.J., John, J.E., Durieux, M.E., and Jones, L.R. (1992). Phospholemman expression induces a hyperpolarization activated chloride current in *Xenopus* oocytes. J. Biol. Chem. *267*, 14551-14554.

Morrison, B.W., Moorman, J.R., Kowdley, G.C., Kobayashi, Y.M., Jones, L.R., and Leder, P. (1995). Mat-8, a novel phospholemman-like protein expressed in human breast tumors, induces a chloride conductance in *Xenopus* oocytes. J. Biol. Chem. 2176-2182.

Murai, T., Kakizuka, T., Ohkubo, H., and Nakanishi, S. (1989). Molecular cloning and sequence analysis of human genomic DNA encoding a novel membrane protein which exhibits a slowly activating potassium channel activity. Biochem. Biophys. Res. Comm. *161*, 176-181.

Muraki, K., Imaizumi, Y., Watanabe, M., Habuchi, Y., and Giles, W.R. (1995). Delayed rectifier K^+ current in rabbit atrial myocytes. Am. J. Physiol. *269*, H524-H532.

Neher, E. and Lux, H.D. (1973). Rapid changes of potassium concentration at the outer surface of exposed single neurons during membrane current flow. J. Gen. Physiol. *61*, 385-399.

Neyroud, N., Tesson, F., Denjoy, I., Leibovici, M., Donger, C., Barhanin, J., Faure, S., Gary, F., Coumel, P., Petit, C., Schwartz, K., and Guicheney, P. (1997). A novel mutation in the potassium channel gene KvLQT1 causes the Jervell and Lange-Nielsen cardioauditory syndrome. Nat. Genet. *15*, 186-189.

Nicholson, C. and Hounsgaard, J. (1983). Diffusion in the slice microenvironment and implications for physiological studies. Fed. Proc. *42*, 2865-2868.

Nicholson, C. and Phillips, J.M. (1981). Ion diffusion modified by tortuosity and volume fraction in the extracellular microenvironment of the rat cerebellum. J. Physiol. (London) *321*, 225-257.

Noble, D. and Tsien, R.W. (1969). Outward membrane currents activated in the plateau range of potentials in cardiac purkinje fibres. J. Physiol. (London) *200*, 205-231.

Noble, S. (1976). Potassium accumulation and depletion in frog atrial muscle. J. Physiol. (London) *258*, 579-613.

Noma, A. and Irisawa, H. (1976). A time- and voltage-dependent potassium current in the rabbit sinoatrial node cell. Pflügers Arch. *366*, 251-258.

Ojeda, C. and Rougier, O. (1974). Kinetic analysis of delayed outward currents in frog atrium. Existence of two kinds of preparations. J. Physiol. (London) *239*, 51-73.

Pragnell, M., Snay, K.J., Trimmer, J.S., MacLusky, N.J., Naftolin, F., Kaczmarek, L.K., and Boyle, M.B. (1990). Estrogen induction of a small, putative K^+ channel mRNA in rat uterus. Neuron *4*, 807-812.

Raber, G., Waldegger, S., Herzer, T., Gulbins, E., Murer, H., Busch, A.E., and Lang, F. (1995). The nitroso-donor S-nitroso-cysteine regulates IsK expressed in *Xenopus* oocytes via a cGMP independent mechanism. Biochem. Biophys. Res. Commun. *207*, 195-201.

Rasmusson, R.L., Clark, J.W., Giles, W.R., Robinson, K., Clark, R.B., Shibata, E.F., and Campbell, D.L. (1990a). A mathematical model of electrophysiological activity in a bullfrog atrial cell. Am. J. Physiol. *259*, H370-H389.

Rasmusson, R.L., Clark, J.W., Giles, W.R., Shibata, E.F., and Campbell, D.L. (1990b). A mathematical model of a bullfrog cardiac pacemaker cell. Am. J. Physiol. *259*, H352-H369.

Rees, S. and Curtis, M.J. (1996). Which cardiac potassium channel subtype is the preferable target for suppression of ventricular arrhythmias? Pharmac. Ther. *69*, 199-217.

Roden, D.M., Bennett, P.B., Snyders, D.J., Balser, J.R., and Hondeghem, L.M. (1988). Quinidine delays I_K activation in guinea pig ventricular myocytes. Circ. Res. *62*, 1055-1058.

Roden, D.M. and George, A.L., Jr. (1996). The cardiac ion channels: Relevance to management of arrhythmias. Annu. Rev. Med. *47*, 135-148.

Romey, G., Attali, B., Chouabe, C., Abitbol, I., Guillemare, E., Barhanin, J., and Lazdunski, M. (1997). Molecular mechanism and functional significance of the minK control of the KvLQT1 channel activity. J. Biol. Chem. *272*, 16713-16716.

Safronov, B.V. and Vogel, W. (1995). Modulation of delayed rectifier K^+ channel activity by external K^+ ions in *Xenopus* axon. Pflügers Arch. *430*, 879-886.

Sakagami, M., Fukazawa, K., Matsunaga, T., Fujita, H., Mori, N., Takumi, T., Ohkubo, H., and Nakanishi, S. (1991). Cellular localization of rat IsK protein in the stria vascularis by immunohistochemical observation. Hear. Res. *56*, 168-172.

Sakura, H., Bond, C., Warren-Perry, M., Horsley, X., Kearney, L., Tucker, S., Adelman, J., Turner, R., and Ashcroft, F.M. (1995). Characterization and variation of a human inwardly-rectifying-K-channel gene (KCNJ6): a putative ATP-sensitive K-channel subunit. FEBS Lett. *367*, 193-197.

Salata, J.J. and Brooks, R.R. (1997). Pharmacology of azimilide dihydrochloride (NE-10064), a class III antiarrhythmic agent. Cardiovasc. Drug Rev. *15*, 137-156.

Salata, J.J., Jurkiewicz, N.K., Jow, B., Folander, K., Guinosso, P.J.J., Raynor, B., Swanson, R., and Fermini, B. (1996a). IK of rabbit ventricle is composed of two currents: evidence for IKs. Am. J. Physiol. *271*, H2477-H2489.

Salata, J.J., Jurkiewicz, N.K., Sanguinetti, M.C., Siegl, P.K., Claremon, D.A., Remy, D.C., Elliot, J.M., and Libby, B.E. (1996b). The novel class III antiarrhythmic agent, L-735,821 is a potent and selective blocker of IKs in guinea pig ventricular myocytes. Circulation *94(8)*, I-529.

Salata, J.J., Jurkiewicz, N.K., Wallace, A.A., Stupienski, R.F.3., Guinosso, P.J., Jr., and Lynch, J.J., Jr. (1995). Cardiac electrophysiological actions of the histamine H1- receptor antagonists astemizole and terfenadine compared with chlorpheniramine and pyrilamine. Circ. Res. *76*, 110-119.

Sanguinetti, M.C., Curran, M.E., Zou, A., Shen, J., Spector, P.S., Atkinson, D.L., and Keating, M.T. (1996). Coassembly of KvLQT1 and minK (IsK) proteins to form cardiac IKs potassium channel. Nature *384*, 80-83.

Sanguinetti, M.C., Jiang, C., Curren, M.E., and Keating, M.T. (1995). A mechanistic link between an inherited and an acquired cardiac arrhythmia: HERG encodes the IKr potassium channel. Cell *81*, 299-307.

Sanguinetti, M.C. and Jurkiewicz, N.K. (1990a). Lanthanum blocks a specific component of I_K and screens membrane surface charge in cardiac cells. Am. J. Physiol. *259*, H1881-H1889

Sanguinetti, M.C. and Jurkiewicz, N.K. (1990b). Two components of cardiac delayed rectifier K^+ current. Differential sensitivity to block by class III antiarrhythmic agents. J. Gen. Physiol. *96*, 195-215.

Sanguinetti, M.C. and Jurkiewicz, N.K. (1991). Delayed rectifier outward K^+ current is composed of two currents in guinea pig atrial cells. Am. J. Physiol. *260*, H393-H399.

Sanguinetti, M.C. and Jurkiewicz, N.K. (1992). Role of external Ca^{2+} and K^+ in gating of cardiac delayed rectifier K^+ currents. Pflügers Arch. *420*, 180-186.

Sanguinetti, M.C. and Jurkiewicz, N.K. (1994). Delayed rectifier potassium channels of cardiac muscle. In Ion channels in the Cardiovascular System: Function and Dysfunction. P.M. Spooner, A.M. Brown, W.A. Catterall, G.J. Kaczorowski, and H.C. Strauss, eds. (Armonk, New York: Futura Publishing Co.Inc.), pp. 121-143.

Sanguinetti, M.C., Jurkiewicz, N.K., Scott, A., and Siegl, P.K.S. (1991). Isoproterenol antagonizes prolongation of refractory period by the class III antiarrhythmic agent E-4031 in guinea pig myocytes. Circ. Res. *68*, 77-84.

Sanguinetti, M.C. and Keating, M.T. (1997). Role of delayed rectifier potassium channels in cardiac repolarization and arrhythmias. News Physiol. Sci. *12*, 152-157.

Shalaby, F.Y., Levesque, P.C., Yang, W.-P., Little, W.A., Conder, M.L., Jenkins-West, T., and Blanar, M.A. (1997). Dominant-negative KvLQT1 mutations underlie the LQT1 form of long QT syndrome. Circulation *96*, 1733-1736.

Shibasaki, T. (1987). Conductance and kinetics of delayed rectifier potassium channels in nodal cells of the rabbit heart. J. Physiol. (London) *387*, 227-250.

Shimbo, K., Brassard, D.L., Lamb, R.A., and Pinto, L.H. (1995). Viral and cellular small integral membrane proteins can modify ion channels endogenous to *Xenopus* oocytes. Biophys. J. *69*, 1819-1829.

Shrier, A. and Clay, J.R. (1986). Repolarization current in embryonic chick atrial heart cell aggregates. Biophys. J. *50*, 861-874.

Simmons, M.A., Creazzo, T., and Hartzell, H.C. (1986). A time-dependent and voltage-sensitive K^+ current in single cells from frog atrium. J. Gen. Physiol. *88*, 739-755.

Smirnov, S.V. and Aaronson, P.I. (1994). Alteration of the transmembrane K^+ gradient during development of delayed rectifier in isolated rat pulmonary arterial cells. J. Gen. Physiol. *104*, 241-264.

Splawski, I., Timothy, K.W., Vincent, G.M., Atkinson, D.L., and Keating, M.T. (1997a). Molecular basis of the long-QT syndrome associated with deafness. N. Engl. J. Med. *336*, 1562-1567.

Splawski, I., Tristani-Firouzi, M., Lehmann, M.H., Sanguinetti, M.C., and Keating, M.T. (1997b). Mutations in the hminK gene cause long QT syndrome and suppress IKs function. Nat. Genet. *17*, 338-340.

Stühmer, W. (1992). Electrophysiological recording from *Xenopus* oocytes. Meth.Enzymol. *207*, 319-339.

Suessbrich, H., Bleich, M., Ecke, D., Rizzo, M., Waldegger, S., Lang, F., Szabo, I., Lang, H.-J., Kunzelmann, K., Greger, R., and Busch, A.E. (1996). Specific blockade of slowly activating IsK channels by chromanols - impact on the role of IsK channels in epithelia. FEBS Lett. *396*, 271-275.

Swanson, R., Folander, K., Antanavage, J., and Smith, J. (1991). The IsK gene is expressed in human heart. Biophys. J. *59*, 452a.

Tai, K. and Goldstein, S.A.N. (1998). The conduction pore of a cardiac potassium channel. Nature *391*, 605-608.

Tai, K., Wang, K., and Goldstein, S.A.N. (1997). MinK potassium channels are heteromultimeric complexes. J. Biol. Chem. *272*, 1654-1658.

Takumi, T., Moriyoshi, K., Aramori, I., Ishii, T., Oiki, S., Okada, Y., Ohkubo, H., and Nakanishi, S. (1991). Alteration of channel activities and gating by mutations of slow IsK potassium channel. J. Biol. Chem. *266*, 22192-22198.

Takumi, T., Ohkubo, H., and Nakanishi, S. (1988). Cloning of a membrane protein that induces a slow voltage-gated potassium current. Science *242*, 1042-1045.

Tesson, F., Donger, C., Denjoy, I., Berthet, M., Bennaceur, M., Petit, C., Coumel, P., Schwartz, K., and Guicheney, P. (1996). Exclusion of KCNE1 (IsK) as a candidate gene for Jervell and Lange-Nielsen syndrome. J. Mol. Cell. Cardiol. *28*, 2051-2055.

Tohse, N. (1990). Calcium-sensitive delayed rectifier potassium current in guinea pig ventricular cells. Am. J. Physiol. *258*, H1200-H1207.

Tsukahara, Y., Houtani, T., Ueyama, T., Ikeda, M., Nakanishi, S., Yamamoto, A., Tashiro, Y., and Sugimoto, T. (1995). A subpopulation of large ganglion neurons express IsK protein mRNA: an *in situ* hybridization analysis in the rat eye. Mol. Brain Res. *29*, 376-380.

Turgeon, J., Daleau, P., Bennett, P.B., Wiggins, S.S., Selby, L., and Roden, D.M. (1994). Block of IKs, the slow component of the delayed rectifier K^+ current, by the diuretic agent indapamide in guinea pig myocytes. Circ. Res. *75*, 879-886.

Tyson, J., Tranebjærg, L., Bellman, S., Wren, C., Taylor, J.F.N., Bathen, J., Aslaksen, B., Jan Sørland, S., Lund, O., Malcolm, S., Pembrey, M., Bhattacharya, S., and Bitner-Clindzicz, M. (1997). IsK and KvLQT1: mutation in either of the two subunits of the slow component of the delayed rectifier potassium channel can cause Jervell and Lange-Nielsen syndrome. Hum. Mol. Genet. *6*, 2179-2185.

Tzounopoulos, T., Guy, H.R., Durell, S., Adelman, J.P., and Maylie, J. (1995a). minK channels form by assembly of at least 14 subunits. Biophys. J. *92*, 9593-9597.

Tzounopoulos, T., Maylie, J., and Adelman, J.P. (1995b). Induction of endogenous channels by high levels of heterologous membrane proteins in *Xenopus* oocytes. Biophys. J. *69*, 904-908.

van den Berg, M.H., Wilde, A.A.M., Robles de Medina, E.O., Meyer, H., Geelen, J.L.M.C., Jongbloed, R.J.E., Wellens, H.J.J., and Geraedts, J.P.M. (1997). The long QT syndrome: a novel missense in the S6 region of the KVLQT1 gene. Hum. Genet. *100*, 356-361.

Varnum, M.D., Busch, A.E., Bond, C.T., Maylie, J., and Adelman, J.P. (1993). The minK channel underlies the cardiac potassium current IKs and mediates species-specific responses to protein kinase C. Proc. Natl. Acad. Sci.USA *90*, 11528-11532.

Varnum, M.D., Maylie, J., Busch, A., and Adelman, J.P. (1995). Persistent activation of minK channels by chemical cross-linking. Neuron *14*, 407-412.

Veldkamp, M.W., van Ginneken, A.C., and Bouman, L.N. (1993). Single delayed rectifier channels in the membrane of rabbit ventricular myocytes. Circ. Res. *72*, 865-878.

Venable, J. and Coggeshell, R. (1965). A simplified lead citrate stain for use in electron microscopy. J. Cell Biol. *25*, 407-408.

Vetter, D.E., Mann, J.R., Wangemann, P., Liu, J., McLaughlin, K.J., Lesage, F., Marcus, D.C., Lazdunski, M., Heinemann, S.F., and Barhanin, J. (1996). The inner ear defects induced by null mutation of the *isk* gene. Neuron *17*, 1251-1264.

Walsh, K.B., Arena, J.P., Kwok, W.M., Freeman, L., and Kass, R.S. (1991). Delayed-rectifier potassium channel activity in isolated membrane patches of guinea pig ventricular myocytes. Am.J.Physiol. *260*, H1390-H1393.

Walsh, K.B., Begenisich, T.B., and Kass, R.S. (1989). Beta-adrenergic modulation of cardiac ion channels. Differential temperature sensitivity of potassium and calcium currents. J. Gen. Physiol. *93*, 841-854.

Walsh, K.B. and Kass, R.S. (1988). Regulation of a heart potassium channel by protein kinase A and C. Science *242*, 67-69.

Walsh, K.B. and Kass, R.S. (1991). Distinct voltage-dependent regulation of a heart-delayed IK by protein kinases A and C. Am. J. Physiol. *261*, C1081-C1090.

Wang, D.W., Kiyosue, T., Sato, T., and Arita, M. (1996). Comparison of the effects of class I anti-arrhythmic drugs, cibenzoline, mexiletine and flecainide, on the delayed rectifier K^+ current of guinea-pig ventricular myocytes. J. Mol. Cell. Cardiol. *28*, 893-903.

Wang, K.-W. and Goldstein, S.A.N. (1995). Subunit composition of minK potassium channels. Neuron *14*, 1303-1309.

Wang, K.-W., Tai, K., and Goldstein, S.A.N. (1996). MinK residues line a potassium channel pore. Neuron *16*, 571-577.

Wang, L. and Duff, H.J. (1996a). Identification and characteristics of delayed rectifier K^+ current in fetal mouse ventricular myocytes. Am. J. Physiol. *270*, H2088-H2093.

Wang, L., Feng, Z.-P., Kondo, C.S., Sheldon, R.S., and Duff, H.J. (1996b). Developmental changes in the delayed rectifier K^+ channels in mouse heart. Circ. Res. *79*, 79-85.

Wang, Q., Curran, M.E., Splawski, I., Burn, T.C., Millholland, J.M., VanRaay, T.J., Shen, J., Timothy, K.W., Vincent, G.M., de Jager, T., Schwartz, P.J., Towbin, J.A., Moss, A.J., Atkinson, D.L., Landes, G.M., Connors, T.D., and Keating, M.T. (1996). Positional cloning of a novel potassium channel gene: KvLQT1 mutations cause cardiac arrhythmias. Nat. Genet. *12*, 17-23.

Wang, Q., Shen, J., Splawski, I., Atkinson, D., Li, Z., Robinson, J.L., Moss, A.J., Towbin, J.A., and Keating, M.T. (1995). SCN5A mutations associated with an inherited cardiac arrhythmia, long QT syndrome. Cell *80*, 805-811.

Wang, Z., Fermini, B., and Nattel, S. (1994). Rapid and slow components of delayed rectifier current in human atrial myocytes. Cardiovasc. Res. *28*, 1540-1546.

Wilde, A.A.M. and Veldkamp, M.W. (1997). Ion channels, the QT interval, and arrhythmias. PACE *20*, 2048-2057.

Wilson, G.G., Sivaprasadarao, A., Findlay, J.B.C., and Wray, D. (1994). Changes in activation gating of IsK potassium currents brought about by mutations in the transmembrane sequence. FEBS Lett. *353*, 251-254.

Wollnik, B., Schroeder, B.C., Kubisch, C., Esperer, H.D., Wieacker, P., and Jentsch, T.J. (1997). Pathophysiological mechanisms of dominant and recessive KvLQT1 K^+ channel mutations found in inherited cardiac arrhythmias. Hum. Mol. Genet. *6*, 1943-1949.

Yamane, T., Furukawa, T., Horikawa, S., and Hiraoka, M. (1993). External pH regulates the slowly activating potassium current IsK expressed in *Xenopus* oocytes. FEBS Lett. *319*, 229-232.

Yang, T., Kupershmidt, S., and Roden, D.M. (1995). Anti-minK antisense decreases the amplitude of the rapidly activating cardiac delayed rectifier K^+ current. Circ. Res. *77*, 1246-1253.

Yang, W.-P., Levesque, P.C., Little, W.A., Conder, M.L., Shalaby, F.Y., and Blanar, M.A. (1997). KvLQT1, a voltage-gated potassium channel responsible for human cardiac arrhythmias. Proc. Natl. Acad. Sci.USA *94*, 4017-4021.

Yao, J.-A., Trybulski, E.J., and Tseng, C.-J. (1998). Quinidine preferentially blocks the slow delayed rectifier potassium channel in the rested state. J. Pharmacol. Exp. Ther. *279*, 856-864.

Yao, J.-A. and Tseng, G.-N. (1997). Azimilide (NE-10064) can prolong or shorten the action potential duration in canine ventricular myocytes: Dependence on blockade of K, Ca, and Na channels. J. Cardiovasc. Electrophysiol. *8*, 184-198.

Yasui, K., Anno, T., Kamiya, K., Boyett, M.R., Kodama, I., and Toyama, J. (1993). Contibution of potassium accumulation in narrow extracellular spaces to the genesis of nicorandil-induced large inward tail current in guinea-pig ventricular cells. Pflügers Arch. *422*, 371-379.

Yue, L., Feng, J., Li, G.R., and Nattel, S. (1996). Transient outward and delayed rectifier currents in canine atrium: properties and role of isolation methods. Am. J. Physiol. *270*, H2157-H2168.

Zeng, J., Laurita, K.R., Rosenbaum, D.S., and Rudy, Y. (1995). Two components of the delayed rectifier K^+ current in ventricular myocytes of the guinea pig type. Theoretical formulation and their role in repolarization. Circ. Res. *77*, 140-152.

APPENDIX 1:

MATHEMATICAL MODEL FOR K^+ ACCUMULATION IN *XENOPUS* OOCYTES

Appendix 1:

We have developed a mathematical model to describe the observed accumulation of K^+ ions during activation of minK or Kv1.2 currents. Our aims were to determine a) whether the observed signs of K^+ accumulation can be explained in terms of the anatomy of the oocyte, and b) to explore whether the data obtained from minK and Kv1.2 can be reproduced by the same model. The fundamental rationale is that K^+ accumulation would be expected to occur at the surface of the oocyte due to a "transport number effect" (Barry, 1984). We will assume that the current through the cell membrane is carried exclusively by K^+ ions, and that the current in the extracellular medium is carried exclusively by species other than K^+. Thus, all K^+ ions transported across the membrane will accumulate at the surface, and will then be removed through a diffusion process driven by the concentration gradient. The extent to which accumulation will develop will depend critically, however, on the presence of anatomical restrictions to diffusion from the membrane surface. Since removal of the vitelline membrane did not reduce the amount of K^+ accumulation (Figure 44), and considering the surface anatomy of the oocyte as depicted in Figure 45, it seems likely that the restriction to diffusion in this preparation is mainly in the form of an unstirred fluid layer (Barry, 1984; Barry and Diamond, 1984). An unstirred layer may develop due to an inability of the superfusion system to exchange the solution immediately adjacent to the surface membrane(s) of the oocyte. Within the layer of microvilli (0 to 1.5 μm from the surface), only a fraction of the volume (approximately 70%, our estimate) is available for dilution of K^+ ions transported across the membrane. Moreover, the average pathlength of diffusion may be increased ("tortuosity"; Nicholson and Phillips, 1981; Nicholson and Hounsgaard, 1983), resulting in a reduced apparent diffusion coefficient. The net effect is the unstirred layer appears severalfold thicker than its actual dimensions. Beyond the layer of microvilli there are no known obstacles to diffusion, and the diffusion process in this region is therefore assumed to be governed by the diffusion coefficient for K^+ in free aqueous solution.

Diffusion of K^+ ions is governed by the equation,

$$\frac{\partial [K^+](r,t)}{\partial t} = \frac{D}{r^2}\frac{\partial}{\partial r}\left[r^2 \frac{\partial}{\partial r}[K^+](r,t)\right], \quad (1)$$

with boundary conditions,

$$\frac{\partial [K^+](r_0,t)}{\partial r} = -\frac{I_K}{DSF}, \quad (2)$$

at the surface of the cell, and

$$[K^+](r_1,t) = [K^+]_{\text{bath}}, \quad (3)$$

at the interface between the unstirred layer and the bath solution. In the equations above, $[K^+](r,t)$ denotes the K^+ concentration (dependent on radius r and time t) in mM, D the diffusion constant in m^2/s, I_K the total K^+ current crossing the membrane (minK or Kv1.2) in A, S the surface area of the cell ($4\pi r_0^2$) in m^2, r_0 the radius of the cell in m, and F is Faraday's constant, 96487 As/mol.

If the unstirred layer within the layer of microvilli contributed substantially to the total K^+ accumulation, there could be a significant difference in $[K^+]$ between the innermost and the outermost aspects of this layer. Ion channels located at the base of the microvilli would then be subject to a different extracellular $[K^+]$ than those located at the tip of the microvilli, which would complicate this analysis considerably. We therefore began by exploring this possibility. For a thin layer (compared to the radius of the cell), we may approximate (1) with

$$\frac{\partial [K^+](r,t)}{\partial t} = D\frac{\partial^2}{\partial r^2}[K^+](r,t). \quad (4)$$

We can then estimate the maximum concentration difference that can occur across the layer of microvilli from the steady-state solution to (4). This solution is obtained by setting the time-derivative in (4) to zero, and imposing the boundary condition in (2), and yields the formula,

$$\frac{\partial}{\partial r}[K^+](r,t) = -\frac{I_K}{DSF}. \quad (5)$$

The maximum concentration difference that could accumulate across a layer of thickness Δr is therefore,

$$\Delta[K^+] = \Delta r \frac{I_K}{DSF}. \quad (6)$$

For the layer of microvilli, we have that $\Delta r = 1.5 \cdot 10^{-6}$ m and $S = 3.14 \cdot 10^{-6}$ m^2. The diffusion coefficient for K^+ in free aqueous solution (at 293K) in $1.92 \cdot 10^{-9}$ m^2/s (Lide, 1992). The maximum concentration difference across this layer per μA of current is then $\Delta[K^+] = 2.6$ μM. Clearly, even if the apparent diffusion constant is several times smaller than that in aqueous solution, the concentration difference across the layer of microvilli for a current of a few μA will be much less than 100 μM. We can therefore conclude that the contribution to K^+ accumulation from the unstirred layer within the layer of microvilli is very small, and that it is reasonable to assume that all ion channels in the membrane are subject to the same extracellular $[K^+]$. Although the approximation in (4) is no longer applicable for a thicker layer, it does provide an indication that a concentration difference in the mM range could accumulate across an unstirred layer of a few hundred μm thickness for a K^+ current of a few μA.

Based on these considerations, we formulated a model in which the oocyte is surrounded by an unstirred fluid layer. This includes the contribution from the microvilli, as well as that from the adjacent surrounding unstirred layer due to laminar flow around the oocyte. The diffusion process in this layer is modeled by solving equation (1) subject to the boundary conditions (2) and (3) using a 10-point finite difference method. This method can be thought of in terms of 10 concentric spherical shells surrounding the cell, and relates the K^+ concentration $[K^+]_n$ in a shell at radius r_n to the concentrations in the two adjacent shells as,

$$\frac{\partial [K^+]_n}{\partial t} = -D\left[\frac{r_{n+\frac{1}{2}}^2}{r_n^2 \Delta r^2}[K^+]_{n+1} - \frac{r_{n+\frac{1}{2}}^2 + r_{n-\frac{1}{2}}^2}{r_n^2 \Delta r^2}[K^+]_n + \frac{r_{n-\frac{1}{2}}^2}{r_n^2 \Delta r^2}[K^+]_{n-1}\right], \quad (7)$$

for $n = 1, 2, \ldots, 9$. At the outermost shell, the boundary condition (3) is enforced by

setting $[K^+]_{10} = [K^+]_{bath}$, and at the innermost shell, the boundary condition (2) is enforced by the equation,

$$\frac{\partial [K^+]_0}{\partial t} = -D\frac{r_{\frac{1}{2}}^2 + r_{-\frac{1}{2}}^2}{r_0^2 \Delta r^2}\left[[K^+]_0 - [K^+]_1\right] + \frac{r_{\frac{1}{2}}^2}{r_0^2 \Delta r}\frac{2I_K}{SF}. \qquad (8)$$

We attempted to reproduce our experimental results using representative recorded current waveforms, scaled to match average values for current integrals, to "drive" the accumulation model derived above. It soon became clear, however, that this model alone could not account for the amounts of accumulation observed in our experiments, at least when using the initial choices for the model parameters. Figure 48 shows simulations obtained assuming an unstirred layer thickness of 250 μm, and using recorded minK and Kv1.2 current waveforms. Clearly, this model is not sufficient to explain more than a small fraction of the K^+ accumulation observed in experiments with minK currents, and provides even less insight into the results obtained when Kv1.2 currents were activated. We therefore deduced that although an unstirred fluid layer must be involved in the K^+ accumulation process, there must be at least one other phenomenon operating. This second mechanism should then be one in which large amounts of accumulation can develop relatively rapidly, so that the large but short-lasting Kv1.2 currents can produce significant accumulation. This suggests that this process is likely to occur very near the surface of the oocyte, in a relatively small volume.

Micrographs showing oocytes at stage IV of development (Dumont and Brummett, 1978; their Figure 28A) show a much more complicated surface anatomy with deep "crypts" (subsurface passageways and infoldings), which appear to be in communication with the extracellular space only through relatively narrow "mouths". Dumont & Brummett also note that during stages V and VI, the oocyte surface becomes much less contoured, and the microvilli become fewer, shorter, and somewhat broader, consistent with our Figure 45. Presumably, this is a gradual process, and it is therefore possible that a significant number of the oocytes used in our experiments could have had a considerably more contoured surface anatomy than Figure 45 would suggest.

Figure 48: K^+ accumulation as predicted by a model including an unstirred fluid layer of 250 μm thickness for minK (left) and Kv1.2 (right) currents. Top panels show the current waveforms used to "drive" the model, middle panels show model-predicted increase in $[K^+]$ at the surface of the oocyte compared to experimental data. Bottom panels show integrals of the computed current waveforms compared to mean experimental data.

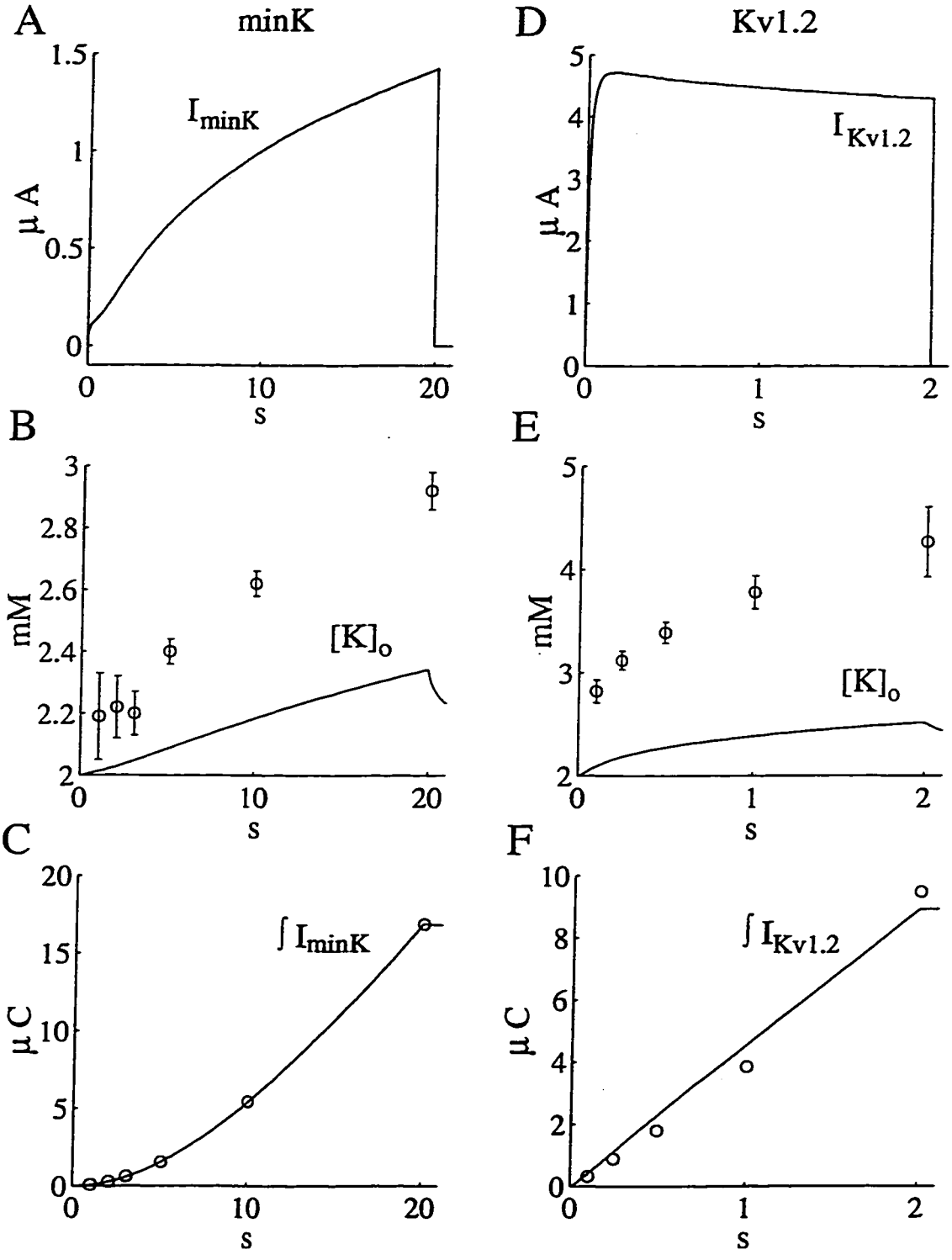
A
minK
1.5
1
0.5
0
μA
I_{minK}
0
10
20
s
D
Kv1.2
5
4
3
2
1
0
μA
$I_{Kv1.2}$
0
1
2
s
B
3
2.8
2.6
2.4
2.2
2
mM
$[K]_o$
0
10
20
s
E
5
4
3
2
mM
$[K]_o$
0
1
2
s
C
20
15
10
5
0
μC
$\int I_{minK}$
0
10
20
s
F
10
8
6
4
2
0
μC
$\int I_{Kv1.2}$
0
1
2
s

Accumulation of K^+ in diffusion-restricted membrane invaginations has been successfully modelled in the context of the cardiac T-tubule system (Yasui et al., 1993), as well as membrane invaginations on the surface of rat pulmonary arterial cells (Smirnov and Aaronson, 1994). Both studies reported that a relatively simple model where K^+ accumulation is governed by the equation,

$$\frac{d[K^+]_c(t)}{dt} = \frac{I_K}{FV_c} - \frac{[K^+]_c - [K^+]_0}{\tau_c}, \quad (9)$$

could successfully reproduce the observed K^+ accumulation process. In this equation, $[K^+]_c$ denotes the K^+ concentration in the crypts, I_K the total K^+ current crossing the membrane, V_c the volume of the crypts, τ_c a time-constant according to which the concentration in the crypts approaches that at the surface if no K^+ current is active, and $[K^+]_0$ the K^+ concentration at the surface (i.e., in the innermost shell of the unstirred layer model). We therefore proceeded to combine our unstirred fluid layer description with this model for the subsurface crypts, to attempt to gain insight into whether accumulation in these could be partially responsible for the accumulation observed in our experimental results. In order to "connect" the two models, it was necessary to modify boundary condition (8) to

$$\frac{\partial [K^+]_0}{\partial t} = \frac{r_{\frac{1}{2}}^2}{r_0^2 \Delta r} \cdot \frac{2V_c}{S} \cdot \frac{[K^+]_c - [K^+]_0}{\tau_c} - D \frac{r_{\frac{1}{2}}^2 + r_{-\frac{1}{2}}^2}{r_0^2 \Delta r^2} \left[[K^+]_0 - [K^+]_1 \right]. \quad (10)$$

Figure 49 shows outputs obtained when this model was used to fit our K^+ accumulation data. In this case, the model has been "tuned" to fit both the minK and the Kv1.2 accumulation data. The radius of the oocyte was set to 0.5 mm, the diffusion constant was assumed to be that for K^+ ions in free aqueous solution (Lide, 1992), and the thickness of the unstirred fluid layer was again set to 250 μm. We then employed a least-squares procedure to find the values of the V_c and τ_c parameters for which the accumulation predicted by the model agreed as closely as possible to the experimental results. Figure 49 shows the result of this analysis, which yielded values for the free parameters of V_c = 6.91 nl, and τ_c = 263 ms. This combined model provides much improved simulations of the observed K^+ accumulation phenomena than the unstirred

Figure 49: K^+ accumulation as predicted by a model including a representation of subsurface "crypts", surrounded by a 250 μm unstirred fluid layer.

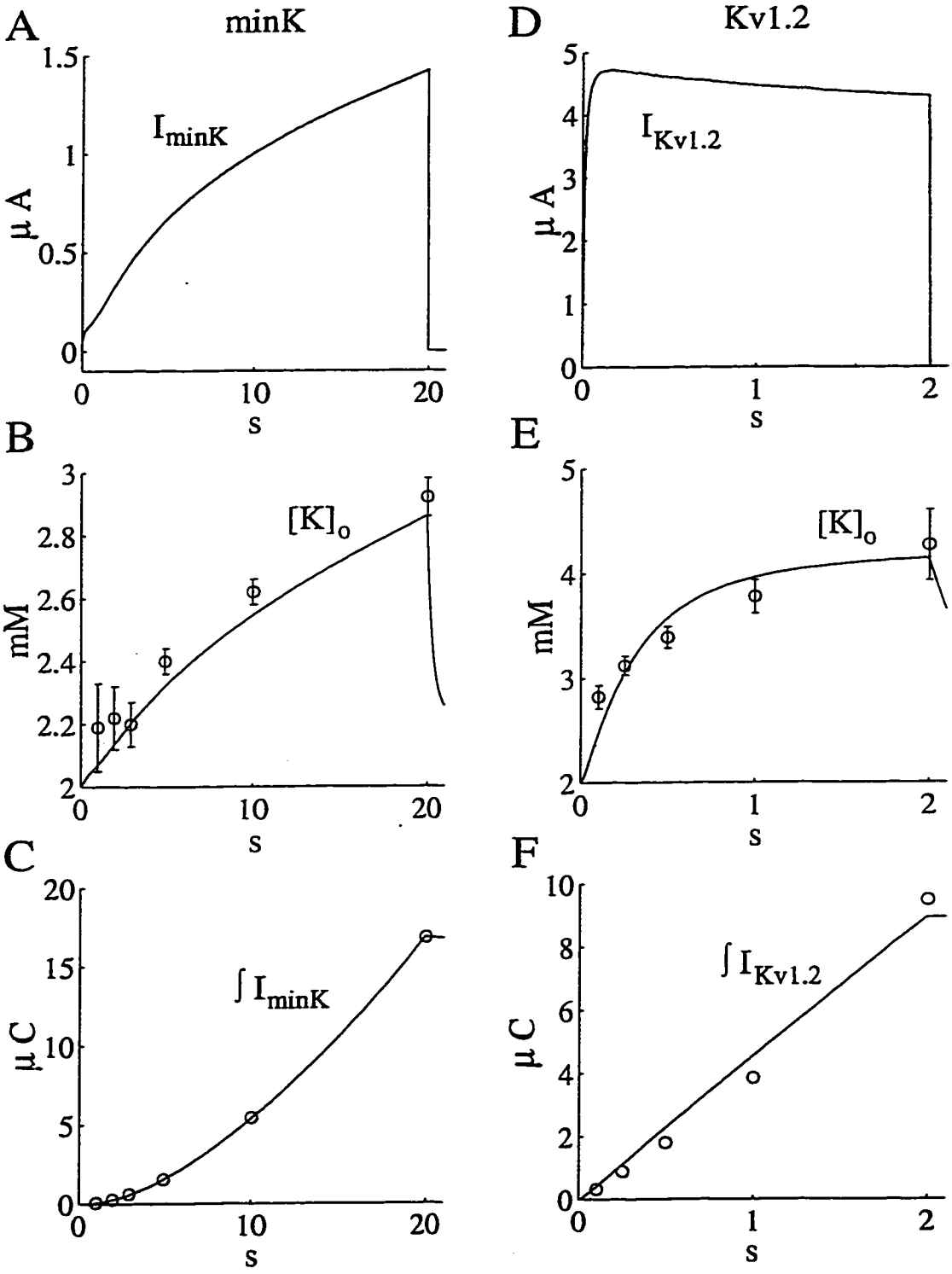
A
minK
1.5
1
0.5
0
μA
I_{minK}
0
10
20
s
B
3
2.8
2.6
2.4
2.2
2
mM
$[K]_o$
0
10
20
s
C
20
15
10
5
0
μC
$\int I_{minK}$
0
10
20
s
D
Kv1.2
5
4
3
2
1
0
μA
$I_{Kv1.2}$
0
1
2
s
E
5
4
3
2
mM
$[K]_o$
0
1
2
s
F
10
8
6
4
2
0
μC
$\int I_{Kv1.2}$
0
1
2
s

fluid layer model alone. It should be noted that the discrepancy in the $[K^+]_o$ waveform for the Kv1.2 data at least in part is due to a corresponding discrepancy in the current integral waveform; ie. that the current waveform used is not entirely representative of the average current integral data.

The fact that a model based solely on the assumption that the cell is surrounded by an unstirred layer comes closer to accounting for accumulation observed during a long-lasting slowly activating current than during a short, rapidly activating current pulse, is interesting and deserves some further analysis. Figure 50 illustrates how the two components of our model contribute to accumulation during the simulation shown in Figure 49. Note that the relative importance of the unstirred fluid layer is much greater in the case of the long-lasting minK current waveform than it is during the short Kv1.2 pulse. This provides an interpretation of the "accumulation volume" results presented in this paper: For the short Kv1.2 current pulses, accumulation occurs primarily within or near the small crypts. For longer-lasting pulses, however, there is sufficient time for a substantial amount of K^+ ions to diffuse away from the surface into the unstirred fluid layer.

- This mathematical model was developed by our colleague, Anders Nygren, at Rice University.

Figure 50: K^+ concentration in the subsurface crypts, and in shells 0 (surface) through 9 of the unstirred fluid layer as a function of time. Note that the unstirred fluid layer contributes a relatively small fraction of the total K^+ accumulation for short pulses (Kv1.2), but becomes more important as pulse duration is increased.

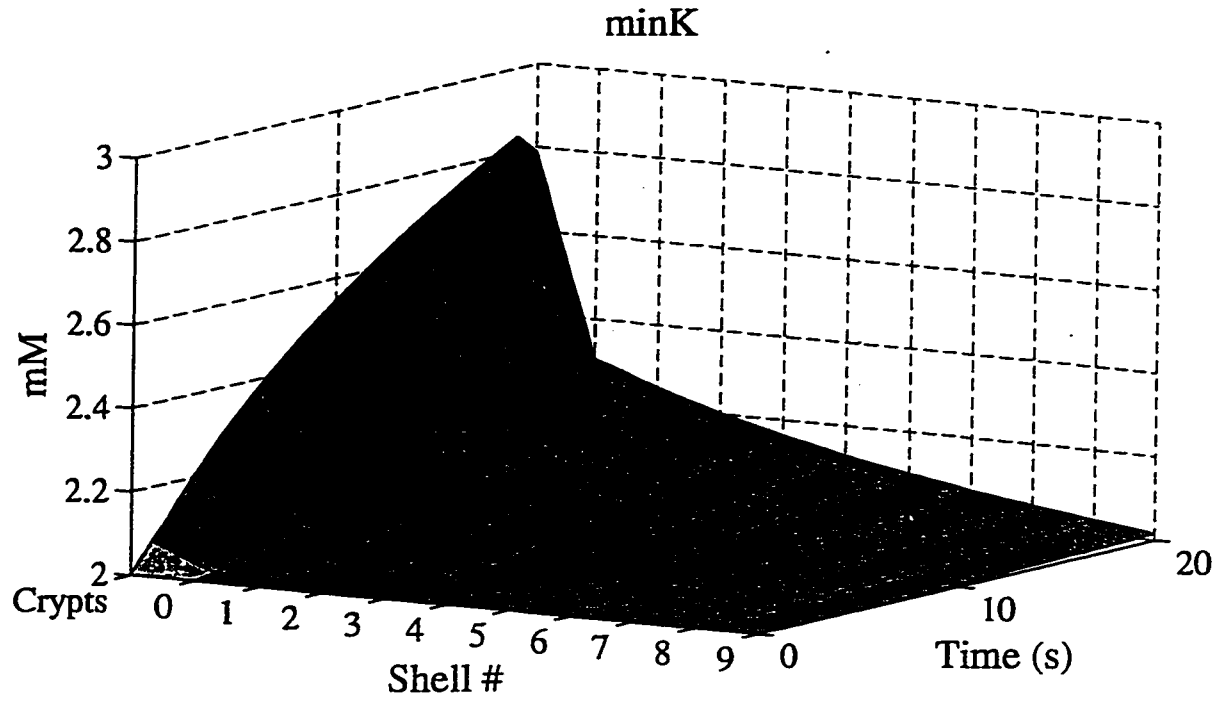
minK
3
2.8
2.6
2.4
2.2
2
mM
Crypts
0 1 2 3 4 5 6 7 8 9
Shell #
0
10
20
Time (s)

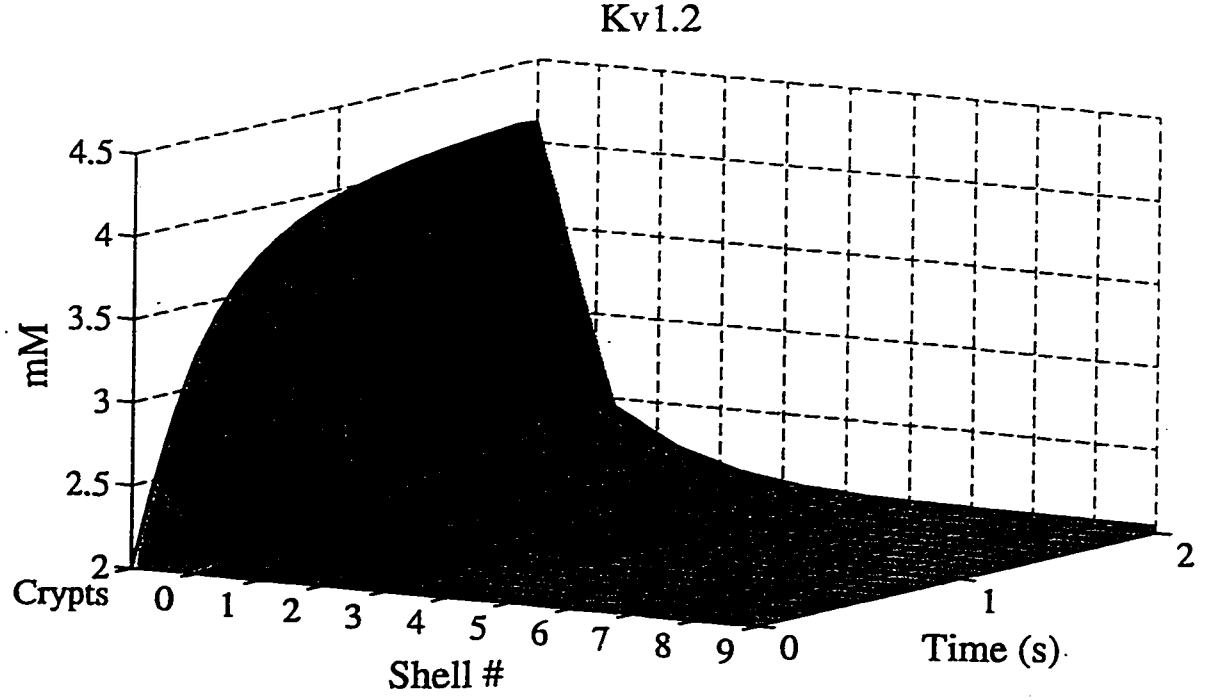
Kv1.2
4.5
4
3.5
3
2.5
2
mM
Crypts
0 1 2 3 4 5 6 7 8 9
Shell #
0
1
2
Time (s)

IMAGE EVALUATION
TEST TARGET (QA-3)

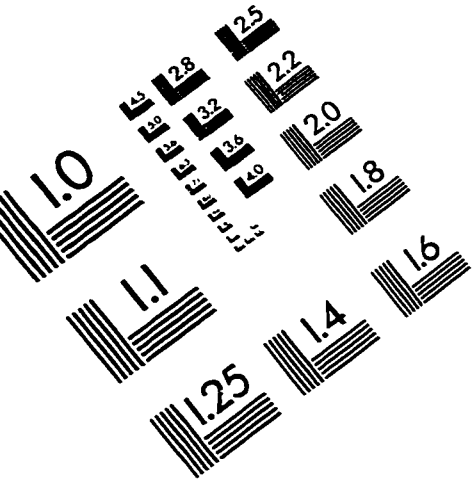

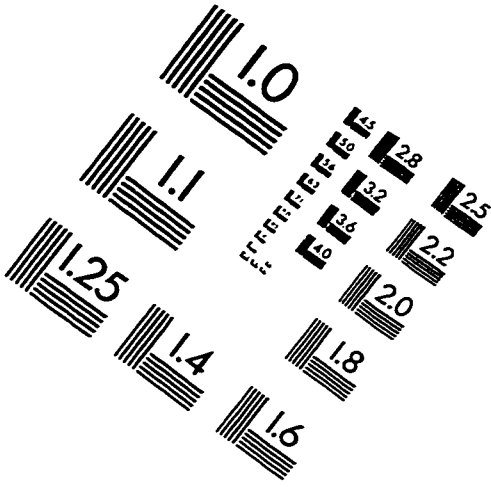

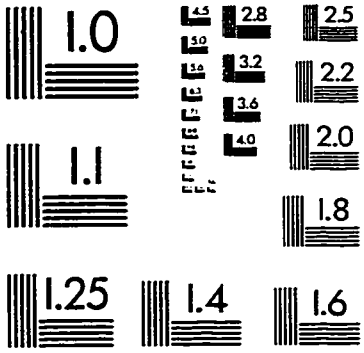

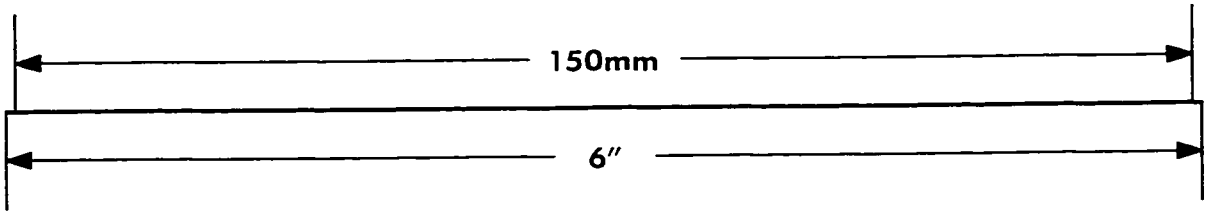

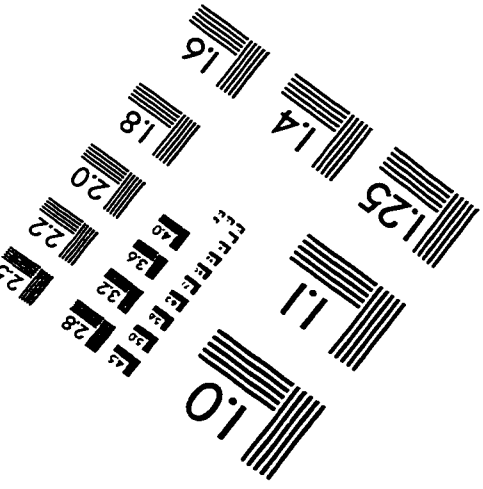

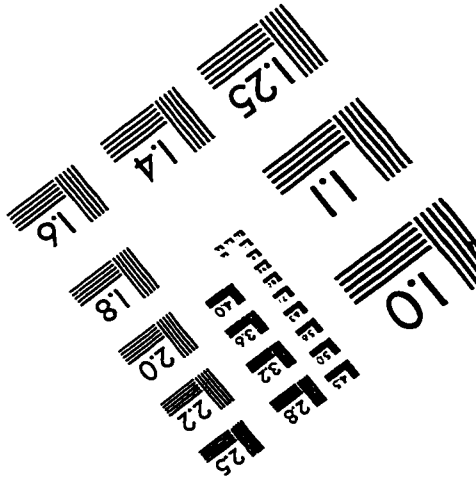

APPLIED IMAGE, Inc
1653 East Main Street
Rochester, NY 14609 USA
Phone: 716/482-0300
Fax: 716/288-5989